UNIVERSITY OF CALIFORNIA SAN DIEGO

Design, Synthesis, and Application of a Fluorescent Ribonucleoside Alphabet

A dissertation submitted in partial satisfaction of the requirements for the degree Doctor of Philosophy

in

Chemistry

by

Paul Theodore Ludford III

Committee in charge:

Professor Yitzhak Tor, Chair
Professor Steven Dowdy
Professor Michael Burkart
Professor Clifford Kubiak
Professor Colleen McHugh

2021

The dissertation of Paul Theodore Ludford III is approved, and it is acceptable in quality and form for publication on microfilm and electronically.

University of California San Diego

2021

DEDICATION

I dedicate this thesis to my parents, Ted and Debbie Ludford.

EPIGRAPH

“An unexamined life is not worth living.”

- Socrates

TABLE OF CONTENTS

LIST OF ABBREVIATIONS

ºC	degrees Celsius
^{13}C	carbon
^{1}H	hydrogen
2-AP	2-aminopurine
^{31}P	phosphorous
3-MI	3-methylpterin riboside
6-MI	6-methylpterin riboside
A	adenosine
Å	angstrom
ABq	AB quartet
Ac_2O	Acetic anhydride
Acetyl-CoA	acetyl coenzyme A
ACN	acetonitrile
ADA	adenosine deaminase
ADA1	human adenosine deaminase 1
ADA2	human adenosine deaminase 2
ATP	adenosine triphosphate
BOP	benzotriazol-1-yloxytris(tris(dimethylamino)phosphonium hexafluorophosphate
br	broad
C	cytidine
CDA	cytidine deaminase
cGMP	cyclic guanosine monophosphate
cm	centimeter
COSY	correlated spectroscopy
d	doublet
DADA2	deficiency of adenosine deaminase 2
DBU	1,8-Diazabicyclo[5.4.0]undec-7-ene
DCM	dichloromethane
dd	doublet of doublets
DEAE	diethylaminoethanol
DMAP	4-dimethylaminopyridine
DMF	dimethylformamide
DMSO	dimethylsulfoxide
$DMSO_2$	dimethylsulfone
DNA	deoxyribonucleic acid
DTT	dithiothreitol
EBV	Epstein Barr Virus
EDTA	ethylenediaminetetraacetic acid
EHNA	erythron-9-(2-hydroxy-3-nonyl)adenine
em	emission
ESI	electrospray ionization
EtOAc	ethyl acetate
EtOH	ethanol
ex	excitation
$FADH_2$	flavin adenine dinucleotide
FDA	Food and Drug Administration
g	gram
G	guanosine

GDA	guanine deaminase
G_n	guanine
GTP	guanosine triphosphate
h	hour
HEPES	4-(2-hydroxyethyl)-1-piperazineethanesulfonic acid
HH ^3J	NMR coupling constant
HIV	human immunodeficiency virus
HPLC	high performance liquid chromatography
HR-ESI-TOF MS	high resolution electrospray ionization time of flight mass spectrometer
HRMS	high resolution mass spectrometry
HTS	high throughput screen
Hz	Hertz
IC_{50}	half maximal inhibitory concentration
K	Kelvin
k_1	binding rate constant
k_{-1}	unbinding rate constant
k_2	deamination rate constant
k_{app}	apparent rate constant
k_{cat}	catalytic turnover rate constant/turnover number
kDA	kilodaltons
K_I	inhibitor constant
K_M	Michaelis-Menten constant
L	liter
LB	Lubria Broth
m	meter, multiplet
M	molar
MALDI	matrix-assisted laser desorption/ionization
MBP	metal-binding pharmacophore
$MeNO_2$	nitromethane
MeOH	methanol
mg	milligram
MHz	Megahertz
min	minutes
mL	milliliter
mm	millimeter
mM	millimolar
mol	mole
^{mth}A	methylthieno[3,4-*d*]pyrimidine-based adenosine analogue
^{mth}C	methylthieno[3,4-*d*]pyrimidine-based cytidine analogue
^{mth}G	methylthieno[3,4-*d*]pyrimidine-based guanosine analogue
$^{mth}G_n$	methylthieno[3,4-*d*]pyrimidine-based guanine analogue
^{mth}GTP	^{mth}G triphosphate
^{mth}U	methylthieno[3,4-*d*]pyrimidine-based uridine analogue
MW	molecular weight
n	refractive index
NADH	nicotinamide adenine dinucleotide
NaOAc	sodium acetate
ng	nanogram
nm	nanometer
nM	nanomolar
NMR	nuclear magnetic resonance

NOESY	Nuclear Overhauser Effect spectroscopy
OD	optical density
OD_{600}	optical density at 600 nanometers
ODE	ordinary differential equation
OEt_2	diethylether/ether
PAGE	polyacrylamide gel electrophoresis
PL	photoluminescence
ppm	parts per million
q	quartet
R^2	correlation coefficient
RNA	ribonucleic acid
rpm	revolutions per minute
RT	room temperature
s	second, singlet
SAM	S-adenosylmethionine
SAR	structure activity relationship
SD	standard deviation
SDS	sodium dodecyl sulfate
STD	standard deviation
T	thymidine
t	time, triplet
$t_{1/2}$	half life
TCEP	tris(2-carboxyethyl)phosphine
TE	buffer
TEA	triethylamine
TEAA	triethylammonium acetate
TEAB	triethylammonium bicarbonate
^{th}A	thieno[3,4-*d*]pyrimidine-based adenosine analogue
^{th}C	thieno[3,4-*d*]pyrimidine-based cytidine analogue
THF	tetrahydrofuran
^{th}G	thieno[3,4-*d*]pyrimidine-based guanosine analogue
$^{th}G_n$	thieno[3,4-*d*]pyrimidine-based guanine analogue
^{th}GTP	^{th}G triphosphate
THU	tetrahydrouridine
^{th}U	thieno[3,4-*d*]pyrimidine-based uridine analogue
TLC	thin layer chromatography
TMS	triflate trimethylsilyltrifluoromethanesulfonate
Tris-HCl	tris(hydroxymethyl)aminomethane
^{tz}A	isothiazolo[4,3-*d*]pyrimidine-based adenosine analogue
^{tz}C	isothiazolo[4,3-*d*]pyrimidine-based cytidine analogue
^{tz}G	isothiazolo[4,3-*d*]pyrimidine-based guanosine analogue
$^{tz}G_n$	isothiazolo[4,3-*d*]pyrimidine-based guanine analogue
^{tz}GTP	^{tz}G triphosphate
^{tz}U	isothiazolo[4,3-*d*]pyrimidine-based uridine analogue
U	unit
U	uridine
UV	ultraviolet
v	volume
Vis	visible light
Zeb	Zebularine
δ	chemical shift

ε	extinction coefficient/molar absorptivity
λ_{abs}	maximum wavelength of absorbance
λ_{abs}^{max}	maximum wavelength of absorbance
λ_{em}	maximum wavelength of emission
λ_{max}	maximum wavelength of absorbance
µg	microgram
µL	microliter
µm	micrometer
µM	micromolar
Φ	quantum yield

LIST OF FIGURES

LIST OF SCHEMES

LIST OF TABLES

LIST OF EQUATIONS

ACKNOWLEDGEMENTS

First and foremost, I would like to thank my parents Ted and Debbie Ludford who have supported me my entire life through highs and lows. None of this would be possible without there tireless efforts in raising me, providing for me, and pushing me to achieve my goals. They have laid the bedrock of which all else has been built on.

I would like to thank my sisters Rebecca and Victoria Ludford who continuously support my goals and aspirations and provide no shortage of guidance and insight. They are there whenever I need them for or for worse, whether I realize it or not.

I would like to thank Professor Yitzhak Tor for all of his guidance and support. He certainly did not need to accept me into his lab, but he did and it has been an excellent experience. He has provided me with his wisdom, experience, and knowledge. I could not be where I am today without his guiding hand.

I would like to thank all of the great people I have spent so much time with in the lab, Andrea Fin, Alex Rovira, Patrycja Hopkins, Yao Li, Kaivin Hadidi, Francois Halle, Yusuke Kawamoto, Alexander Braun, Deyuan Cong, Yu Wu, Phil Bartels, Kfir Steinbuch, Marcela Bucardo, Kasper Beck, Ryosuke Koyama, Ryo Watabe, Yoshimasa Makita, Alessandro Volonterio, Helena Roura, Chiara Miti, Jonas Feldman, Julia Friedrich, Moritz Hommrich, Xiyuan Lu, Jamie Lam, Shenghua Yang, John Lopp, Aaron Levy, Jackie Tu, Yumo Lin, Tyler Lam, Darlene Woodward, Anthony Greene, Benjamin Huang, Juliana Fox, Mason Gatz, Ruxandra Dane, Marina Banasevic, Francis Yu. I have spent an enormous amount of time with them and they with me. There are plenty of ups and downs shared among us and those experiences I will always cherish. They have made working in the Tor lab through the years a far more enjoyable and rich experience.

I would like to thank the Cohen Lab for being excellent collaborators and for sharing their immense knowledge of metal-binding pharmacophores. It was an absolute joy working with all of them and especially Rebecca Adamek, Stephanie Duggan, and Professor Seth Cohen.

I would like to thank the facilities managers and staff. None of this is possible without them. Dr. Milan Gembicky, Dr. Jake Bailey, and Dr. Curtis Moore have been a tremendous help in growing crystals and obtaining crystal structures. Dr. Anthony Mrse has been provided no end of insight into NMR spectra and experiments that could be helpful or key to obtaining the information I need. He has always been willing to help interpret data that may be confusing and to provide suggestions for experiments that may clear up confusion. Dr. Yongxuan Su, the Mass spectrometry facility manager, has been able to provide beautiful high-resolution mass spectrometry data, softening the blow when it is not the mass you were expecting. And of course, Robyn Swanland who has answered any and all day to day questions I have regarding UCSD bureaucracy.

Finally, I would like to thank my wife, Xin Guo, for all her love and support. She is there whenever I need her, no matter what kind of day I have, the best, the worst, the most average. Life is that much brighter when she is around.

Chapter 2 is adapted from work currently being drafted for submission: Ludford III, P. T.; Yang, S.; Tor, Y. “The Next Generation of Emissive RNA Alphabets” *in preparation*. Permission to use materials from the manuscript was also obtained from co-authors Shenghua Yang and Yitzhak Tor. The dissertation author will be the first author.

Chapter 3 is adapted from the work: Adamek, R. N.* and Ludford III, P. T.*; Duggan, S. M.; Tor, Y.; Cohen, S. M. “Identification of Adenosine Deaminase Inhibitors by Metal-binding Pharmacophore Screening” *ChemMedChem*, *22*, 2151-2156. (*Shared first co-authorship). Permission to use materials from the manuscript was also obtained from co-authors Rebecca Adamek, Stephanie Duggan, Seth Cohen, and Yitzhak Tor. The dissertation author is the first co-author.

Chapter 4 is adapted from the work: Ludford III, P. T.; Li, Y.; Yang, S.; Tor, Y. “Cytidine Deaminase Can Deaminate Fused Pyrimidine Ribonucleosides” *Org. Biomol. Chem.*, *in press*.

Permission to use materials from the manuscript was also obtained from co-authors Yao Li, Shenghua Yang, and Yitzhak Tor. The dissertation author is the first author.

Chapter 5 is adapted from work currently being drafted for submission: Ludford III, P. T.; Bartels, P. L.; Tor, Y. “Deconvoluting the Activity of Human Adenosine Deaminase 1 and 2” *in preparation*. Permission to use materials from the manuscript was also obtained from co-authors Phillip Bartels and Yitzhak Tor. The dissertation author will be the first author.

VITA

2013 Bachelor of Science, Chemistry – Rutgers University

2017 Master of Science, Chemistry – University of California San Diego

2021 Doctor of Philosophy, Chemistry – University of California San Diego

PUBLICATIONS

Ludford, P.; Aydin, F.; Dutt, M. “Design and Characterization of Nanostructured Biomaterials via the Self-assembly of Lipids” *MRS Proceedings* **2013**, *1498*, 233-238.

Aydin, F.; Ludford, P.; Dutt, M. “Phase segregation in bio-inspired multi-component vesicles encompassing double tail phospholipid species” *Soft Matter* **2014**, *10*, 6096-6108.

Ludford III, P. T.; Rovira, A. R.; Fin, A.; Tor, Y. "Fluorescing Isofunctional Ribonucleosides: Assessing Adenosine Deaminase Activity and Inhibition" *ChemBioChem* **2019**, *20*, 718-726. *cover feature*

Li, Y.; Ludford III, P. T.; Fin, A.; Rovira, A. R.; Tor, Y. "Enzymatic Synthesis and Applications of Fluorescent Cyclic Dinucleotides" *Chem. Eur. J.* **2020**, *26*, 6076-6084.

Ludford III, P. T.; Tor, Y. “Ascertaining the Activity and Inhibition of Adenosine Deaminase” *Methods in Enzymology* **2020**, *639*, 71-90.

Adamek, R. N.* and Ludford III, P. T.*; Duggan, S. M.; Tor, Y.; Cohen, S. M. “Identification of Adenosine Deaminase Inhibitors by Metal-binding Pharmacophore Screening” *ChemMedChem*, *22*, 2151-2156. (*Shared first co-authorship)

Beck, K. M.; Krogh, M. B.; Hornum, M.; Ludford III, P. T.; Tor, Y.; Nielsen, P. “Double-headed Nucleotides As Xeno Nucleic Acids: Information Storage and Polymerase Recognition” *Org. Biomol. Chem.* **2020**, *18*, 7213-7223.

Ludford III, P. T.; Li, Y.; Yang, S.; Tor, Y. “Cytidine Deaminase Can Deaminate Fused Pyrimidine Ribonucleosides” *Org. Biomol. Chem.*, *in press*.

Bucardo, M.; Wu, Y.; Ludford III, P. T.; Fin, A.; Tor, Y. “Real-time Monitoring of Human Guanine Deaminase Activity by an Emissive Guanine Analog” *ACS Chem. Bio.*, *in press*.

Cong, D.; Li, Y.; Ludford III, P. T.; Tor, Y. “Isomorphic Fluorescent Nucleosides Facilitate a Real Time Monitoring of RNA Depurination by Ribosome Inactivating Proteins”, *submitted*.

ABSTRACT OF THE DISSERTATION

Design, Synthesis, and Application of a Fluorescent Ribonucleoside Alphabet

by

Paul Theodore Ludford III

Doctor of Philosophy in Chemistry

University of California San Diego, 2021

Professor Yitzhak Tor, Chair

A new fluorescent ribonucleoside alphabet consisting of pyrimidines and purines, all derived from methylthieno[3,4-*d*]pyrimidine as the heterocyclic core, is described. Photophysical analyses reveal surprisingly large bathochromic shifts relative to previous alphabets derived from thieno[3,4-*d*]pyrimidine and isothiazole[4,3-*d*]pyrimidine. Biochemical analyses with adenosine deaminase, T7 RNA Polymerase, and guanine deaminase indicate the varying degrees of tolerance for a methyl moiety on the Hoogsteen face by different enzymes.

These results indicate that the analogues can act as useful probes in the same capacity as previous alphabets and provide insight into enzyme tolerance to structural perturbations on the Hoogsteen face.

Separately, the enzymatic conversion of a visibly emitting adenosine analogue, ^{tz}A, to the corresponding fluorescent inosine analogue, ^{tz}I, by adenosine deaminase (ADA) is monitored via fluorescence intensity changes. The Cohen Lab at UC San Diego has a library of over 300 compounds comprised of metal-binding pharmacophores which they have tested as novel inhibitors of a variety of metalloenzymes. The new method of monitoring ADA activity is utilized in collaboration with the Cohen Lab to screen their library of metal binding pharmacophores (MBPs) in a high throughput format as inhibitors of ADA. Several inhibitors are discovered and derivatives of the hit compounds are tested against ADA to develop a structure activity relationship. Finally, a new compound is designed and synthesized based on the findings of the structure activity relationship and found to be the most potent derivative of the original hit compound.

With the new methylthieno[3,4-*d*]pyrimidine based alphabet in hand, the tolerance of Cytidine Deaminase (CDA) to expanded heterocycles is explored. The molecules used are ^{mth}C, thC, and ^{tz}C, three fluorescent cytidine analogues where the pyrimidine core is fused to three distinct five-membered heterocycles at the 5/6 positions. The reaction between each analogue and CDA is monitored by absorption and emission spectroscopy, revealing shorter reaction times for all three analogues than the native substrate. Pseudo-first order and Michaelis-Menten kinetic analyses provide further insight into the enzymatic deamination reactions and assist in drawing comparison to established structure activity relationships. Finally, each analogue is used to analyze two known inhibitors of CDA, zebularine and tetrahydrouridine, as a proof of concept for potential screening assays.

Continuing on the success of the CDA assays, human adenosine deaminase 1 (ADA1) and 2 (ADA2) are studied. The newly synthesized adenosine analogue, ^{mth}A, as well as the two

previously reported analogues thA and ^{tz}A are used to monitor ADA1 and ADA2 activity and probe their tolerance for steric hindrance on the Hoogsteen face. ADA2 is found to tolerate the missing nitrogen in thA and the perturbing methyl in ^{mth}A on the Hoogsteen face far more than ADA1. Further it is found to react faster with ^{tz}A and thA than adenosine, the native substrate. An assay is then developed in which both ADA1 and ADA2 are present, but one is “turned off” by excess selective inhibitor so that the other enzymes activity can be monitored using ^{mth}A, thA, or ^{tz}A.

Chapter 1

Introduction

1.1 Introduction to Nucleosides

Nucleosides are the building blocks of two types of biopolymers, RNA and DNA. They fall under two categories, ribonucleosides and deoxyribonucleosides. The former make up RNA and the latter make up DNA. There are four different nucleosides in each category, guanosine, adenosine, cytidine, and uracil (RNA) or thymine (DNA) (Fig. 1.1, 1.2). The key difference between ribonucleosides and deoxyribonucleosides is a hydroxyl moiety attached to the 2nd carbon (2' position) on the ribose (Fig. 1.1, 1.2). The nucleobases are split into two categories: purines and pyrimidines (Fig. 1.1). Our interest for the remainder of the paper will be in the context of RNA.

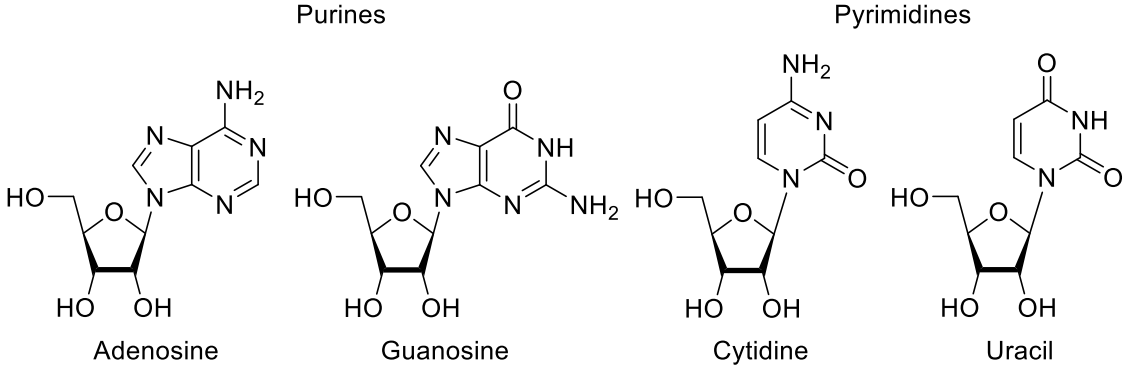

Figure 1.1 Canonical Ribonucleosides

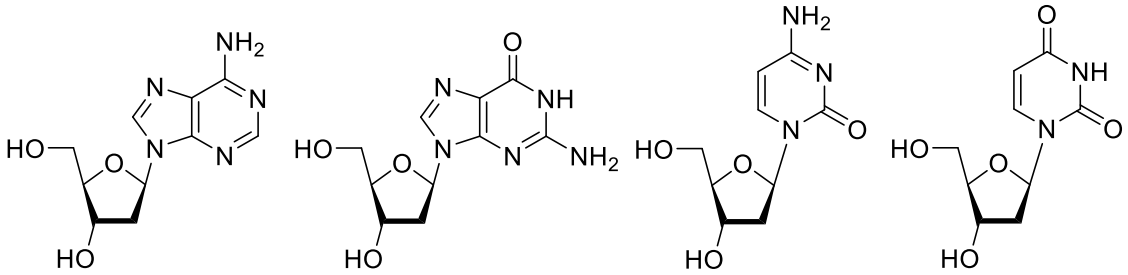

Figure 1.2 Canonical Deoxyribonucleosides

As nucleosides make up RNA and DNA, they are directly involved in the central dogma or flow of information in cells.[1–4] This makes them extremely valuable targets for observing cellular processes, particularly RNA because it acts as an intermediate between DNA and proteins. However, there are many forms of RNA and they are not all fully understood. rRNA and tRNA facilitate translation and have complex secondary structure. In addition, tRNA undergoes many posttranscriptional modifications that are critical for proper function.[2–4] Non-coding RNA (ncRNA) in particular still has much to be discerned. These ncRNA may regulate gene expression at the level of transcription, processing of other RNA, as well as translation.[5] Some RNA strands also function as enzymes, referred to as ribozymes or riboswitches.[6]

Not only are ribonucleosides the building blocks of RNA, but they also make up the core structure of many secondary messengers and cofactors. Examples include cyclic GMP, a signaling molecule in cells, ATP, nature's energy unit, NADH and $FADH_2$, nature's redox reagents, SAM, nature's methylating agent, and acetyl-CoA, nature's acetylating unit (Fig. 1.3).[7–18] These and many more molecules based on ribonucleosides are directly involved in many cellular processes.

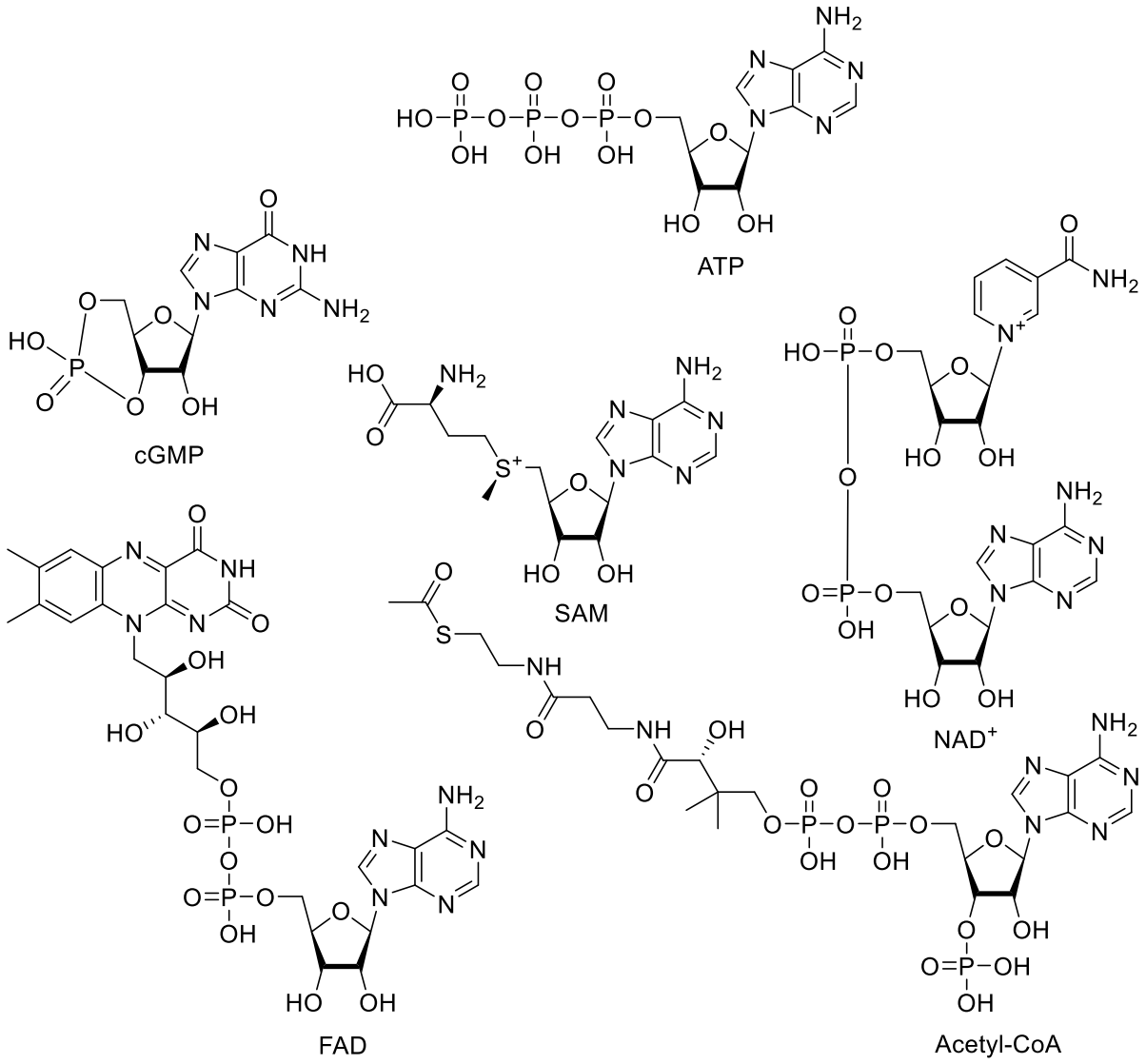

Figure 1.3 Secondary Messengers and Cofactors

Due to ribonucleosides being so integral to cellular processes, many different techniques for observing them and changes to them have been developed and pursued. These techniques include but are not limited to: nuclear magnetic resonance (NMR), X-ray crystallography, fluorescence, UV-Vis based spectroscopy, and electron paramagnetic resonance.[19–20]

The ultimate goal in many cases is to monitor activity in real time. This becomes acutely apparent when monitoring enzymatic processes where critical time windows are narrow. Fluorescence and UV-Vis spectroscopy can provide the means to observe molecules in real

time. However, a major drawback of the canonical nucleosides is that their main absorption bands are below 300 nm, a region that is exceptionally crowded by biological molecules. Further, the canonical nucleosides have sub picosecond excited state lifetimes and quantum yields below one hundredth of a percent making them essentially dark.

Another technique that has been used to observe nucleosides and their derivatives is radiolabeling.[21] Isotopes such as ^{32}P, ^{14}C, and ^{3}H have been incorporated into nucleotides and nucleosides via biosynthesis or chemical synthesis. The main advantage of radiolabeling is that they maintain the same structure as native nucleosides to such a degree that they are recognized just as well. We can define this property “isofunctionality” and describe it as the ability to be recognized by biological systems as well as the native counterpart. Likewise, the structural resemblance of the modified molecule to the native molecule can be defined as “isomorphicity”.[22] In both aspects, radiolabeling produces the most isofunctional and isomorphic nucleoside analogues and radiolabeled nucleosides can be considered to have reached the upper limit of each property. The downside of radiolabeled nucleoside analogues, unfortunately, is the difficulty in measurement, the delicacy required in handling them, the short lifespans of them, and the lack of methods to monitor them in real-time.

The lack of real-time monitoring in most of the methods mentioned above and the lack of fluorescence in the native nucleosides has led to the development of fluorescent nucleoside analogues. Their structures and photophysical properties vary widely and require a plethora of synthetic procedures to make.[19]

1.2 Properties to Consider When Choosing or Designing a Fluorophore

A major challenge in the development of fluorescent ribonucleoside analogues is the lack of predictability of photophysical properties of any molecule. A molecule can be

hypothesized to fluoresce, but any quantifiable properties are only determined after extensive experimentation with the final product. As a result, one can spend a large amount of time and energy synthesizing a promising looking molecule only to find out after synthesis that the molecule does not have the desired photophysical properties. Contending with this problem while also trying to minimize structural perturbation can be quite difficult. We will elaborate on some of the properties that one may seek to take advantage of in a fluorophore.

There are two properties of a fluorophore that one must at minimum determine to begin to describe that fluorophore. Those properties are the molar absorptivity (ε) and the quantum yield (Φ). The former describes the amount of light particles a molecule will absorb at a given concentration and the latter describes the number of light particles emitted for every light particle absorbed.[23]

The molar absorptivity, sometimes referred to as the extinction coefficient, of a molecule is determined by measuring the absorbance of samples with varying concentrations of that molecule. The absorbance values are then plotted against concentration and a line is fit to the data. The slope of the resulting line is the molar absorptivity. The quantum yield can be determined in a number of different ways. The method used herein is the relative quantum yield, determined by comparison to another reported chromophore. When the molar absorptivity and the quantum yield are multiplied together one obtains the brightness. A high brightness is considered highly desirable and improving either the quantum yield or the molar absorptivity will result in a higher brightness.[23]

In addition to these fundamental properties of the fluorophore, one may also be interested in the excited state lifetime. The excited state lifetime is the length of time the fluorophore will remain in the excited state before relaxation to the ground state. The longer the lifetime, the longer the amount of time a sample of the fluorophore will emit. We will not elaborate further in this document, but it is worth noting that lengthening the lifetime of the

fluorophore lengthens the time window with which one can observe events at a molecular level.[23]

One may also be interested in the sensitivity of the fluorophore to its surroundings. The polarity, viscosity, and pH can have a drastic effect on the emission of a fluorophore.[23] The change in the Stokes Shift, or difference in energy between the absorption and emission maxima, relative to the polarity of the solvent is referred to as the sensitivity to polarity. In certain circumstances a high sensitivity to polarity can be extremely useful such as when observing binding of the fluorophore by a protein. Upon binding, the fluorophore which was in polar solvated surroundings suddenly becomes introduced to nonpolar desolvated surroundings. If the fluorophore is emissive in a polar environment but not a nonpolar environment, one may see a sudden quenching of the fluorophore upon addition of the binding enzyme. Likewise, if the fluorophore is emissive in a nonpolar environment but not a polar environment, one may see the exact opposite upon addition of the binding enzyme.

All of the properties described above are worth considering when choosing a fluorophore for an experiment or when designing a new fluorophore.

1.3 Different Types of Fluorescent Ribonucleosides

A multitude of approaches have been taken to designing fluorescent nucleosides. The structural modifications of nucleosides have included extending the pi system of the nucleobase, expanding the ring system of the nucleobase, or substituting the nucleobase entirely for a known fluorophore. The fluorescent analogues can be categorized into five families: extended analogues, expanded analogues, pteridine analogues, chromophoric analogues, and isomorphic analogues. There are some overlapping similarities between each of the families.[19–20,24–27]

The extension approach has been implemented heavily at the 5-position of pyrimidines (Fig. 1.4). Structures such as an alkyne linked to a larger fluorophore, thiophenes,

selenophenes, and furans have been attached at the 5-position of uridine.[28] Extensions have also been made off of the 8 position in purines notably in 8-vinyladenosine.[9] The upside of the extension approach is that it leaves the Watson-Crick face intact for base pairing.

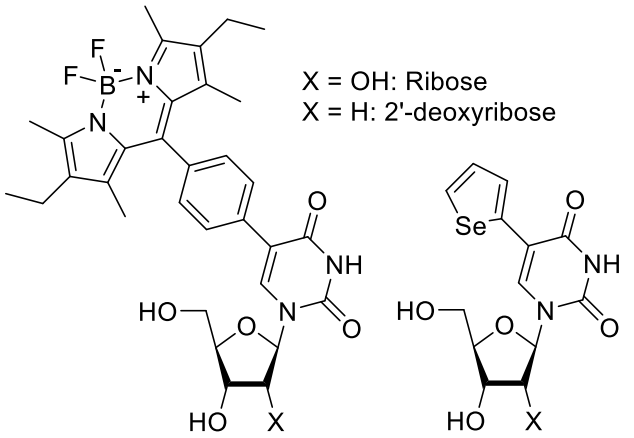

Figure 1.4 Examples of Extended Nucleoside Analogues

The expanded ring approach involves fusing additional rings onto the target nucleoside (Fig. 1.5). Etheno-adenosine, an adenosine analogue, expands the aromatic ring system by forming a five-member ring with an ethene between the exocyclic amine at the 6 position and the N1 position.[29–32] This however interferes with the Watson-Crick face. tc^0 expands the ring system of cytidine by connecting a benzene ring to the exocyclic amine and an ether linkage at the 5-position.[25] This analogue preserves the Watson-Crick face but also increases the steric bulk.

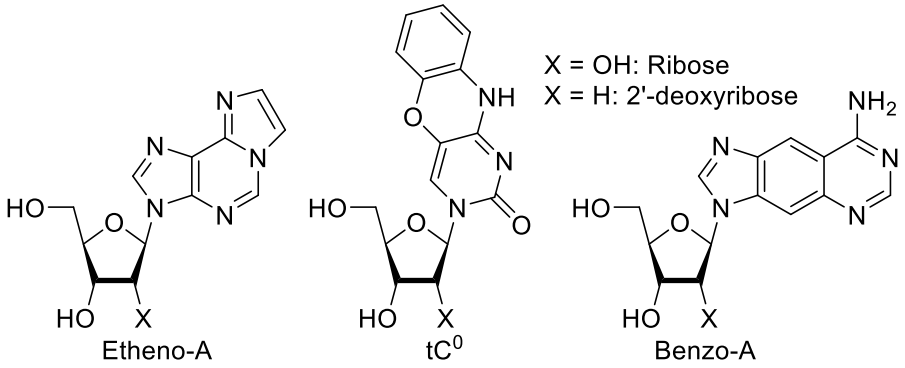

Figure 1.5 Examples of Expanded Nucleoside Analogues

Pteridines are naturally occurring molecules.[27,33] Analogues of them have been used as fluorescent purine analogues. Examples are 3-MI and 6-MI, two guanosine analogues (Fig. 1.6). The pteridine analogues reported quantum yields are quite high (0.39-0.68) and their absorption bands are above 300 nm, a highly desirable trait given that the native nucleosides absorb in the mid to upper 200 nm range.

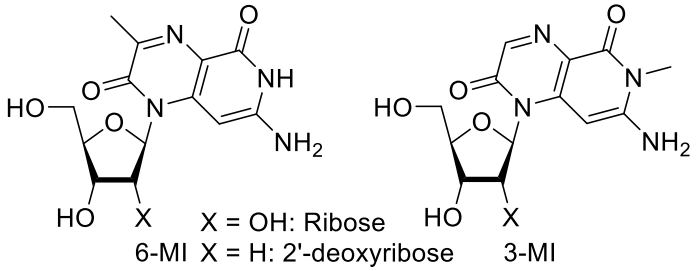

Figure 1.6 Structures of 3-MI and 6-MI

Chromophoric analogues forego attempts at preserving the original nucleobase structure and instead aim for desirable photophysical properties (Fig. 1.7).[26,34] These analogues tend to have high quantum yields and red-shifted absorption and emission bands. They retain the sugar, but they cannot base pair as the Watson-Crick face is almost certainly removed. They can however still base stack which can be suitable for some applications.[19,26,34]

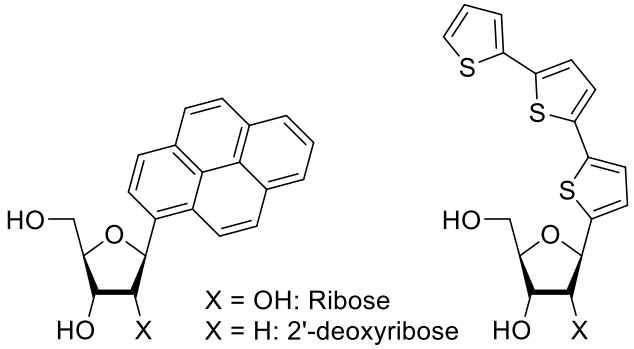

Figure 1.7 Examples of Chromophoric Analogues

The isomorphic analogues aim to be as structurally and electronically close to the native nucleosides as possible while still providing desirable photophysical features (Fig. 1.8). These analogues provide the best opportunity to monitor processes involving the native nucleosides

with minimal interference. However, the synthesis of these analogues is often quite challenging. Perhaps one of the oldest isomorphic analogues described is 2-aminopurine (2-AP), an adenosine analogue with the exocyclic amine moved from the 6 position to the 2 position. This seemingly small modification results in a quantum yield of 0.68 and a main absorption band at 303 nm and is a good example of how unpredictable photophysical characteristics can often be.[35–38] Unfortunately, it is severely quenched when incorporated into oligomers highlighting the large drawbacks even the most promising fluorophores can have.[19,39]

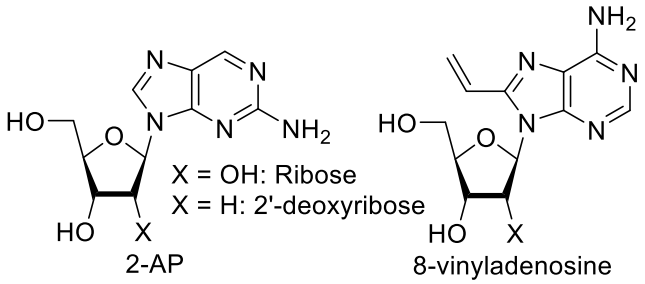

Figure 1.8 Examples of Isomorphic Analogues

1.4 Evolution of Fluorescent Ribonucleosides in the Tor Lab

The Tor Lab has reported a number of fluorescent nucleosides over the years. The emphasis in general has been to remain as isomorphic as possible, with some exceptions for improved photophysical characteristics.

Some of the early molecules developed in the Tor Lab were the 5 substituted uridine analogues. The substitutions included a thiophene, furan, thiazole, and oxazole (Fig. 1.9).[40–42] These analogues were found to be sensitive to changes in viscosity. When placed in a high viscosity environment the quantum yield improved significantly suggesting the main method of relaxation was rotational. The 5-furan uridine analogue emission was shown to be enhanced when adjacent to an abasic site in incorporated into a DNA duplex as compared to when it was adjacent to guanosine.[43] This is a useful trait for detecting the formation of abasic sites in DNA. The C analogue equivalent of the 5-furan-uridine analogue when placed in an oligomer was

shown to emit differently depending on whether it base-paired with guanosine, 8-oxoguanosine, or thymidine.[44] A particularly useful trait for observing mismatched bases or the oxidation of guanosine.

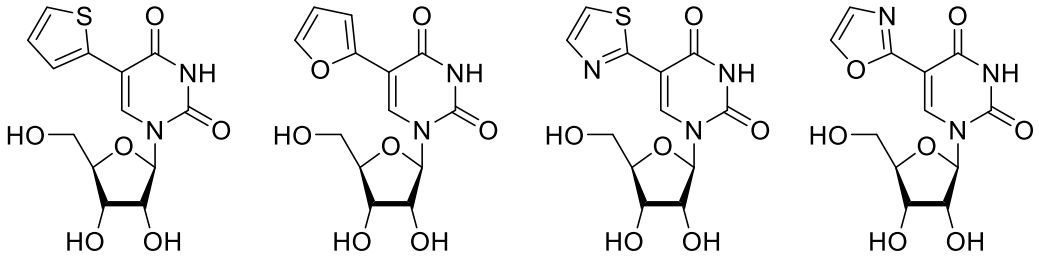

Figure 1.9 Structure of 5-substituted Uridine Analogues

While the above-mentioned fluorescent nucleoside analogues were being exploited, another uridine analogue, thU, was developed (Fig. 1.10).[45] thU unlike the previous analogues, had a thiophene ring fused to the pyrimidine core at the 5/6 positions. This resulted in a high quantum yield of 0.41, an absorption band at 304 nm, and an emission band at 412 nm. thU was shown to detect abasic sites like the 5-furan uridine analogue and was used to monitor the activity of ricin.[46]

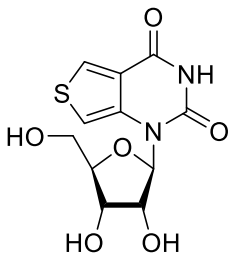

Figure 1.10 Structure of thU

thU inspired a new generation of fluorescent nucleoside analogues, the thieno[3,4-d]pyrimidine based alphabet (Fig. 1.11). This alphabet included thU, thC, thA, and thG all of which were found to be highly fluorescent with quantum yields ranging from 0.21 to 0.46 (Fig. 1.11).[47] The triphosphate derivative of thG, thGTP, was found to be accepted by T7 RNA Polymerase during in vitro transcription and an oligomer containing thG corresponding to the Hammerhead Ribozyme substrate was used to monitor the ribozymes activity in real time by fluorescence.[48]

thG was also found to successfully initiate strands during in vitro transcription when placed in the reaction in high excess (5x NTP concentration). This allowed for site specific incorporation into desired RNA strands including the Hammerhead Ribozyme.[49]

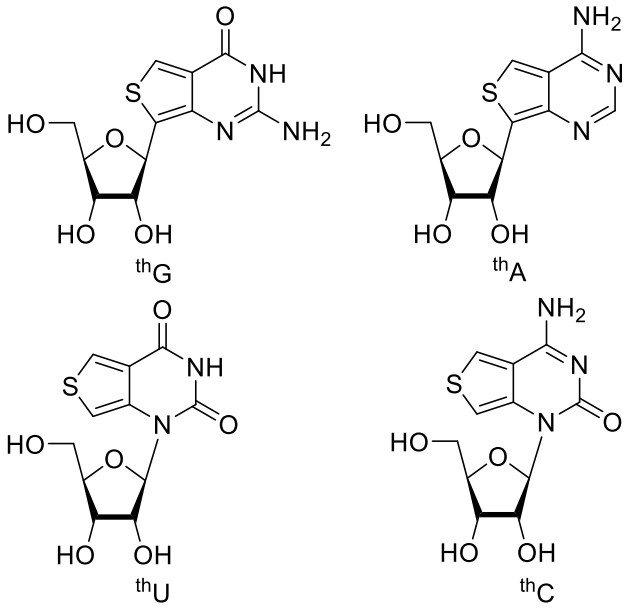

Figure 1.11 Thieno[3,4-d]pyrimidine based alphabet

thA has also been used in many applications. Two such applications were the monitoring of adenosine deaminase (ADA) activity, and the biosynthesis of a fluorescent SAM analogue using thA as the core structure.[50,51] In the former, thA was tested as a substrate of ADA and a Michaelis-Menten analysis was performed. The K_M was found to larger than that for adenosine, but excitingly thA was recognized as a substrate by ADA. Two inhibitors, Pentostatin and EHNA, were then analyzed using thA to monitor ADA activity. In the latter, the SAM analogue based on thA and the enzyme M. Taq1 were used to methylate a linear DNA strand. M. Taq1 also recognized the SAM analogue as a substrate.

The thieno[3,4-d]pyrimidine based alphabet was a success, but it had some shortcomings. One clear drawback was the slower reaction rate observed for thA with ADA as compared to the reaction between adenosine and ADA.[50] It seemed that the isofunctionality of the alphabet might be improved by reinstalling the N7 atom to the analogues. This inspired the

design and synthesis of the isothiazole[4,3-d]pyrimidine based alphabet performed by Dr. Alexander R. Rovira and Dr. Andrea Fin (Fig. 1.12).[52]

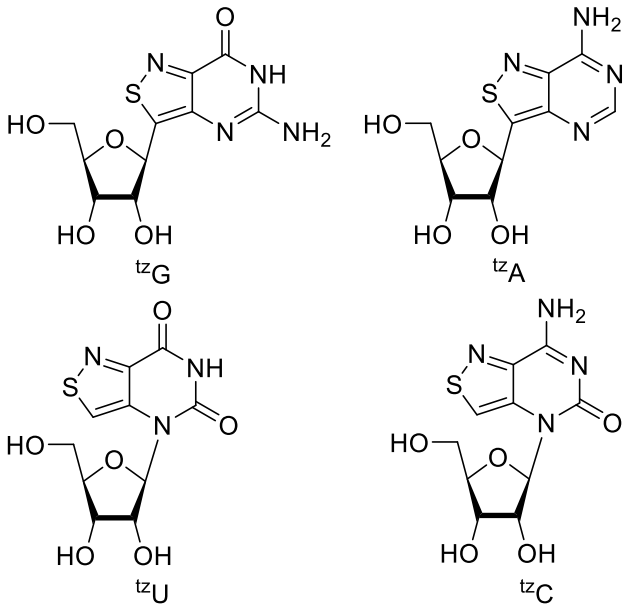

Figure 1.12 Isothiazole[4,3-d]pyrimidine based alphabet

The isothiazole[4,3-d]pyrimidine based adenosine analogue, ^{tz}A, was tested with ADA and compared to that of thA. It was found to have a K_M slightly smaller than that reported for adenosine, a huge success.[52] The isofunctionality was clearly improved for at least the purine analogues, but the photophysical characteristics were significantly diminished. The extinction coefficients of each analogue were larger than the corresponding thieno[3,4-d]pyrimidine based analogue, but the quantum yields dramatically decreased. In the case of ^{tz}U, the quantum yield was 0.01, a complete and total reversal of the success of thU. Further, the emission bands of all analogues but the guanosine analogue were blue shifted relative to their thieno[3,4-d]pyrimidine based counterparts. The results of these findings clearly showed the struggle between developing the most isomorphic and isofunctional nucleosides and developing analogues with highly desirable photophysical features.

This led us to the conclusion that we may need to sacrifice some of the isomorphic and isofunctional behavior to further improve the photophysical features, hopefully beyond those of the thieno[3,4-d]pyrimidine alphabet.

We thus set out to design and synthesize a new fluorescent nucleoside analogue alphabet. We noted that the reintroduction of the N7 and thus a more polar Hoogsteen face led to a large reduction in the quantum yield and blue shifting in the emission. We hypothesized the introduction of a greasier moiety might cause the reverse to occur. We therefore chose to attach a methyl moiety to the Hoogsteen face of the thiophene in the thieno[3,4-d]pyrimidine based precursor yielding a methylthieno[3,4-d]pyrimidine based alphabet (Fig. 1.13).

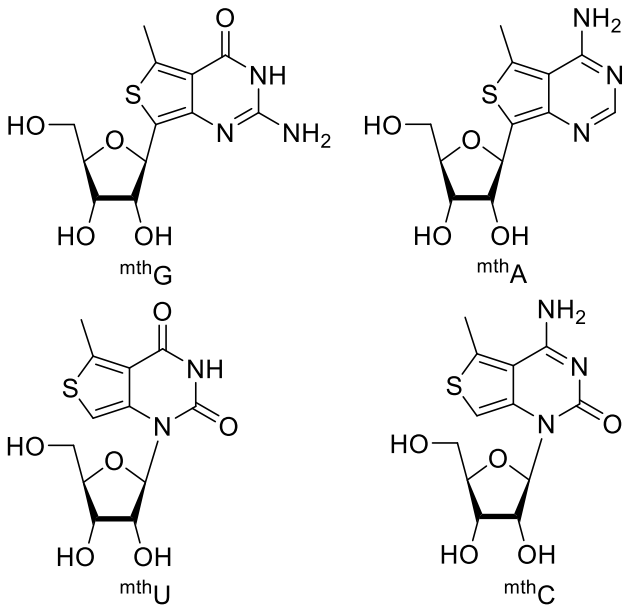

Figure 1.13 Methylthieno[3,4-d]pyrimidine based alphabet

1.5 References

1. Crick, F.H.C. *Symp Soc Exp Biol.*, **1958**, *12*, 138–163.
2. Weeks, K. M. *Biopolymers* **2015,** *103* (8), 438–448.
3. Roundtree, I. A.; Evans, M. E.; Pan, T.; He, C. *Cell*, **2017**, *169*, 1187–1200.
4. Lyons, S. M.; Fay, M. M.; Ivanov, P. *FEBS Lett.*, **2018**, *592*, 2828–2844.

5. Cech, T. R.; Steitz, J. A. *Cell* **2014**, *157* (1), 77–94.

6. Serganov, A.; Patel, D. J. *Nat Rev Genet* **2007,** *8* (10), 776–790.

7. Jenal, U.; Reinders, A.; Lori, C. *Nat. Rev. Microbiol.* **2017,** *15*, 271–284.

8. Ying, W. H. *Antioxid. Redox Signaling* **2008,** *10* (2), 179–206.

9. Pankiewicz, K. W.; Watanabe, K. A.; Lesiak-Watanabe, K.; Goldstein, B. M.; Jayaram, H. N. *Curr. Med. Chem.* **2002,** *9* (7), 733–741.

10. Pergolizzi, G.; Butt, J. N.; Bowater, R. P.; Wagner, G. K. *Chem. Commun.* **2011,** *47* (47), 12655–12657.

11. Collins, Y.; Chouchani, E. T.; James, A. M.; Menger, K. E.; Cocheme, H. M.; Murphy, M. P. *J. Cell Sci.* **2012,** *125* (4), 801–806.

12. Struck, A.-W.; Thompson, M. L.; Wong, L. S.; Micklefield, J. *ChemBioChem* **2012,** *13* (18), 2642–2655.

13. Deen, J.; Vranken, C.; Leen, V.; Neely, R. K.; Janssen, K. P. F.; Hofkens, J. *Angew. Chem. Int. Ed.* **2017,** *56* (19), 5182–5200.

14. Chiang, P. K.; Gordon, R. K.; Tal, J.; Zeng, G. C.; Doctor, B. P.; Pardhasaradhi, K.; McCann, P. P. *The FASEB Journal* **1996,** *10* (4), 471–80.

15. Loenen, W. A. M. *Biochem. Soc. Trans.* **2006,** *34* (2), 330–333.

16. McDaniel, B. A. M.; Grundy, F. J.; Artsimovitch, I.; Henkin, T. M. *Proc. Natl. Acad. Sci. U. S. A.* **2003,** *100* (6), 3083–3088.

17. Winkler, W. C.; Nahvi, A.; Sudarsan, N.; Barrick, J. E.; Breaker, R. R. *Nature Structural Biology* **2003,** *10* (9), 701–707.

18. Singh, S.; Zhang, J. J.; Huber, T. D.; Sunkara, M.; Hurley, K.; Goff, R. D.; Wang, G. J.; Zhang, W.; Liu, C. M.; Rohr, J.; Van Lanen, S. G.; Morris, A. J.; Thorson, J. S. *Angew. Chem., Int. Ed.* **2014,** *53* (15), 3965–3969.

19. Sinkeldam, R. W.; Greco, N. J.; Tor, Y. *Chem. Rev.* **2010,** *110* (5), 2579–2619.

20. Tanpure, A. A.; Pawar, M. G.; Srivatsan, S. G. *Isr. J. Chem.* **2013,** *53* (6–7), 366–378.

21. James Slater, R. *Reviews in Cell Biology and Molecular Medicine*, Wiley-VCH Verlag GmbH & Co. KGaA: 2006.

22. Sinkeldam, R. W.; Tor, Y. *Org. Biomol. Chem.* **2007,** *5* (16), 2523–2528.

23. Lakowicz, J. R. *Principles of fluorescence spectroscopy*. Second edition. New York : Kluwer Academic/Plenum, 1999.

24. Okamoto, A.; Saito, Y.; Saito, I. *Journal of Photochemistry and Photobiology C: Photochemistry Reviews* **2005,** *6* (2–3), 108–122.

25. Wilhelmsson, L. M. *Quarterly Reviews of Biophysics* **2010,** *43* (2), 159–183.

26. Xu, W.; Chan, K. M.; Kool, E. T. *Nat Chem* **2017,** *9* (11), 1043–1055.

27. Hawkins, M. E. *Cell Biochemistry and Biophysics* **2001**, *34* (2), 257–281.

28. Nuthanakanti, A; Boerneke, M. A.; Hermann, T.; Srivatsan, S. G. *Angew. Chem. Int. Ed.* **2017,** *56*, 2640–2644.

29. Jahnz-Wechmann, Z.; Framski, G. R.; Januszczyk, P. A.; Boryski, J. *Front Chem* **2016,** *4*.

30. Gruber, B. A.; Leonard, N. J. *Proc. Natl. Acad. Sci. U. S. A.* **1975,** *72* (10), 3966–3969.

31. Leonard, N. J. B., J. R. *Crit. Rev. Biochem.* **1984,** *15* (2), 125–199.

32. Barrio, J. R.; Secrist, J. A.; Leonard, N. J. *Proc. Natl. Acad. Sci. U. S. A.* **1972,** *69* (8), 2039–2042.

33. Driscoll, S. L.; Hawkins, M. E.; Balis, F. M.; Pfleiderer, W.; Laws, W. R. *Biophys. J.* **1997,** *73* (6), 3277–3286.

34. Teo, Y. N.; Kool, E. T. *Chem. Rev.* **2012,** *112* (7), 4221–4245.

35. Jones, A. C.; Neely, R. K. *Quarterly Reviews of Biophysics* **2015,** *48* (2), 244–279.

36. Serrano-Andres, L.; Merchan, M.; Borin, A. C. *Proc. Natl. Acad. Sci. U. S. A.* **2006,** *103* (23), 8691–8696.

37. Ward, D. C.; Reich, E.; Stryer, L. *J. Biol. Chem.* **1969,** *244* (5), 1228–1237.

38. Jean, J. M.; Hall, K. B. *Proc. Natl. Acad. Sci. U. S. A.* **2001,** *98* (1), 37–41.

39. Dallmann, A.; Dehmel, L.; Peters, T.; Mügge, C.; Griesinger, C.; Tuma, J.; Ernsting, N. P. *Angew. Chem. Int. Ed.* **2010,** *49* (34), 5989–5992.

40. Greco, N. J.; Tor, Y. *Tetrahedron* **2007,** *63* (17), 3515–3527.

41. Greco, N. J.; Tor, Y. *Nat. Protocols* **2007,** *2* (2), 305–316.

42. Sinkeldam, R. W.; Greco, N. J.; Tor, Y. *ChemBioChem*, **2008**, *9*, 706–709.

43. Greco, N. J.; Tor, Y. *J. Am. Chem. Soc.* **2005,** *127* (31), 10784–10785.

44. Greco, N. J.; Sinkeldam, R. W.; Tor, Y. *Org. Lett.*, **2009**, *11* (5), 1115–1118.

45. Srivatsan, S. G.; Weizman, H.; Tor, Y. *Org. Biomol. Chem.* **2008,** *6* (8), 1334–1338.

46. Srivatsan, S. G.; Greco, N. J.; Tor, Y. *Angew. Chem., Int. Ed.* **2008,** *47* (35), 6661–6665.

47. Shin, D.; Sinkeldam, R. W.; Tor, Y. Emissive RNA Alphabet. *J. Am. Chem. Soc.* **2011,** *133* (38), 14912–14915.

48. McCoy, L. S.; Shin, D.; Tor, Y. *J. Am. Chem. Soc.* **2014,** *136* (43), 15176–15184.

49. Li, Y.; Fin, A.; McCoy, L. S.; Tor, Y. *Angew. Chem. Int. Ed.* **2017,** *56,* 1303–1307.

50. Sinkeldam, R. W.; McCoy, L. S.; Shin, D.; Tor, Y. *Angew. Chem., Int. Ed.* **2013,** *52* (52), 14026–14030.

51. Vranken, C.; Fin, A.; Tufar, P.; Hofkens, J.; Burkart, M. D.; Tor, Y. *Org. Biomol. Chem.* **2016,** *14* (26), 6189–6192.

52. Rovira, A. R.; Fin, A.; Tor, Y. *J. Am. Chem. Soc.* **2015,** *137*, 14602–14605.

53. Rovira, A. R.; Fin, A.; Tor, Y. *Chem. Sci.* **2017,** *8*, 2983–2993.

Chapter 2

Development of a Fluorescent Ribonucleoside Alphabet

2.1 Introduction

Fluorescent ribonucleosides, which have been developed to address the lack of emission in native ribonucleosides, have been used as probes for RNA structural analysis, biophysical analysis, and discovery assays.[1–9] Some desirable characteristics of fluorescent ribonucleosides include red shifted emission, structural similarity, high brightness, and sensitivity to the surrounding environment. To improve isomorphicity researchers have tried to minimize changes to the Watson-Crick pairing face and in more recent years even the Hoogsteen pairing face.[10–19] Efforts to improve isomorphicity have in the past had the side effect of decreased quantum yield and blue shifted emission.[15,16] This suggests that diminishing isomorphicity might reverse this phenomenon. As many analogues are ultimately intended for enzymatic analyses, a better understanding of the tolerable limit of structural perturbation for enzymes would be helpful for designing even more highly tuned probes in the future.

Our lab has previously published two isomorphic and "isofunctional" alphabets based on the thieno[3,4-*d*]pyrimidine and isothiazole[4,3-d]pyrimidine scaffolds.[15,16] The reinstallation of the "N7" (in reference to a purine numbering system) in the isothiazolo-based alphabet resulted in improved isofunctionality, when tested with a variety of different enzymes, but dramatically lowered the quantum yield and for the most part blue shifted the emission.[15,16] We hypothesized that if increasing isomorphicity with the reinstallation of a polar "N7" moiety diminished

photophysical characteristics, then decreasing isomorphicity with the introduction of a nonpolar moiety such as a methyl group might improve those desired characteristics. This would have the dual benefit of allowing us to probe enzymes tolerance for structural perturbations at the "N7" position and thereby expand what structures might be considered isofunctional.

Herein, we set out to synthesize a ribonucleoside analogue alphabet based off of a methylthieno[3,4-*d*]pyrimidine core. Our hope being that they would improve some photophysical characteristics from previous generations and provide insight into how far an analogue could deviate from the native structure while still being recognized as a substrate by enzymes. This is facilitated by synthesizing a key precursor and building the U, C, A, and G analogues from there. We then analyze the extinction coefficient, quantum yield, Stokes shift, and sensitivity to polarity of each analogue and compare to previous alphabets. Finally, we observe the reactions between various enzymes and the corresponding analogue to see how the structural perturbation on the Hoogsteen face is tolerated.

2.2 Synthesis of a Methyl Thiophene Precursor

Synthesis of the methylthieno[3,4-*d*]pyrimidine based alphabet began with the design of a methylthiophene precursor that could be used as a starting point for the synthesis of each nucleoside (Fig. 2.1). Dongwon et. al. had previously used a similar, commercially available, and relatively cheap thiophene precursor to synthesize all four ribonucleoside analogues (Fig. 2.1).[15] The thiophene precursor contained a methyl ester and an amine at the 2 and 3 positions providing a structural basis for constructing a pyrimidine ring. Ideally, the methylthiophene precursor would contain the same structural elements so that reactions used to build the four nucleobases of the thiophene alphabet could be applied.

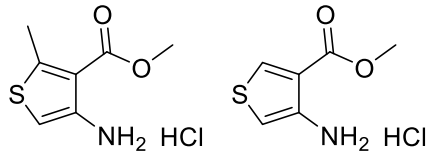

Methylthiophene Thiophene

Figure 2.1 Structures of a Methylthiophene and Thiophene Based Nucleoside Precursor

The ester moiety was not the only option however. An imidazole precursor with a cyano-group attached at the same position as the ester moiety has been previously reported (Fig. 2.2).[20] This was kept in mind as a potential alternative structure to pursue, particularly for the adenosine analogue, but ultimately decided against.

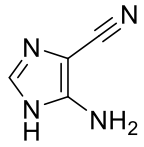

Imidazole Precursor

Figure 2.2 Structure of an Imidazole Based Nucleoside Precursor

Thiophene synthesis has been thoroughly explored and reported, but this is not true for methylthiophenes. The synthetic pathways of the thiophene precursor used to build thieno[3,4-*d*]pyrimidine based nucleosides was reported in four steps (Scheme 2.1).[21] Synthesis begins with a Michael addition between methyl thioglycolate and methyl acrylate. The resulting thioether is cyclized using a Claisen condensation protocol and sodium hydride as the base. The ketone on the cyclized thioether is then converted to an oxime by treatment with hydroxylamine hydrochloride in the presence of mild base and heat. The oxime is then aromatized by treatment with hydrochloric acid. Only one step, the cyclization, required column chromatography making the route fairly attractive.[21]

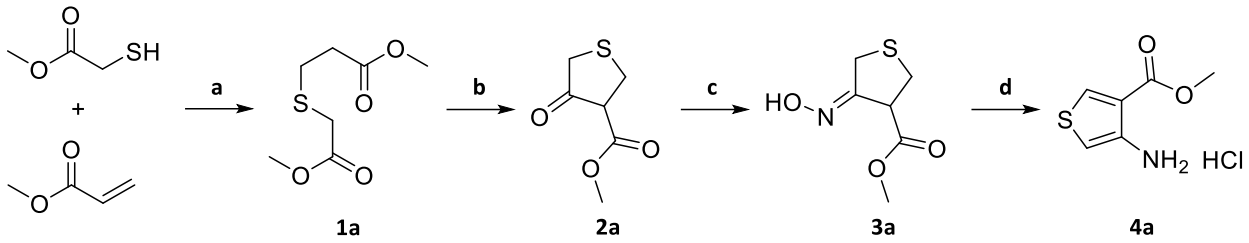

Scheme 2.1 Synthetic Route to the Thiophene Precursor. [a]Reagents and Conditions: (a) Piperidine, 50ºC, 2 h, 99%; (b) NaH (60% in mineral oil), THF, 70ºC, overnight, 35%; (c) **1**, $BaCO_3$, hydroxylamine hydrochloride, MeOH, 70ºC, overnight, 98%; (d) 2M HCl in OEt_2, OEt_2, MeOH, RT, 24 h, 91%.

Upon review of the synthetic pathway, we hypothesized that the addition of a methyl group would be possible because the moiety would be relatively inert. We thus substituted methyl crotonate for methyl thioglycolate and proceeded down the same route (Scheme 2.2). The Michael addition resulted in full conversion, but the Claisen condensation gave a lower yield. The conversion of the ketone to an oxime also appeared to be comparable to the original route, but the aromatization gave a slightly lower yield. It was also observed that the methylthiophene was light and acid sensitive and thus needed to be placed under vacuum and wrapped in aluminum foil after isolating it as a solid.

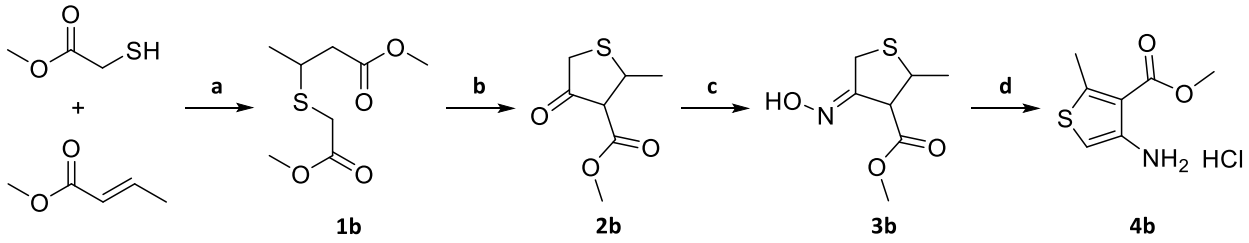

Scheme 2.2 Synthetic Route to the Methylthiophene Precursor. [a]Reagents and Conditions: (a) Piperidine, 50ºC, 2 h; (b) NaH (60% in mineral oil), THF, 70ºC, overnight, 19% over two steps; (c) **1**, $BaCO_3$, hydroxylamine hydrochloride, MeOH, 70ºC, overnight; (d) 2M HCl in OEt_2, Oet_2, MeOH, RT, 24 h, 78% over two steps.

2.3 Synthesis of a Guanosine Analogue

Synthesis of the guanosine analogue, ^{mth}G, began with the cyclization of the six-member ring. The methylthiophene precursor **4b** was treated with chloroformamidine and heat to yield

the nucleobase, **5**. The exocyclic amine on the nucleobase was then protected with a DMF-protecting group by treatment with dimethylformamide dimethyl acetal giving **6**. The protected nucleobase, 6, was then glycosylated with a benzoate protected ribose, β-D-ribofuranose 1-acetate 2,4,5-tribenzoate, in the presence of tin (IV) chloride yielding the protected nucleoside, **7**. **7** was then deprotected by placing it in methanolic ammonia and refluxing overnight. This gave the nucleoside analogue ^{mth}G. All steps followed the conditions of those reported for the corresponding thieno[3,4-*d*]pyrimidine based guanosine analogue, thG. All reactions were successful on the first attempt.

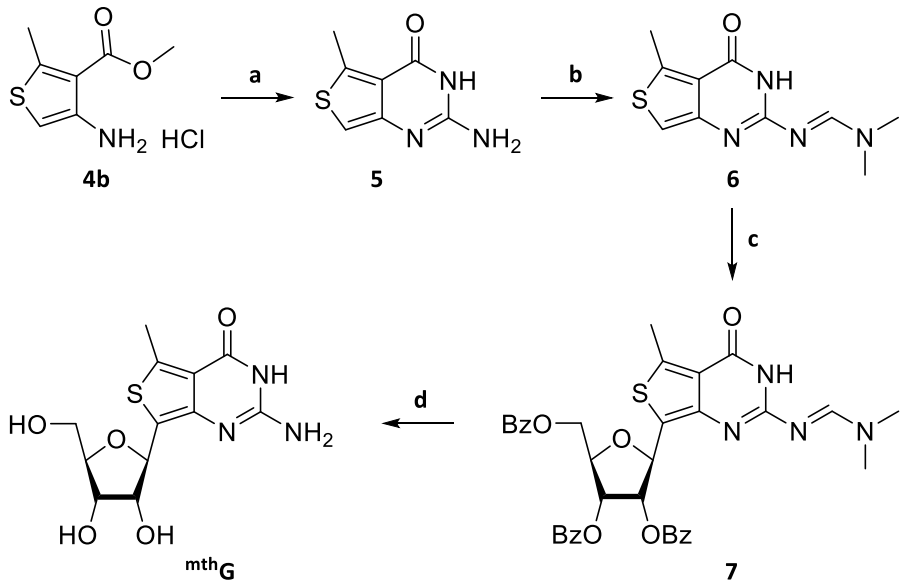

Scheme 2.3 Synthetic Route to ^{mth}G. Reagents and Conditions: (a) Chloroformamidine hydrochloride, $DMSO_2$, 125ºC, 2 h, 99%. (b) Dimethylformamide dimethyl acetal, DMF, RT, overnight, 95%. (c) β-D-ribofuranose 1-acetate 2,4,5-tribenzoate, tin (IV) chloride, $MeNO_2$, 65ºC, overnight, 25%. (d) Ammonia saturated MeOH, 65ºC, overnight, 63%.

The first cyclization and protection reactions gave excellent yields of 99% and 95%, respectively. However, the glycosylation gave a 25% yield, falling short of the 64% reported for the thiophene route. Likewise, the deprotection yield of 63% was lower than that reported for thG. ^{mth}G was also found to degrade slightly when left in the presence of light as seen by thin layer chromatography in which multiple new faint fluorescent bands would appear. These

results and observations suggest that ^{mth}G needs to be handled carefully and kept out of light and in a freezer.

2.4 Synthesis of Adenosine and Inosine Analogues

Synthesis of the adenosine analogue started with the same approach as that used for the thieno[3,4-*d*]pyrimidine based adenosine analogue (Scheme 2.4). The first step was to install a formal protecting group on the exocyclic amine of the methylthiophene precursor. This was done by treating **4b** with sodium acetate and formic acid. The protection was comparable in yield (80%) to that reported for the thiophene precursor (84%). The second step was to glycoscylate **8** with the same ribose sugar as used for the ^{mth}G route. The reaction was performed in nitromethane with tin (IV) chloride as the activator. To our surprise, the methylthiophene precursor glycosylated better (48%) than the thiophene precursor (32%). The next step, cyclization of the six-member ring, was performed by first removing the formal protection with acid treatment. After drying overnight, the intermediate was treated with formamidine acetate to yield **10**, the protected inosine analogue.

In our attempts in the first route (Scheme 2.4) the isomers of **10** were not separated but pushed forwards in the hope that they would be easier to separate at a later step. The reported yields of the two isomers came from later attempts, but the total yield remained the same. Following the reported thA pathway, **10** was treated with P_2S_5 and heat. The yield was surprisingly low at 14% and it only appeared to produce one isomer. However, we took the product, **11**, and pushed forward by treating with methanolic ammonia and refluxing overnight. This gave ^{mth}A in modest yield of 57%. Upon obtaining a crystal of the ^{mth}A, we found out from the crystal structure that it was in fact the alpha configuration. This was a major setback and indicated a new approach would be needed since the sulfonylation reaction gave such poor results.

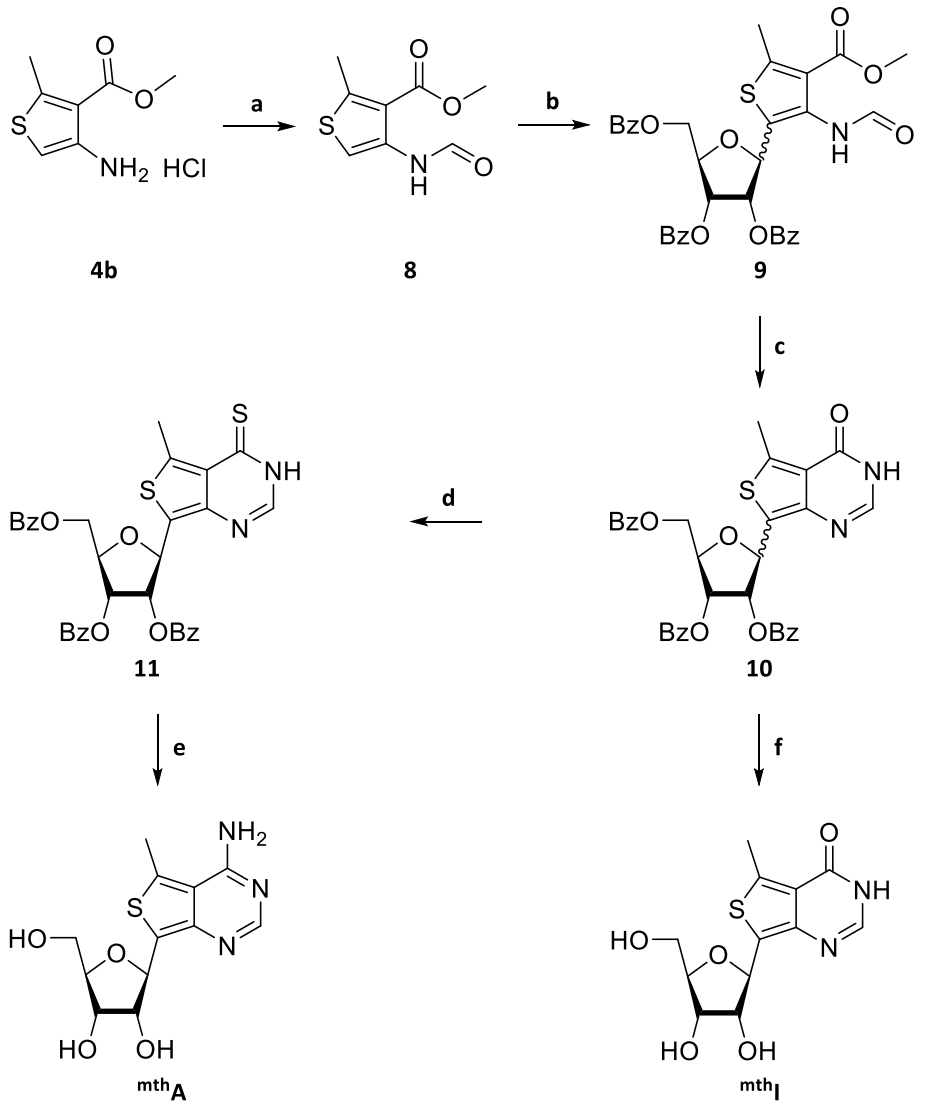

Scheme 2.4 First Attempted Synthetic Route to ^{mth}A. Reagents and Conditions: (a) NaOAc, formic acid (90%), 60ºC, 2 h, 80%. (b) β-D-ribofuranose 1-acetate 2,4,5-tribenzoate, tin (IV) chloride, $MeNO_2$, 60ºC, overnight, 48%. (c) i) 15% HCl (aq.) in MeOH, $CHCl_3$, RT, 2 h; ii) formamidine acetate, EtOH, 90ºC, 4 h, β-52%, α-18% over two steps. (d) P_2S_5, Pyridine, 115ºC, 2 h, β-0%, α-14%. (e) methanolic ammonia, 65ºC, overnight, α-57%. (f) NH_4OH (aq. saturated), methylamine (aq. saturated), RT, overnight, β-74%.

We decided to rethink the synthetic pathway and instead pursued the synthesis and subsequent glycosylation of the ^{mth}I nucleobase, **12** (Scheme 2.5). The thinking was that this new route would lower the number of total steps and potentially give higher yields particularly on the six-member ring cyclization. Synthesis began by cyclizing **4b** using formamidine acetate. Initial results were quite promising as the yield was 89% for the first step in the pathway. The

glycosylation of **12** with the ribose sugar used in previous routes at first glance was successful giving a nice yield of 75%. However, a preliminary crystal structure of what was thought to be compound **10** revealed that the product was in fact glycosylated at the "N3" (in reference to the purine numbering system) position instead of the desired carbon (Fig. 2.3).

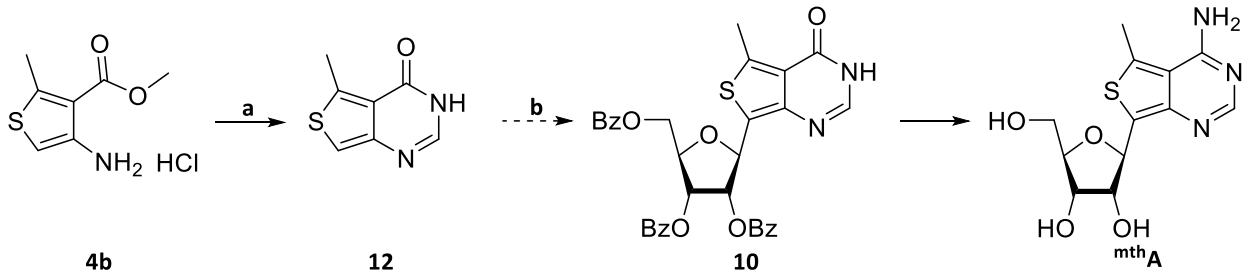

Scheme 2.5 Proposed Alternative Synthetic Route to ^{mth}A. Reagents and Conditions: (a) formamidine acetate, EtOH, 90ºC, 4 h, 89%. (b) β-D-ribofuranose 1-acetate 2,4,5-tribenzoate, tin (IV) chloride, $MeNO_2$, 60ºC, overnight, failed.

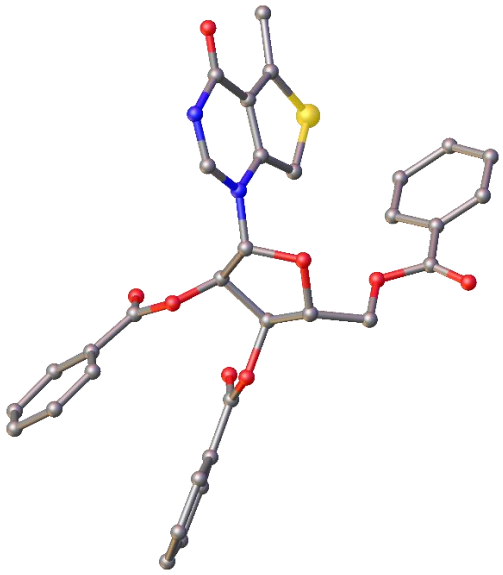

Figure 2.3 Preliminary Crystal Structure of N-glycosylated ^{mth}I Nucleobase

As this was a significant setback, we decided to rethink the synthetic route again. We reapproached the original route but tried a new method for the activation of the carbonyl in compound **10**. Compound **10** was treated with BOP in the presence of DBU and then ammonia was bubbled in to displace the activated carbonyl. The reaction was evaporated to a crude

residue and then placed in methanolic ammonia and heated at 65ºC overnight. This gave the desired ^{mth}A in the beta conformation in 43% yield. In a roundabout way, the original route ended up being mostly successful, but it required a different activation step. To also obtain ^{mth}I, some of each isomer of compound **10** was placed in a 50:50 ratio of saturated ammonium hydroxide (aq.) and saturated methylamine (aq.) overnight (Scheme 2.7).

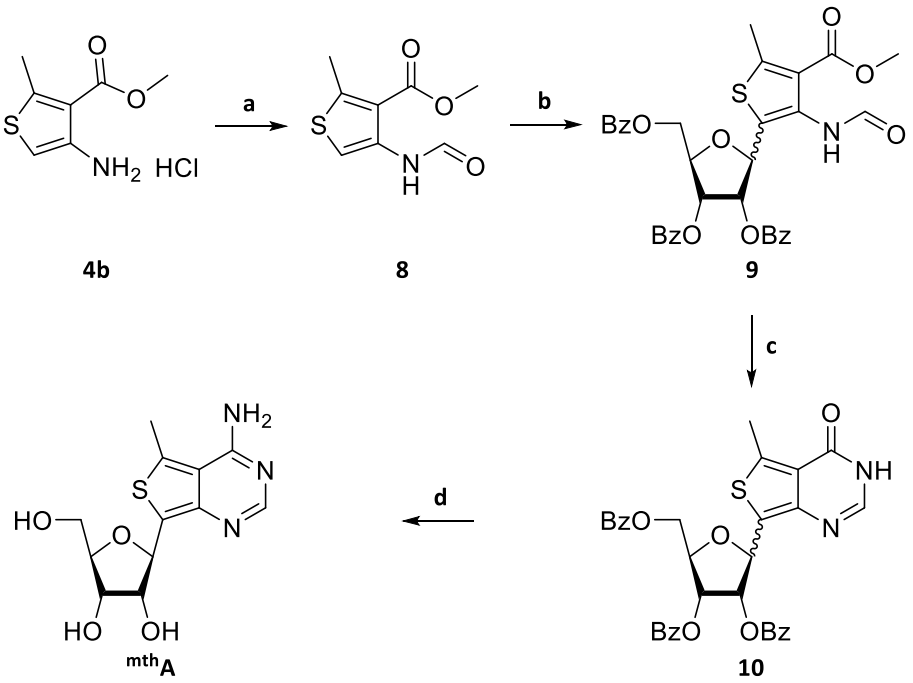

Scheme 2.6 Final Synthetic Route to ^{mth}A. Reagents and Conditions: (a) NaOAc, formic acid (90%), 60ºC, 2 h, 80%. (b) β-D-ribofuranose 1-acetate 2,4,5-tribenzoate, tin (IV) chloride, $MeNO_2$, 60ºC, overnight, 48%. (c) i) 15% HCl (aq.) in MeOH, $CHCl_3$, RT, 2 h; ii) formamidine acetate, EtOH, 90ºC, 4 h, β-52%, α-18% over two steps. (d) i) BOP, DBU, NH_3, DMF, RT, 1 h; ii) methanolic ammonia, 65ºC, overnight, 43% over two steps.

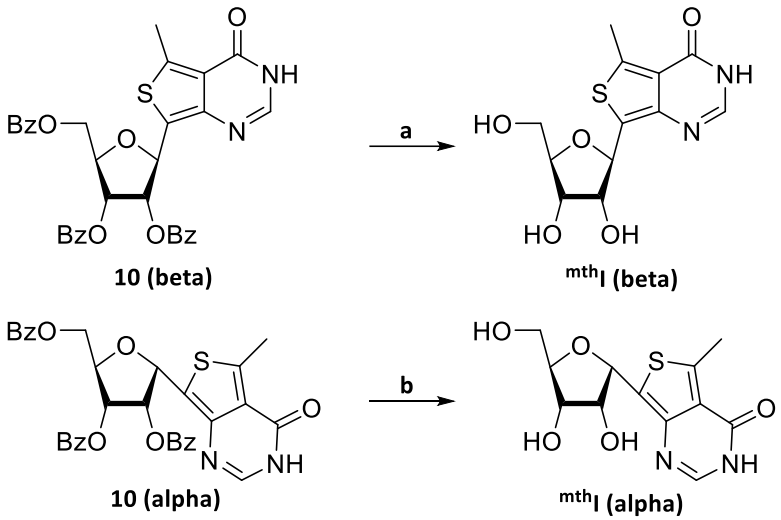

Scheme 2.7 Synthetic Route to ^{mth}I. Reagents and Conditions: (a) NH_4OH (aq. saturated), methylamine (aq. saturated), RT, overnight, 74%. (b) NH_4OH (aq. saturated), methylamine (aq. saturated), RT, overnight, 43%.

2.5 Synthesis of Cytidine and Uridine Analogues

Synthesis of ^{mth}C and ^{mth}U initially followed the thieno[3,4-*d*]pyrimidine C and U analogue route. The methylthiophene precursor was treated with potassium cyanate in acetic acid (30%) to form the urea, **13**, in 94% yield. The urea was exposed to the strong base sodium methoxide to cyclize the six-member ring giving the ^{mth}U nucleobase, **14**, in 91% yield. The nucleobase was then glycosylated by activation with *N,O*-bis(trimethylsilyl)acetamide and subsequent addition of TMS triflate and β-D-ribofuranose 1-acetate 2,4,5-tribenzoate. The resulting benzoate protected ^{mth}U, **15**, was then divided and deprotected to give ^{mth}U or pushed forward towards ^{mth}C. Compound **15** was deprotected with a 50:50 mixture of saturated NH_4OH (aq.) and saturated methylamine (aq.) to give ^{mth}U in 85% yield (Scheme 2.8).

In converted **15** to ^{mth}C we initially attempted the same activation as that used to form thC. Treatment of **15** with 2,4,6-triisopropylbenzenesulfonyl chloride showed no reaction on thin layer chromatography even when used in large excess or in excess heat, base (TEA), or catalyst (DMAP). We therefore tested another reaction. 1,2,4-triazole was reacted with phosphoryl (V) chloride in pyridine and the resulting solution used to activate the carbonyl on

15. After activation, seen by consumption of starting material on thin layer chromatography, the activated intermediate was treated with saturated ammonium hydroxide for a short period. This gave the benzoate protected ^{mth}C, **16**, in modest yield of 37%. Compound **16** was then deprotected with methanolic ammonia and heat to give ^{mth}C in 75% yield (Scheme 2.8).

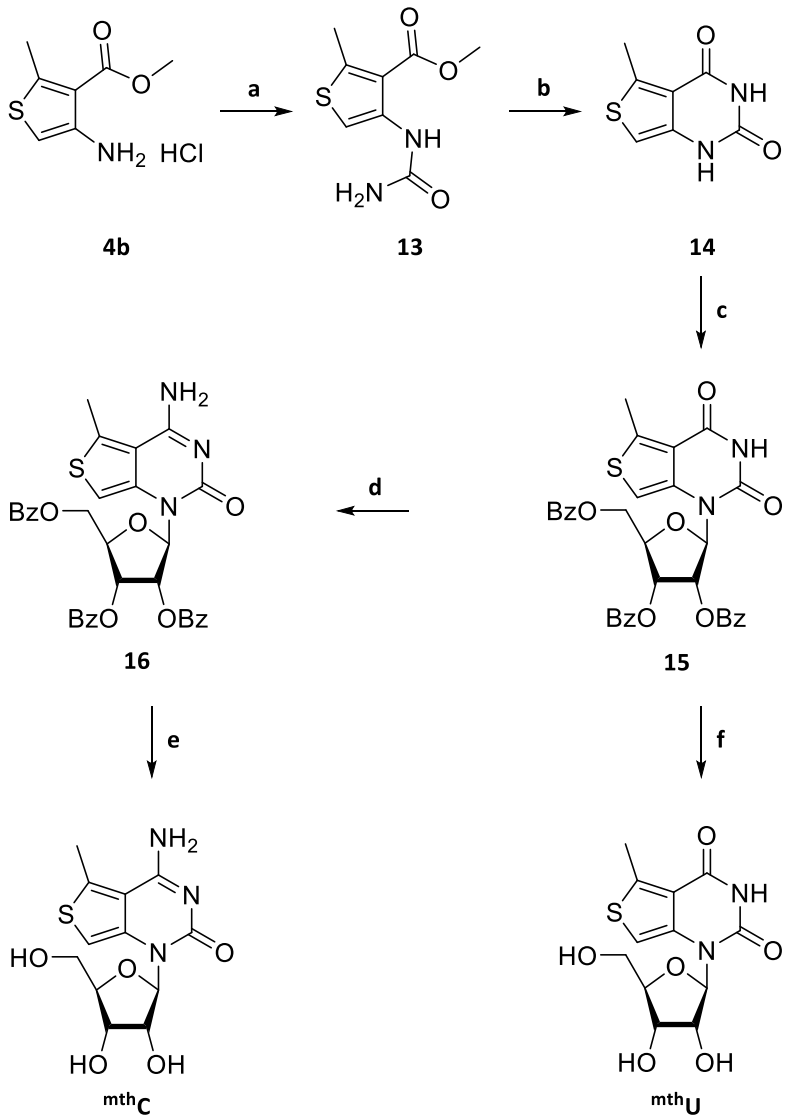

Scheme 2.8 Synthetic Route to ^{mth}C and ^{mth}U. Reagents and Conditions: (a) Potassium cyanate, acetic acid (30%), RT, overnight, 94%. (b) Sodium methoxide, MeOH, RT, 15 h, 91%. (c) *N,O*-bis(trimethylsilyl)acetamide, β-D-ribofuranose 1-acetate 2,4,5-tribenzoate, trimethylsilyl trifluoromethanesulfonate, ACN, 85ºC, 3 h, 85%. (d) i) Phosphoryl (V) Chloride, 1,2,4-triazole, pyridine, RT, 1 h; ii) Saturated ammonium hydroxide, RT, 3 h, 37%. (e) Ammonia saturated MeOH, 65ºC, overnight, 75%. (f) NH_4OH (aq. saturated), methylamine (aq. saturated), RT, overnight, 85%.

2.6 Photophysical Characterization of the Ribonucleoside Alphabet

Once all methylthieno[3,4-d]pyrimidine based analogues had been obtained, we sought to analyze their photophysical properties. Initially we sought to determine the extinction coefficients and quantum yields. Absorption spectra were measured at multiple concentrations and the values plotted against concentration to determine the slope of the resulting line. The extinction coefficients determined in this manner are contained in Table 2.1. Quantum yields were next obtained by taking a sample with an absorbance under 0.07, exciting at the respective λ_{max}, and recording the emission at each wavelength. The quantum yield was calculated for each analogue using equation 2.1 and quinine (^{mth}A) or 2-aminopurine (all others) as a standard.

$$\Phi = \Phi_{STD} \frac{I}{I_{STD}} \frac{OD_{STD}}{OD} \frac{n^2}{n_{STD}^2}$$

Equation 2.1 Relative Quantum Yield

Φ is the quantum yield, Φ_{STD} is the quantum yield, I is the integrated area of the emission band, I is the integrated area of the emission band of the standard, OD is the optical density at the exciting wavelength, OD_{STD} is the optical density at the exciting wavelength of the standard, n is the refractive index of the solvent the sample is in, n_{STD} is the refractive index of the solvent the standard is in.

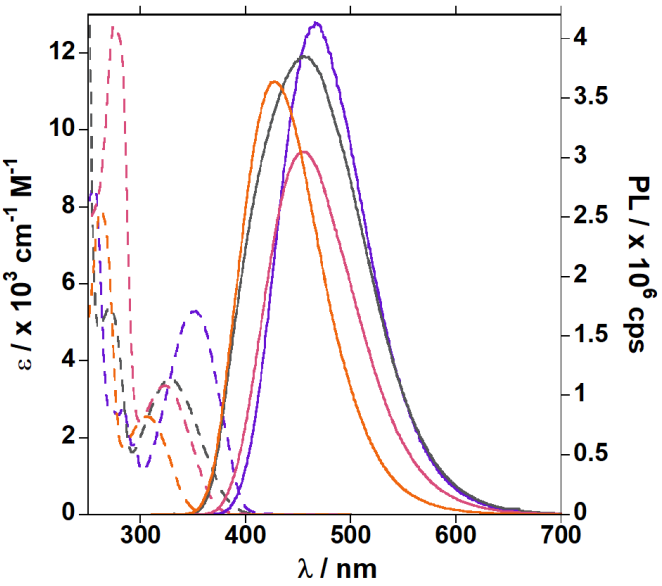

Figure 2.4 Absorption (dashed) and Emission (solid) Spectra of ^{mth}A (purple), ^{mth}G (grey), ^{mth}C (pink), and ^{mth}U (orange).

The sensitivity to polarity of each ribonucleoside analogue was examined. Mixtures of water and 0, 20%, 40%, 60%, 80%, and 100% dioxane were prepared. An aliquot of each analogue was added to a mixture and the absorption and emission spectra (exciting at the λ_{max}) were recorded (Figs. 2.5–2.9, 2.12). Reichardt's dye was added to separate water and dioxane mixtures in parallel and the λ_{max} recorded.[22] The $E_T(30)$ value of each water and dioxane mixture was calculated from those λ_{max} values according to Equation 2.2 (Table 2.2). The Stokes Shift of each ribonucleoside analogue at each ratio of water to dioxane was calculated from the emission and absorption spectra. Stokes Shifts were then plotted against $E_T(30)$ values and the slope of a linear gave the sensitivity to polarity (Fig. 2.10).

$$E_T(30) = \frac{28591}{\lambda_{abs}^{max}}$$

Equation 2.2 $E_T(30)$ Equation

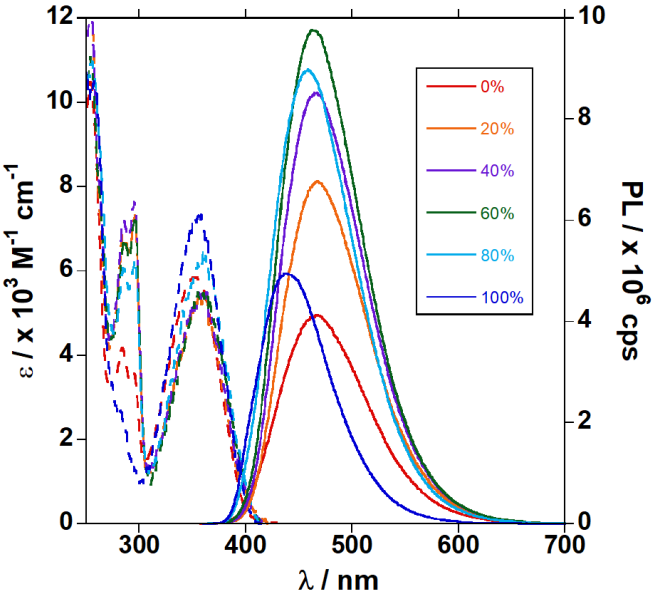

Figure 2.5 [mth]A Absorption and Emission Spectra in Various Mixtures of Water and Dioxane. Absorption (dashed lines) and emission (solid lines) spectra of [mth]A in water (red), dioxane (blue), and mixtures of 20% (orange), 40% (purple), 60% (green), and 80% (light blue) v/v dioxane in water

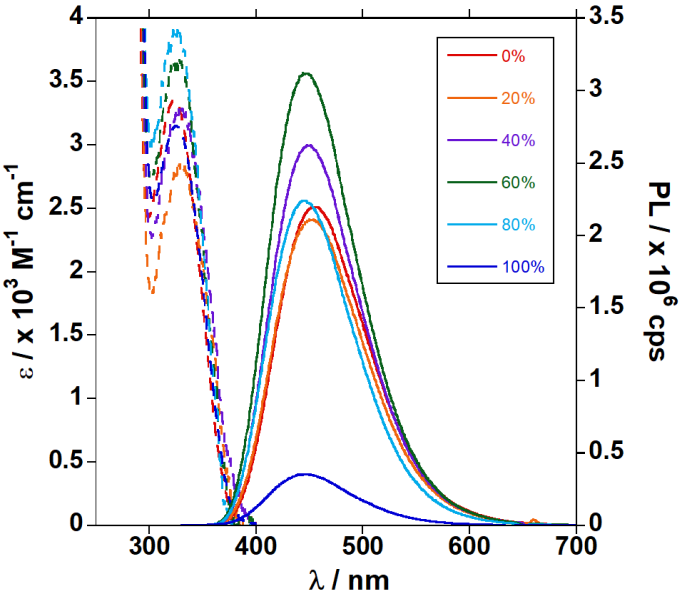

Figure 2.6 [mth]C Absorption and Emission Spectra in Various Mixtures of Water and Dioxane. Absorption (dashed lines) and emission (solid lines) spectra of [mth]C in water (red), dioxane (blue), and mixtures of 20% (orange), 40% (purple), 60% (green), and 80% (light blue) v/v% dioxane in water

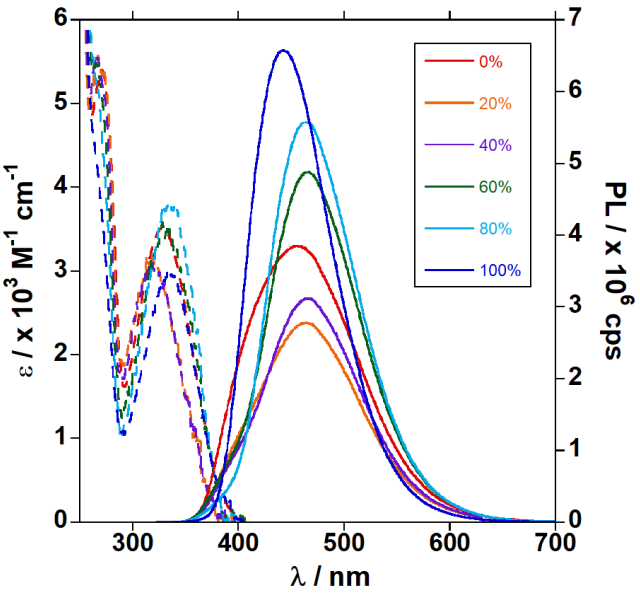

Figure 2.7 ^{mth}G Absorption and Emission Spectra in Various Mixtures of Water and Dioxane. Absorption (dashed lines) and emission (solid lines) spectra of ^{mth}G in water (red), dioxane (blue), and mixtures of 20% (orange), 40% (purple), 60% (green), and 80% (light blue) v/v dioxane in water

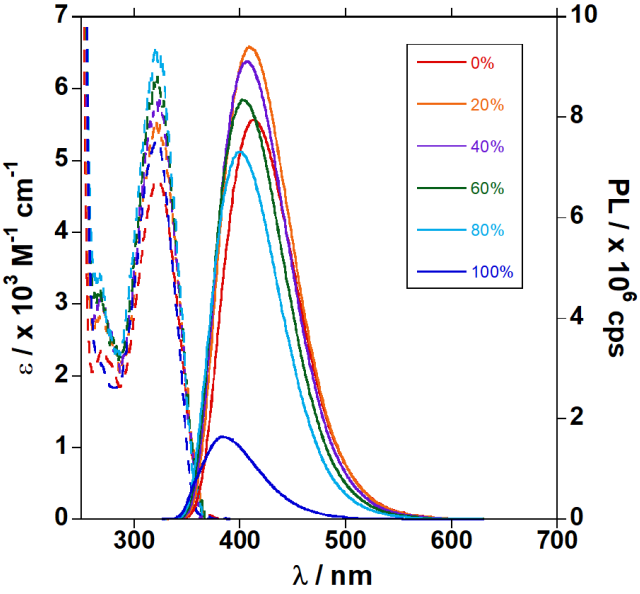

Figure 2.8 ^{mth}I Absorption and Emission Spectra in Various Mixtures of Water and Dioxane. Absorption (dashed lines) and emission (solid lines) spectra of ^{mth}I in water (red), dioxane (blue), and mixtures of 20% (orange), 40% (purple), 60% (green), and 80% (light blue) v/v dioxane in water

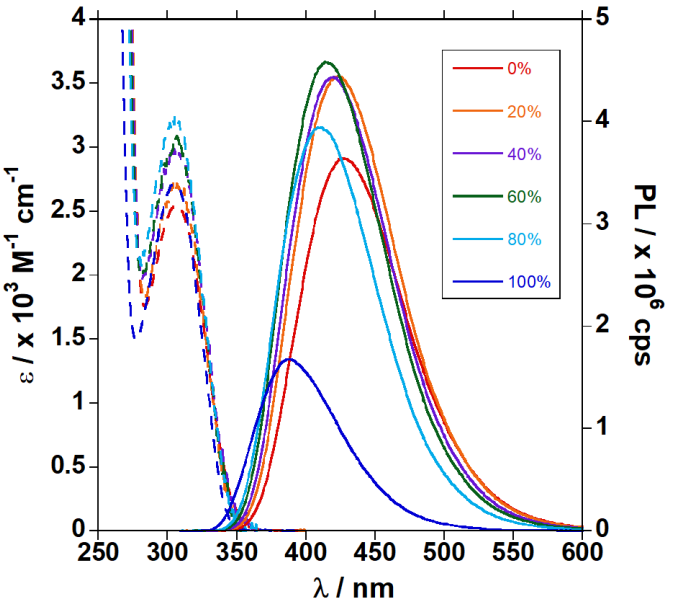

Figure 2.9 ^{mth}U Absorption and Emission Spectra in Various Mixtures of Water and Dioxane. Absorption (dashed lines) and emission (solid lines) spectra of ^{mth}U in water (red), dioxane (blue), and mixtures of 20% (orange), 40% (purple), 60% (green), and 80% (light blue) v/v dioxane in water

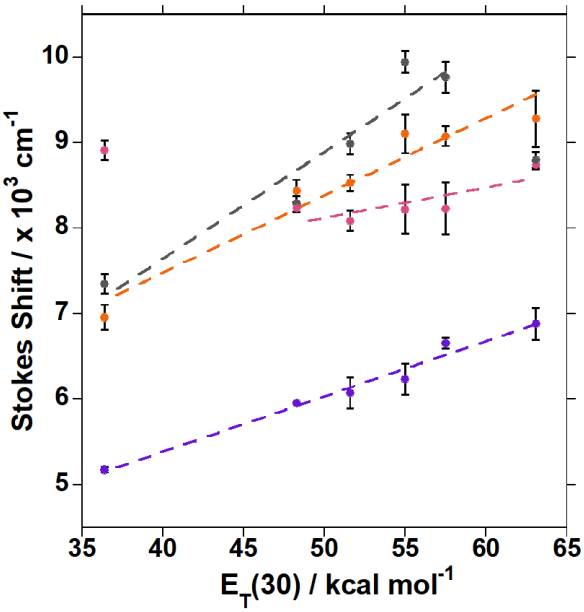

Figure 2.10 Methylthieno[3,4-*d*]pyrimidine Based Alphabet Sensitivity to Polarity. Stokes shift correlation versus solvent polarity ($E_T(30)$) of water/dioxane mixtures for ^{mth}A (purple), ^{mth}C (pink), ^{mth}G (grey), ^{mth}U (orange)

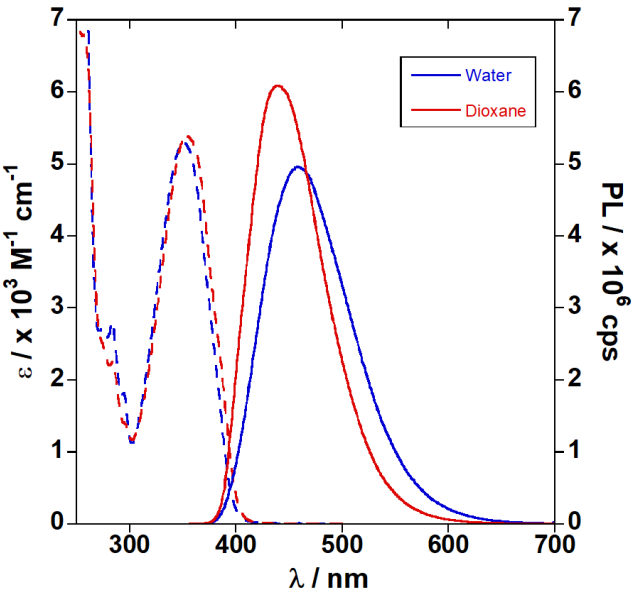

Figure 2.11 [mth]A Alpha Emission (solid) and Absorption (dashed) Spectra in Water (blue) and Dioxane (red)

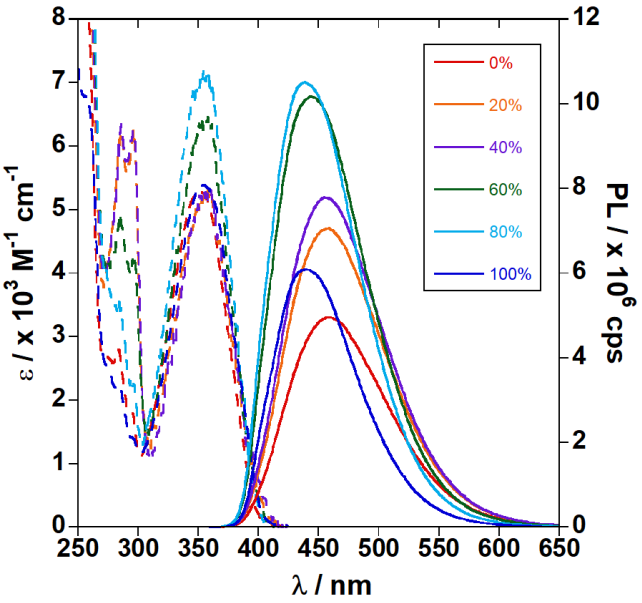

Figure 2.12 [mth]A alpha Absorption and Emission Spectra in Various Mixtures of Water and Dioxane. Absorption (dashed lines) and emission (solid lines) spectra of [mth]U in water (red), dioxane (blue), and mixtures of 20% (orange), 40% (purple), 60% (green), and 80% (light blue) v/v dioxane in water

Each of the methylthieno[3,4-d]pyrimidine based analogues displayed absorption bands above 300 nm, significantly red shifted compared to the native ribonucleosides. [mth]U has an absorption maximum at 306 nm in water, about the same as that of [th]U (304 nm) and slightly

lower than ^{tz}U (312 nm). The extinction coefficient in water (2550 M^{-1} cm^{-1}) is smaller than thU (3160 M^{-1} cm^{-1}) and ^{tz}U (5170 M^{-1} cm^{-1}), but the quantum yield at 0.29 was much improved upon compared to ^{tz}U (0.01). The emission maxima of ^{mth}U (427 nm) was significantly red shifted relative to thU (409 nm) and ^{tz}U (392 nm).[15,16]

^{mth}C displayed an absorption maximum at 323 nm in water that fell right in the middle of thC (320 nm) and ^{tz}C (325 nm). The extinction coefficient in water (3350 M^{-1} cm^{-1}) is also smaller than the thC (4530 M^{-1} cm^{-1}) and ^{tz}C (5450 M^{-1} cm^{-1}), but the quantum yield at 0.24 was again much improved upon compared to ^{tz}C (0.05). As with ^{mth}U relative to thU and ^{tz}U, the emission maxima of ^{mth}C (455 nm) was remarkably red shifted relative to thC (429 nm) and ^{tz}C (411 nm).[15,16]

^{mth}G displayed an absorption maximum at 327 nm in water, somewhat higher than thG (321 nm) and somewhat lower than ^{tz}C (333 nm). The extinction coefficient in water (3510 M^{-1} cm^{-1}) is also smaller than the thG (4150 M^{-1} cm^{-1}) and ^{tz}G (4870 M^{-1} cm^{-1}), but the quantum yield at 0.42 was yet again much improved upon compared to ^{tz}G (0.25) and approaching that of thG (0.46). The emission maxima of ^{mth}G (465 nm) was slightly red shifted relative to thG (453 nm) and ^{tz}G (459 nm). The emission spectrum also indicated that ^{mth}G, like the thG, exists in two tautomeric forms as shown by the two overlapping emission bands.[15,16]

Finally, ^{mth}A has an absorption maximum at 353 nm in water, which is somewhat higher than thA (341 nm) and ^{tz}A (338 nm). The extinction coefficient in water (5830 M^{-1} cm^{-1}) is smaller than the thA (7440 M^{-1} cm^{-1}) and ^{tz}A (7790 M^{-1} cm^{-1}), but the quantum yield at 0.21 was improved upon compared to ^{tz}A (0.05) and the same as thA (0.21). The emission maxima of ^{mth}A (465 nm) displayed a large red shift relative to thA (420 nm) and ^{tz}A (410 nm).[15,16]

Overall, the methyl moiety at the “N7” position (in reference to the purine numbering system) appeared to cause a significant bathochromic shift in the emission bands of all methylthieno alphabet analogues relative to the thieno and isothiazolo alphabet analogues.

Quantum yields were highly improved compared to the isothiazole derivatives, but somewhat diminished relative to the thieno derivatives.

Table 2.1 Photophysical Properties of Methylthieno[3,4-*d*]pyrimidine Nucleoside Analogues

	Solvent	$\lambda_{abs}(\varepsilon)^a$	$\lambda_{em}(\Phi)^a$	Φε	Stokes Shift[a]	Polarity Sensitivity[b]
^{mth}G	Water	327 (3.5 ± 0.1)	456 (0.42 ± 0.02)	1470	8700 ± 100	130 ± 10
	Dioxane	334 (3.6 ± 0.1)	443 (0.61 ± 0.03)	2200	7200 ± 120	
^{mth}A	Water	353 (5.8 ± 0.1)	467 (0.21 ± 0.01)	1230	6900 ± 180	65 ± 4
	Dioxane	355 (6.2 ± 0.1)	440 (0.23 ± 0.01)	1660	5300 ± 100	
^{mth}U	Water	306 (2.6 ± 0.1)	427 (0.30 ± 0.01)	765	9300 ± 330	90. ± 8
	Dioxane	305 (2.7 ± 0.1)	387 (0.12 ± 0.01)	353	7000 ± 150	
^{mth}C	Water	323 (3.4 ± 0.1)	455 (0.24 ± 0.01)	804	8900 ± 100	36 ± 12
	Dioxane	325 (3.2 ± 0.1)	445 (0.03 ± 0.01)	95	8300 ± 110	
^{mth}I	Water	322 (4.7 ± 0.1)	414 (0.56 ± 0.01)	2660	6900 ± 100	69 ± 6
	Dioxane	322 (5.3 ± 0.1)	382 (0.11 ± 0.01)	580	4900 ± 100	

Table 2.2 $E_T(30)$ Experimental Values for Water and Dioxane Mixtures

Water v/v% In Dioxane	Reported $E_T(30)$ (kcal mol^{-1})	Experimental $E_T(30)$ (kcal mol^{-1})
0	36.4	35.1
20	48.3	47.8
40	51.6	51.8
60	55.0	55.4
80	57.5	58.3
100	63.1	-

2.7 Testing Enzyme Recognition of the Ribonucleoside Alphabet as Substrates

Once we had obtained each ribonucleoside analogue, we wanted to test whether the methyl moiety would be tolerated by enzymes. We first chose bovine adenosine deaminase (ADA) as a representative enzyme because it has been used to compare the isofunctionality of thA and ^{tz}A in the past.[16] We placed adenosine, ^{tz}A, thA, and ^{mth}A in the presence of ADA and monitored the reaction by absorbance and emission (analogues only). The resulting data were plotted against time and first order curve fit to them yielding k_{app} and $t_{1/2}$ values (Fig. 2., Table 2.3). ^{tz}A was found to have the smallest $t_{1/2}$ followed closely by adenosine and then far behind was thA. Interestingly, ^{mth}A was still able to be deaminated, albeit slowly, indicating that ADA could still recognize the adenosine analogue as a substrate even though it had a perturbing methyl moiety at the equivalent of the "N7" position.

We next chose guanine deaminase (GDA) to observe if the methylthieno[3,4-d]pyrimidine based guanine analogue, **5** or $^{mth}G_n$, would be recognized. As with the ADA experiments we tested GDA with the native substrate guanine and the two previous alphabets guanine analogues, $^{tz}G_n$ and $^{th}G_n$, in parallel with $^{mth}G_n$ (Fig. 2., Table 2.3). Similar to findings in the past, $^{tz}G_n$ reacted slightly slower than guanine with GDA and $^{th}G_n$ did not react at all.[23] Further, $^{mth}G_n$ did not react with GDA either. These results were in line with expectations as the GDA binding pocket only has a few points of contact with the substrate as opposed to the ADA binding pocket which has an additional ribose for recognition.

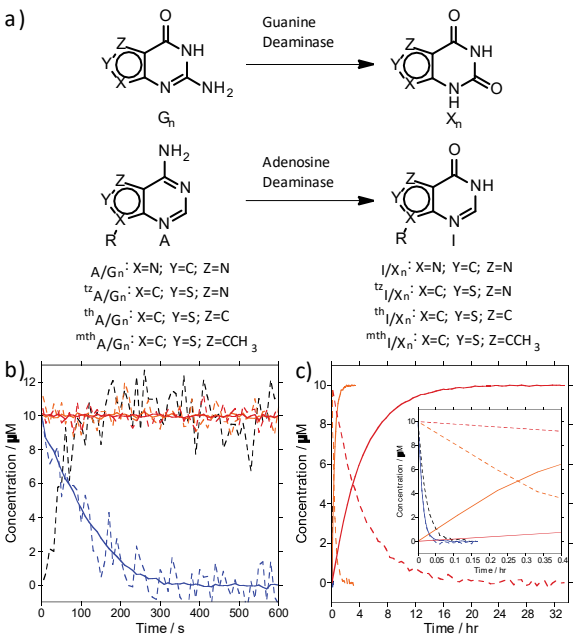

Figure 2.13 GDA and ADA Reactions with Various Substrates. (a) Deamination of G to X, $^{tz}G_n$ to $^{tz}X_n$, $^{th}G_n$ to $^{th}X_n$, and $^{mth}G_n$ to $^{mth}X_n$ by guanine deaminase and deamination of A to I, ^{tz}A to ^{tz}I, ^{th}A to ^{th}I, and ^{mth}A to ^{mth}I by adenosine deaminase. (b) Enzymatic deamination of G to X (black), $^{tz}G_n$ to $^{tz}X_n$ (blue), $^{th}G_n$ to $^{th}X_n$ (orange), and $^{mth}G_n$ to $^{mth}X_n$ (red) with GDA monitored by absorption (dashed) at 270, 355, 355, and 355 nm, respectively, and monitored by emission at 450 nm (upon excitation at 328, 360, and 360 nm, respectively) from 0 to 600 seconds. (c) Enzymatic deamination of A to I (black), ^{tz}A to ^{tz}I (blue), ^{th}A to ^{th}I (orange), and ^{mth}A to ^{mth}I (red) with ADA monitored by absorption (dashed) at 260, 340, 340, and 353 nm, respectively, and monitored by emission at 410, 391, and 420 nm (upon excitation at 322, 318, and 332 nm, respectively), respectively, from 0 to 32 hours or (inset) 0 to 0.4 hours.

Table 2.3 Kinetic Properties of Enzymatic Reactions of A, ^{tz}A, ^{th}A, and ^{mth}A with ADA and G_n, $^{tz}G_n$, $^{th}G_n$, and $^{mth}G_n$ with GDA

		ADA		GDA	
	Alphabet	**k_{app} (x 10^{-4} s^{-1})**	**$t_{1/2}$ (x 10^2 s)**	**k_{app} (x 10^{-2} s^{-1})**	**$t_{1/2}$ (s)**
Abs	**A/G_n**	120 ± 10	0.57±0.01	2.1 ± 0.2	33 ± 4
	^{tz}A/$^{tz}G_n$	220 ± 10	0.32±0.02	0.95 ± 0.16	74 ± 13
	thA/$^{th}G_n$	7.0 ± 0.5	9.8±0.6	No Rxn	No Rxn
	^{mth}A/$^{mth}G_n$	0.64 ± 0.09	110±20	No Rxn	No Rxn
Em	**^{tz}A/$^{tz}G_n$**	220 ± 10	0.31±0.02	0.90 ± 0.02	77 ± 2
	thA/$^{th}G_n$	7.0 ± 0.5	9.6±0.2	No Rxn	No Rxn
	^{mth}A/$^{mth}G_n$	0.64 ± 0.06	110±10	No Rxn	No Rxn

To further demonstrate the retained isofunctionality and utility, ^{mth}G and ^{mth}GTP (Scheme 2.9) were used for in vitro transcription. To compare to previous alphabets and the native ribonucleosides, reactions with guanosine, ^{tz}G, ^{th}G, GTP, ^{tz}GTP, and ^{th}GTP were also run in

parallel. Guanosine, ^{tz}G, thG, and ^{mth}G were added in high concentration (10 mM) to in vitro transcription reactions of a representative RNA strand (Fig. 2.13). The resulting strands initiate with the nucleoside or nucleoside analogue and then elongate with the native NTPs. GTP, ^{tz}GTP, thGTP, and ^{mth}GTP were used as the sole guanosine triphosphate source in in vitro transcription reactions of the same representative RNA (Fig. 2.13). The resulting strands were separated by gel electrophoresis and compared under UV light (Fig. 2.13). All lanes containing reactions with G analogues fluoresced under long wave (365 nm) UV light indicating they were successfully incorporated. Target strands were extracted and MALDI MS analysis confirmed the desired strands were transcribed. This indicated ^{mth}G and ^{mth}GTP were faithful surrogates of guanosine and GTP during transcription both by initiation and elongation.

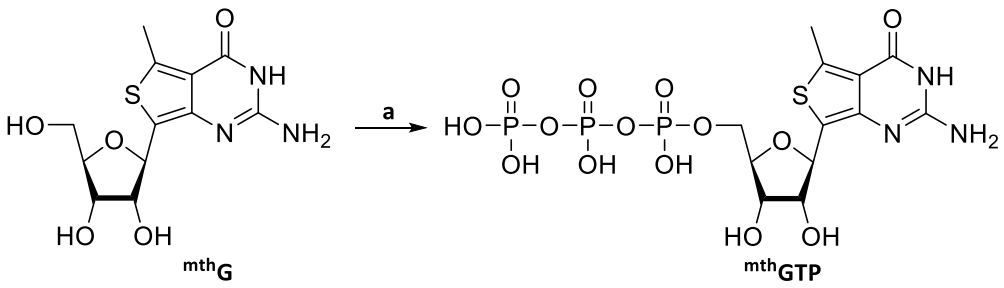

Scheme 2.9 Synthesis of ^{mth}GTP. Reagents and Conditions: (a) i) $POCl_3$, trimethyl phosphate, 0ºC, 2 h; ii) Bistributylammonium pyrophosphate, tributylamine, DMF, 0ºC, 1 h, 5%.

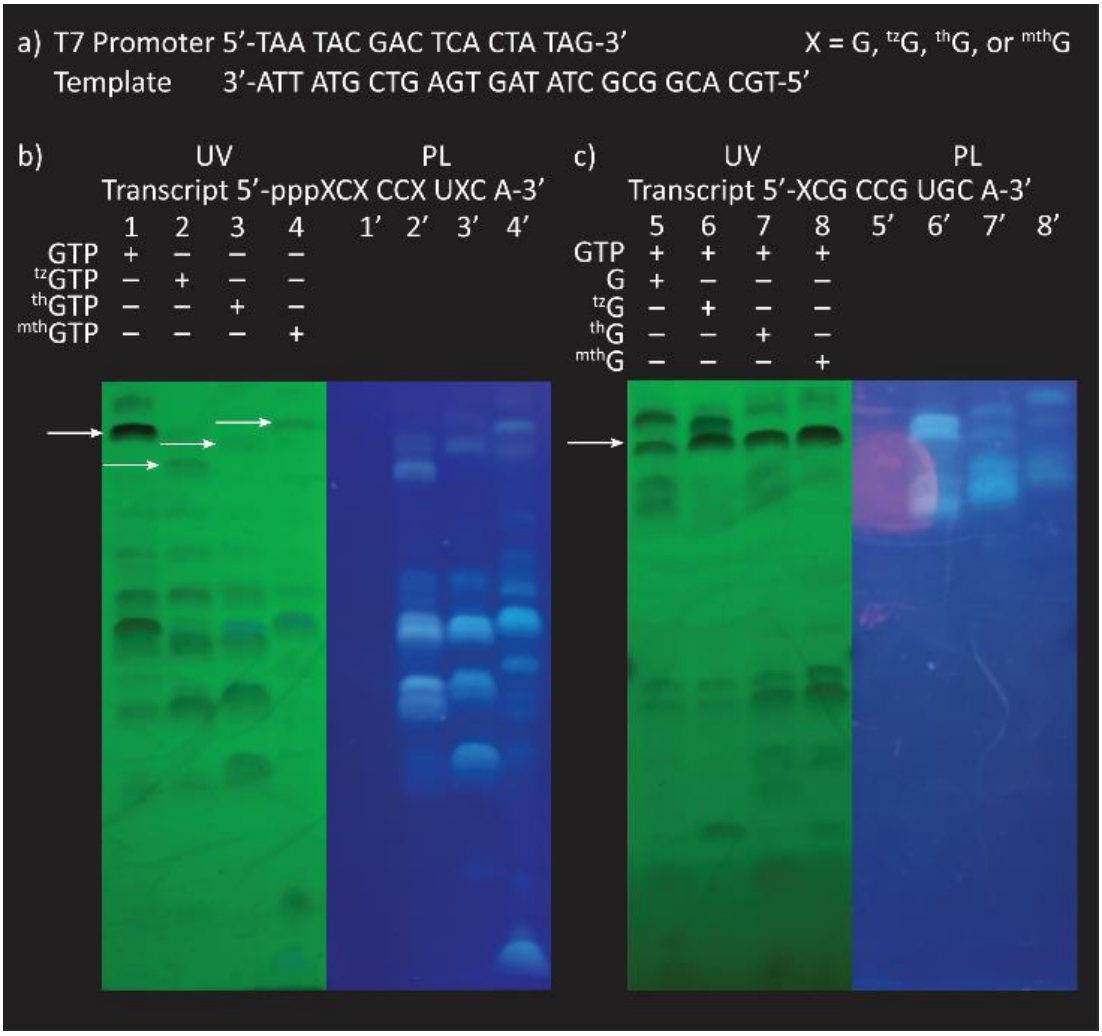

Figure 2.14 Transcription reactions with T7 Promoter and template. a) T7 Promoter and Template strand sequences; b) Gel separation of transcription reaction using template with 2 mM ATP, UTP, and CTP and 2 mM GTP, ^{tz}GTP, thGTP, or ^{mth}GTP; c) Gel separation of transcription reaction using template with 2 mM of all natural NTPs and 10 mM guanosine, ^{tz}G, thG, or ^{mth}G. The white arrows indicate the target transcript of each reaction. UV shadowing was observed at 254 nm, photoluminescence (PL) was observed at 365 nm.

More enzymes including cytidine deaminase (CDA) and human adenosine deaminase 1 (ADA1) and 2 (ADA2) were also investigated using the new and previous alphabets.[24]

Subsequent chapters will further elaborate on those studies findings.

2.8 Analysis of Stereochemistry via NMR Spectra

Each molecule synthesized in pursuit of the methylthieno alphabet was characterized by ^{1}H and ^{13}C NMR in addition to other characterization methods such as crystallography or mass spectrometry. The glycosylation step in the synthetic routes of each analogue can potentially give either of two stereoisomers. However, only one, the beta configuration, is relevant to the biological applications we wished to investigate. We therefore needed to identify whether a beta or an alpha configured nucleoside was obtained from each synthetic pathway. The first approach was to grow a crystal and discern the crystal structure, but this proved difficult for some of the nucleosides. Crystal structures of ^{mth}I in the beta configuration (Fig. 2.13), ^{mth}A in the alpha configuration (Fig. 2.14), ^{mth}U (Fig. 2.15), and the benzoate protected ^{mth}U, **15** (Fig. 2.16), were discerned. Using these structures and comparing ^{1}H and ^{13}C NMR, we were able to confirm the stereochemistry of all analogues except ^{mth}G.

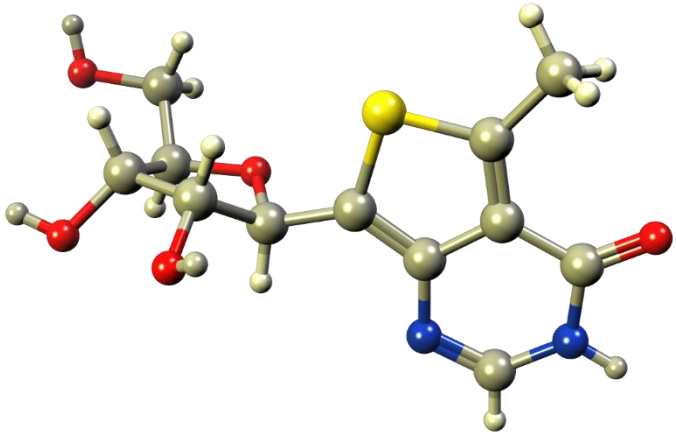

Figure 2.15 Crystal structure of ^{mth}I

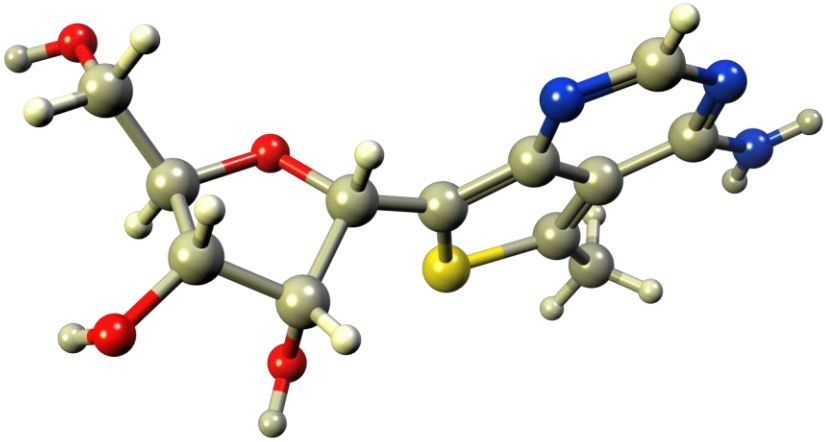

Figure 2.16 Crystal structure of ^{mth}A in the alpha configuration

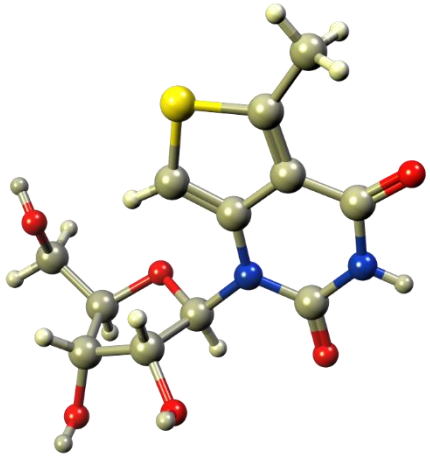

Figure 2.17 Crystal structure of ^{mth}U

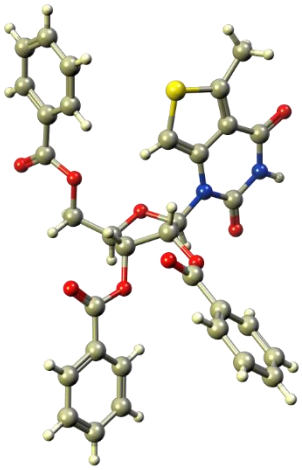

Figure 2.18 Crystal structure of **15**

To determine the configuration of ^{mth}G, COSY and NOESY NMR experiments were run on each of the ribonucleoside analogues. The COSY spectra were taken to help assign the proton signals to each of the respective protons in the molecule. The sugar protons signals are distinct but need to be identified so that NOESY correlations can be predicted. We hypothesized that the H1' proton would in an aprotic deuterated solvent show NOESY correlation with the 2'-OH proton. The ^{mth}U NOESY spectrum indeed showed a distinct NOESY correlation between the H1' and the 2-OH' (Fig. 2.71). ^{mth}C showed a NOESY correlation between the H1' and the 2-OH' though it was not as strong as that of ^{mth}U (Fig. 2.75). ^{mth}A in the beta configuration and ^{mth}G also showed a NOESY correlation between the H1' and the 2-OH', although they appeared as a shoulder due to the close proximity of the two proton peaks in each spectrum (Figs. 2.31, 2.47). ^{mth}I in the beta configuration also showed a NOESY correlation between the H1' and the 2-OH' (Fig. 2.55). ^{mth}A and ^{mth}I in the alpha configuration showed no NOESY correlation between the H1' and the 2-OH' (Figs. 2.51, 2.59).

After assigning the proton signals to each respective proton in the molecule using the COSY spectra, the HH ^{3}J-couplings and chemical shifts were compared across the ribonucleosides and across stereochemical conformations (Table 2.3, 2.4). Interestingly, it was

found that the H1’ in ribonucleosides in the beta conformation would display a HH ^{3}J-coupling of ~6–7 Hz whereas the H1’ in ribonucleosides in the alpha conformation would display a HH ^{3}J-coupling of ~3 Hz. We also noted that the H2’ signal would move up field of the H3’ signal and likewise the H3’ signal would move downfield of the H2’ signal, effectively trading places in a sense. These two trends may suggest that stereochemistry can be discerned from a ^{1}H proton NMR and COSY experiment. The evidence is stronger for the purine analogues and therefore C-nucleosides due to the five independent data points of ^{mth}A in the beta configuration, ^{mth}A in the alpha configuration, ^{mth}I in the beta configuration, ^{mth}I in the alpha configuration, and ^{mth}G.

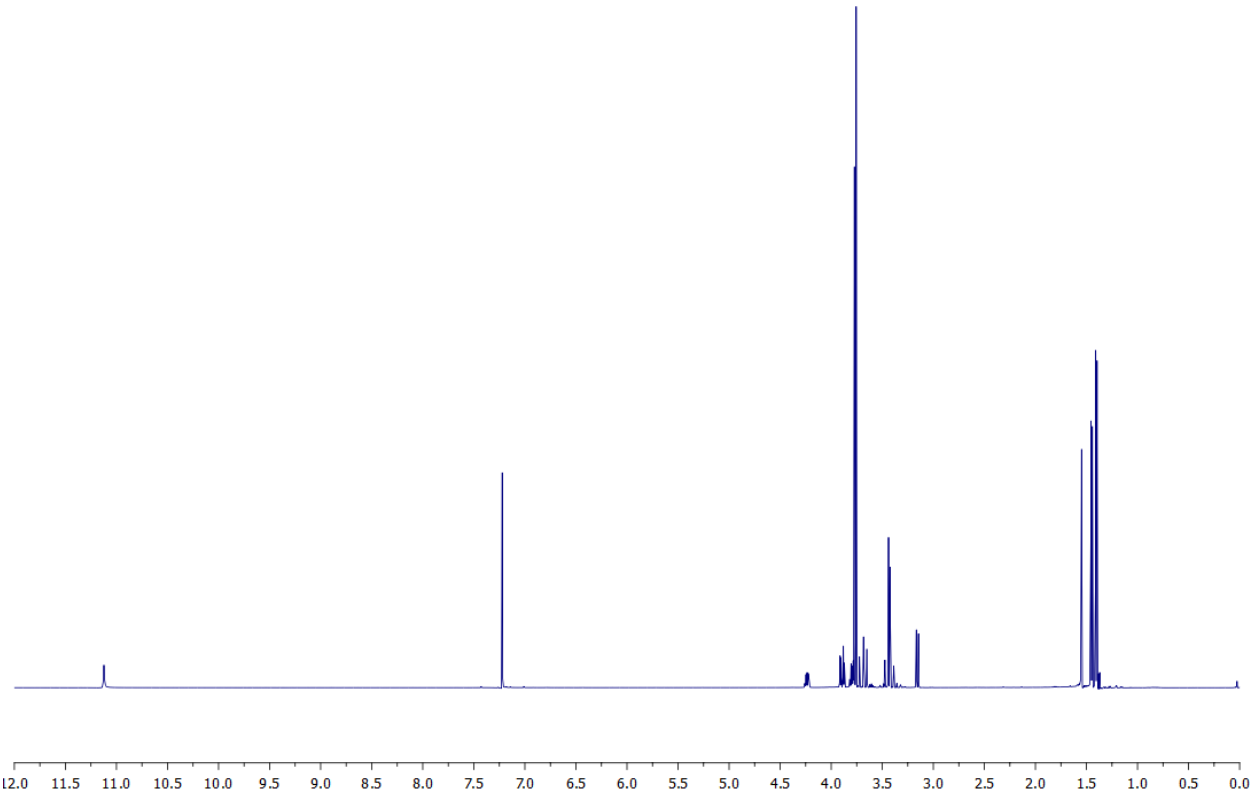

Figure 2.19 ^{1}H NMR spectra of **2b** in $CDCl_3$

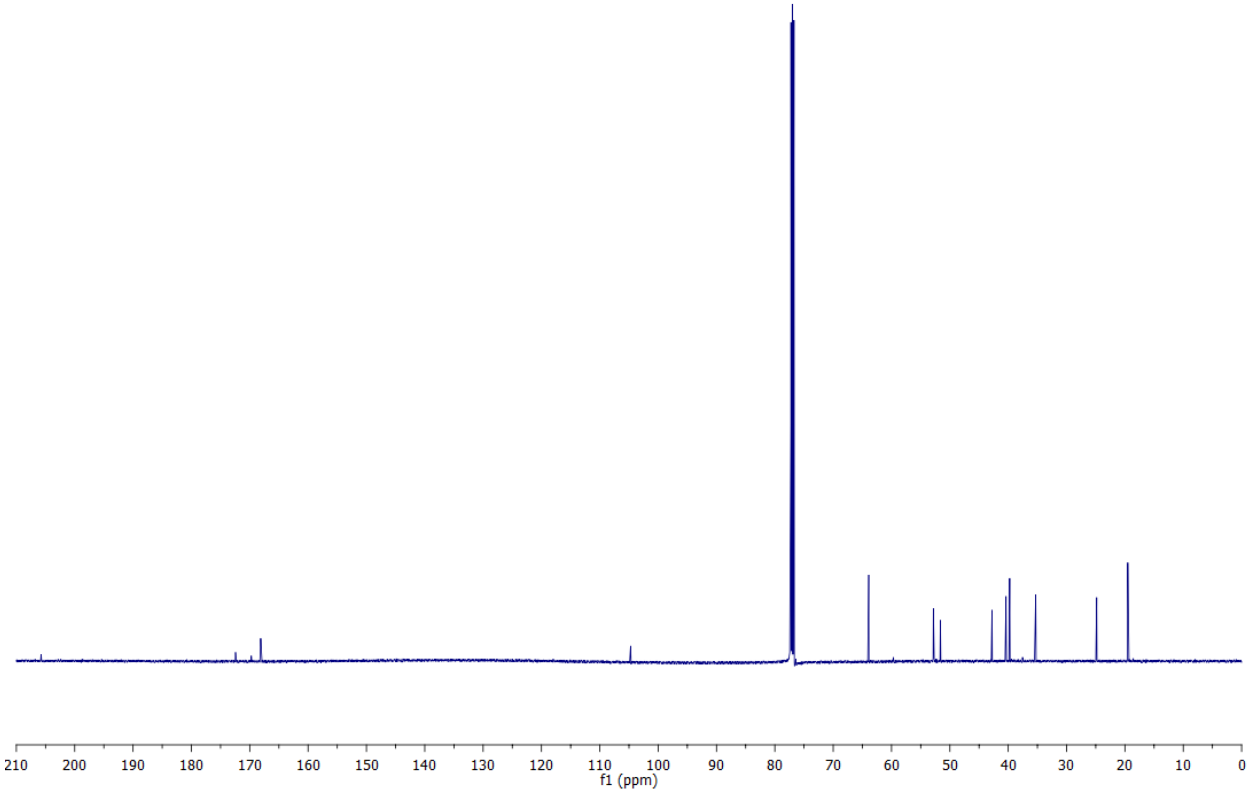

Figure 2.20 ^{13}C NMR spectra of **2b** in $CDCl_3$

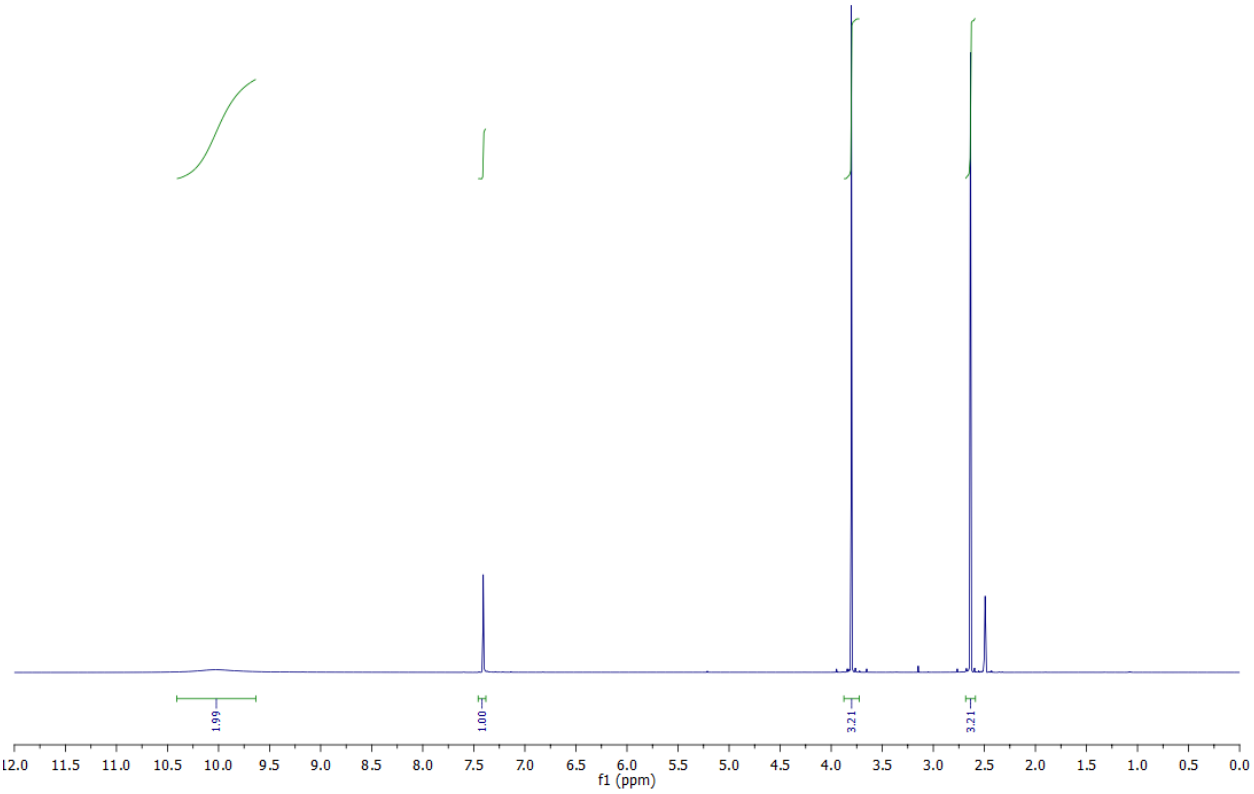

Figure 2.21 ^{1}H NMR spectra of **4b** in DMSO-d_6

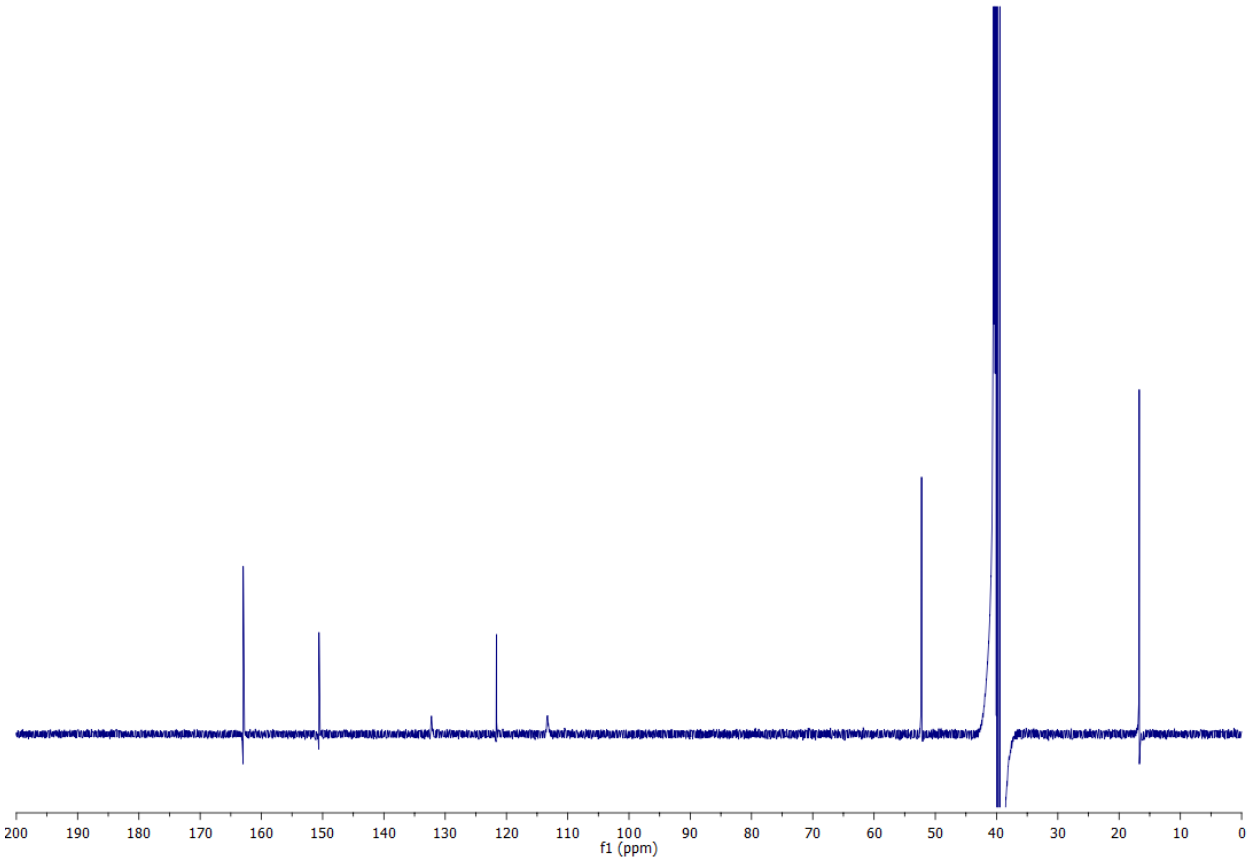

Figure 2.22 ^{13}C NMR spectra of **4b** in DMSO-d_6

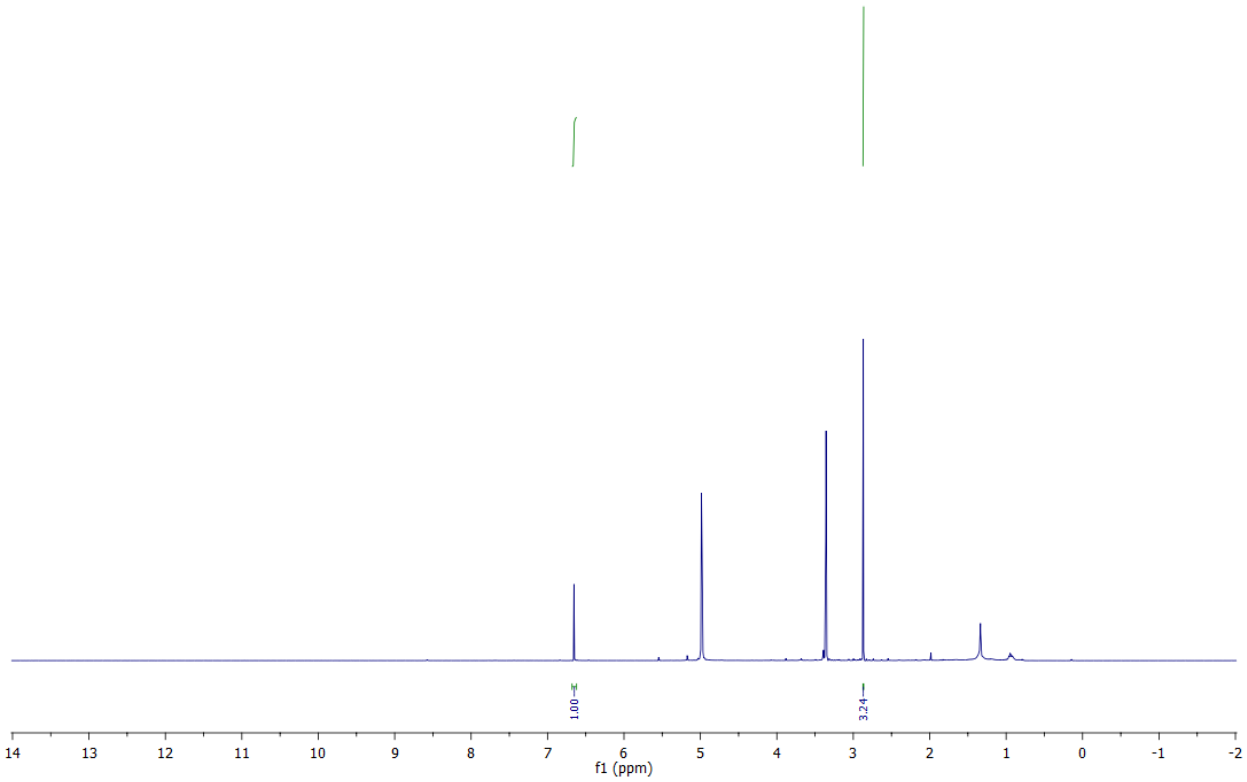

Figure 2.23 ^{1}H NMR spectra of **5** in CD_3OD

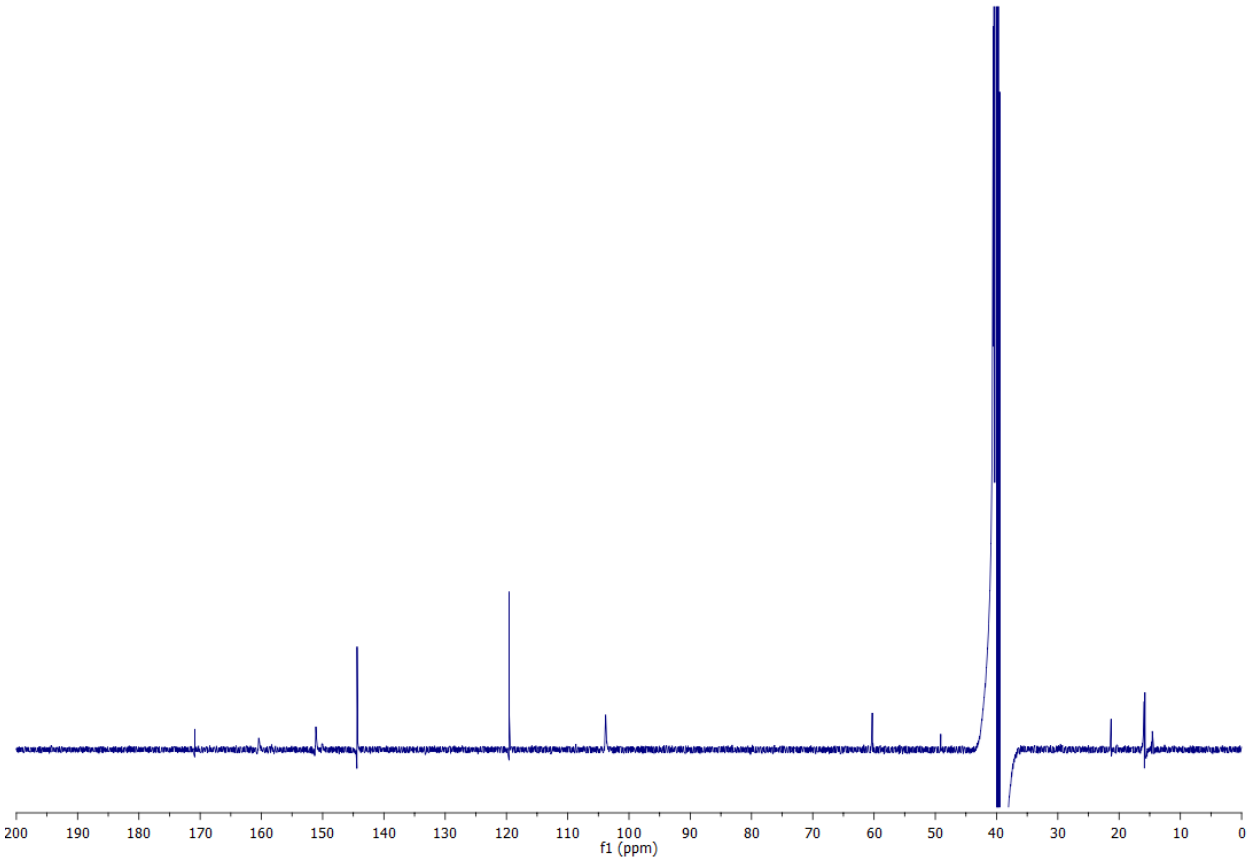

Figure 2.24 ^{13}C NMR spectra of **5** in DMSO-d_6

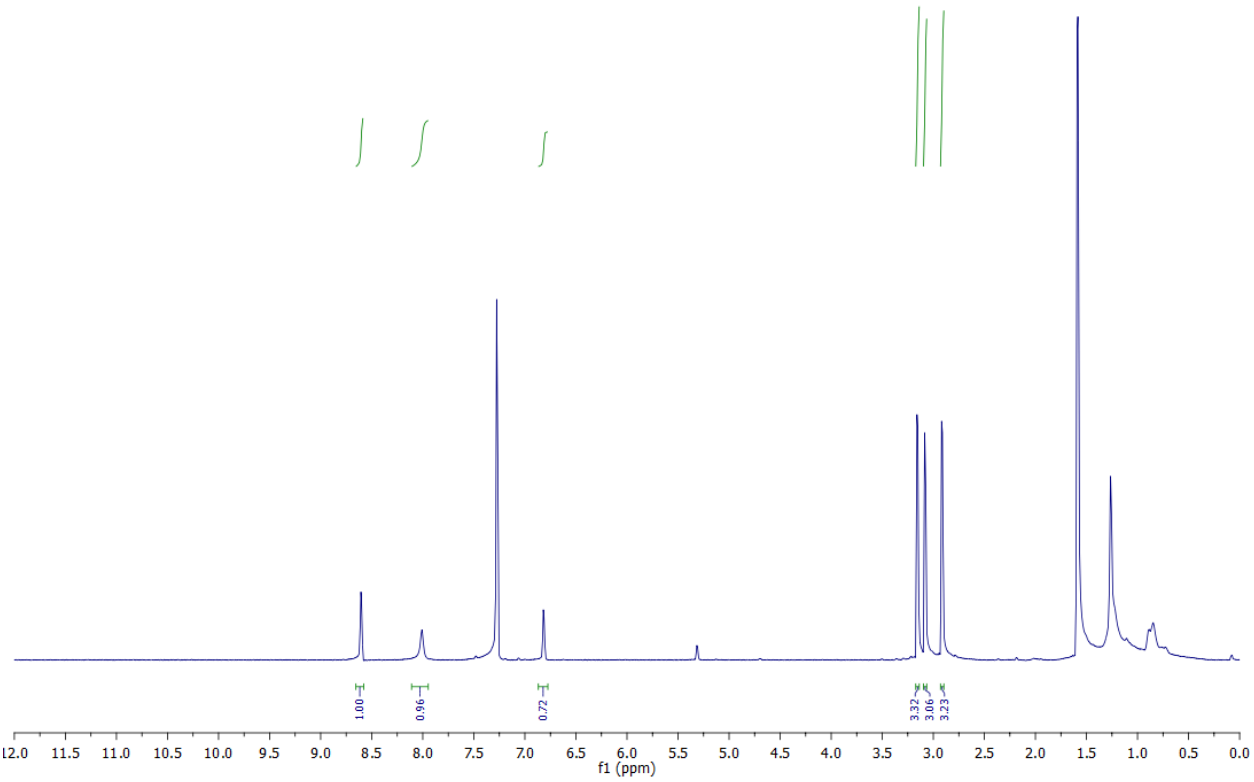

Figure 2.25 ^{1}H NMR spectra of **6** in $CDCl_3$

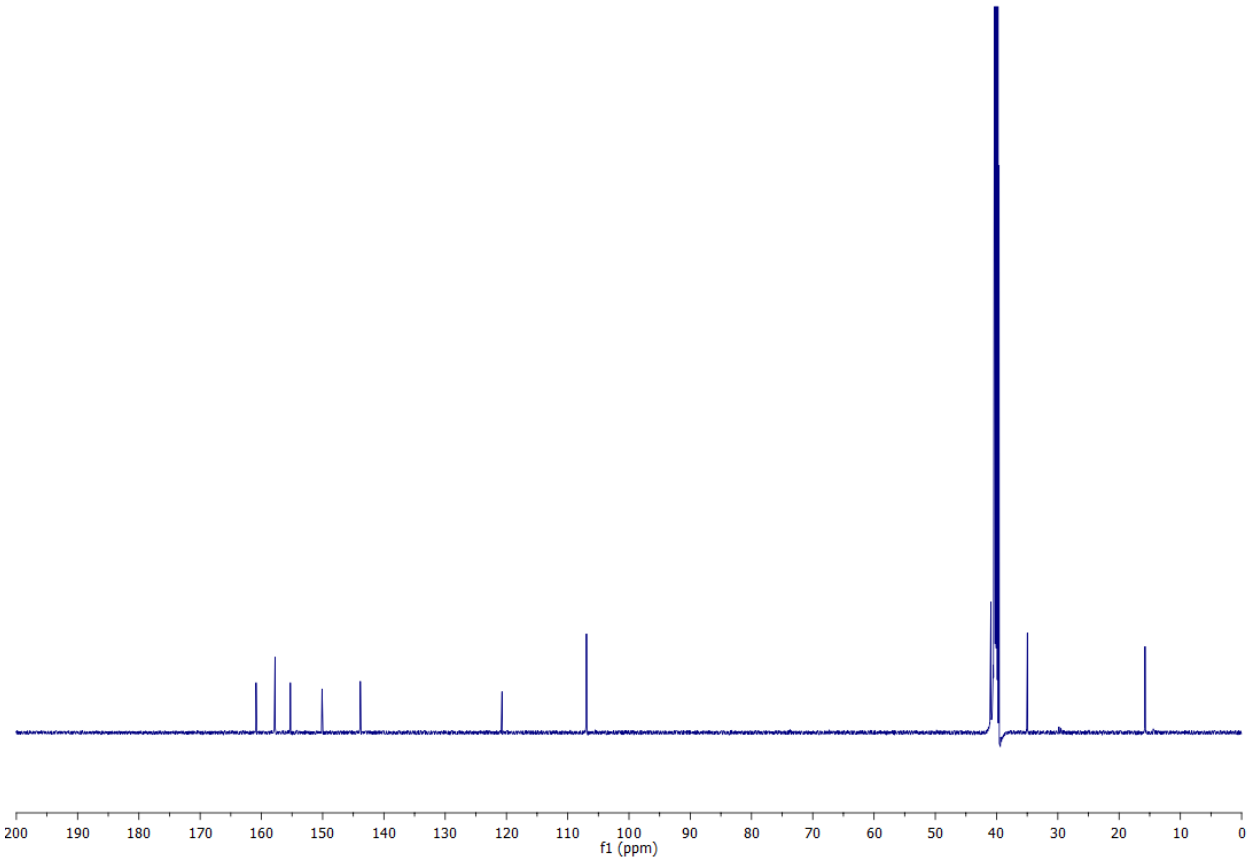

Figure 2.26 ^{13}C NMR spectra of **6** in DMSO-d_6

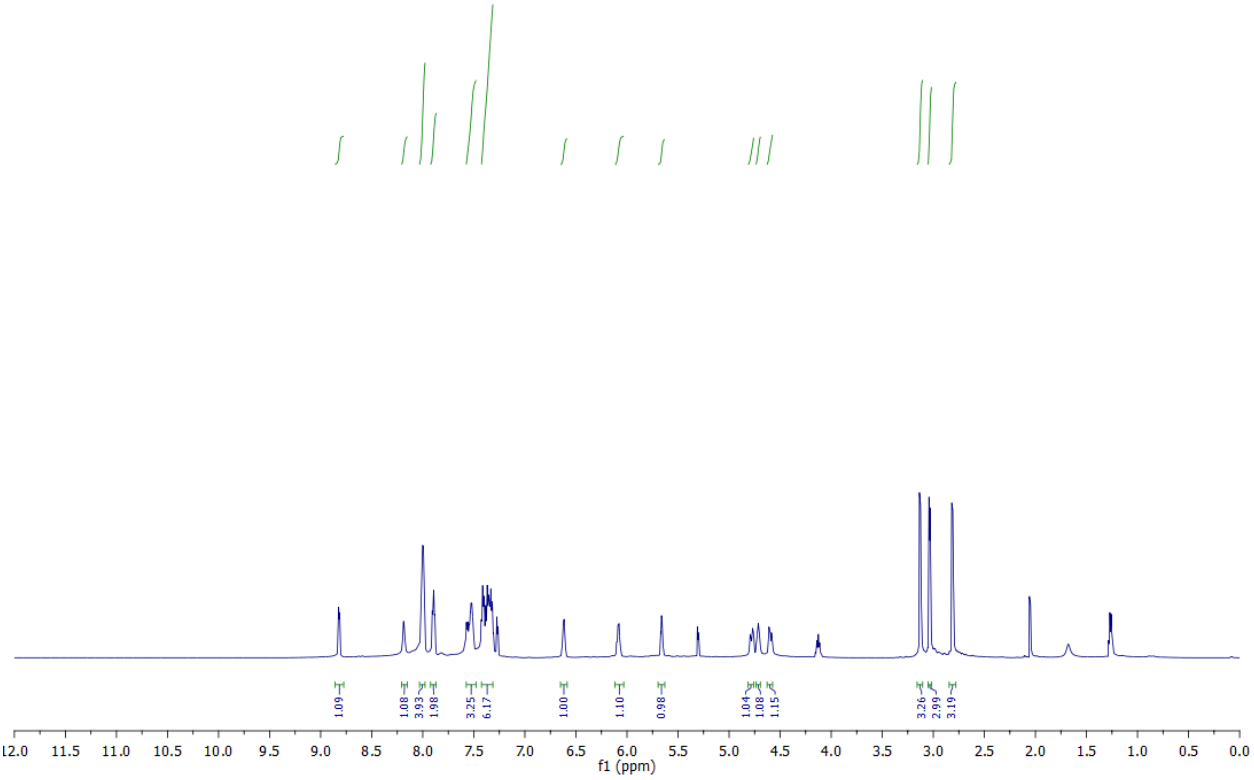

Figure 2.27 ^{1}H NMR spectra of **7** in $CDCl_3$

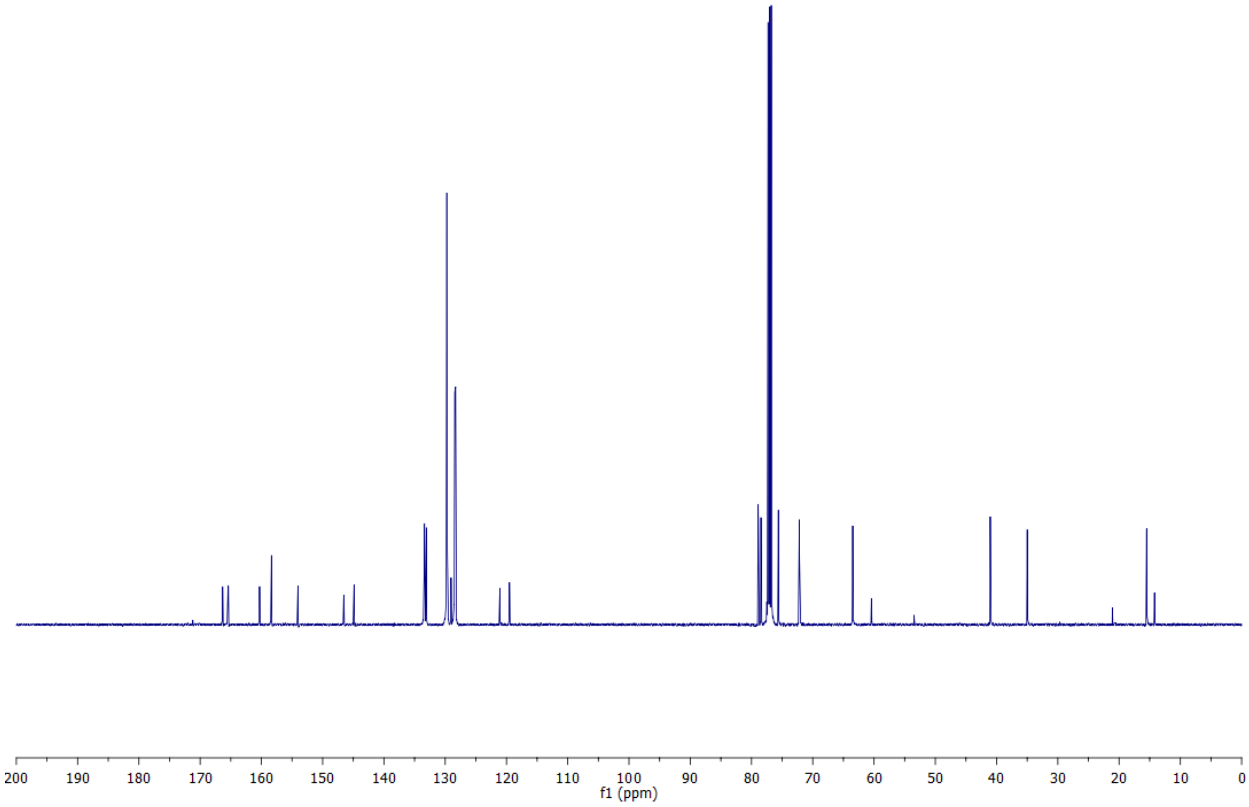

Figure 2.28 ^{13}C NMR spectra of **7** in $CDCl_3$

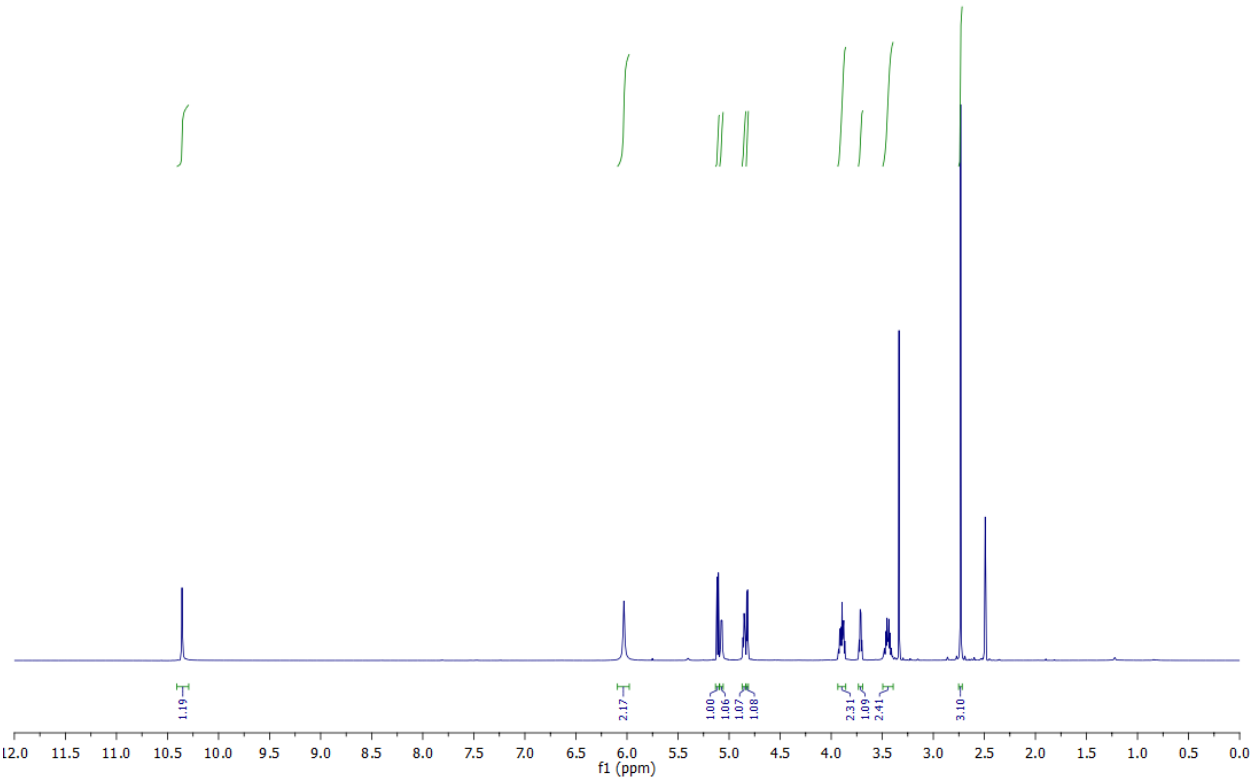

Figure 2.29 ^{1}H NMR spectra of ^{mth}G in DMSO-d_6

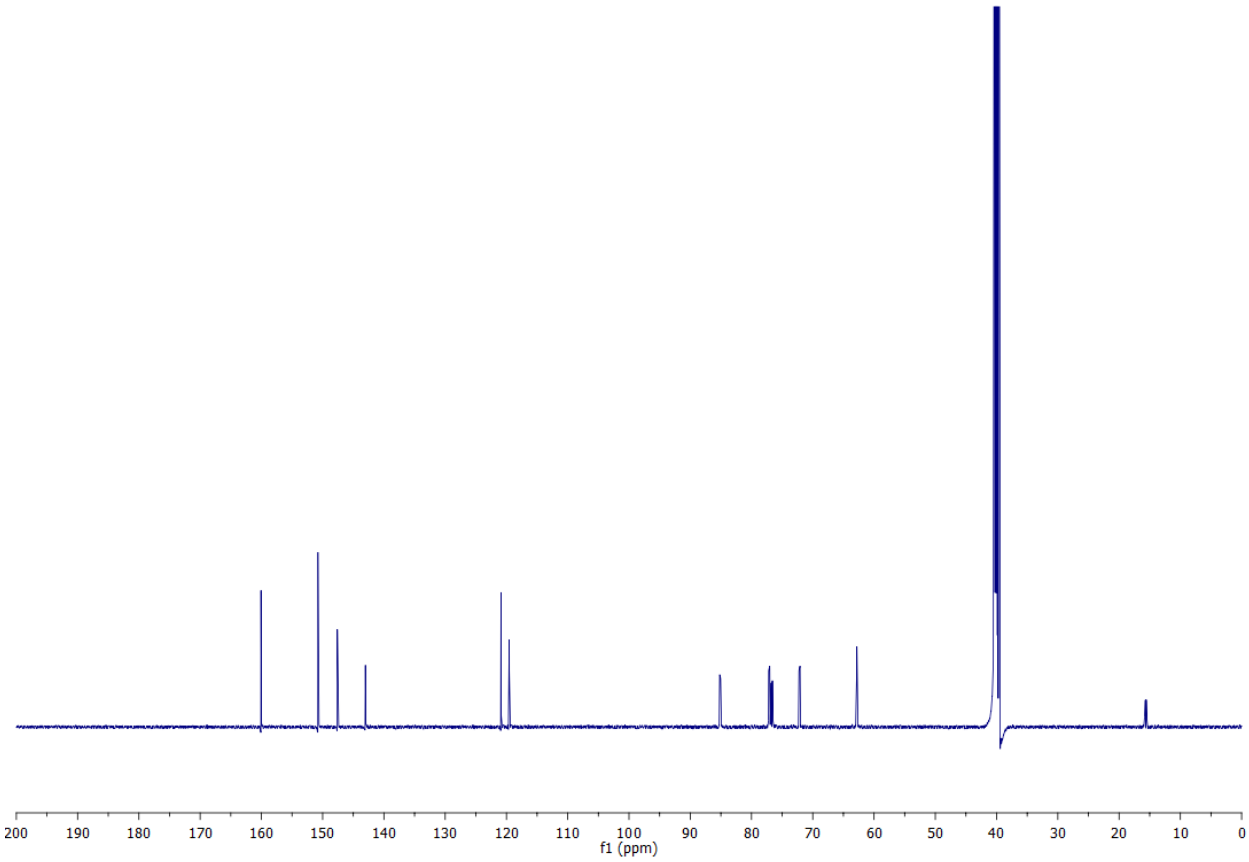

Figure 2.30 ^{13}C NMR spectra of ^{mth}G in DMSO-d_6

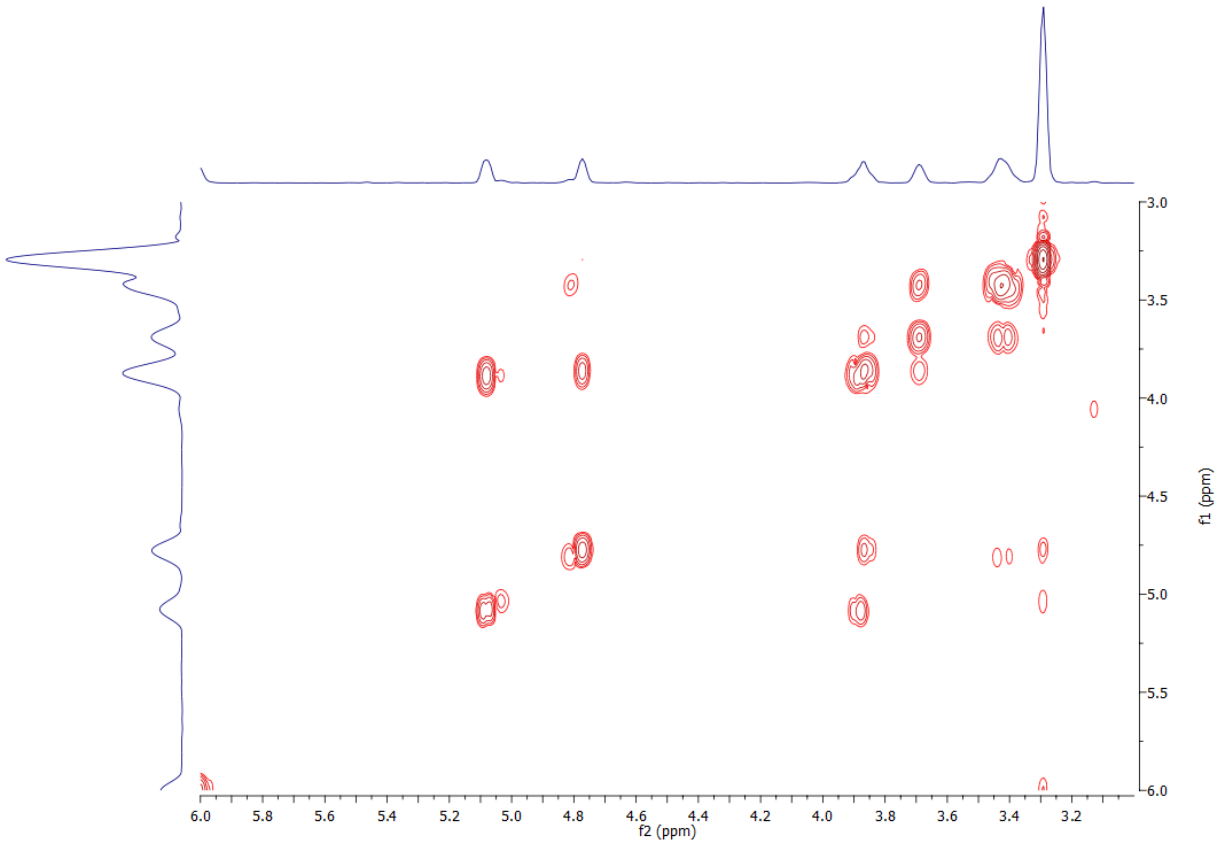

Figure 2.31 Relevant COSY correlations of ^{mth}G in DMSO-d_6; H-1' correlated with H-2'; H-2' correlated with H-3' and 2'-OH; H-3' correlated with H-4' and 3'-OH; H-4' correlated with H-5'; H-5' correlated with 5'-OH.

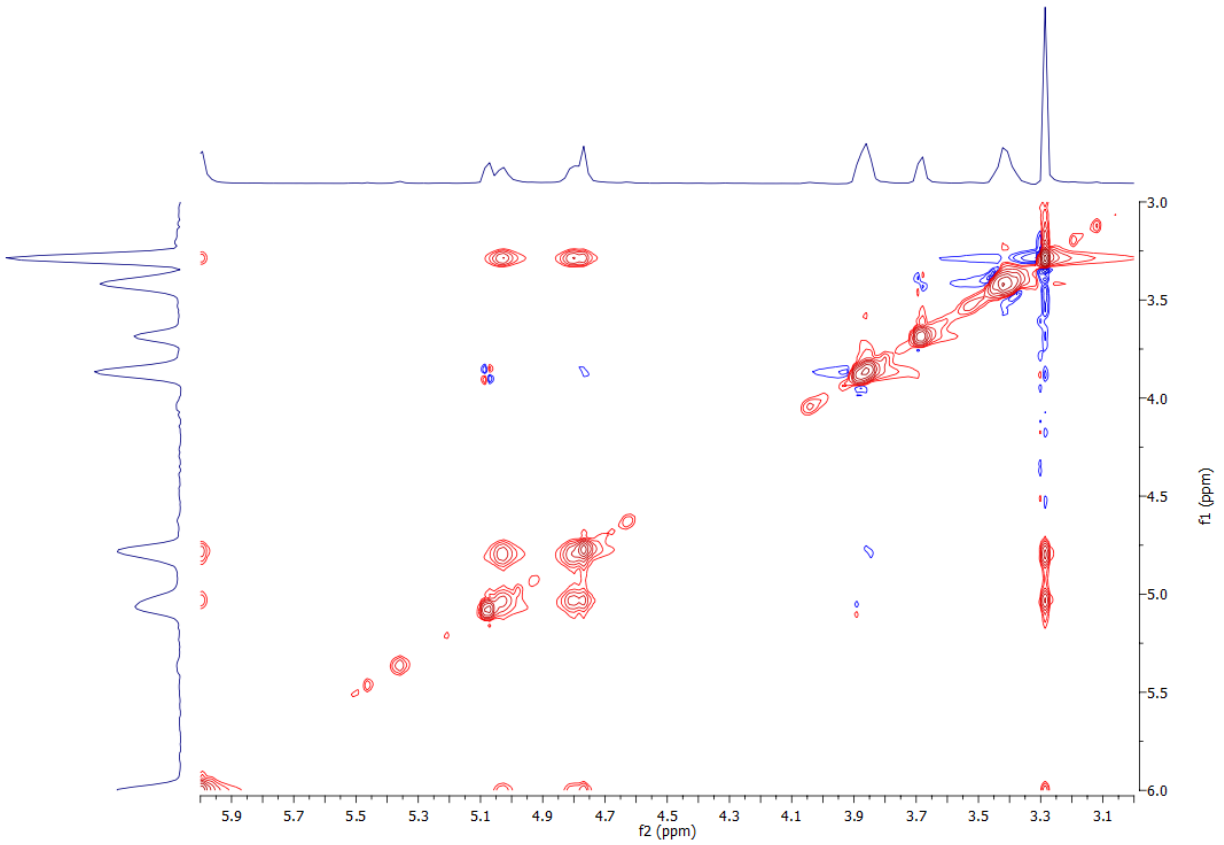

Figure 2.32 Relevant NOESY correlations of ^{mth}G in DMSO-d_6; H-1' correlated with H-2' and 2'-OH; H-2' correlated with H-3'; H-4' correlated with H-5'.

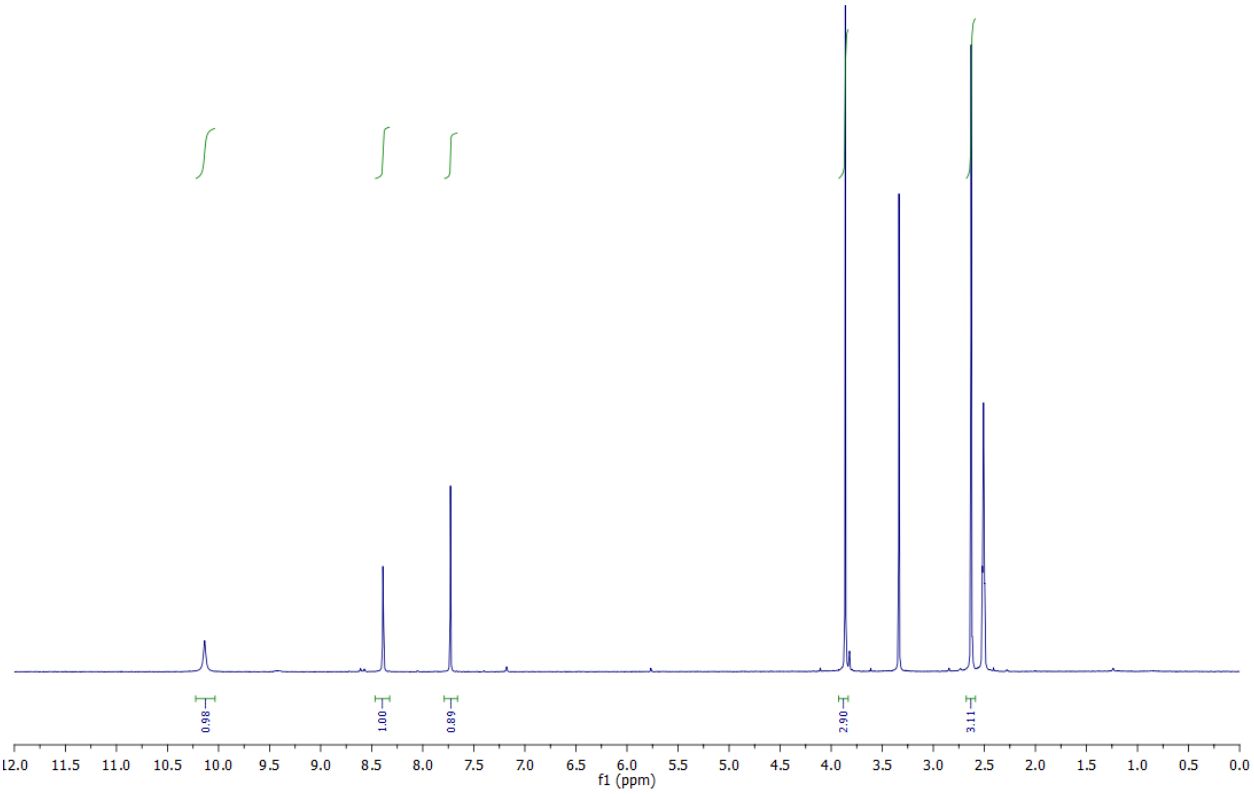

Figure 2.33 ^{1}H NMR spectra of **8** in DMSO-d_6

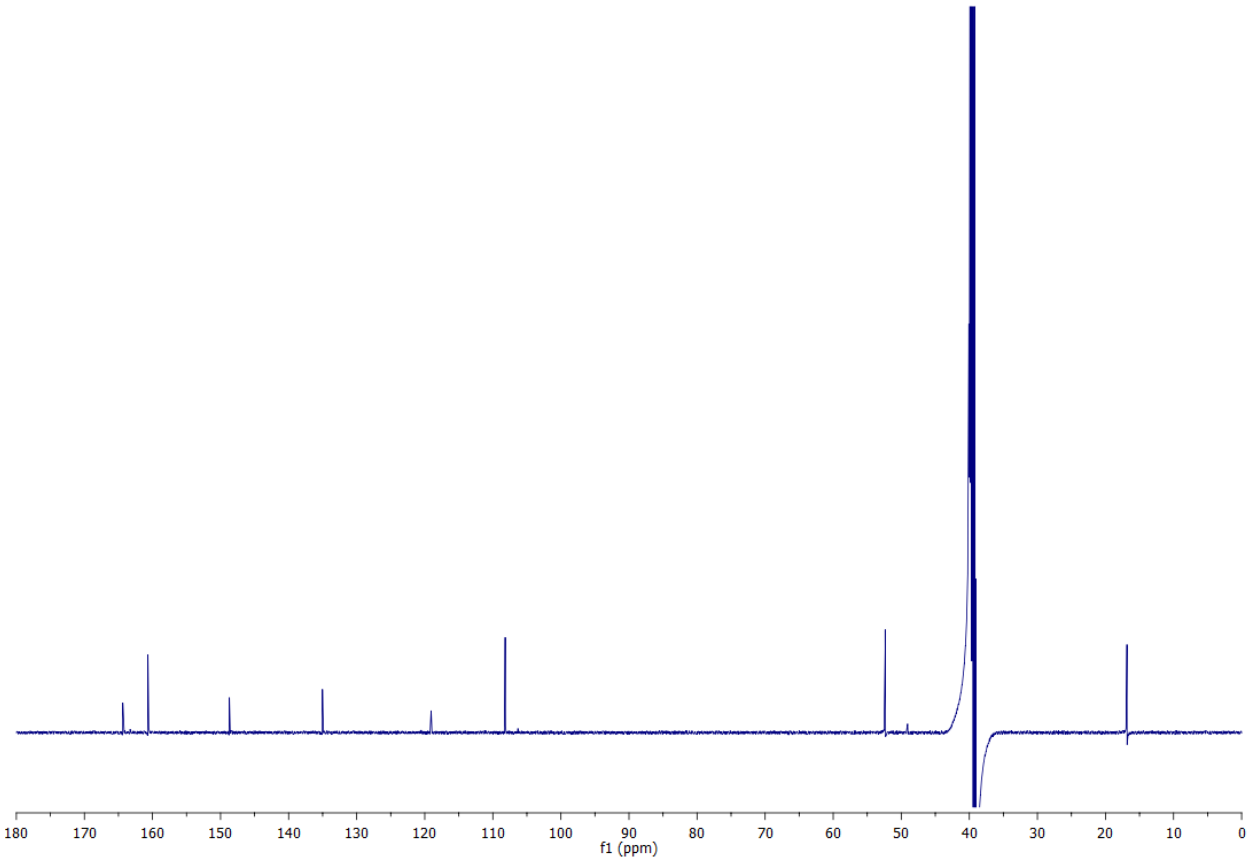

Figure 2.34 ^{13}C NMR spectra of **8** in DMSO-d_6

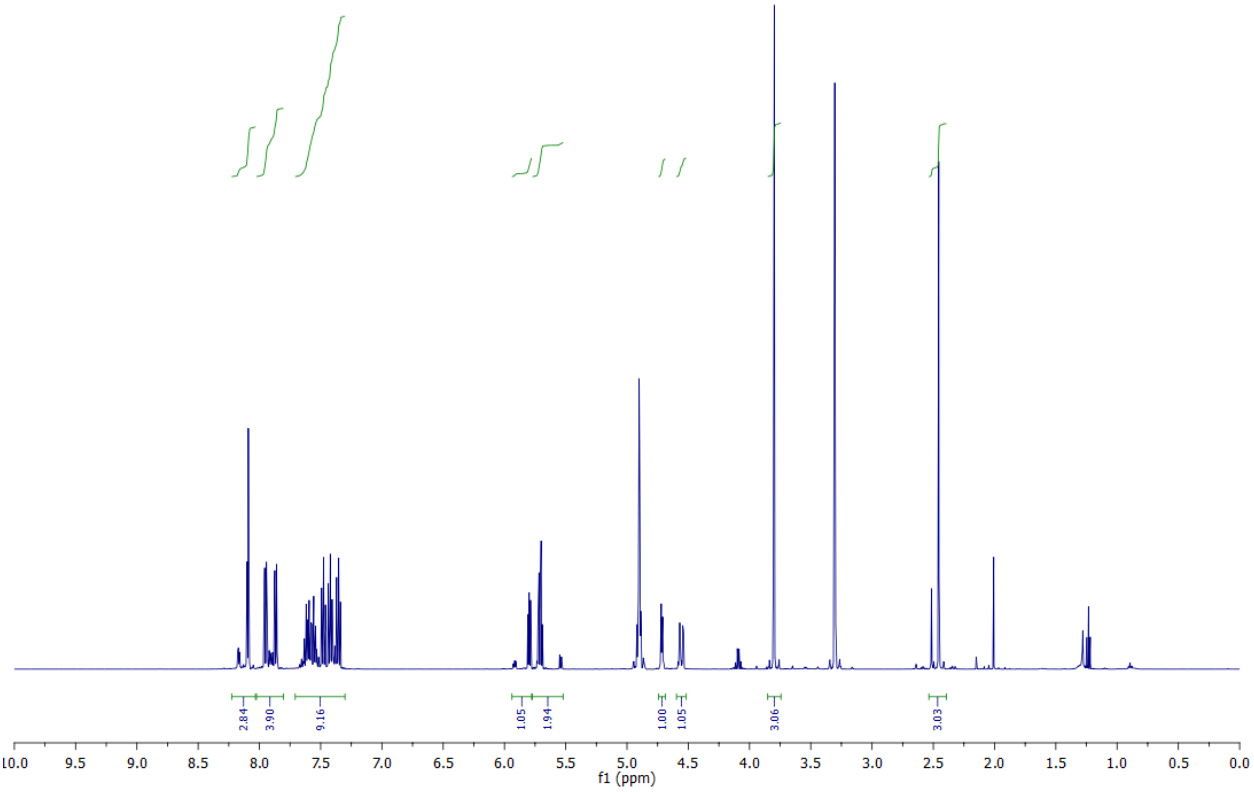

Figure 2.35 ^{1}H NMR spectra of **9** in CD_3OD

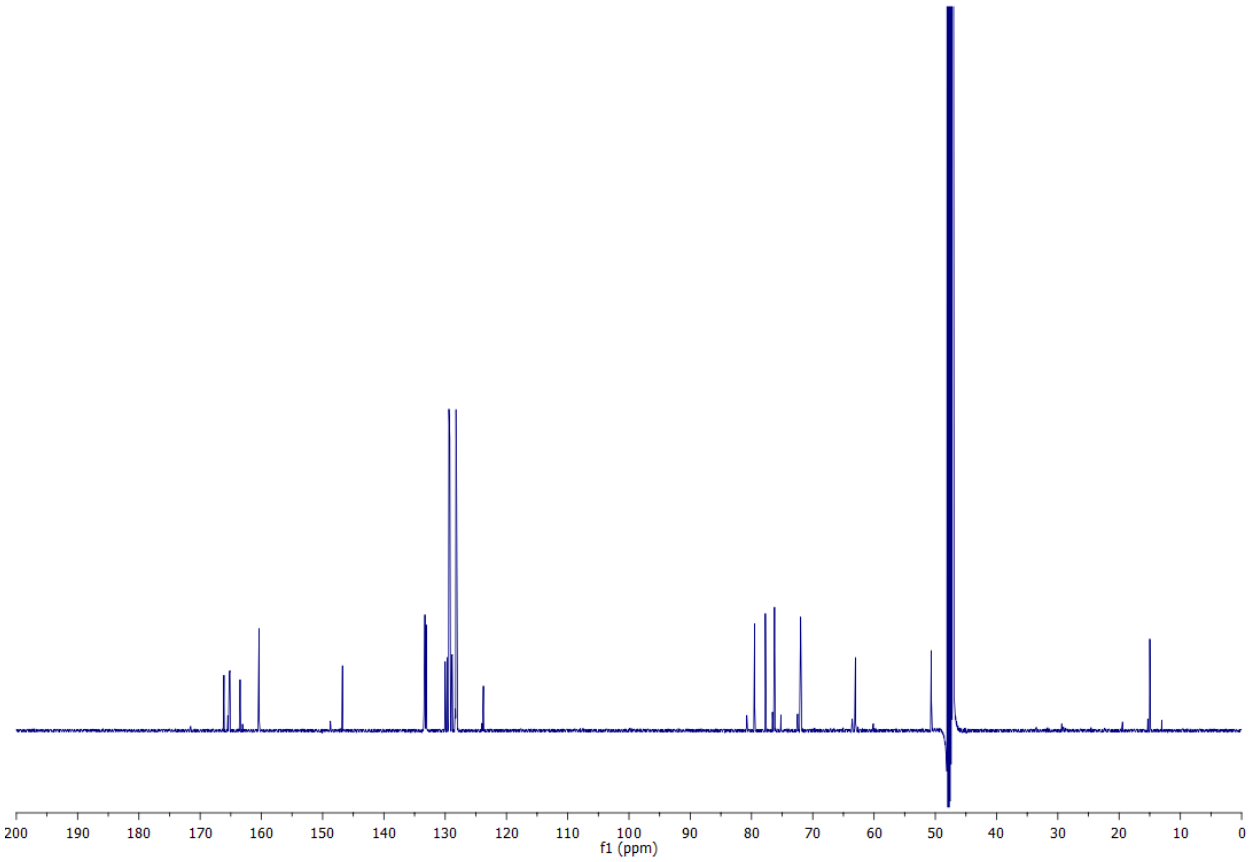

Figure 2.36 ^{13}C NMR spectra of **9** in CD_3OD

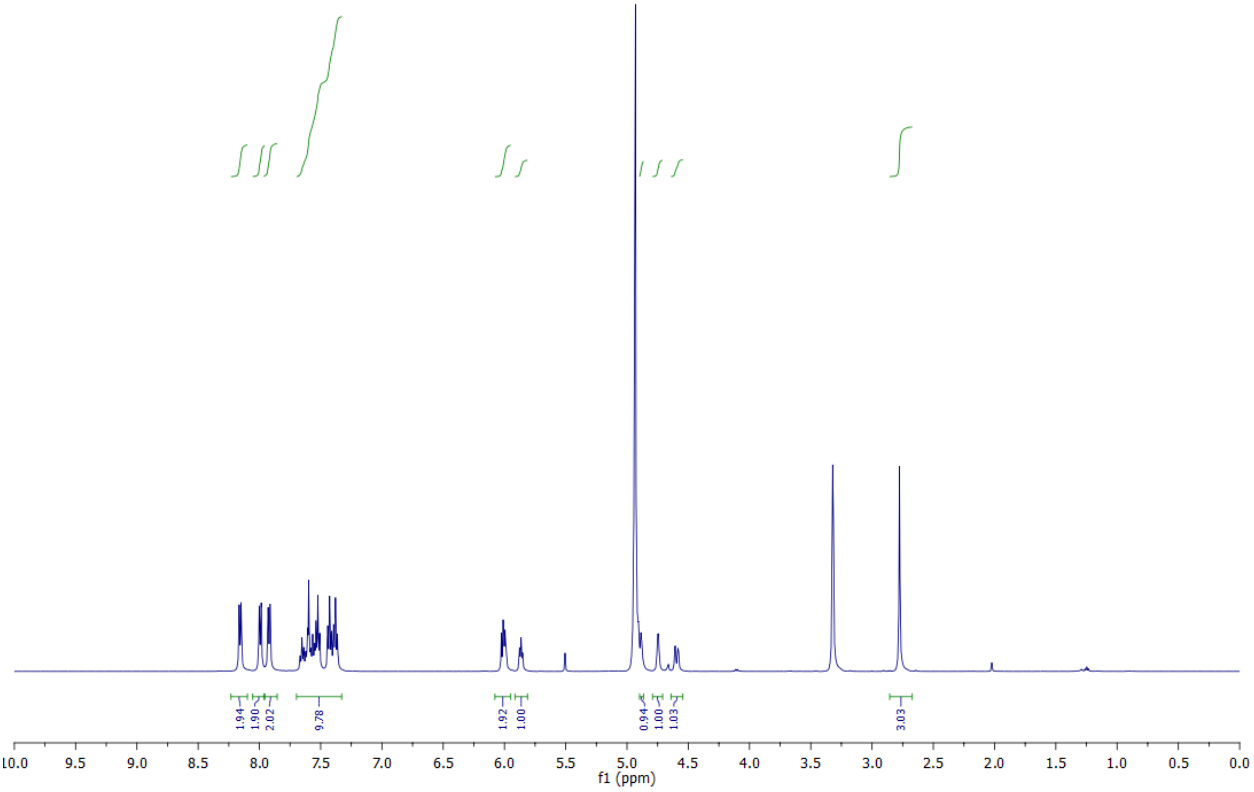

Figure 2.37 ^{1}H NMR spectra of **10** in the β configuration in CD_3OD

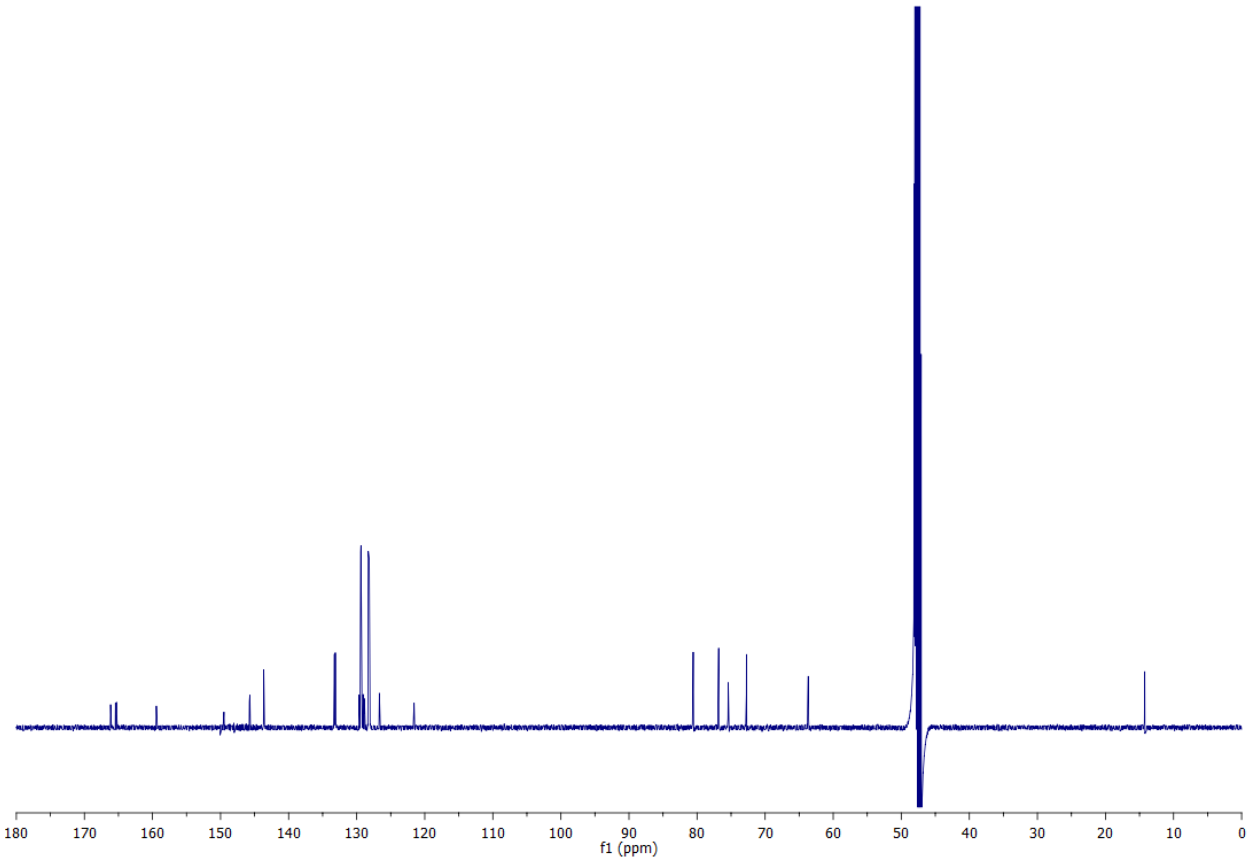

Figure 2.38 ^{13}C NMR spectra of **10** in the β configuration in CD_3OD

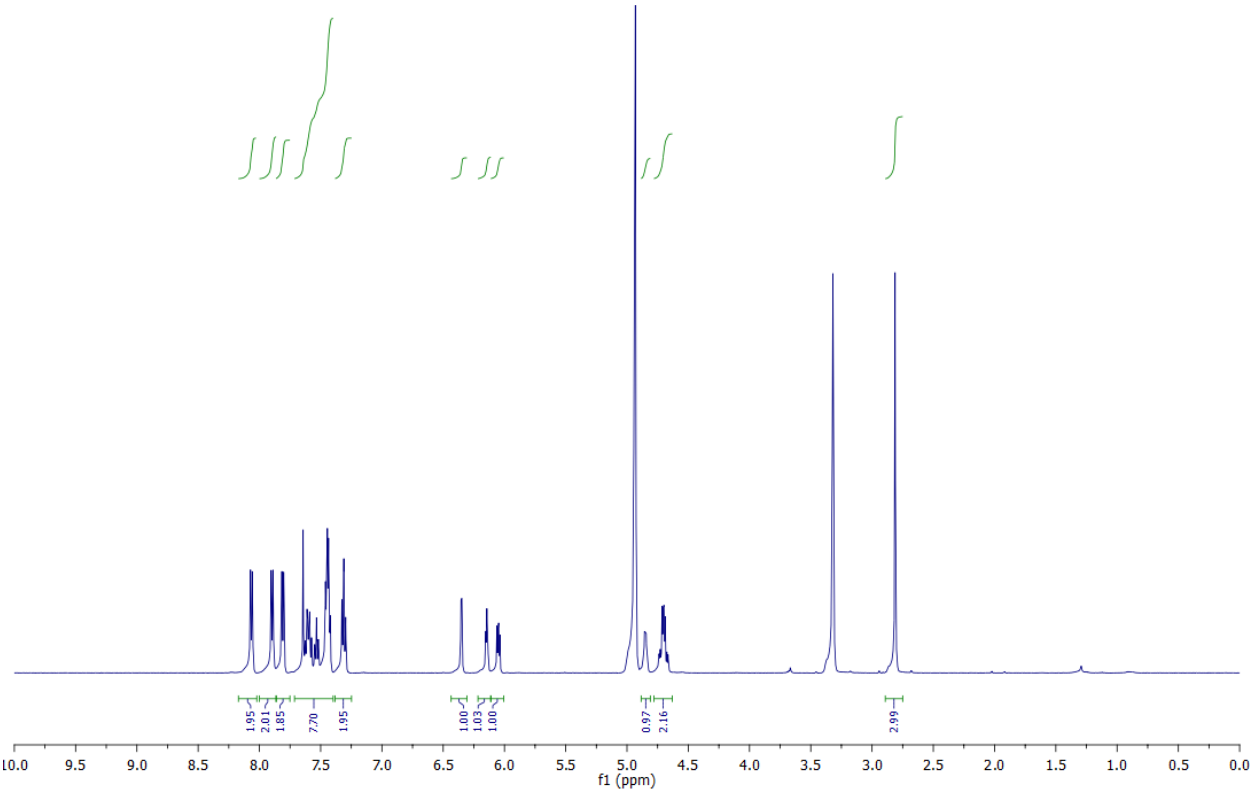

Figure 2.39 ^{1}H NMR spectra of **10** in the α configuration in CD_3OD

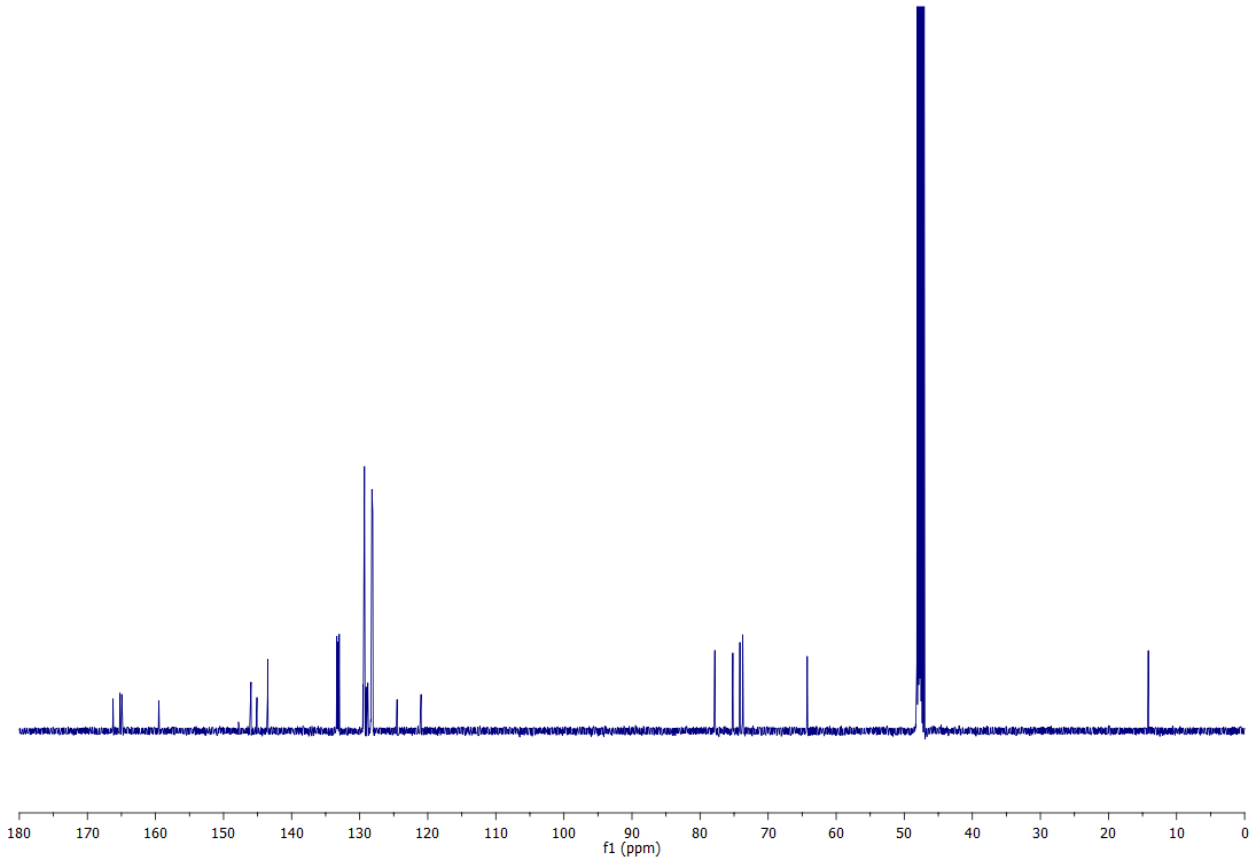

Figure 2.40 ^{13}C NMR spectra of **10** in the α configuration in CD_3OD

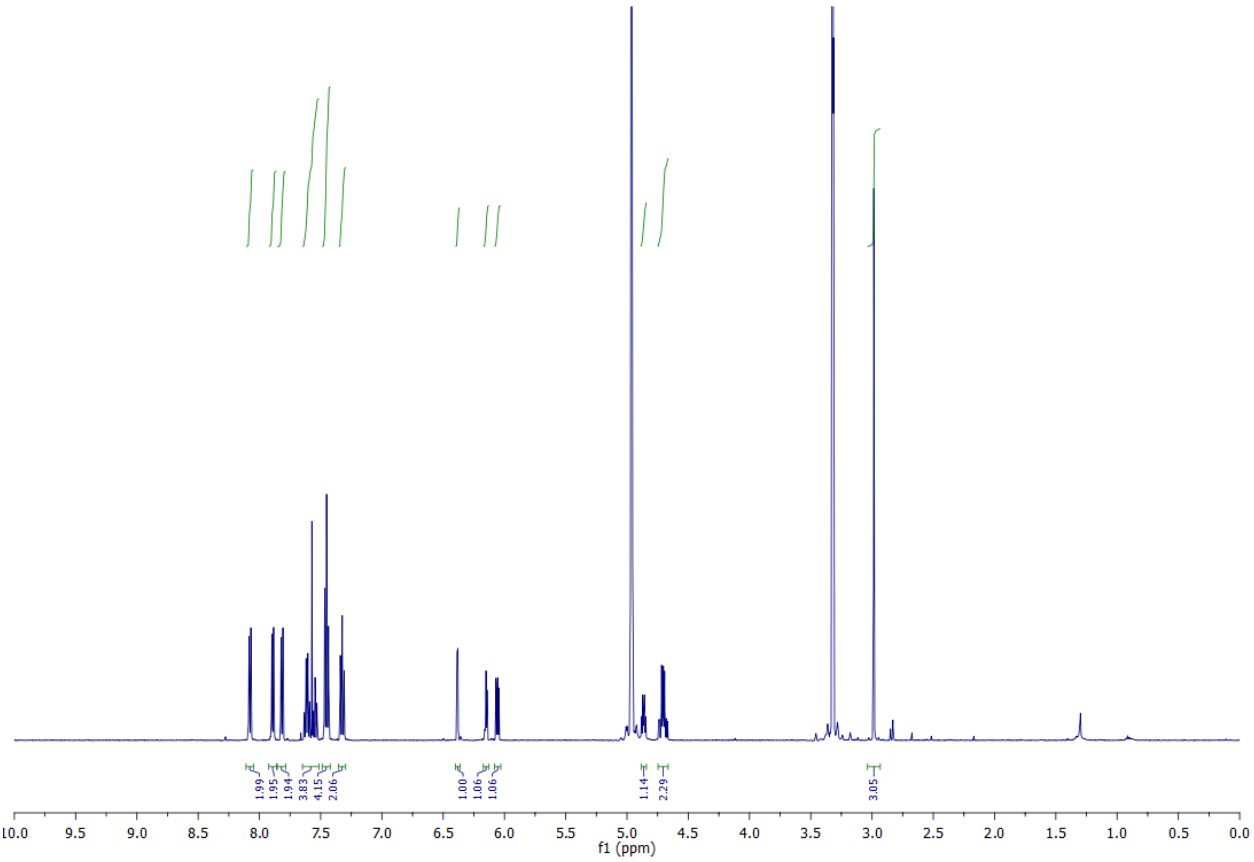

Figure 2.41 ^{1}H NMR spectra of **11** in the α configuration in CD_3OD

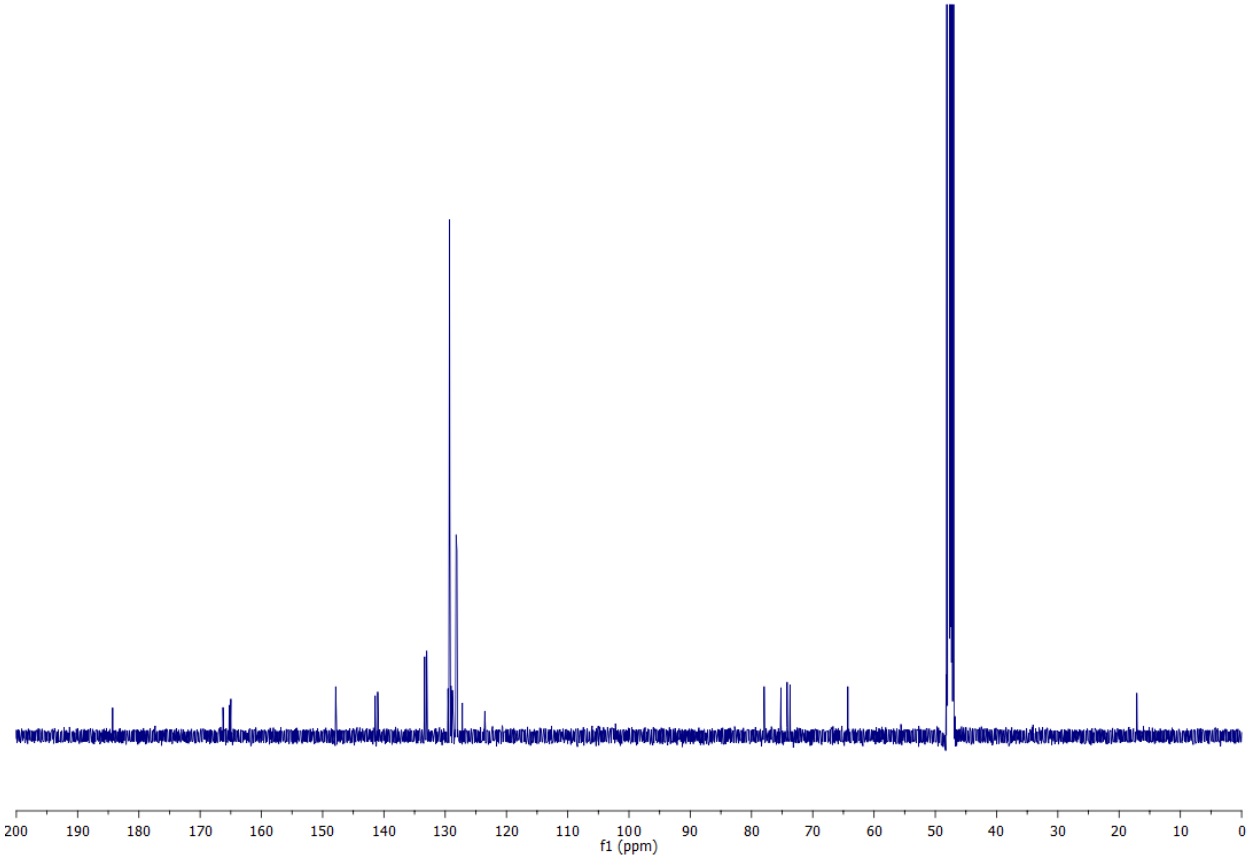

Figure 2.42 ^{13}C NMR spectra of **11** in the α configuration in CD_3OD

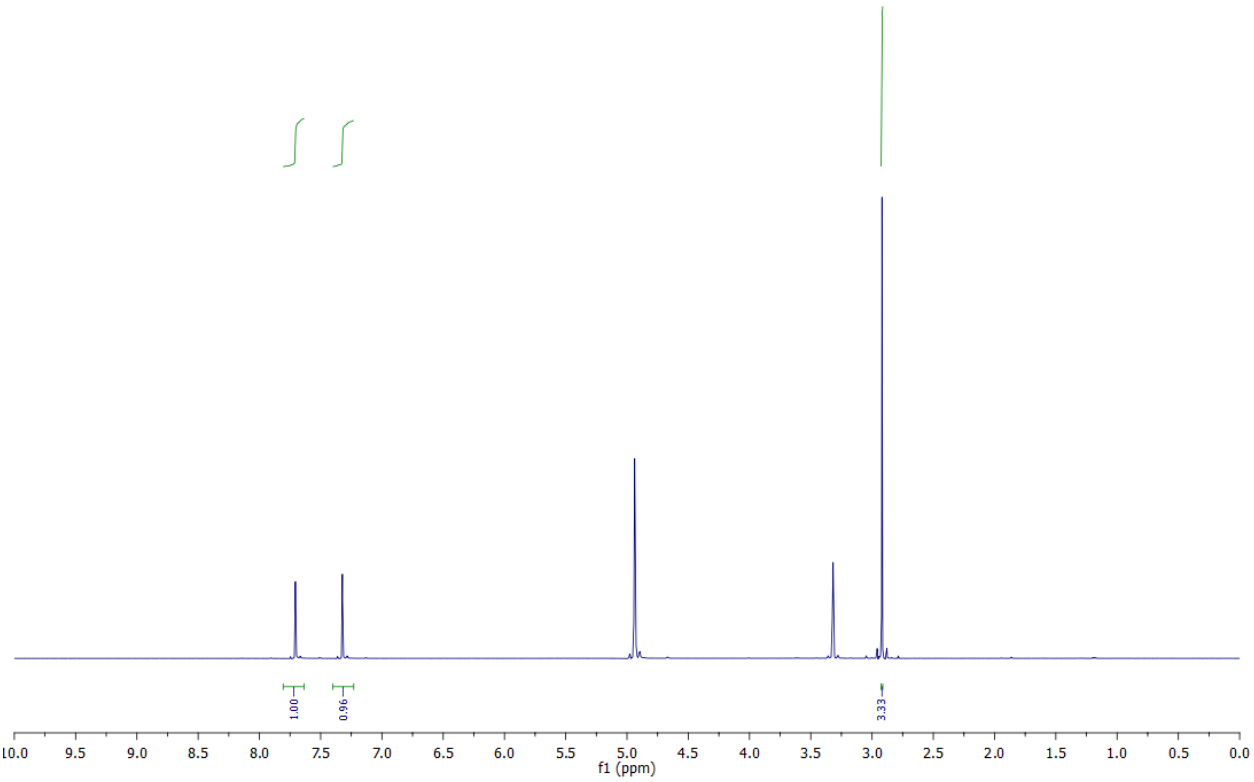

Figure 2.43 ^{1}H NMR spectra of **12** in CD_3OD

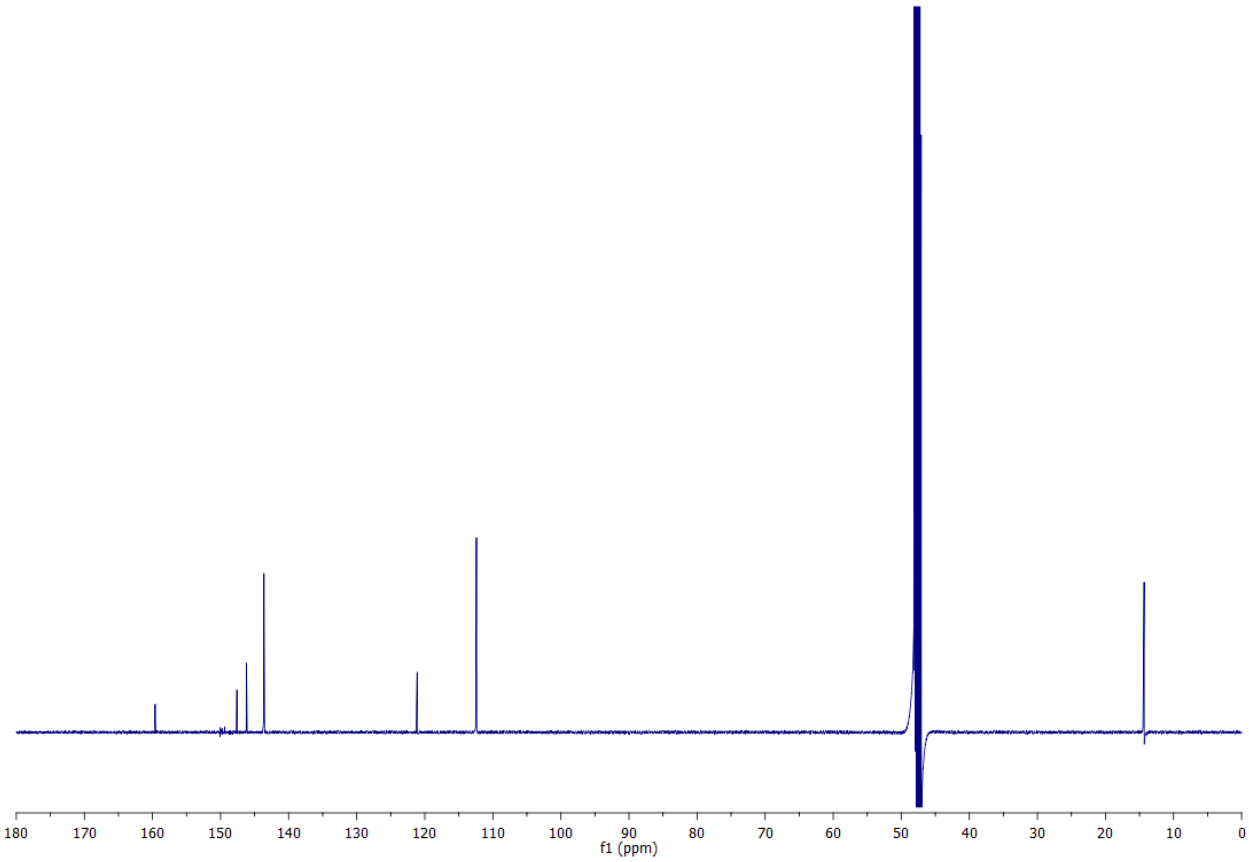

Figure 2.44 ^{13}C NMR spectra of **12** in CD_3OD

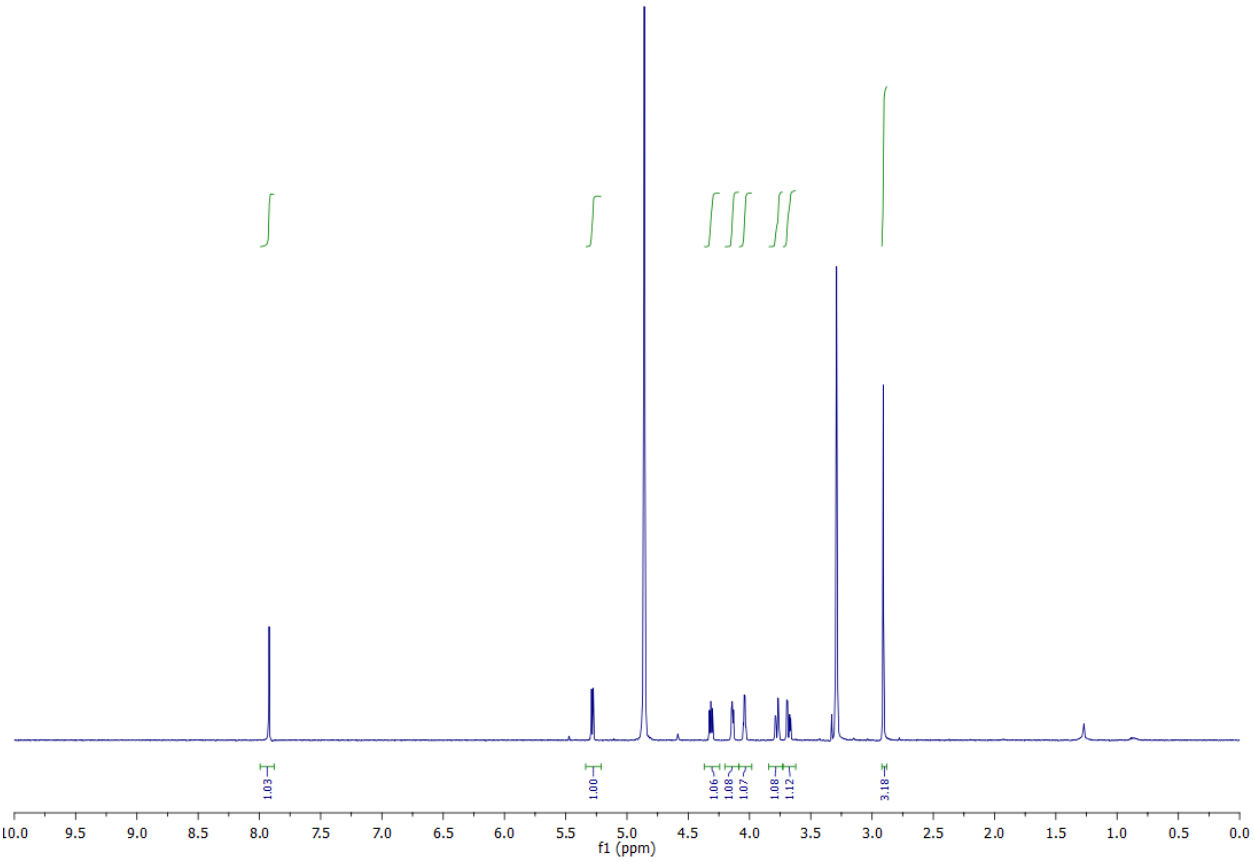

Figure 2.45 ^{1}H NMR spectra of ^{mth}A in CD_3OD

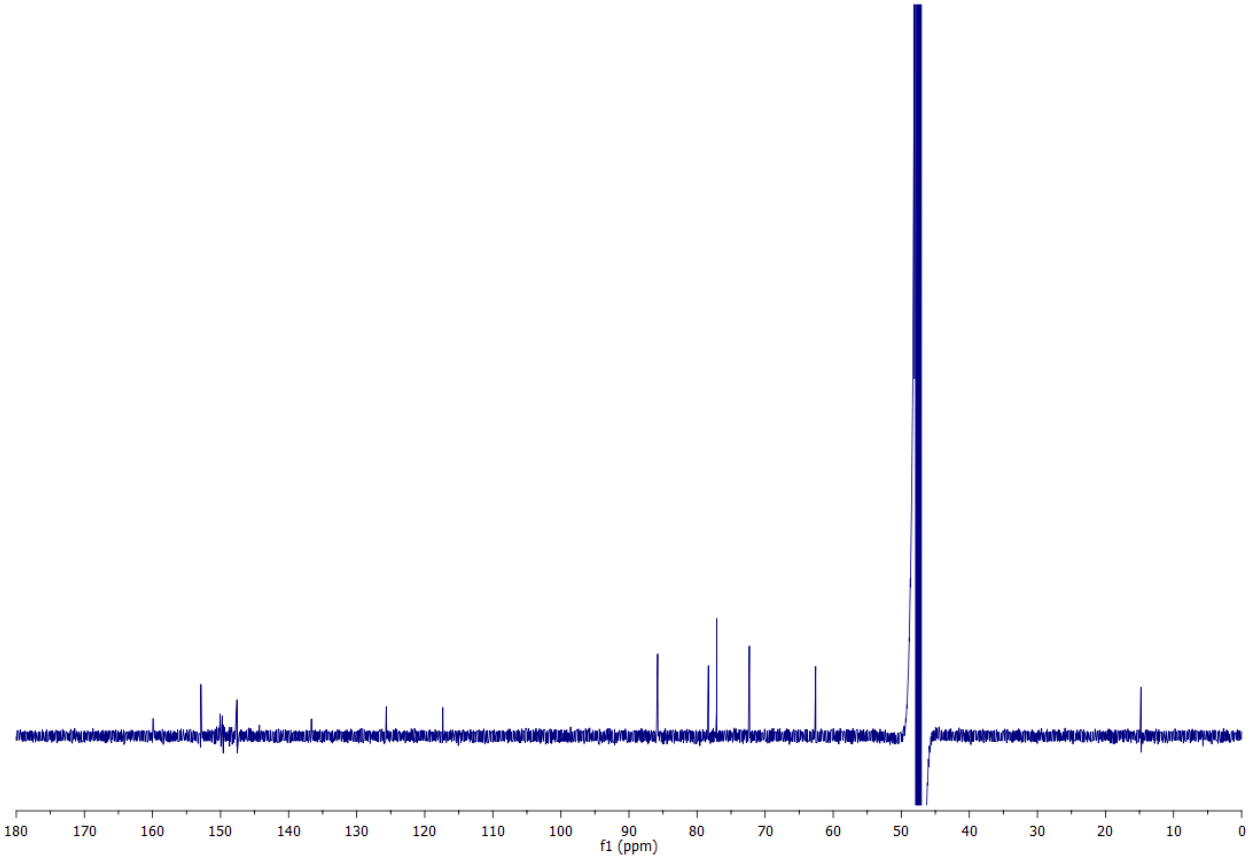

Figure 2.46 ^{13}C NMR spectra of ^{mth}A in CD_3OD

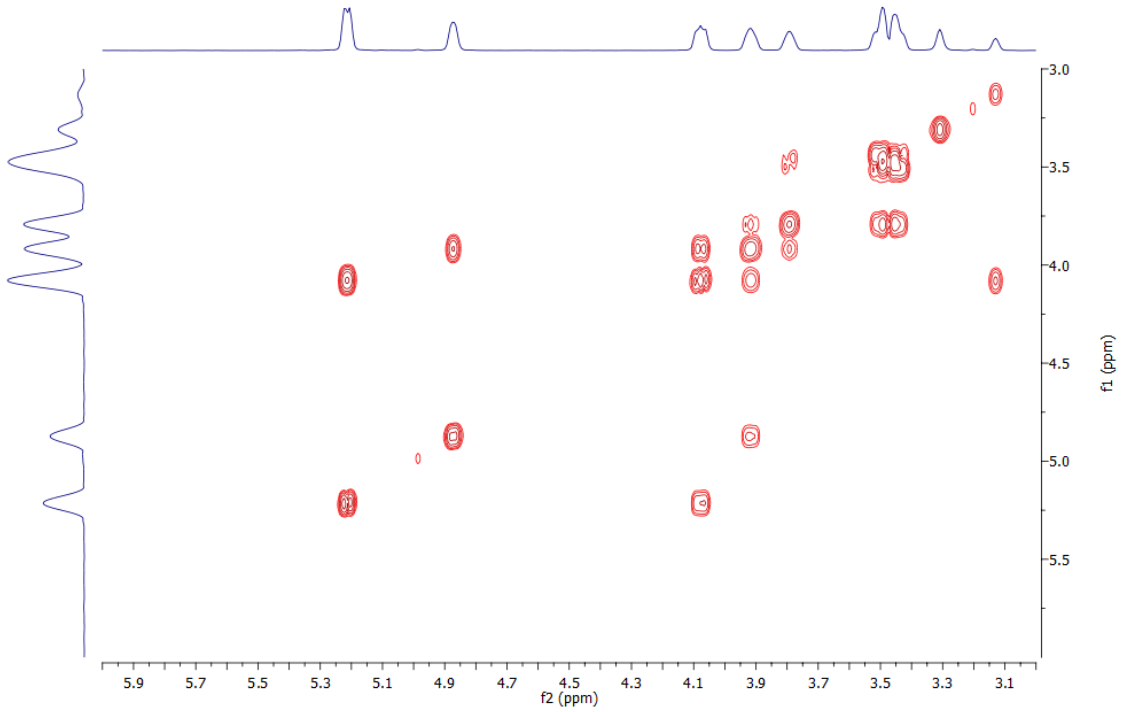

Figure 2.47 Relevant COSY correlations of ^{mth}A in DMSO-d_6; H-1' correlated with H-2'; H-2' correlated with H-3'; H-3' correlated with H-4' and 3'-OH; H-4' correlated with H-5'.

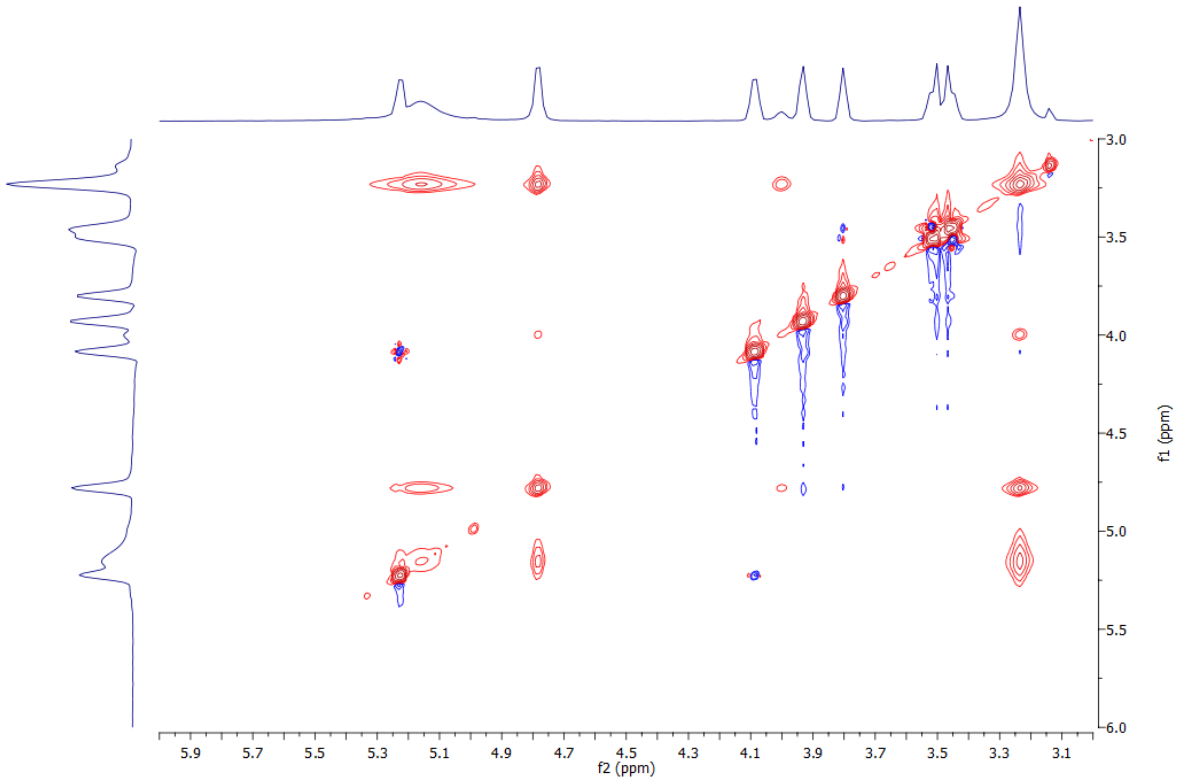

Figure 2.48 Relevant NOESY correlations of ^{mth}A in DMSO-d_6; H-1' correlated with H-2' and 2'-OH; H-4' correlated with H-5'.

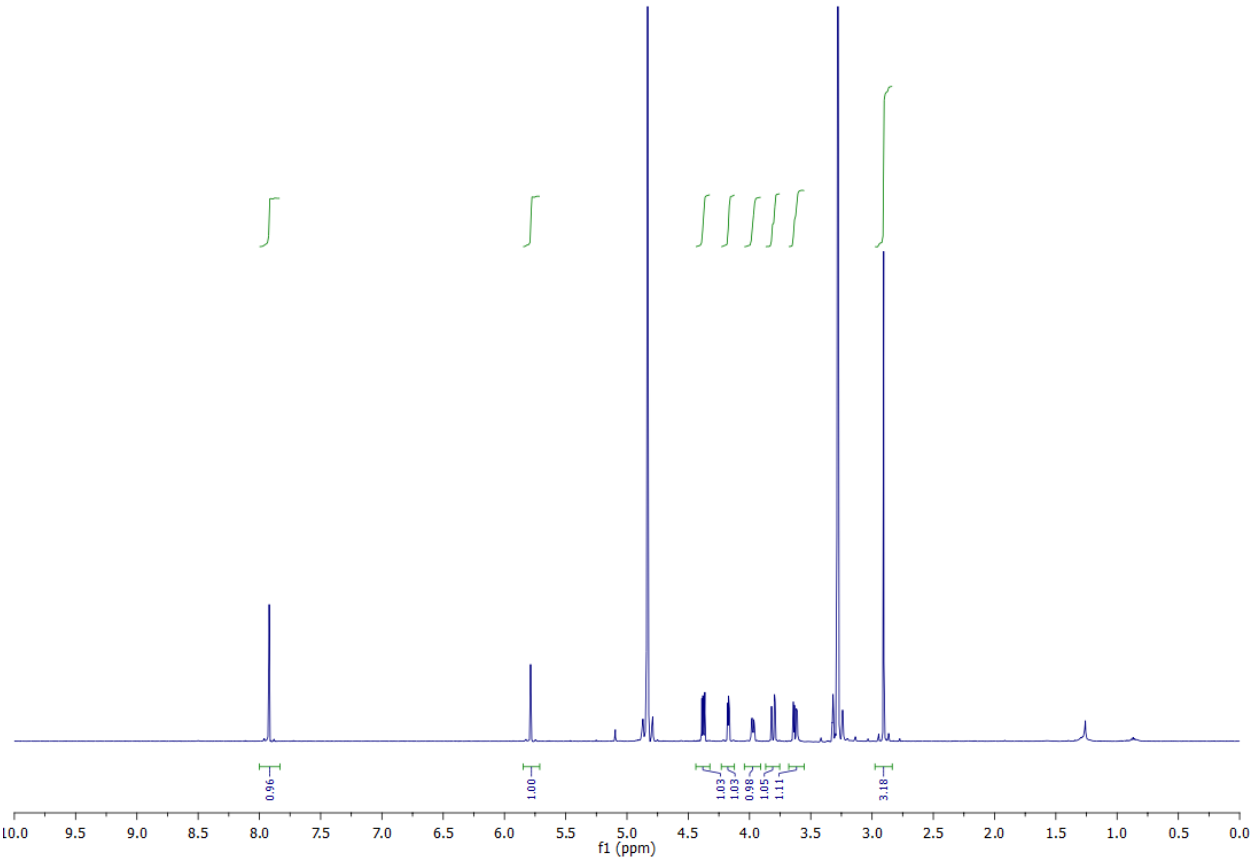

Figure 2.49 ^{1}H NMR spectra of ^{mth}A in the alpha configuration in CD_3OD

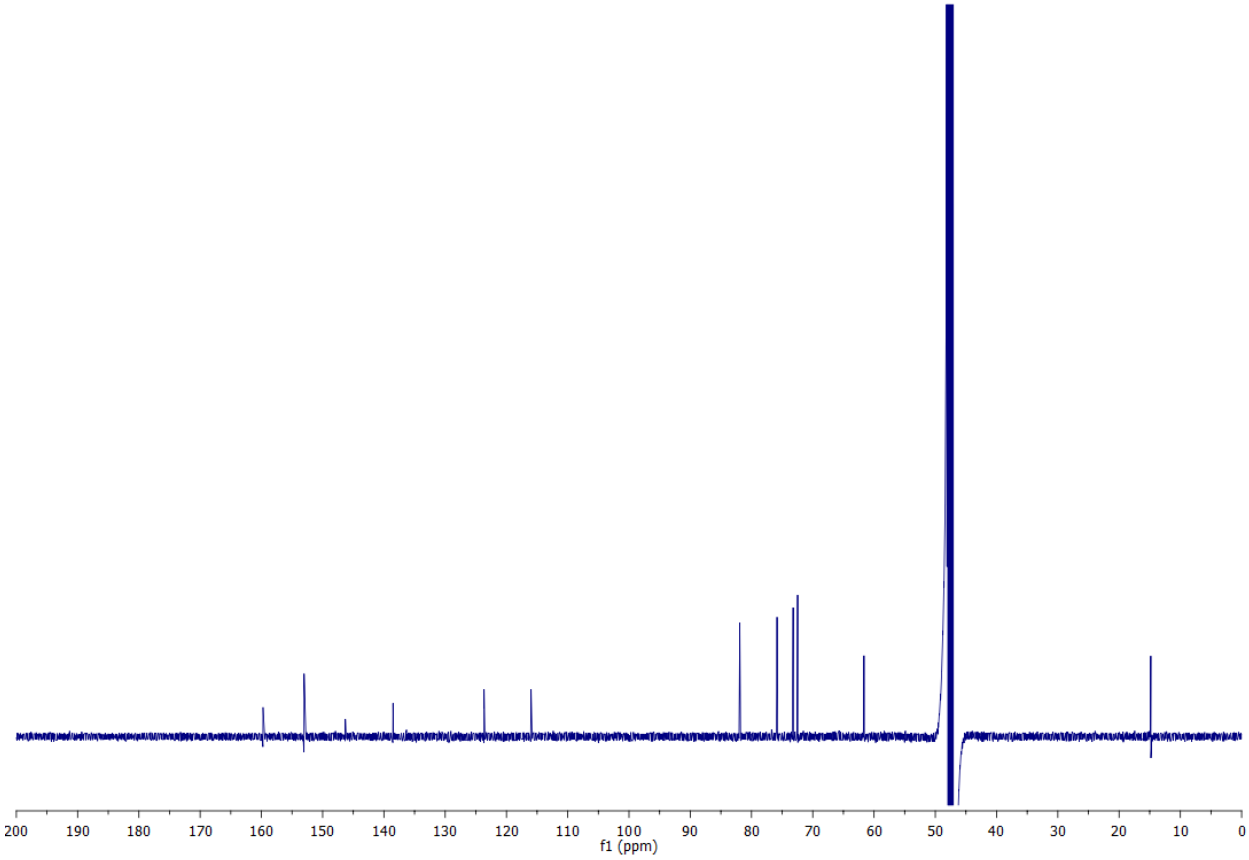

Figure 2.50 ^{13}C NMR spectra of ^{mth}A in the alpha configuration in CD_3OD

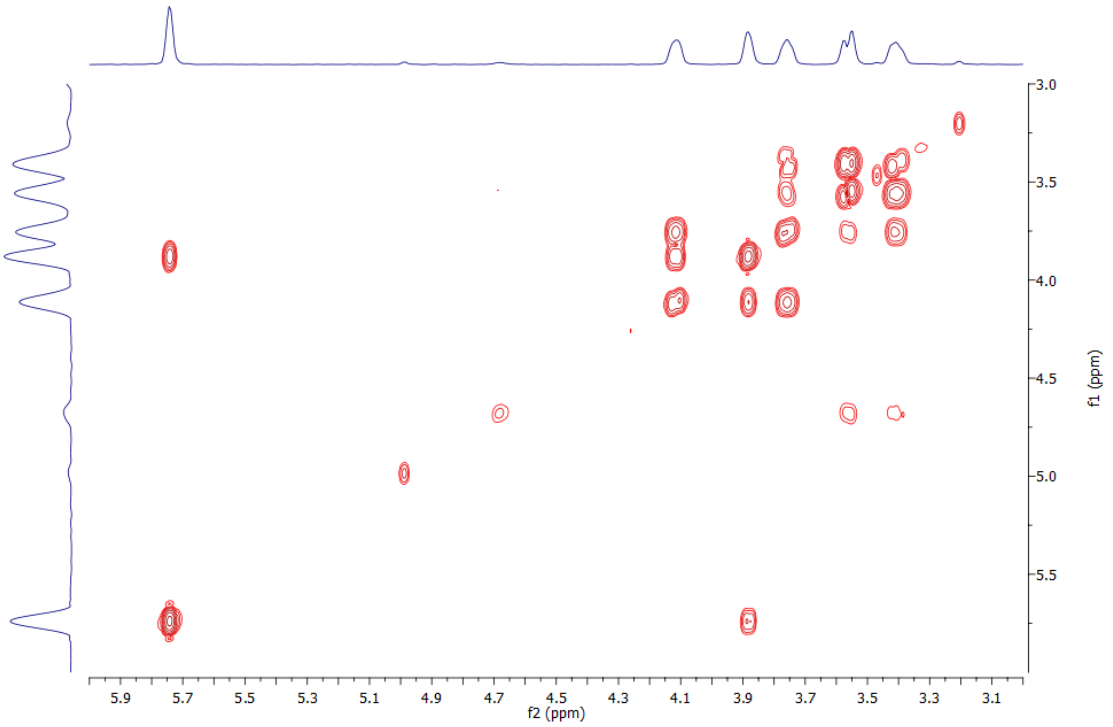

Figure 2.51 Relevant COSY correlations of ^{mth}A in the alpha configuration in DMSO-d_6; H-1' correlated with H-2'; H-2' correlated with H-3'; H-3' correlated with H-4'; H-4' correlated with H-5'.

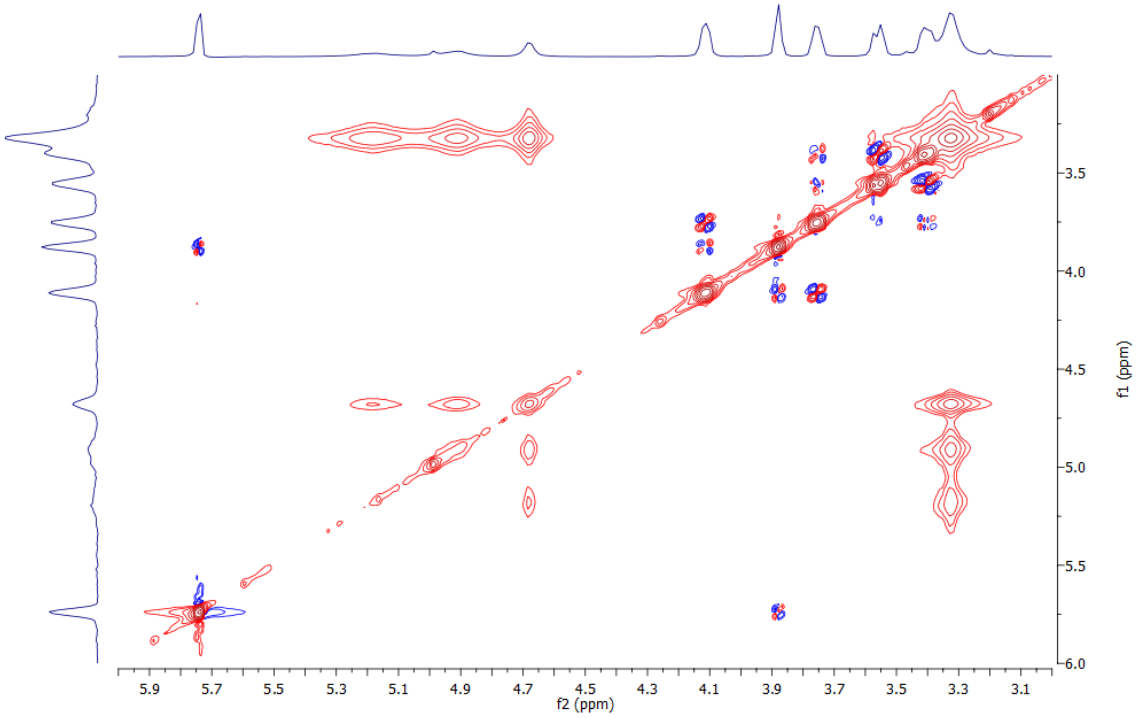

Figure 2.52 Relevant NOESY correlations of ^{mth}A in the alpha configuration in DMSO-d_6; H-1' correlated with H-2'; H-2' correlated with H-3'; H-3' correlated with H-4'; H-4' correlated with H-5'.

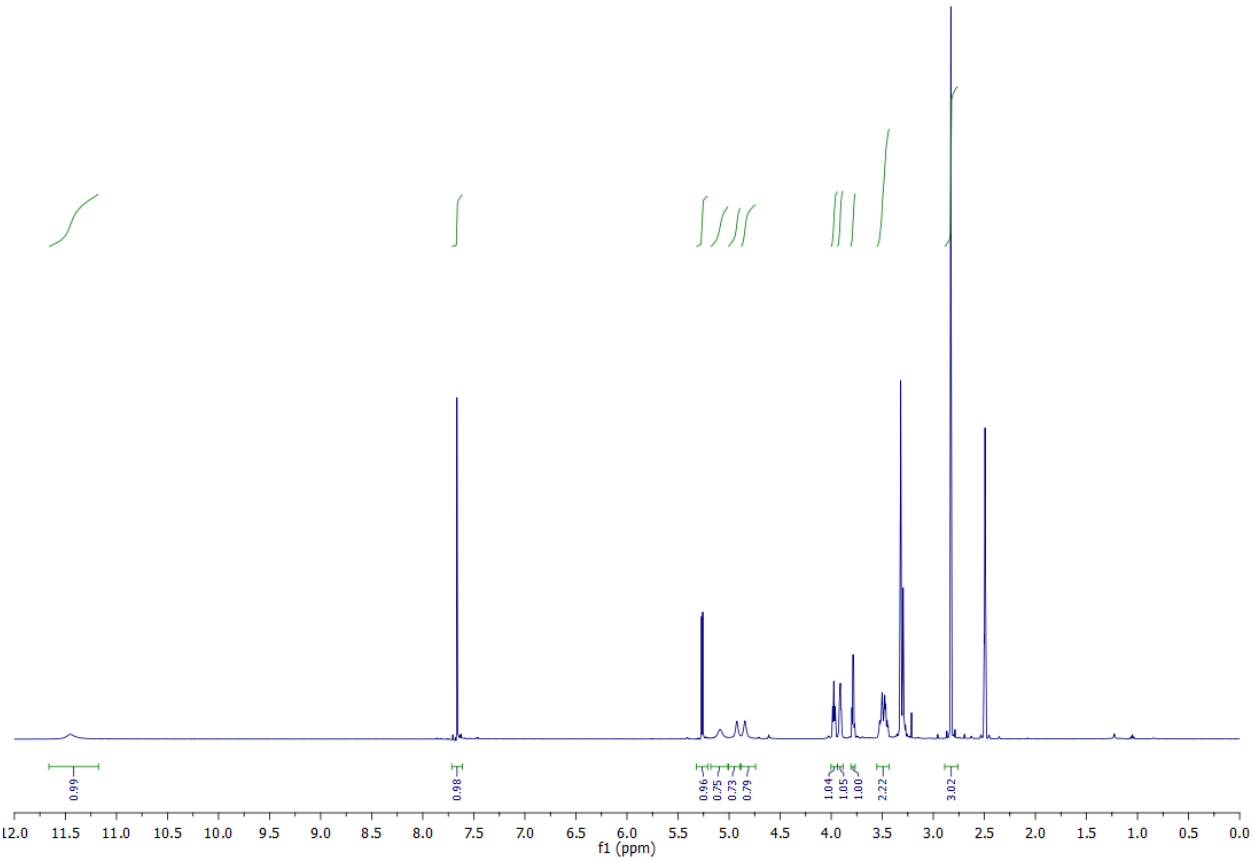

Figure 2.53 ^{1}H NMR spectra of ^{mth}I in DMSO-d_6

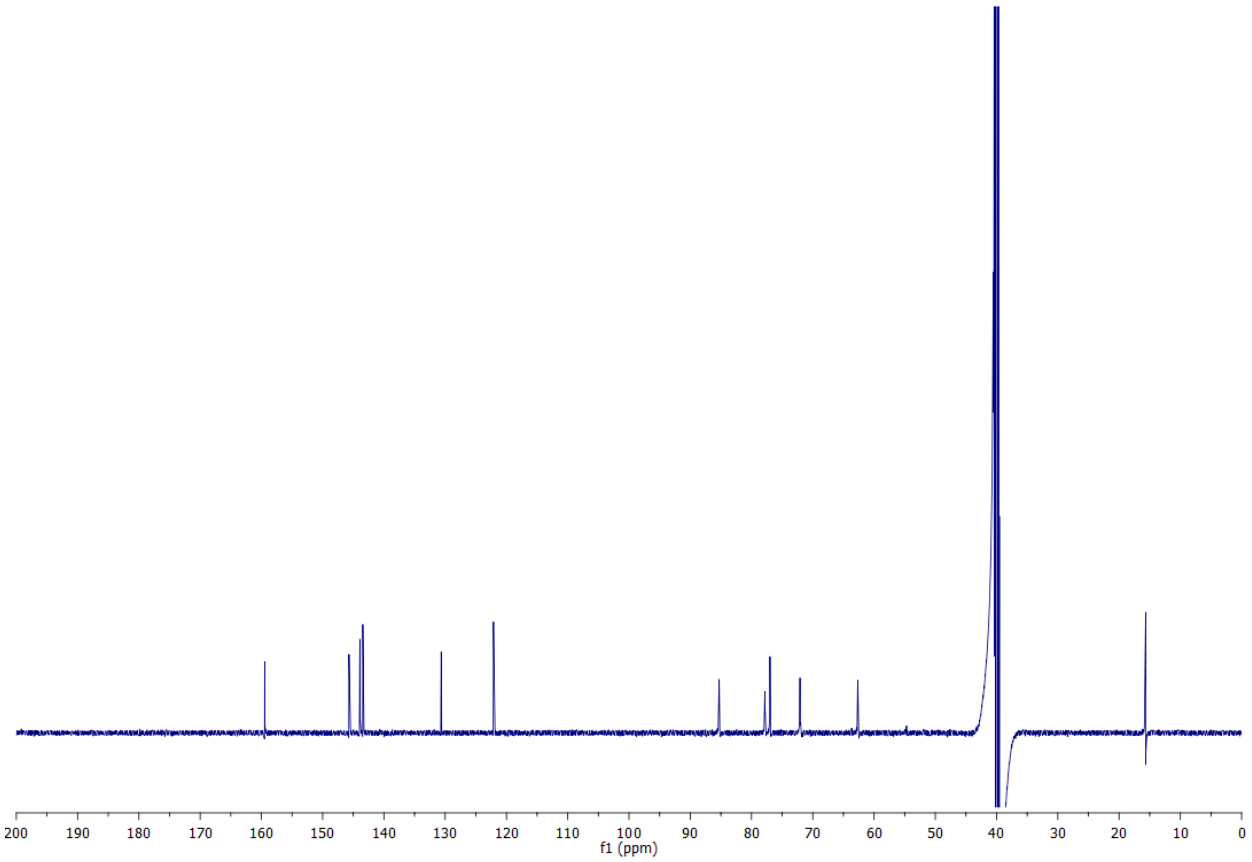

Figure 2.54 ^{13}C NMR spectra of ^{mth}I in DMSO-d_6

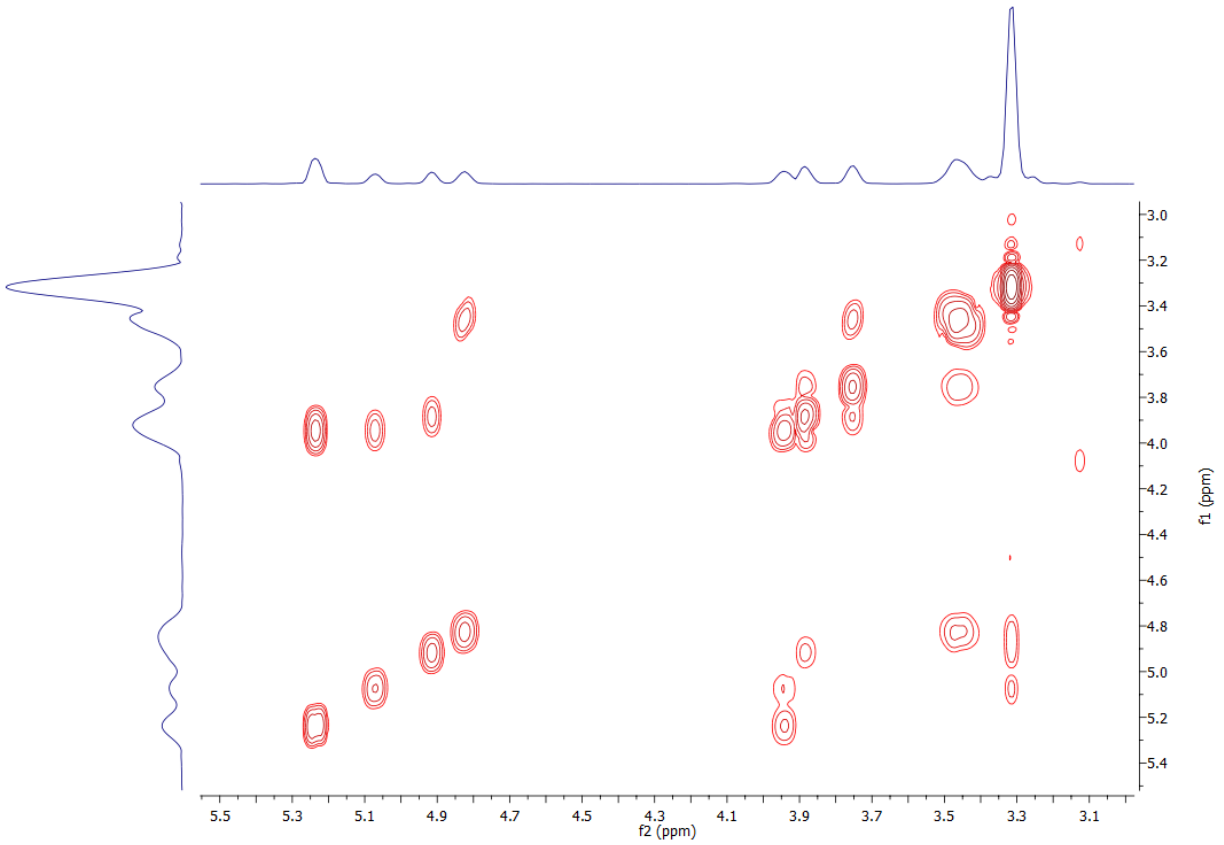

Figure 2.55 Relevant COSY correlations of ^{mth}I in DMSO-d_6; H-1' correlated with H-2'; H-2' correlated with H-3' and 2'-OH; H-3' correlated with H-4' and 3'-OH; H-4' correlated with H-5'; H-5' correlated with 5'-OH.

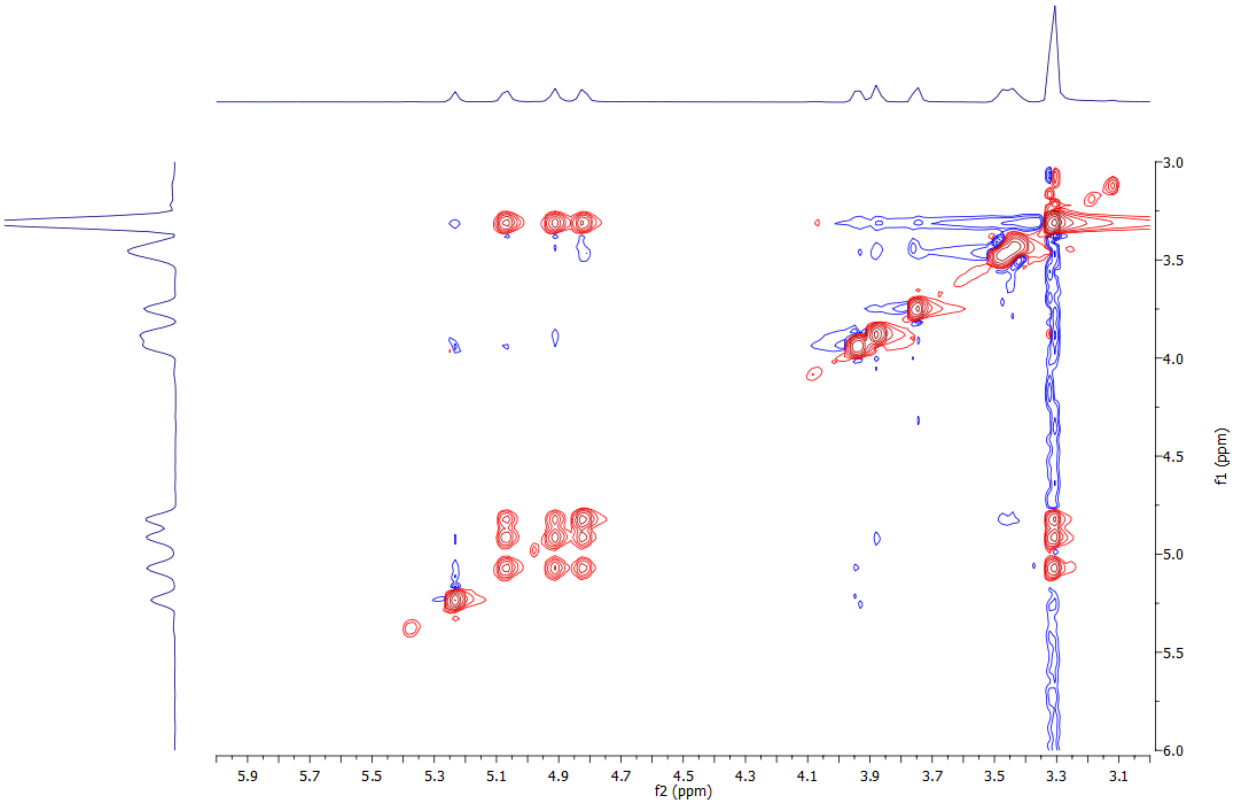

Figure 2.56 Relevant NOESY correlations of ^{mth}I in DMSO-d_6; H-1' correlated with H-2' and 2'-OH; H-2' correlated with H-3' and 2'-OH; H-3' correlated with 3'-OH; H-4' correlated with H-5'; H-5' correlated with 5'-OH.

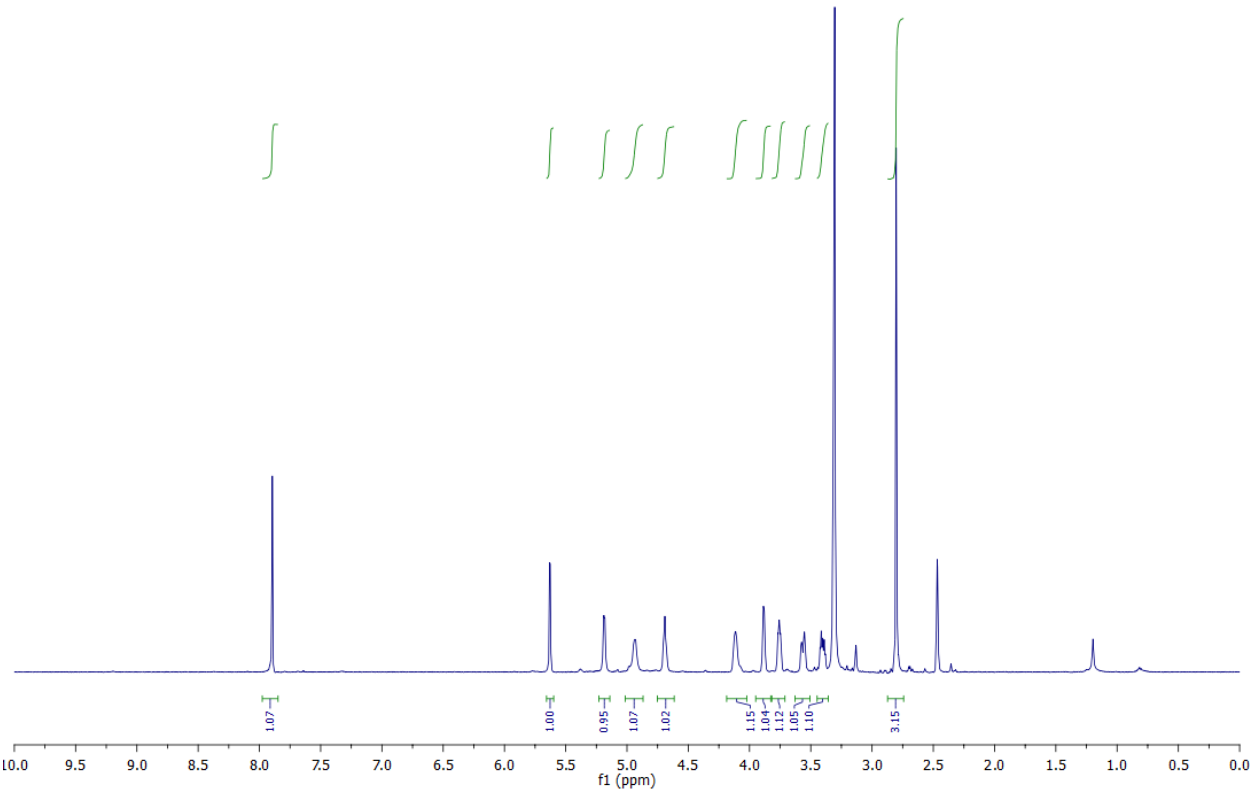

Figure 2.57 ^{1}H NMR spectra of ^{mth}I in the alpha configuration in DMSO-d_6

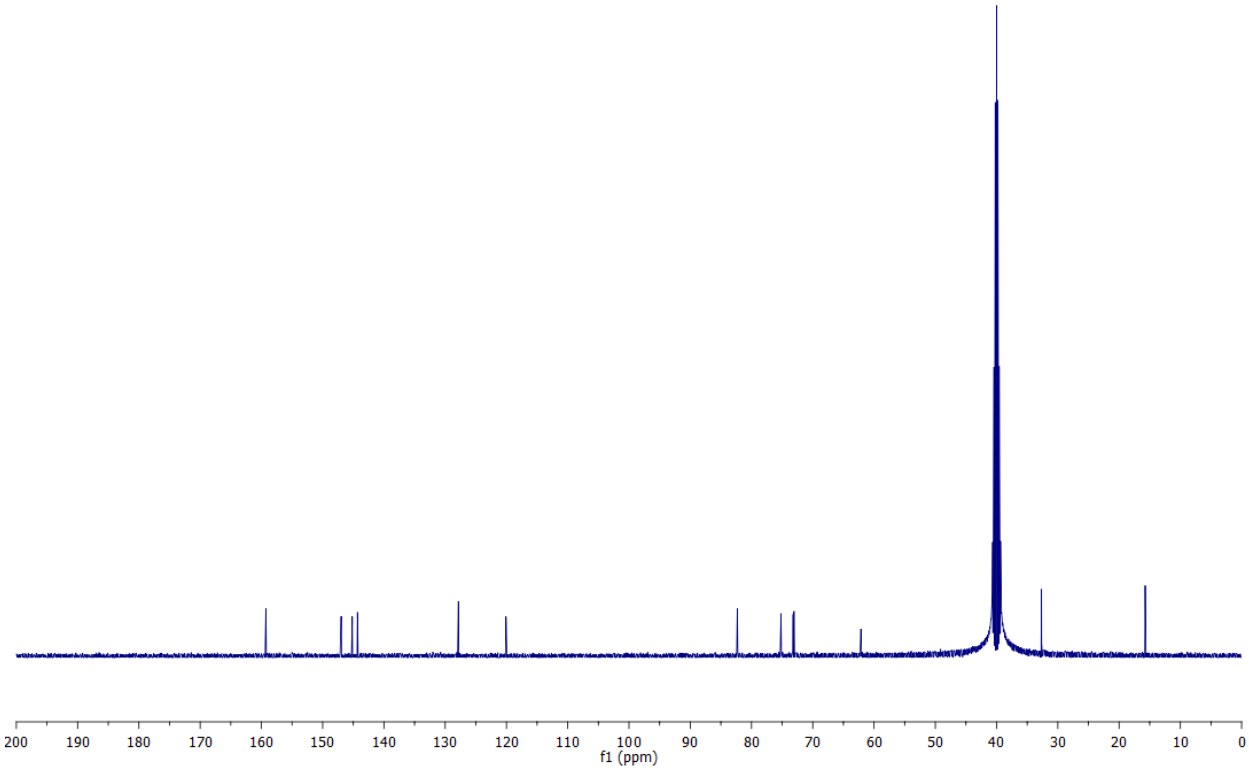

Figure 2.58 ^{13}C NMR spectra of ^{mth}I in the alpha configuration in DMSO-d_6

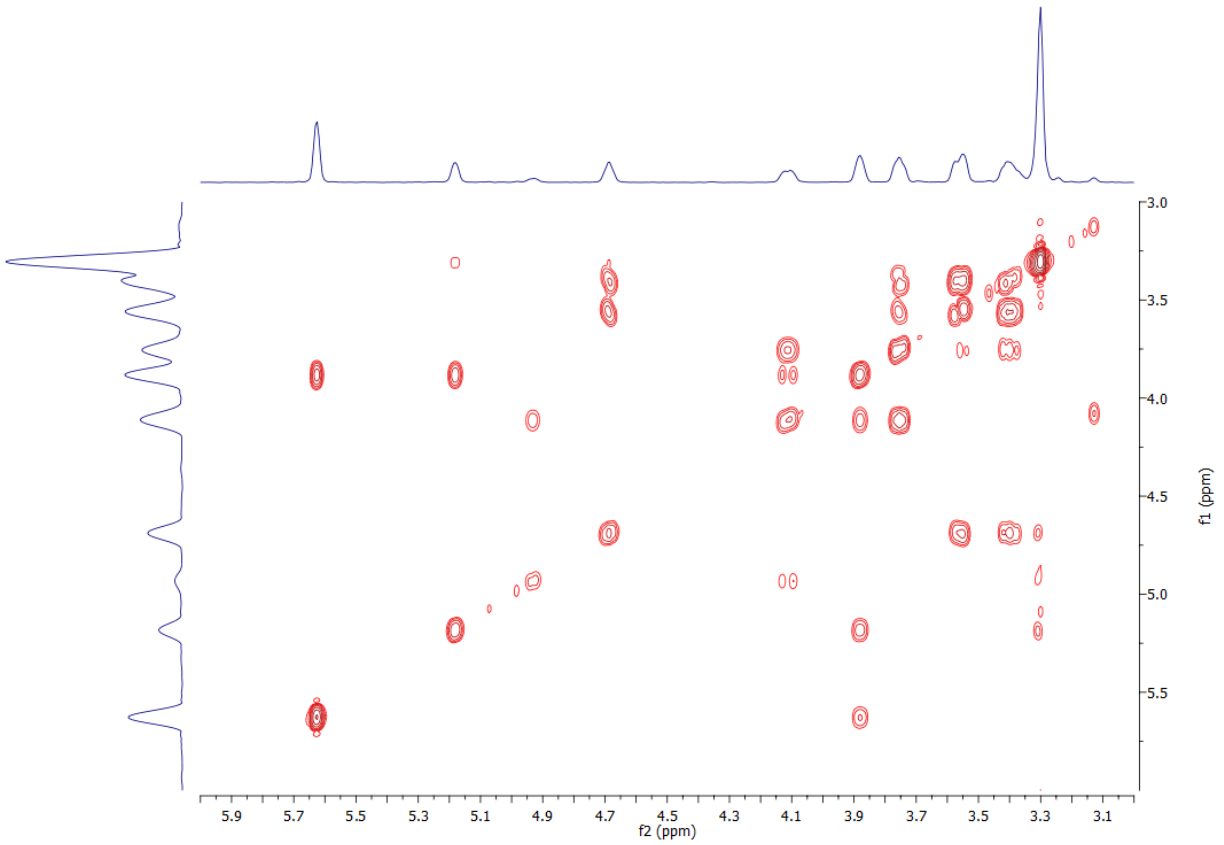

Figure 2.59 Relevant COSY correlations of ^{mth}I in the alpha configuration in DMSO-d_6; H-1' correlated with H-2'; H-2' correlated with H-3' and 2'-OH; H-3' correlated with H-4' and 3'-OH; H-4' correlated with H-5'; H-5' correlated with 5'-OH.

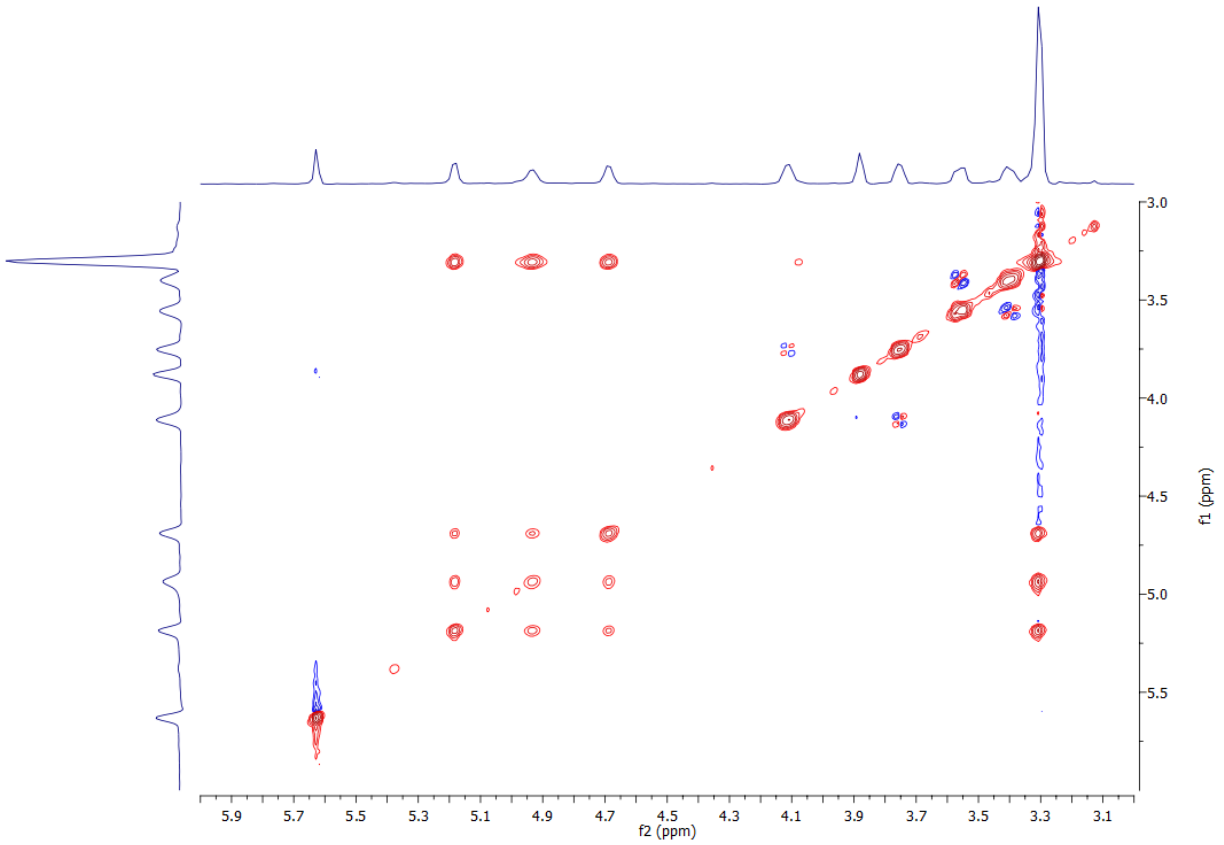

Figure 2.60 Relevant NOESY correlations of ^{mth}I in the alpha configuration in DMSO-d_6; H-1' correlated with H-2' and 2'-OH; H-2' correlated with H-3' and 2'-OH; H-3' correlated with 3'-OH; H-4' correlated with H-5'; H-5' correlated with 5'-OH.

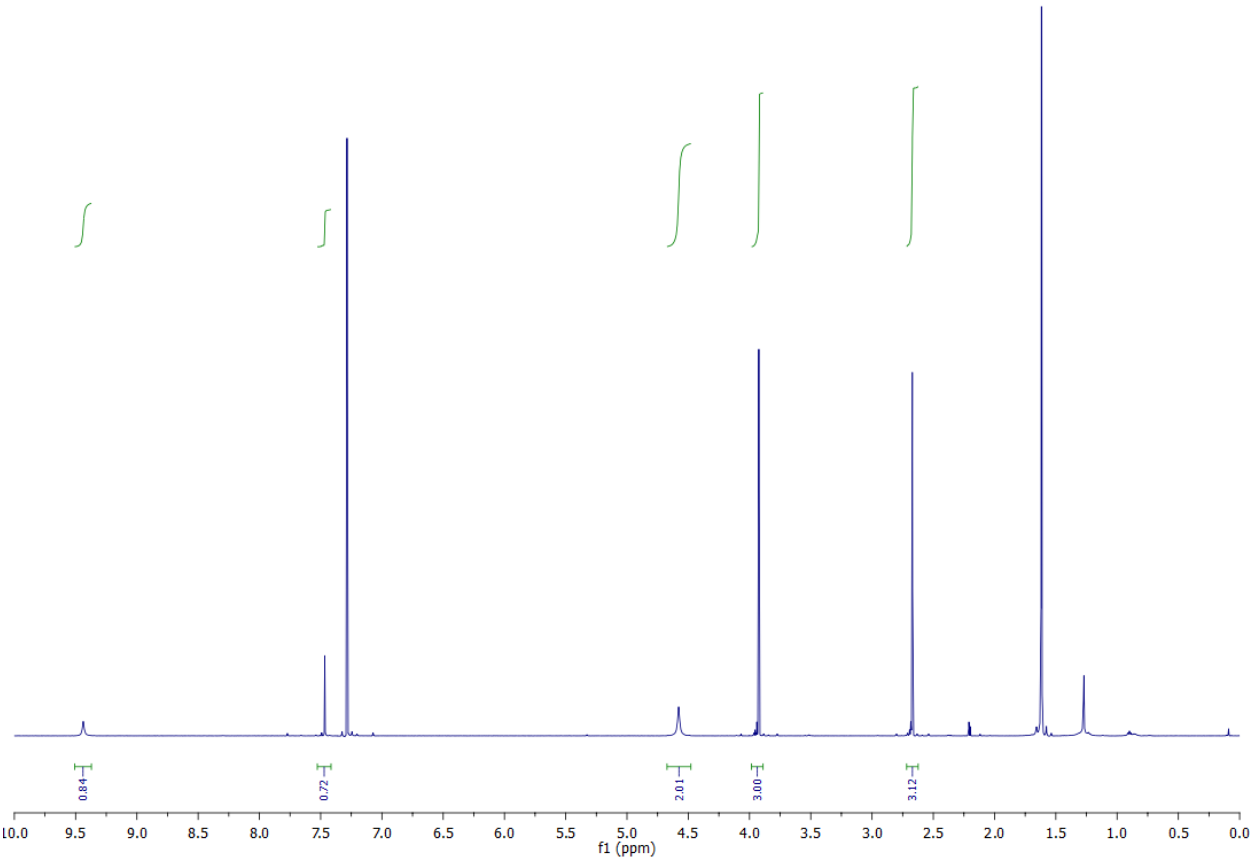

Figure 2.61 ^{1}H NMR spectra of **13** in $CDCl_3$

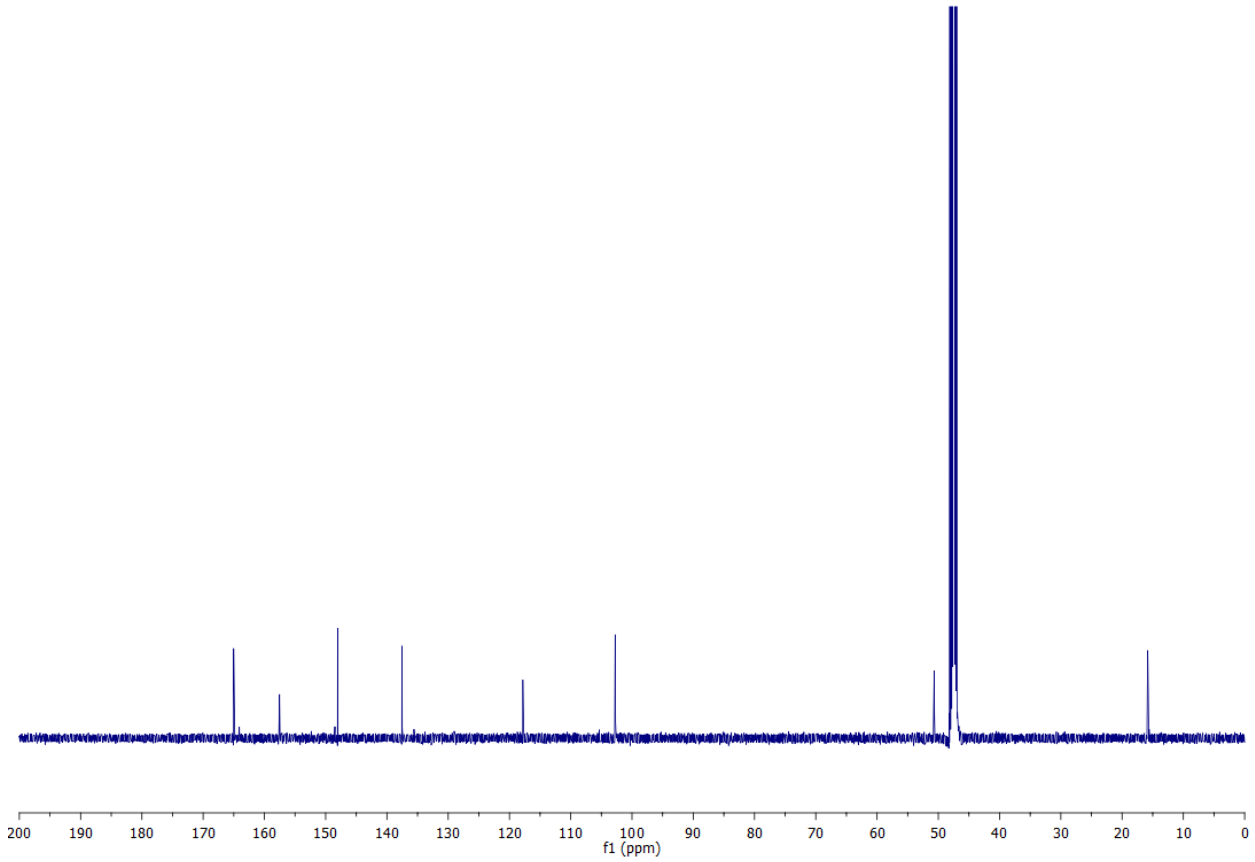

Figure 2.62 ^{13}C NMR spectra of **13** in CD_3OD

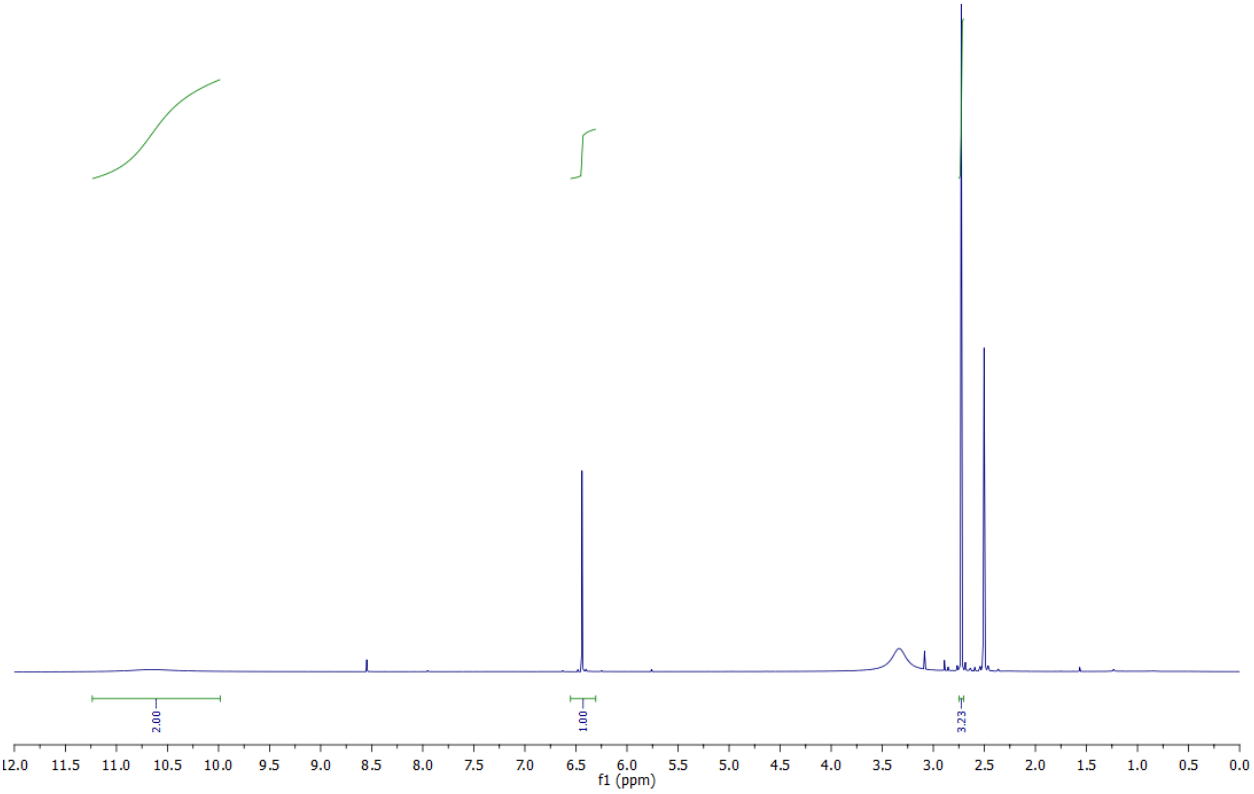

Figure 2.63 ^{1}H NMR spectra of **14** in DMSO-d_6

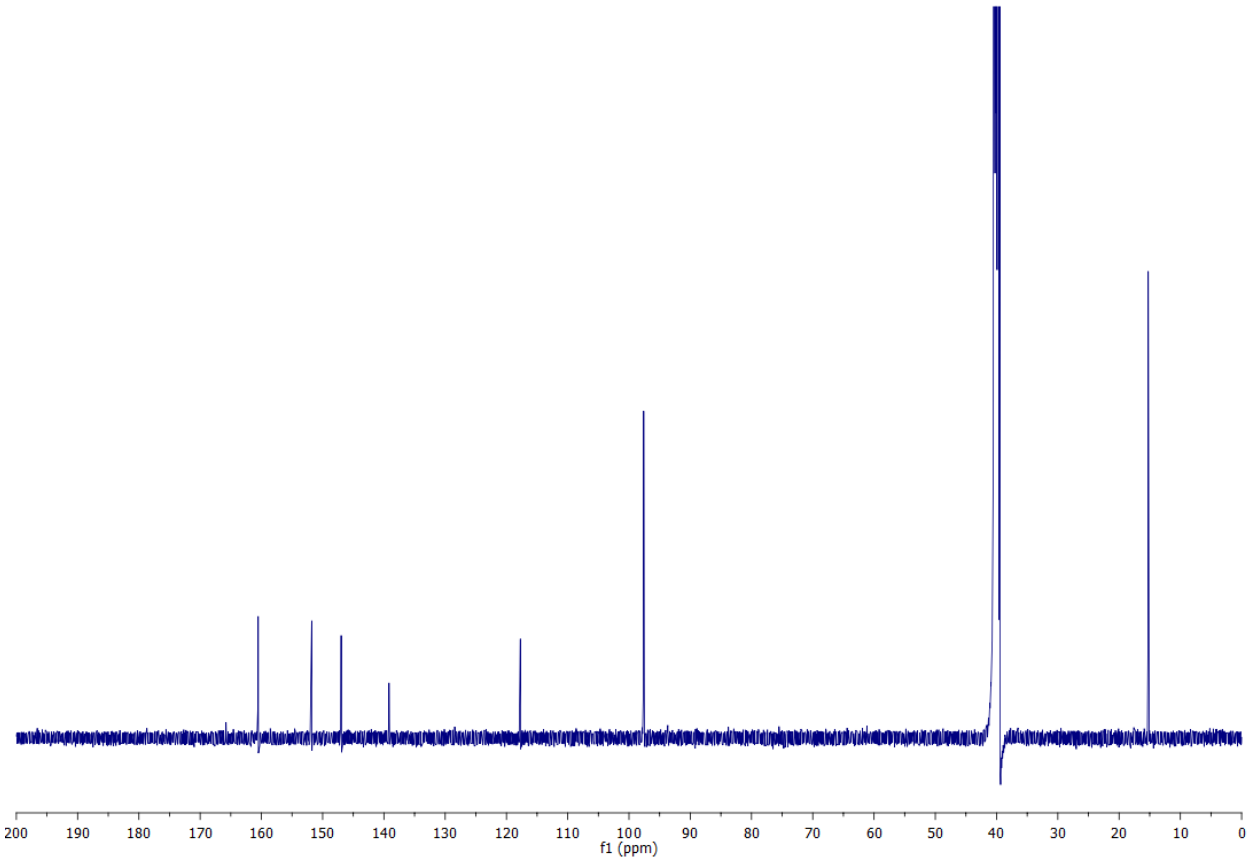

Figure 2.64 ^{13}C NMR spectra of **14** in DMSO-d_6

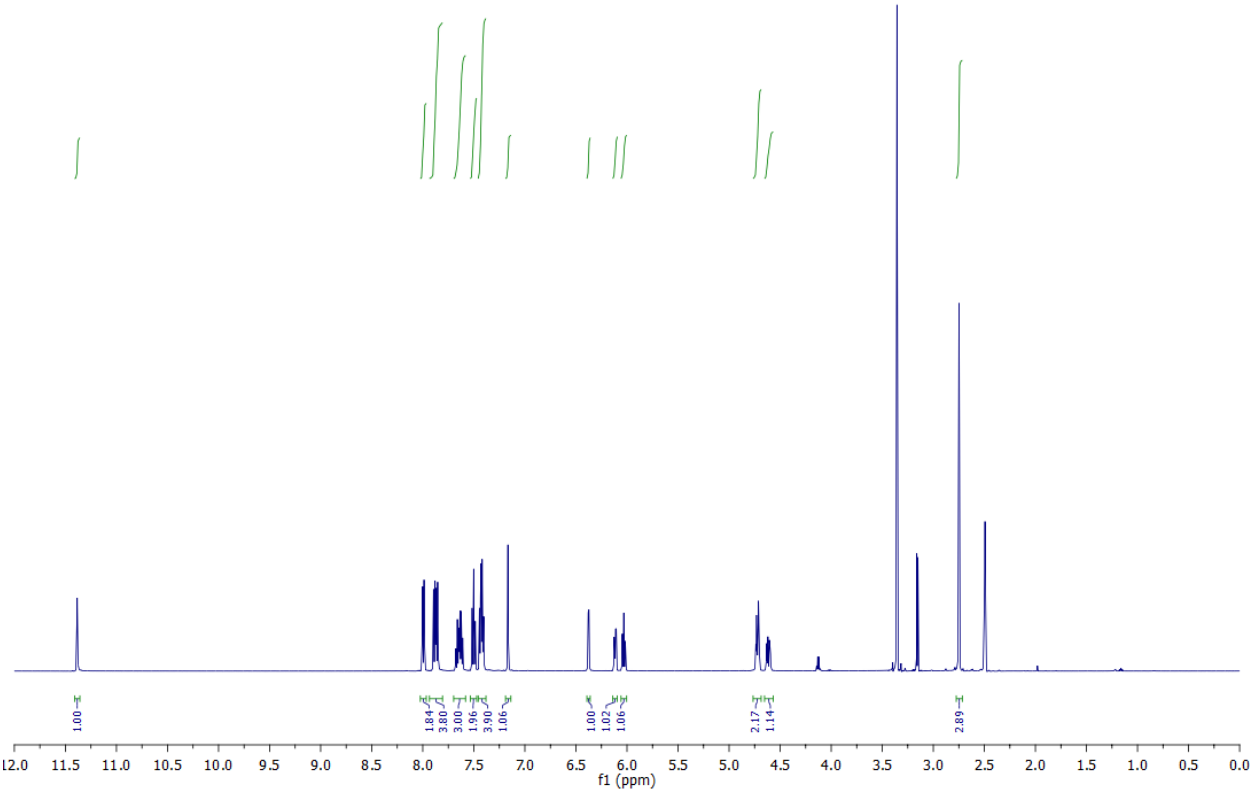

Figure 2.65 ^{1}H NMR spectra of **15** in DMSO-d_6

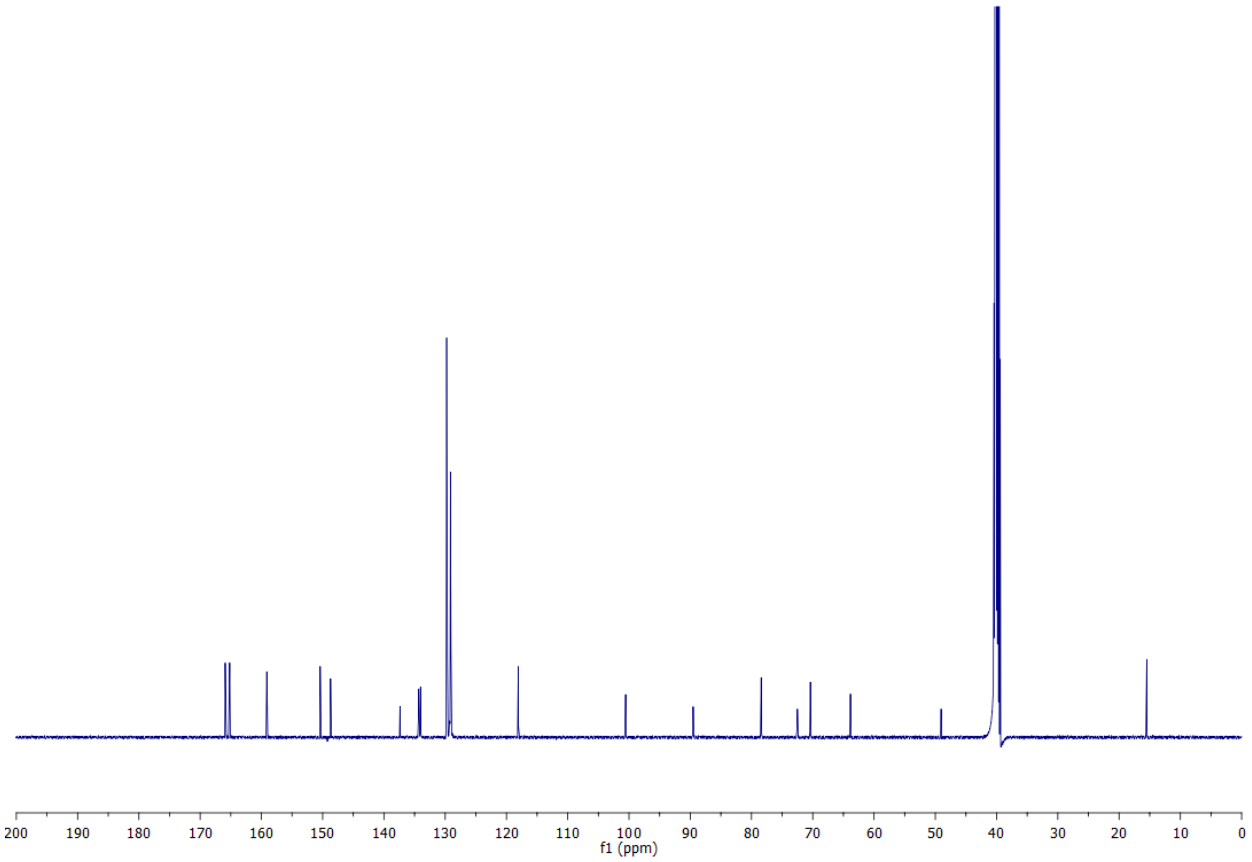

Figure 2.66 ^{13}C NMR spectra of **15** in DMSO-d_6

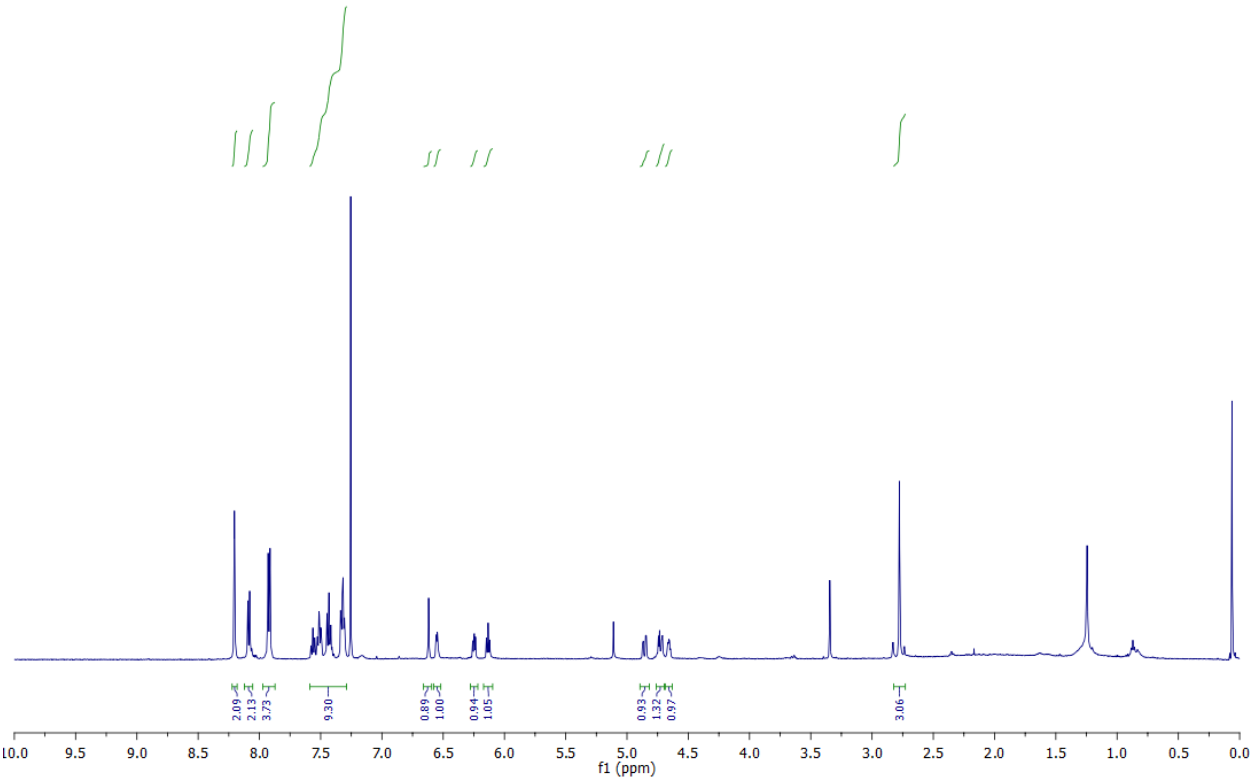

Figure 2.67 ^{1}H NMR spectra of **16** in $CDCl_3$

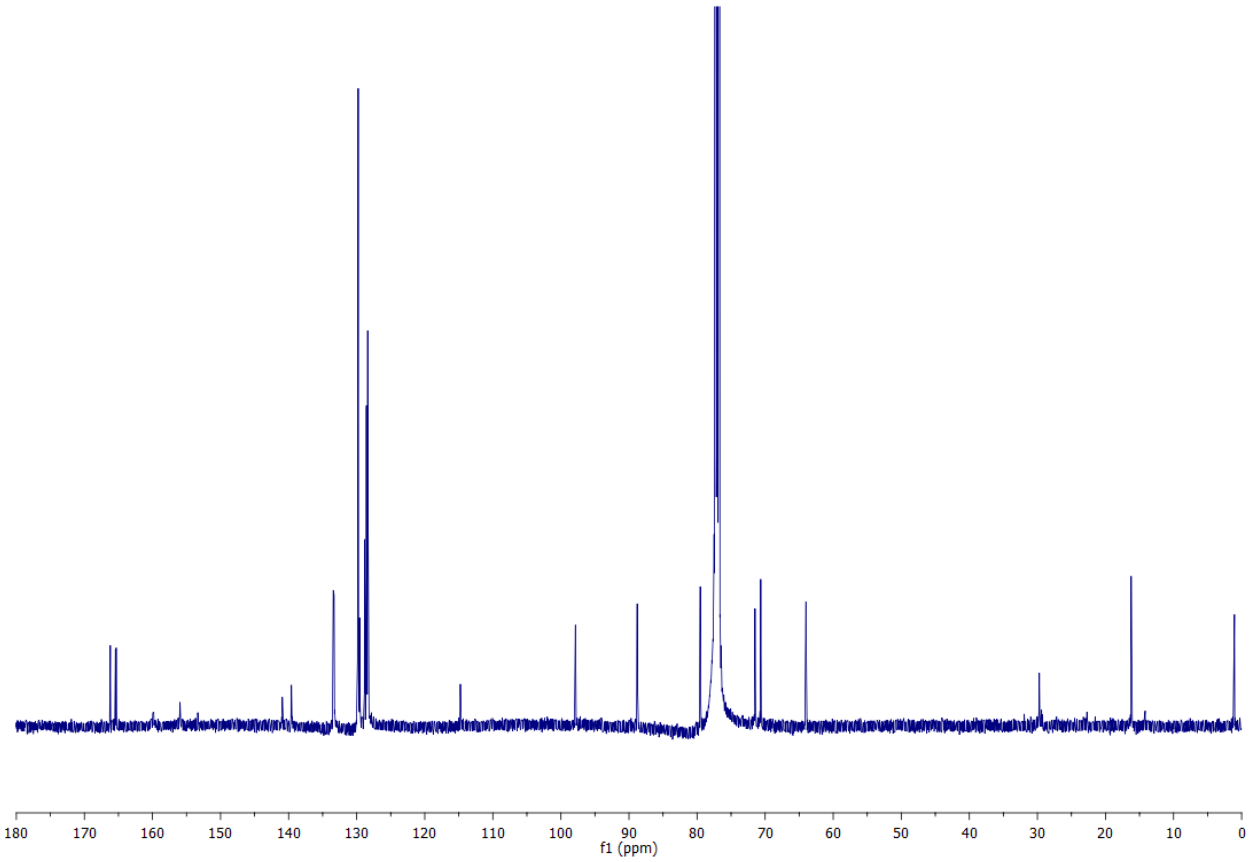

Figure 2.68 ^{13}C NMR spectra of **16** in $CDCl_3$

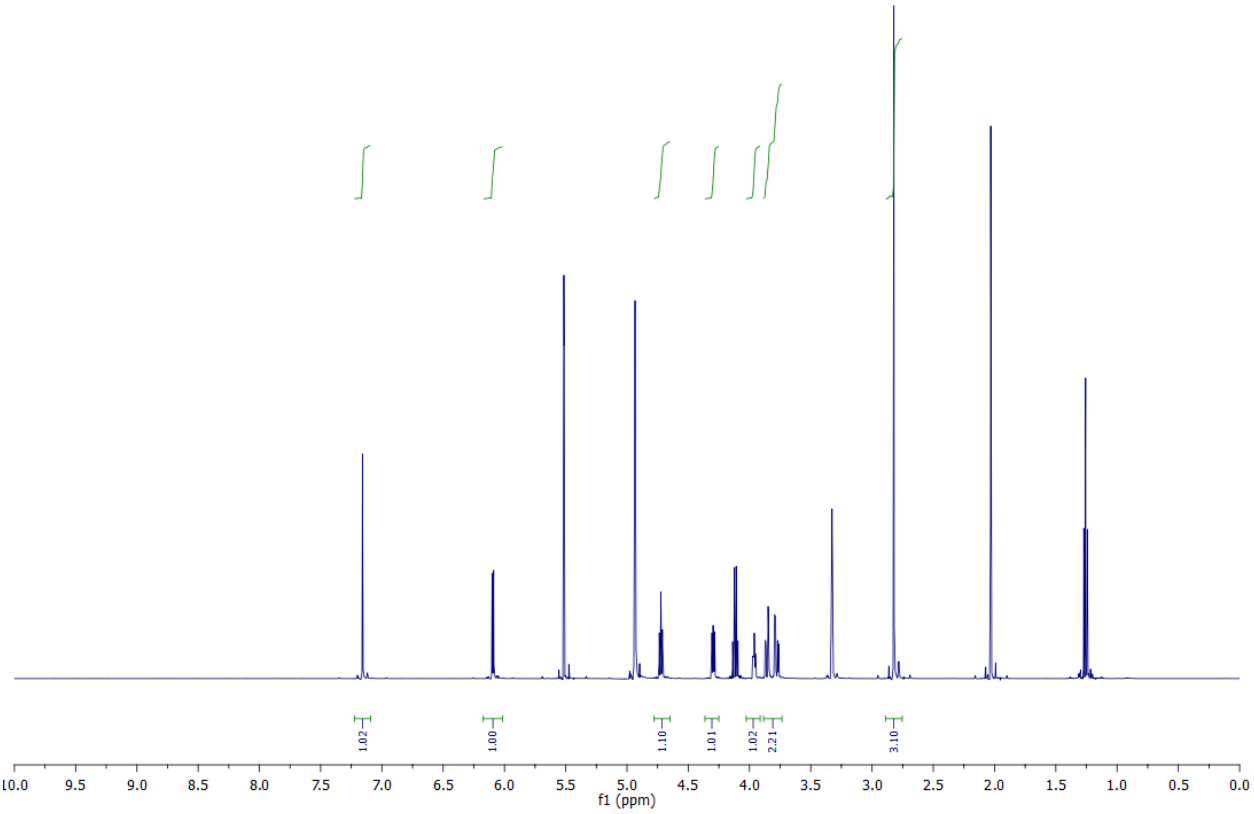

Figure 2.69 ^{1}H NMR spectra of ^{mth}U in CD_3OD

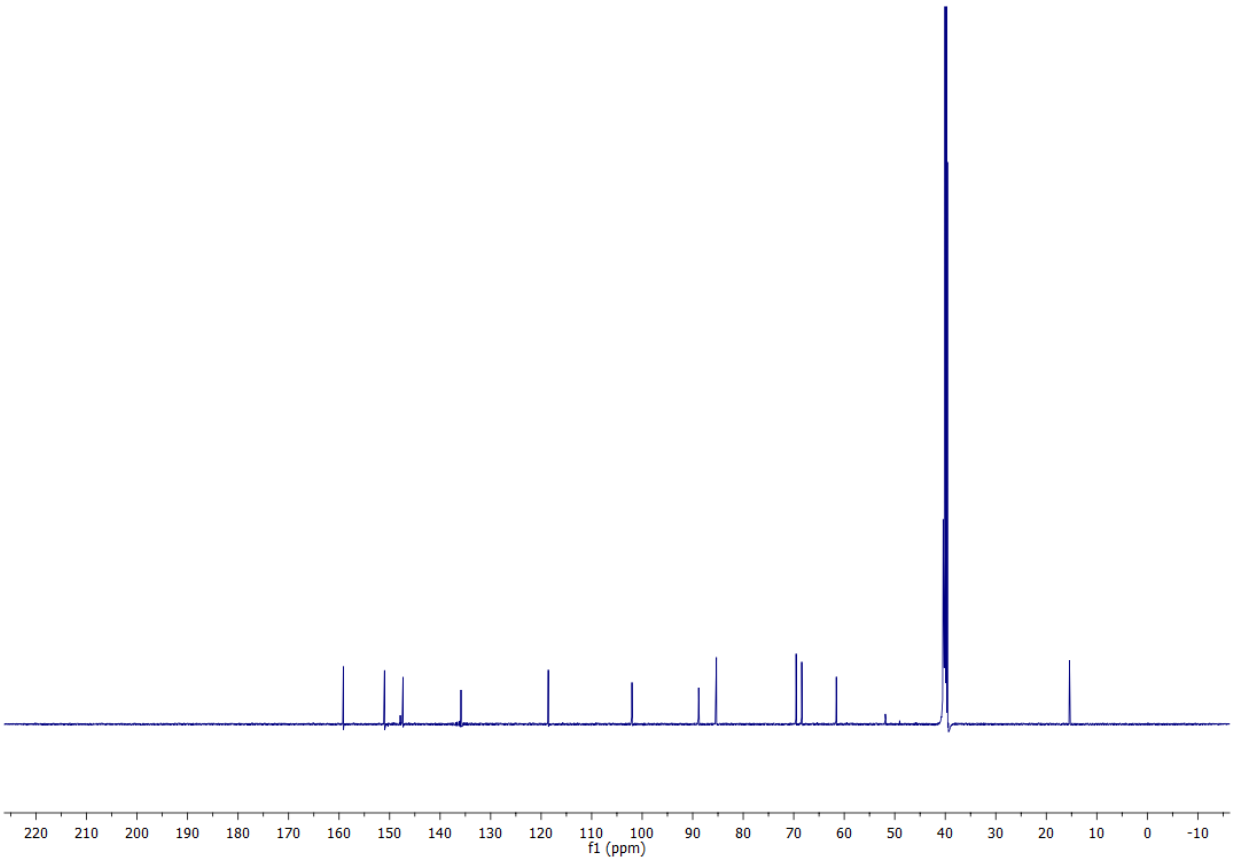

Figure 2.70 ^{13}C NMR spectra of ^{mth}U in CD_3OD

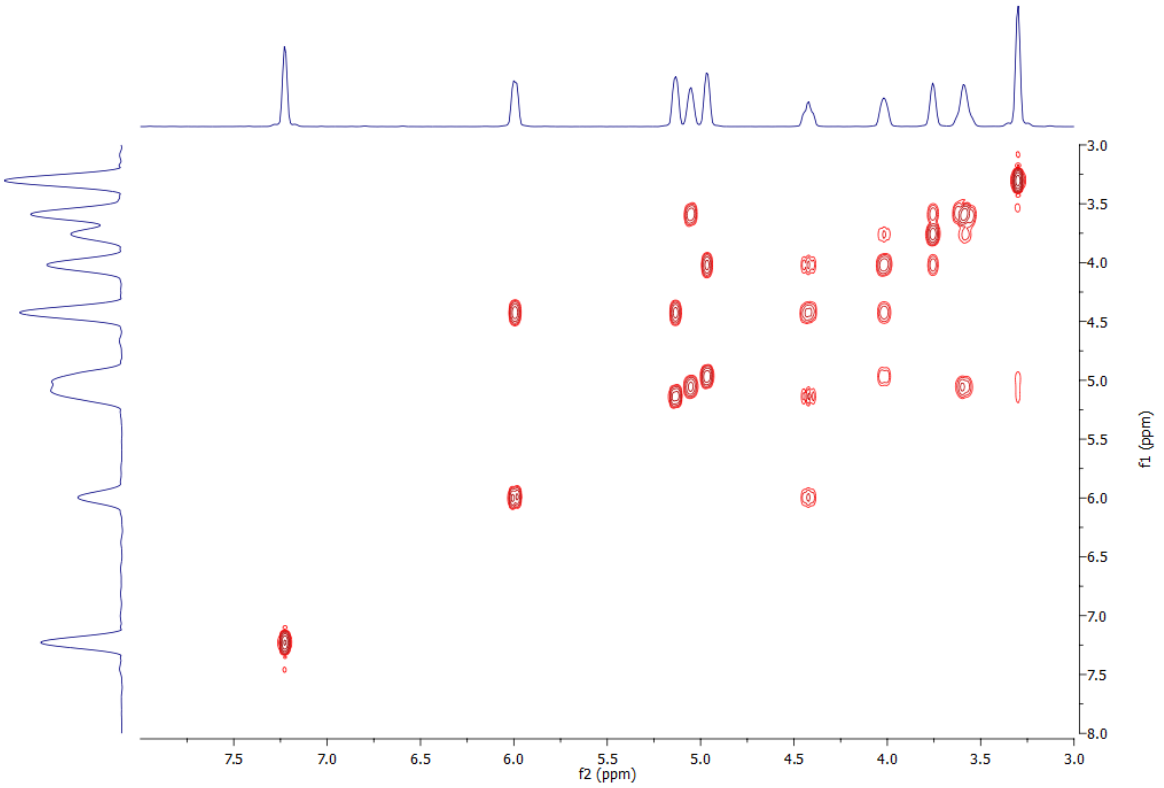

Figure 2.71 Relevant COSY correlations of ^{mth}U in DMSO-d_6; H-1' correlated with H-2'; H-2' correlated with H-3' and 2'-OH; H-3' correlated with H-4' and 3'-OH; H-4' correlated with H-5'; H-5' correlated with 5'-OH.

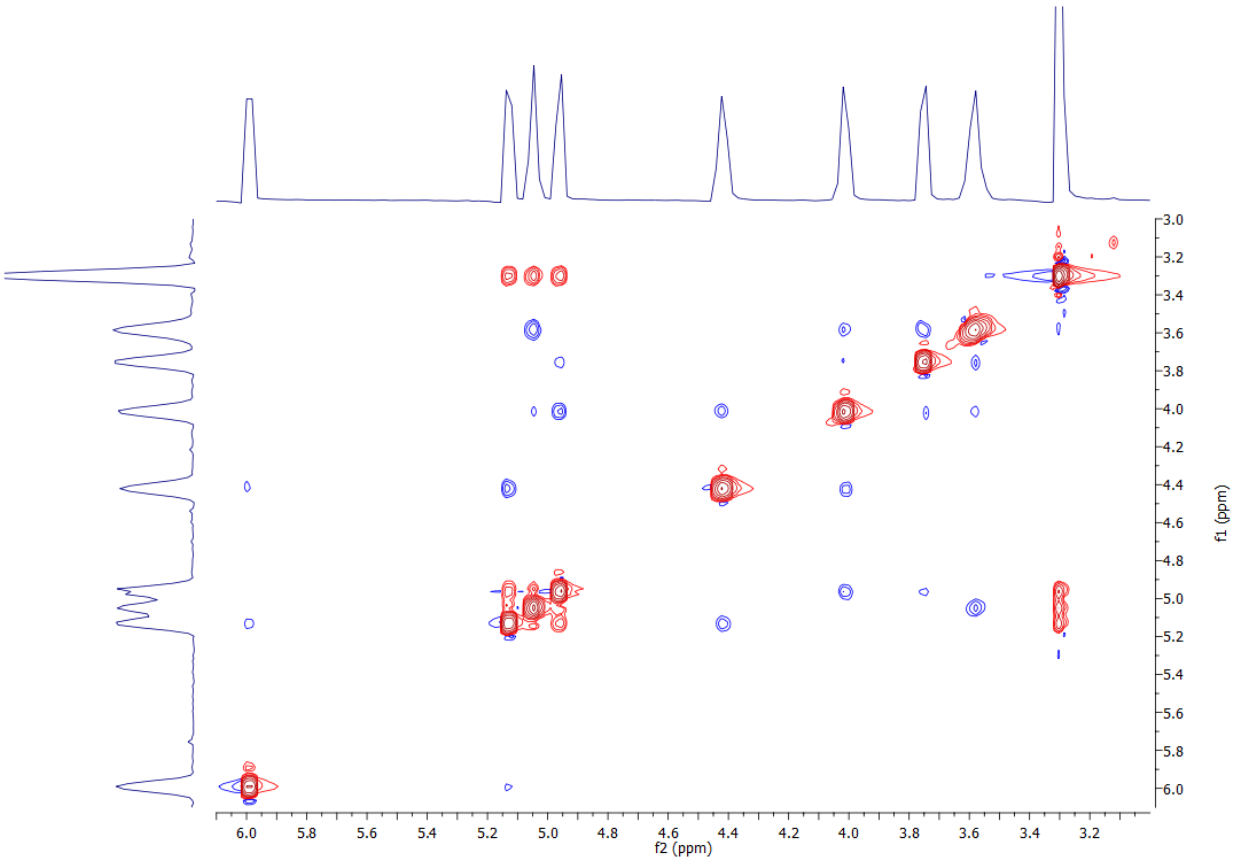

Figure 2.72 Relevant NOESY correlations of ^{mth}U in DMSO-d_6; H-1’ correlated with H-2’ and 2’-OH; H-2’ correlated with H-3’ and 2’-OH; H-3’ correlated with H-4’ and 3’-OH; H-4’ correlated with H-5’; H-5’ correlated with 5’-OH.

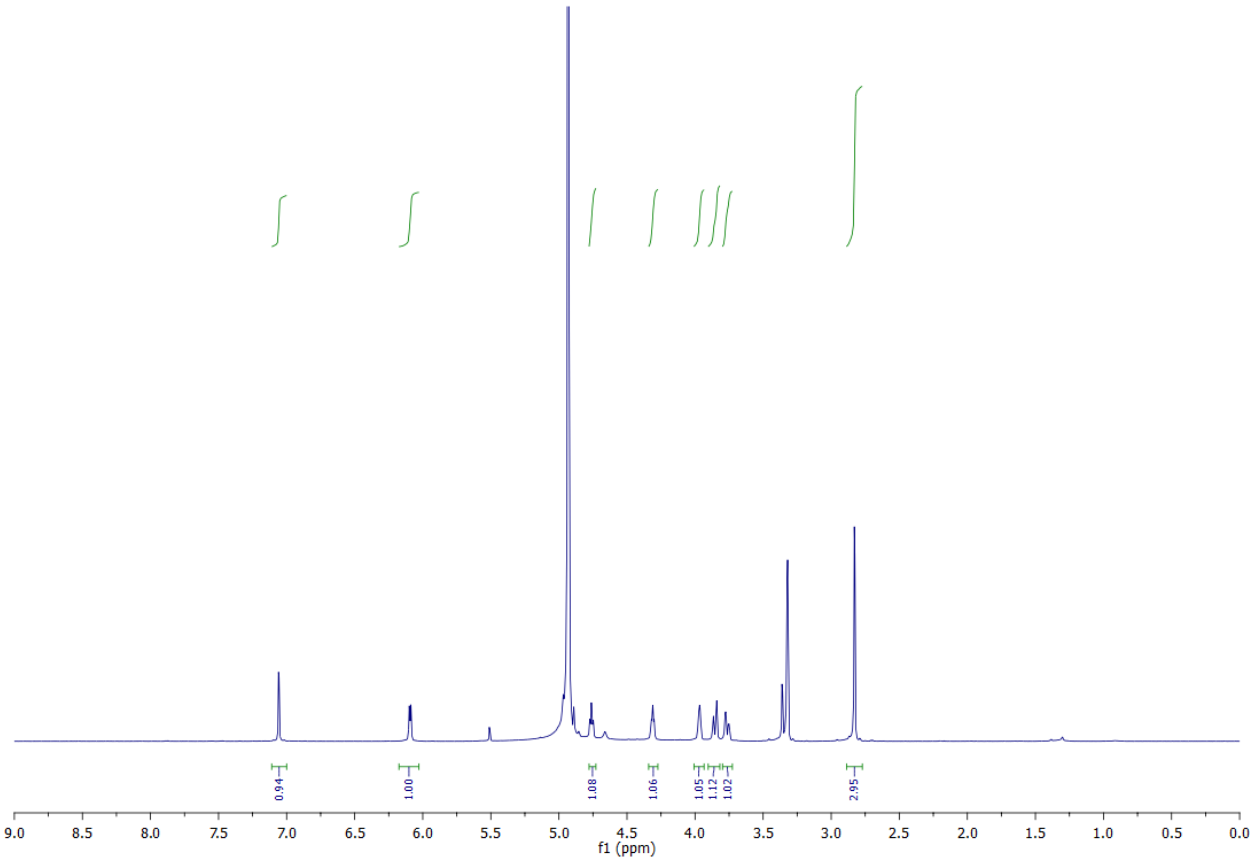

Figure 2.73 ^{1}H NMR spectra of ^{mth}C in CD_3OD

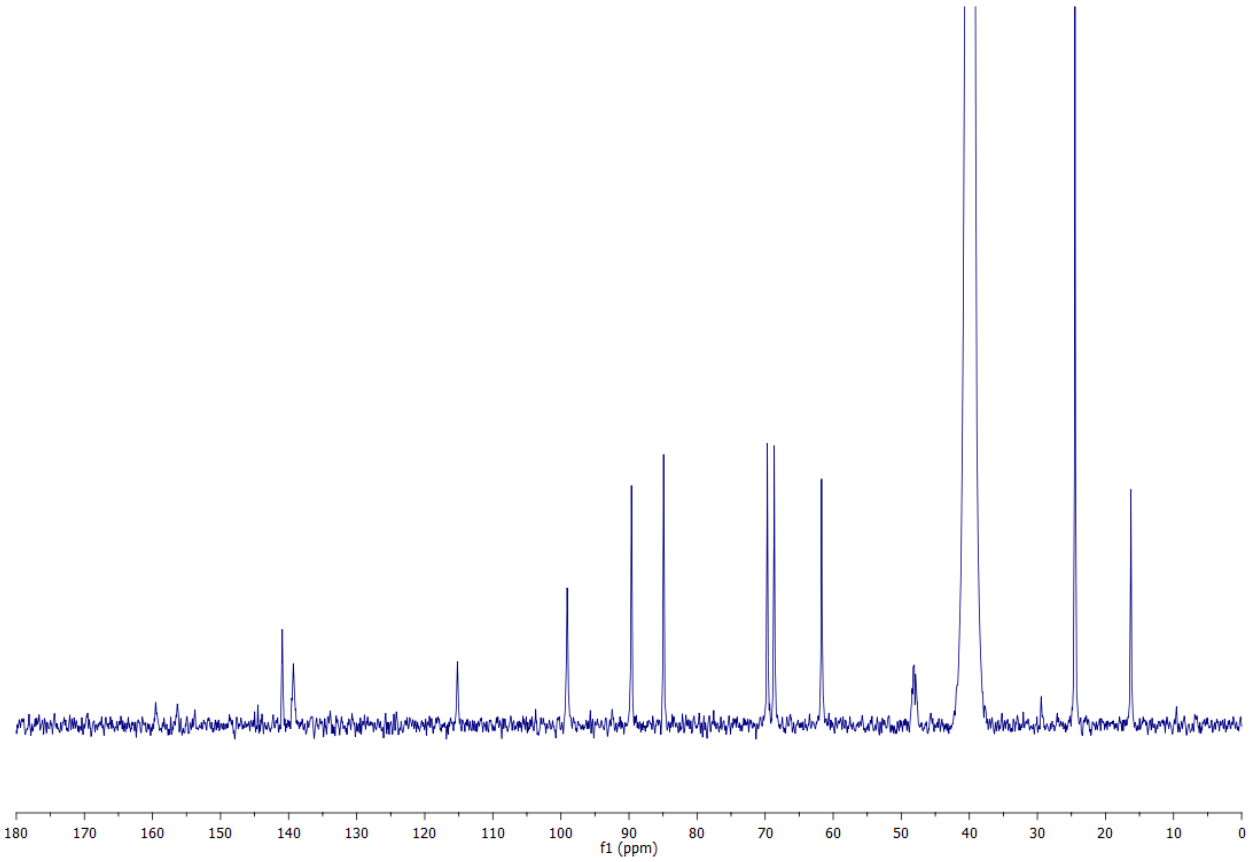

Figure 2.74 ^{13}C NMR spectra of ^{mth}C in CD_3OD

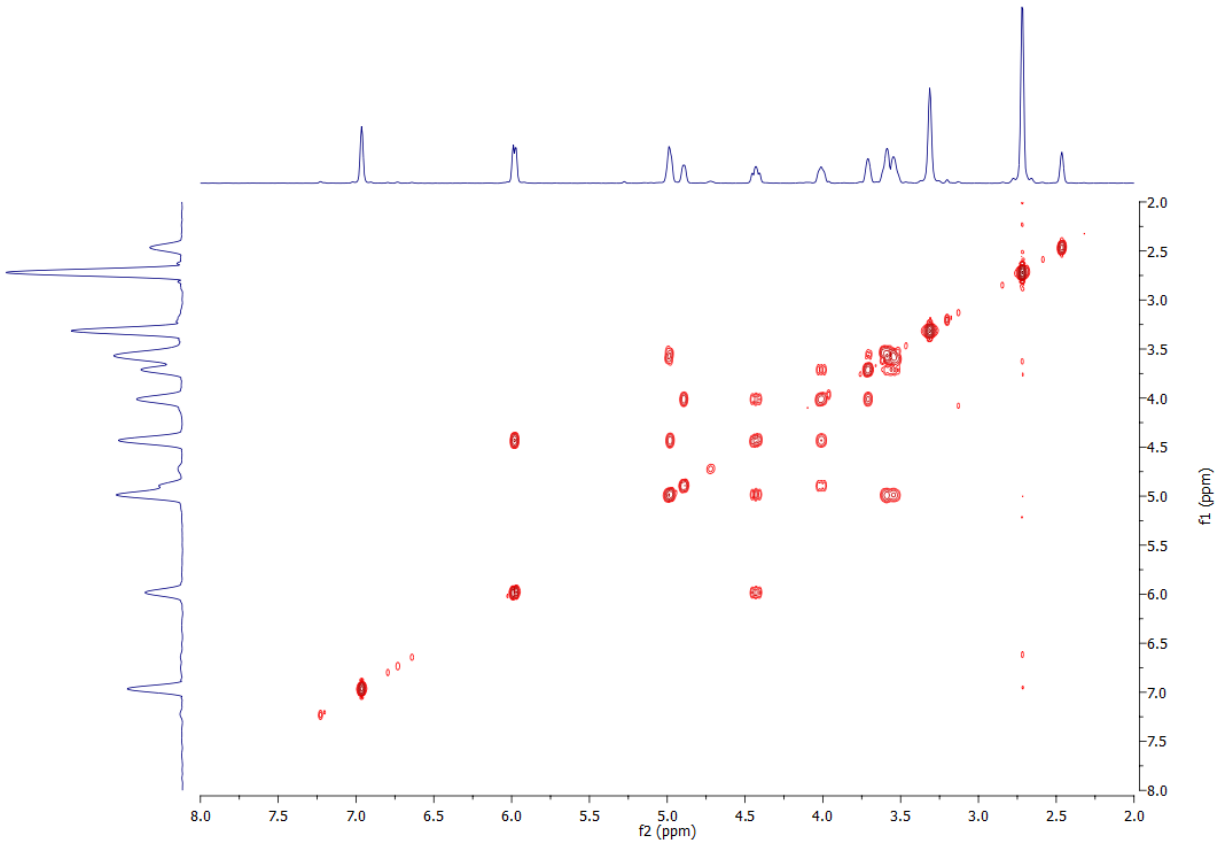

Figure 2.75 Relevant COSY correlations of ^{mth}C in DMSO-d_6; H-1' correlated with H-2'; H-2' correlated with H-3' and 2'-OH; H-3' correlated with H-4' and 3'-OH; H-4' correlated with H-5'; H-5' correlated with 5'-OH.

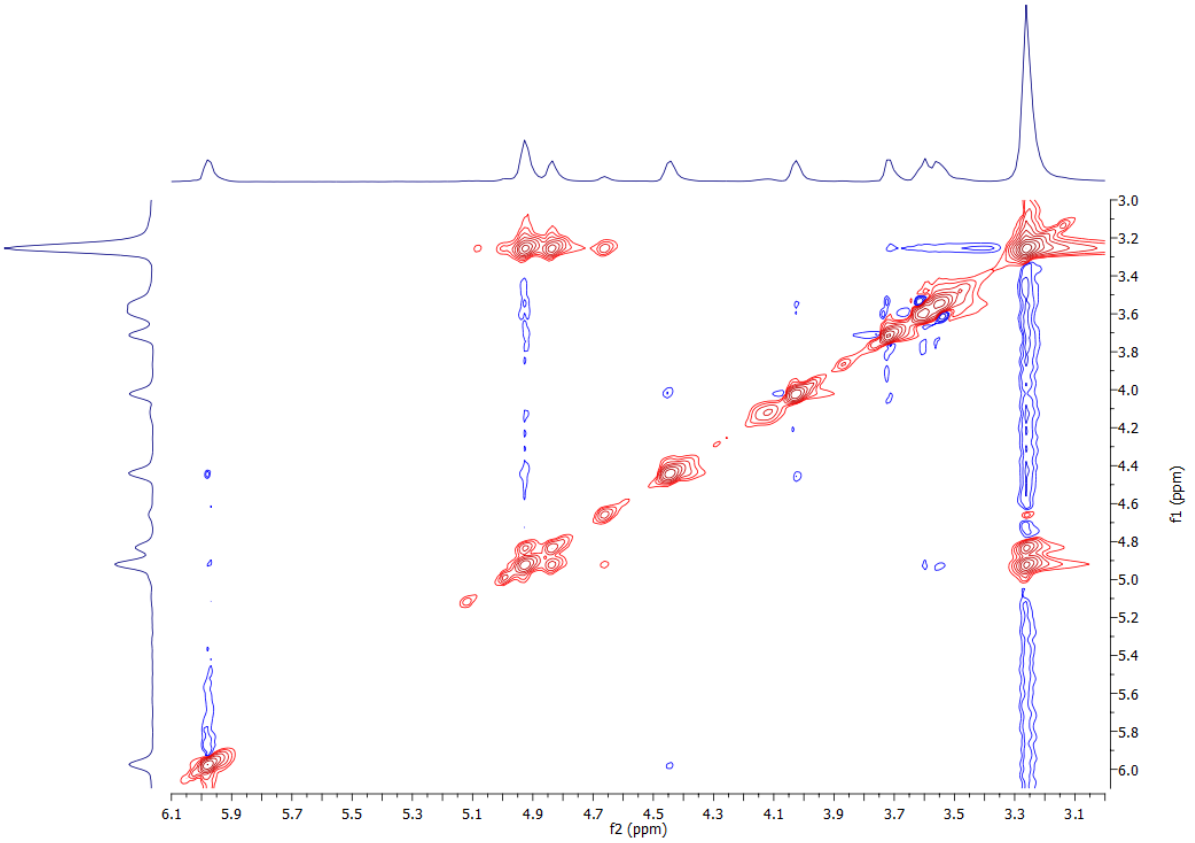

Figure 2.76 Relevant NOESY correlations of ^{mth}C in DMSO-d_6; H-1' correlated with H-2' and 2'-OH; H-2' correlated with H-3'; H-3' correlated with H-4'; H-4' correlated with H-5'; H-5' correlated with 5'-OH.

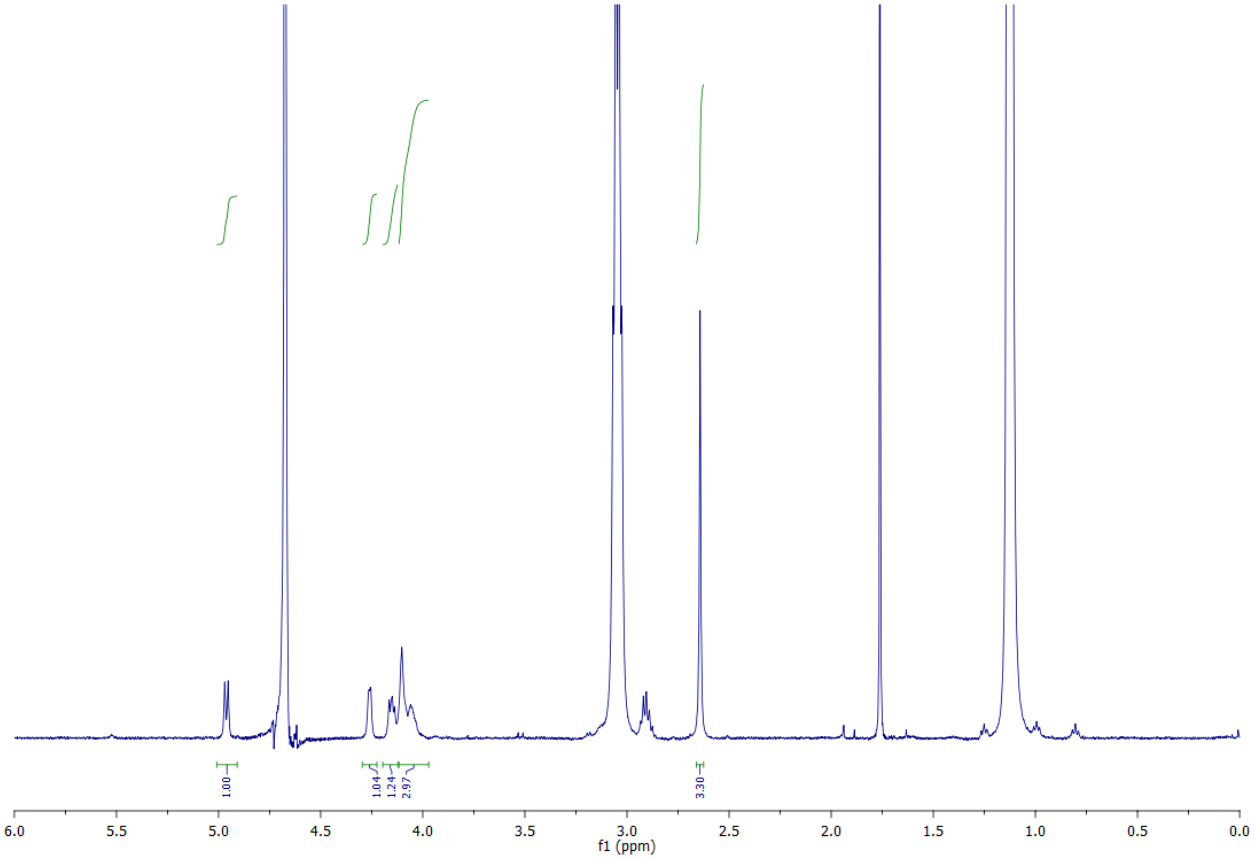

Figure 2.77 ^{1}H NMR spectra of ^{mth}GTP in D_2O

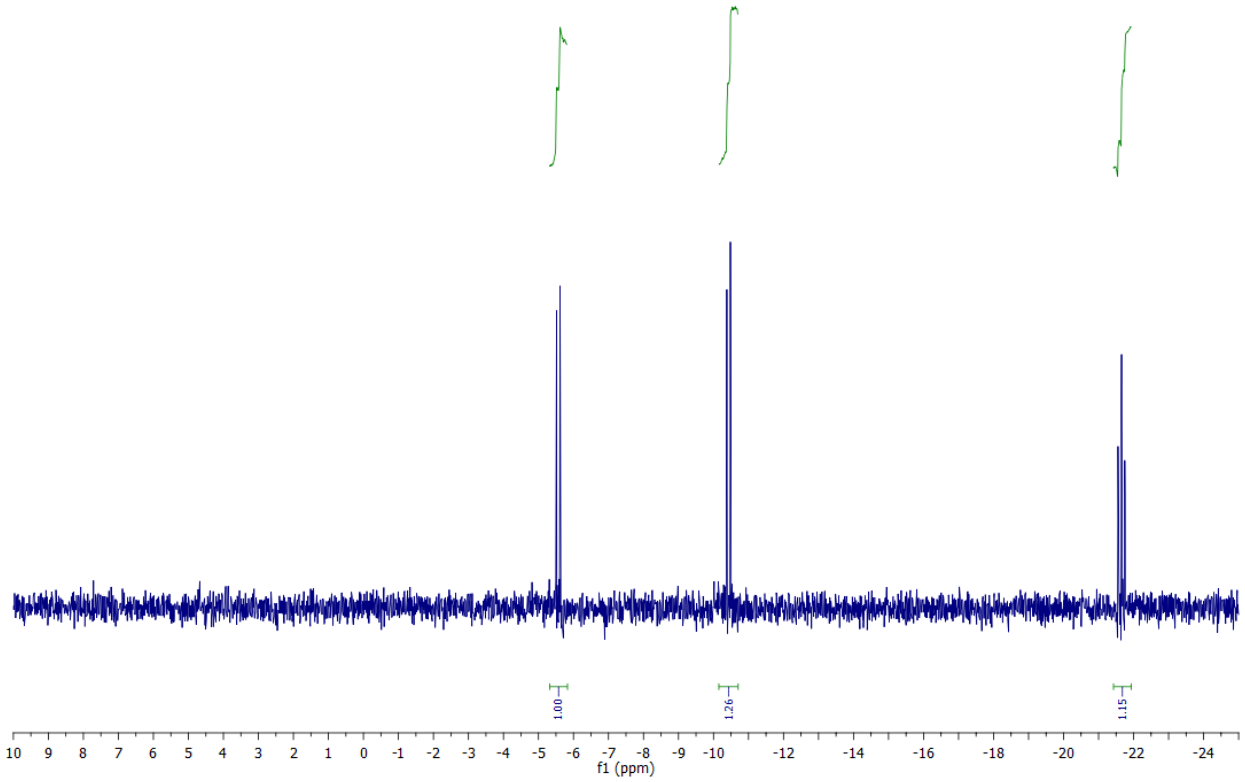

Figure 2.78 ^{31}P NMR spectra of ^{mth}GTP in D_2O

Table 2.4 Chemical Shifts of Protons of the Methylthieno[3,4-*d*]pyrimidine Based Alphabet

	Chemical Shifts (ppm) From ^{1}H NMR in DMSO-d_6						
	^{mth}Aβ (40°C)	**^{mth}Aα (25°C)**	**^{mth}Iβ (25°C)**	**^{mth}Iα (25°C)**	**^{mth}G (25°C)**	**^{mth}U (25°C)**	**^{mth}C (35°C)**
H1’	5.24	5.74	5.24	5.63	5.11	6.00	5.98
H2’	4.10	3.88	3.95	3.88	3.89	4.43	4.45
H3’	3.95	4.12	3.89	4.12	3.88	4.02	4.03
H4’	3.81	3.76	3.76	3.76	3.71	3.76	3.72
H5’	3.53, 3.47	3.56, 3.41	3.46	3.56, 3.40	3.44	3.60	3.61, 3.55
CH_3	2.85	2.84	2.80	2.80	2.73	2.72	2.73
H2	7.90	7.88	7.64	7.89	N/A	N/A	N/A
H9	N/A	N/A	N/A	N/A	N/A	7.23	6.95
2’-OH	5.11	5.17	5.08	5.19	5.07	5.14	4.93
3’-OH	4.73	4.92	4.92	4.94	4.82	4.97	4.83
5’-OH	5.11	4.68	4.83	4.69	4.85	5.06	4.93
6-NH_2	7.20	7.21	N/A	N/A	N/A	N/A	N/A
*N*1-H	N/A	N/A	11.44	N/A	10.34	11.12	N/A
2-NH_2	N/A	N/A	N/A	N/A	6.03	N/A	N/A

Table 2.5 HH ^{3}J-Couplings of Protons of the Methylthieno[3,4-*d*]pyrimidine Based Alphabet

	HH ^{3}J-couplings (Hz)						
	^{mth}Aβ (40ºC)	^{mth}Aα (25ºC)	^{mth}Iβ (25ºC)	^{mth}Iα (25ºC)	^{mth}G (25ºC)	^{mth}U (25ºC)	^{mth}C (35ºC)
H1’	7 d	3.25 d	6.5 d	3.25 d	6.75 d	7 d	6.75 d
H2’	6.75, 5.25 dd	4.5, 2.5 dd	12.5, 5 dd			13.25, 6.75 dd	13, 6.75 dd
H3’		8.25, 4.25 dd	9.75, 4 dd				12, 4.75 dd
H4’	8, 4.25 dd	m	8.75, 4.5 dd	m	8, 5 dd	7, 4 dd	m
H5’							
2’-OH			5 d			6 d	
3’-OH			5 d		4.5 d	5.5 d	6 d
5’-OH			6 t			5.25 t	

Note d = doublet, t = triplet, dd = doublet of doublets, m = multiplet

2.9 Experimental Procedures

2.9.1 Synthetic Procedures

Reagents were purchased from Sigma-Aldrich, TCI, and Acros and were used without further purification unless otherwise specified. Solvents were purchased from Sigma-Aldrich and Fisher Scientific, and dried by standard techniques. NMR solvents were purchased from Cambridge Isotope Laboratories (Andover, MA). All reactions were monitored with analytical TLC (Merck Kieselgel 60 F_{254}). Column chromatography were carried out with Teledyne ISCO Combiflash Rf with silica gel particle size 40–63 μm. NMR spectra were obtained on Varian Mercury 300 MHz, Jeol 500 MHz, and Varian VX 500 MHz. Mass spectra were obtained on an Agilent 6230 HR-ESI-TOF MS at the Mass Spectrometry Facility at the UCSD Chemistry and Biochemistry Department.

^{tz}GTP, thGTP, ^{tz}G, thG, thA, ^{tz}A, $^{tz}G_n$, and $^{th}G_n$ were all synthesized according to previously reported procedures.[15,16,19,23,25]

Methyl 2-methyl-4-oxotetrahydrothiophene-3-carboxylate (2b)

Piperidine (0.31 g, 0.36 mL, 3.7 mmol) was added to a mixture of methyl thioglycolate (19.3 g, 16.2 mL, 182 mmol) and methyl crotonate (20.0 g, 21.2 mL, 200. Mmol) in a round

bottom flask while stirring at room temperature. The solution was heated to 50ºC and stirred for 2 hours. The solution was allowed to cool and the piperidine and excess reagent evaporated off to afford a yellow liquid.

In a separate round bottom flask, 60 wt% sodium hydride in mineral oil (8.75 g, 219 mmol) was added to dry THF (540 mL) under argon while stirring at room temperature. To the mixture was added the yellow liquid slowly over several hours while stirring at room temperature. Excess pressure was released through a needle. The resulting mixture was brought to 70ºC and stirred overnight. The next day the solution was brought to room temperature and quenched with water (200 mL). The pH was adjusted to 1 with concentrated HCl solution and the solution extracted with DCM three times. The organic layer was dried with sodium sulfate and evaporated to a residue. The resulting residue was purified using column chromatography with a gradient of 0 to 20% EtOAc in hexanes yielding **2b** as a clear, yellow liquid (6.6 g, 19%). ^{1}H NMR (300 MHz, $CDCl_3$): δ 11.12 (s), 3.91-3.15 (m), 1.55-1.40 (m). ^{13}C NMR (125 MHz, $CDCl_3$): δ 205.75, 172.43, 168.12, 104.71, 63.91, 52.83, 51.62, 42.78, 40.38, 39.75, 35.29, 24.84, 19.51. ESI-HRMS calculated for $C_7H_{10}O_3S$ $[M+Na]^+$ 197.0243, found 197.0246.

Methyl 4-amino-2-methylthiophene-3-carboxylate hydrochloride (4b)

To a solution of **2b** (6.60 g, 38 mmol) in methanol (280 mL) was added barium carbonate (17.2 g, 87.1 mmol) and hydroxylamine hydrochloride (6.06 g, 87.1 mmol) while stirring at room temperature. The solution was refluxed overnight at 70ºC. The next day the solution was cooled to room temperature and then filtered. The filtrate was dried to a white solid, suspended in water, and extracted three times with ethyl acetate. The organic phase was dried with sodium sulfate and evaporated to a clear, yellow residue.

The yellow residue was dissolved in dry ether (71 mL) and methanol (19 mL) under argon while stirring at room temperature. To the solution was added 2 M HCl in ether (45 mL) and stirring continued at room temperature for 24 hours. The resulting precipitate (6.1 g, 78%)

was filtered, rinsed with cold ether, and collected without further purification to yield **4b** (6.1 g, 78%) as a pink solid. ^{1}H NMR (300 MHz, DMSO-d_6): δ 10.03 (br s, 2H), 7.41 (s, 1H), 3.80 (s, 3H), 2.64 (s, 3H). ^{13}C NMR (125 MHz, DMSO-d_6): δ 162.97, 150.60, 132.24, 121.64, 113.29, 52.24, 16.70. ESI-HRMS calculated for $C_7H_{10}NO_2S$ $[M+H]^+$ 172.0427, found 172.0426.

2-Amino-5-methylthieno[3,4-*d*]pyrimidin-4(3*H*)-one (5)

Dimethyl sulfone (16.3 g) was heated to 125ºC. Solid **4b** (1.0 g, 4.8 mmol) and chloroformamidine hydrochloride (830 mg, 7.2 mmol) were ground up into a finely mixed powder and added to the liquid dimethyl sulfone. The resulting solution was stirred for 2 hours. The mixture was cooled, dissolved in water (82 mL), and basified with concentrated ammonium hydroxide. The solution was vigorously stirred for 1 hour. The resulting precipitate was filtered and collected to yield a cream solid (860 mg, 99%). ^{1}H NMR (300 MHz, CD_3OD): δ 6.65 (s, 1H), 2.87 (s, 3H). ^{13}C NMR (125 MHz, DMSO-d_6): δ 170.87, 160.44, 151.11, 144.38, 119.56, 103.80, 15.87. ESI-HRMS calculated for $C_7H_8N_3OS$ $[M+H]^+$ 182.0383, found 182.0381.

I-*N,N*-dimethyl-*N'*-(5-methyl-4-oxo-3,4-dihydrothieno[3,4-*d*]pyrimidin-2-yl)formimidamide (6)

Solid **5** (860 mg, 4.8 mmol) was dried under high vacuum next to P_2O_5 overnight. DMF was placed on activated molecular sieves under argon and allowed to sit overnight. The next day solid **5** was purged with argon and dissolved in the dry DMF (18 mL) while stirring at room temperature. Dimethyl formamide dimethyl acetal (1.3 mL, 9.6 mmol) was added and the mixture stirred overnight. The next day the brown solution was evaporated to a residue and then co-evaporated a second time with DMF. The resulting residue was purified using column chromatography with a gradient of 0 to 4% MeOH in DCM yielding **6** as a white solid (1.07 g, 95%). ^{1}H NMR (300 MHz, $CDCl_3$): δ 8.61 (s, 1H), 8.01 (s, 1H), 6.82 (s, 1H), 3.16 (d, J = 3.8 Hz, 3H), 3.08 (d, J = 3.7 Hz, 3H), 2.91 (d, J = 3.9 Hz, 3H). ^{13}C NMR (125 MHz, DMSO-d_6): δ 160.87, 157.77, 155.27, 150.10, 143.85, 120.73, 106.94, 40.93, 34.97, 15.76. ESI-HRMS calculated for $C_{10}H_{13}N_4OS$ $[M+H]^+$ 237.0805, found 237.0803.

(2*R*,5*R*)-2-((benzoyloxy)methyl)-5-(2-((l-(dimethylamino)methylene)amino)-5-methyl-4-oxo-3,4-dihydrothieno[3,4-*d*]pyrimidin-7-yl)tetrahydrofuran-3,4-diyl dibenzoate (7)

Solid **6** (600 mg, 2.54 mmol), dried under high vacuum next to P_2O_5 overnight, under argon was dissolved in $MeNO_2$ (11.3 mL) that was dried on molecular sieves. The solution was brought to 50ºC and β-D-ribofuranose 1-acetate 2,4,5-tribenzoate (1.35 g, 2.67 mmol) was added while stirring. The solution was brought to 70C and freshly distilled tin (IV) chloride (0.62 mL, 5.3 mmol) was added slowly. After 3 hours, more β-D-ribofuranose 1-acetate 2,4,5-tribenzoate (0.68 mg, 1.35 mmol) was added. The solution was stirred overnight. The next day the solution was allowed to cool to room temperature and poured into saturated sodium bicarbonate (49 mL). DCM (49 mL) was added and the mixture stirred vigorously for 1.5 hour. The two phases were separated and the water phase extracted once with DCM. The organic layers were combined and evaporated to a residue. The residue was purified by column chromatography with a gradient of 0 to 1% MeOH in DCM. The desired fractions were collected, evaporated, and purified with column chromatography a second time with a gradient of 0 to 80% EtOAc in hexanes. The desired fractions were evaporated to yield **7** (440 mg, 25%) as a yellow foam. ^{1}H NMR (300 MHz, $CDCl_3$): δ 8.82 (d, *J* = 5.1 Hz, 1H), 8.19 (s, 1H), 8.02-7.97 (m, 4H), 7.92-7.87 (m, 2H), 7.60-7.49 (m, 3H), 7.44-7.30 (m, 6H), 6.65-6.59 (m, 1H), 6.12-6.03 (m, 1H), 5.68-5.64 (m, 1H), 4.81-4.75 (m, 1H), 4.74-4.69 (m, 1H), 4.62-4.56 (m, 1H), 3.13 (d, *J* = 5.5 Hz, 3H), 3.04 (d, *J* = 5.3 Hz, 3H), 2.81 (d, *J* = 5.4 Hz, 3H). ^{13}C NMR (125 MHz, $CDCl_3$): δ 171.19, 166.33, 165.43, 165.39, 160.30, 158.35, 154.02, 146.54, 144.86, 133.39, 133.34, 133.07, 129.74, 129.68, 129.50, 129.04, 128.43, 128.38, 128.30, 121.06, 119.51, 78.91, 78.46, 75.61, 72.18, 63.48, 41.03, 34.99, 15.50. ESI-HRMS calculated for $C_{36}H_{33}N_4O_8S$ $[M+H]^+$ 681.2014, found 681.2011.

2-amino-7-((2*R*,5*R*)-3,4-dihydroxy-5-(hydroxymethyl)tetrahydrofuran-2-yl)-5-methylthieno[3,4-*d*]pyrimidin-4(3*H*)-one (^{mth}G)

A solution of **7** (430 mg, 0.63 mmol) in methanolic ammonia (25 mL) was refluxed at 65ºC overnight. The next day the solution was allowed to cool to room temperature and evaporated to a residue. The residue was purified by column chromatography with a gradient of 0 to 18% MeOH in DCM. The desired fractions were combined and evaporated to afford ^{mth}G (125 mg, 63%) as an off-white powder. ^{1}H NMR (300 MHz, DMSO-d_6): δ 10.34 (d, J = 6.4 Hz, 1H), 6.03 (s, 2H), 5.11 (d, J = 6.6 Hz, 1H), 5.07 (d, J = 5.4 Hz, 1H), 4.85 (t, J = 5.6 Hz, 1H), 4.82 (d, J = 4.4 Hz, 1H), 3.93-3.86 (m, 2H), 3.71 (q, J = 2.7 Hz, 1H), 3.49-3.39 (m, 2H), 2.73 (s, 3H). ^{13}C NMR (125 MHz, DMSO-d_6): δ 160.06, 150.77, 147.61, 143.02, 120.88, 119.55, 85.11, 77.11, 76.68, 72.16, 62.80, 15.64. ESI-HRMS calculated for $C_{12}H_{16}N_3O_5S$ $[M+H]^+$ 314.0805, found 314.0800.

Methyl 4-formamido-2-methylthiophene-3-carboxylate (8)

To a mixture of **4b** (1.0 g, 4.8 mmol) and sodium acetate (670, 8.2 mmol) was added 90% formic acid (12 mL) and the solution stirred 1 hour at room temperature. The solution was heated to 60ºC and stirred for an additional 2 hours. The resulting dark red solution was poured into water (12 mL) and stirred vigorously for 20 minutes. A precipitate formed and was filtered off with Celite. The filtrate was collected and extracted three times with ethyl acetate. The organic layers were combined, washed with saturated $NaHCO_3$ followed by brine, and evaporated to a residue. The residue was purified by column chromatography with a gradient of 0 to 25% EtOAc in Hexanes. The desired fractions were combined and evaporated to yield **8** (1.0 g, 80%) as a pale pink solid. ^{1}H NMR (300 MHz, DMSO-d_6): δ 10.14 (s, 1H), 8.39 (d, J = 1.7 Hz 1H), 7.73 (s, 1H), 3.86 (s, 3H), 2.63 (s, 3H). ^{13}C NMR (125 MHz, DMSO-d_6): δ 164.36, 160.67, 148.71, 135.03, 119.06, 108.19, 52.36, 16.83. ESI-HRMS calculated for $C_8H_{10}NO_3S$ $[M+H]^+$ 200.0376, found 200.0377.

(2*R*)-2-((benzoyloxy)methyl)-5-(3-formamido-4-(methoxycarbonyl)-5-methylthiophen-2-yl)tetrahydrofuran-3,4-diyl dibenzoate (9)

Solid **8** (1.15 g, 5.77 mmol) and β-D-ribofuranose 1-acetate 2,4,5-tribenzoate (2.91 g, 5.77 mmol) under argon were suspended in $MeNO_2$ (17 mL) while stirring at room temperature. The suspension was brought to 65C and tin (IV) chloride (0.81 mL, 6.9 mmol) was added slowly over several hours. The solution was then allowed to stir overnight. The solution was brought to room temperature. Saturated aqueous KF was added and the solution stirred vigorously for 2 hours. Celite was then added and the suspension mixed vigorously stirred for 1 hour. The suspension was then filtered, rinsed with DCM, and the filtrate extracted three times with DCM. The organic layers were combined and evaporated to a black residue. The black residue was purified by column chromatography with a gradient of 0 to 40% EtOAc in Hexanes. The desired fractions were combined and evaporated to yield **9** (1.71 g, 46%) as a yellow foam. ^{1}H NMR (300 MHz, CD_3OD): δ 8.21-8.04 (m, 3H), 7.97-7.85 (m, 4H), 7.68-7.33 (m, 9H), 5.92-5.78 (m, 1H), 5.75-5.68 (m, 2H), 4.73-4.70 (m, 1H), 4.59-4.53 (m, 1H), 3.80 (s, 3H), 2.46 (s, 3H). ^{13}C NMR (125 MHz, CD_3OD): δ 166.11, 165.48, 165.34, 165.24, 165.14, 163.47, 163.08, 160.37, 148.75, 146.76, 133.46, 133.38, 133.31, 133.29, 133.17, 133.07, 130.00, 129.68, 129.39, 129.36, 129.34, 129.29, 129.25, 128.95, 128.86, 128.24, 128.23, 128.16, 123.99, 123.76, 80.77, 79.49, 77.47, 76.58, 76.24, 75.19, 72.48, 71.98, 63.56, 63.03, 50.72, 50.65, 15.31, 14.98. ESI-HRMS calculated for $C_{34}H_{29}NO_{10}S$ $[M+Na]^+$ 666.1404, found 666.1401.

(2*R*)-2-((benzoyloxy)methyl)-5-(5-methyl-4-oxo-3,4-dihydrothieno[3,4-*d*]pyrimidin-7-yl)tetrahydrofuran-3,4-diyl dibenzoate (10)

Solid **9** (1.04 g, 1.6 mmol) was dissolved in chloroform (6.5 mL) while stirring at room temperature. To the solution was added 15 v/v% saturated HCl in methanol (26 mL) and stirring continued for 2 hours. Excess solvent was then evaporated off and the residue co-evaporated with methanol twice followed by acetonitrile twice. The resulting orange foam was dried under high vacuum overnight. In a separate container, formamidine acetate (1.6 g, 15 mmol) was

dried under high vacuum overnight. Both containers were argon purged, the formamidine acetate suspended in ethanol (7 mL), and the intermediate dissolved in ethanol (16 mL). The suspension was transferred to the intermediate solution, triethylamine (0.21 mL, 1.5 mmol) was added, and the solution brought to 90ºC. Stirring continued 4 hours. The solution was allowed to cool and solvent evaporated off to reveal a black solid. The solid was triturated with water to yield a white solid. The water was extracted with DCM twice. The organic phase was combined with the white solid. The solution was purified by column chromatography with a gradient of 0 to 50% EtOAc in Hexanes. The desired fractions were combined and evaporated to yield **10** (β-isomer: 508 mg, 52%, α-isomer: 176 mg, 18%) as a yellow foam. B-isomer: ^{1}H NMR (300 MHz, CD_3OD): δ 8.16 (d, J = 7.5 Hz, 2H), 7.99 (d, J = 8.2 Hz, 2H), 7.92 (d, J = 8.0 Hz, 2H), 7.70-7.33 (m, 10H), 6.03-5.98 (m, 2H), 5.86 (t, *J* = 6.1 Hz, 1H), 4.90 (dd, *J* = 12.7, 2.7 Hz, 1H), 4.75 (q, *J* = 3.1 Hz, 1H), 4.60 (dd, *J* = 12.0, 1.7 Hz, 1H), 2.78 (s, 3H). ^{13}C NMR (125 MHz, CD_3OD): δ 166.15, 165.44, 165.27, 159.43, 149.50, 145.76, 145.69, 143.66, 133.32, 133.27, 133.14, 129.65, 129.42, 129.37, 129.33, 129.05, 128.30, 128.15, 126.67, 121.57, 80.56, 76.82, 75.42, 72.74, 63.66, 14.23; α-isomer: ^{1}H NMR (300 MHz, CD_3OD): δ 8.07 (d, *J* = 7.3 Hz, 2H), 7.90 (d, *J* = 7.3 Hz, 2H), 7.81 (d, *J* = 7.3 Hz, 2H), 7.66-7.40 (m, 8H), 7.31 (d, *J* = 7.8 Hz, 2H), 6.35 (d, *J* = 3.5 Hz, 1H), 6.14 (t, *J* = 4.0 Hz, 1H), 6.05 (dd, *J* = 7.2, 4.6 Hz, 1H), 4.88-4.81 (m, 1H), 4.70 (qd, *J* = 11.8, 4.5 Hz, 2H), 2.81 (s, 3H). ^{13}C NMR (125 MHz, CD_3OD): δ 166.24, 165.21, 164.96, 159.51, 147.81, 145.96, 145.09, 143.52, 133.35, 133.22, 133.00, 129.51, 129.32, 129.30, 129.23, 129.05, 128.80, 128.27, 128.21, 128.08, 124.51, 120.98, 77.83, 75.18, 74.15, 73.72, 64.25, 14.14. ESI-HRMS (mixture of both isomers) calculated for $C_{33}H_{27}N_2O_8S$ $[M+H]^+$ 611.1483, found 611.1473.

(2R,5R)-2-(4-amino-5-methylthieno[3,4-d]pyrimidin-7-yl)-5-(hydroxymethyl)tetrahydrofuran-3,4-diol (^{mth}A)

Solid **10** (100 mg, 0.17 mmol) was dissolved in dry DMF (1.4 mL) under argon. DBU (0.04 mL, 0.25 mmol) was added followed by BOP (96 mg, 0.22 mmol) and the solution stirred

at room temperature for 1 hour. Ammonia gas was then bubbled into the solution for 10 minutes and stirred for another 30 minutes. The solution was then evaporated to a residue, suspended in water and the water extracted three times with DCM. The organic layer was evaporated to a residue and purified by column chromatography with a gradient of 0 to 10% MeOH in DCM. The desired fractions were combined and evaporated to a residue. The residue was dissolved in MeOH (4 mL) and placed in an ice bath. Ammonia was bubbled into the solution for 10 minutes, then the reaction was sealed and placed in a heat bath and stirred at 70ºC overnight. The reaction was allowed to cool and then evaporated to a residue. The residue was purified with column chromatography to yield ^{mth}A (21 mg, 43%) as a pale yellow powder. ^{1}H NMR (300 MHz, CD_3OD): δ 7.90 (s, 1H), 7.20 (br s, 1H), 5.24 (d, *J* = 6.8 Hz, 1H), 5.11 (br s, 1H), 4.73 (s, 1H), 4.10 (t, *J* = 6.0 Hz, 1H), 3.95 (s, 1H), 3.81 (q, *J* = 4.0 Hz, 1H), 3.52, 3.47 (dABq, *J* = 11.7, 4.2 Hz, 2H), 2.85 (s, 3H). ^{13}C NMR (125 MHz, CD_3OD): δ 159.91, 152.89, 147.59, 136.65, 125.66, 117.34, 85.79, 78.33, 77.12, 72.31, 62.58, 14.79. ESI-HRMS calculated for $C_{12}H_{14}N_3O_4S$ $[M-H]^-$ 296.0711, found 296.0710.

7-((2*S*,5*R*)-3,4-dihydroxy-5-(hydroxymethyl)tetrahydrofuran-2-yl)-5-methylthieno[3,4-*d*]pyrimidine-4(3*H*)-thione (11 alpha)

A suspension of **10** (430 mg, 0.70 mmol) and P_2S_5 (1550 mg, 3.5 mmol) in dry pyridine (14 mL) was refluxed at 115ºC for 2.5 hours. After cooling to room temperature, the solution was evaporated to a residue and suspended in water (70 mL). The suspension was extracted with DCM (4 x 25 mL) and the combined extracts dried over sodium sulfate and evaporated to a residue. The residue was purified with column chromatography with a gradient of 0 to 1% MeOH in DCM. The desired fractions were combined and evaporated. The reaction yielded only one isomer, the alpha configuration, of **11** (57 mg, 14%) as a yellow solid. ^{1}H NMR (300 MHz, CD_3OD): δ 8.09-8.06 (m, 2H), 7.91-7.87 (m, 2H), 7.83-7.80 (m, 2H), 7.64-7.51 (m, 4H), 7.48-7.43 (m, 4H), 7.35-7.30 (m, 2H), 6.38 (d, *J* = 3.6 Hz, 1H), 6.15 (t, *J* = 4.0 Hz, 1H), 6.06 (dd, *J* = 7.2, 4.6 Hz, 1H), 4.86 (dt, *J* = 7.2, 4.5 Hz, 1H), 4.71 (qd, *J* = 11.9, 4.6 Hz, 2H), 2.99 (s, 3H).

^{13}C NMR (125 MHz, CD_3OD): δ 184.28, 166.27, 165.25, 164.98, 147.87, 141.42, 141.01, 133.35, 133.22, 133.02, 129.54, 129.30, 129.24, 129.05, 128.83, 128.27, 128.22, 128.09, 127.20, 123.53, 77.94, 75.19, 74.19, 73.71, 64.27, 73.72, 17.10. ESI-HRMS calculated for $C_{33}H_{26}N_2O_7S_2$ $[M+Na]^+$ 649.1074, found 649.1072.

(2*S*,5*R*)-2-(4-amino-5-methylthieno[3,4-*d*]pyrimidin-7-yl)-5-(hydroxymethyl)tetrahydrofuran-3,4-diol (^{mth}A alpha)

Solid **11** (57 mg, 0.090 mmol) was dissolved in methanol (7 mL). The solution was placed in an ice bath and then ammonia gas was bubbled into the solution for 10 minutes. The reaction was sealed and placed in a heat bath and stirred at 70ºC overnight. The reaction was allowed to cool and then evaporated to a residue. The residue was purified with column chromatography with a gradient of 0 to 20% methanol in DCM to yield ^{mth}A in the alpha configuration (15 mg, 57%) as a pale yellow powder. ^{1}H NMR (300 MHz, CD_3OD): δ 7.92 (s, 1H), 5.78 (d, *J* = 2.8 Hz, 1H), 4.38 (dd, *J* = 8.2, 4.3 Hz, 1H), 4.18 (t, *J* = 3.6 Hz 1H), 3.99-3.95 (m, 1H), 3.52, 3.47 (dABq, *J* = 12.2, 3.2 Hz, 2H), 2.85 (s, 3H). ^{13}C NMR (125 MHz, CD_3OD): δ 159.73, 153.04, 146.30, 138.52, 123.66, 115.98, 81.91, 75.83, 73.20, 72.47, 61.64, 14.81. ESI-HRMS calculated for $C_{12}H_{16}N_3O_4S$ $[M+H]^+$ 298.0856, found 298.0856.

7-((2*R*,5*R*)-3,4-dihydroxy-5-(hydroxymethyl)tetrahydrofuran-2-yl)-5-methylthieno[3,4-*d*]pyrimidin-4(3*H*)-one (^{mth}I)

Solid **10** (50 mg, 0.082 mmol) was suspended in saturated NH_4OH (1.3 mL), saturated methylamine (1.3 mL), and methanol (0.5 mL). The solution was stirred at room temperature for 24 hours. The solution was evaporated to a residue and purified with column chromatography with a gradient of 0 to 20% MeOH in DCM. The desired fractions were combined and evaporated to yield ^{mth}I (18 mg, 74%) as a white solid. ^{1}H NMR (300 MHz, DMSO-d_6): δ 11.44 (s, 1H), 7.64 (s, 1H), 5.24 (d, *J* = 6.5 Hz, 1H), 5.08 (d, *J* = 4.6 Hz, 1H), 4.92 (d, *J* = 3.0 Hz, 1H), 4.83 (t, *J* = 5.1 Hz, 1H), 3.95 (q, *J* = 4.6 Hz, 1H), 3.89 (s, 1H), 3.76 (q, *J* = 4.2 Hz, 1H), 3.53-3.41 (m, 2H), 2.80 (s, 3H). ^{13}C NMR (125 MHz, DMSO-d_6): δ 159.46, 145.71, 143.93, 143.45,

130.65, 122.12, 85.28, 77.81, 76.98, 72.09, 62.65, 15.66. ESI-HRMS calculated for $C_{12}H_{15}N_2O_5S$ $[M+H]^+$ 299.0696, found 299.0695.

7-((2*S*,5*R*)-3,4-dihydroxy-5-(hydroxymethyl)tetrahydrofuran-2-yl)-5-methylthieno[3,4-*d*]pyrimidin-4(3*H*)-one (^{mth}I alpha)

^{mth}I in the alpha configuration was prepared in the same method as described for ^{mth}I. Solid **10** in the alpha configuration (53 mg, 0.084 mmol) was suspended in saturated NH_4OH (1.3 mL), saturated methylamine (1.3 mL), and methanol (0.5 mL). The solution was stirred at room temperature for 24 hours. The solution was evaporated to a residue and purified with column chromatography with a gradient of 0 to 20% MeOH in DCM. The desired fractions were combined and evaporated to yield ^{mth}I (11 mg, 43%) as a white solid. ^{1}H NMR (300 MHz, DMSO-d_6): δ 7.89 (s, 1H), 5.63 (d, *J* = 2.5 Hz, 1H), 5.19 (d, *J* = 3.3 Hz, 1H), 4.93 (s, 1H), 4.69 (t, *J* = 5.1 Hz, 1H), 4.12 (s, 1H), 3.88 (d, *J* = 2.4 Hz, 1H), 3.78-3.73 (m, 1H), 3.59-3.53 (m, 1H), 3.43-3.37 (m, 1H), 2.80 (s, 3H). ^{13}C NMR (125 MHz, DMSO-d_6): δ 159.27, 146.98, 145.17, 144.32, 127.84, 120.08, 82.31, 75.19, 73.20, 73.07, 62.14, 15.74. ESI-HRMS calculated for $C_{12}H_{15}N_2O_5S$ $[M+H]^+$ 299.0696, found 299.0695.

5-methylthieno[3,4-*d*]pyrimidin-4(3*H*)-one (12)

Solid **4b** (1.0 g, 4.8 mmol) was placed in a round bottom and dissolved in ethanol (70 mL) while stirring at room temperature. Formamidine acetate (4.8 g, 46 mmol) and triethylamine (0.64 mL, 4.6 mmol) were added while stirring. The solution was then brought to reflux at 90ºC and stirred for 15 hours. The solution was then cooled to room temperature. The solution was evaporated to a solid. The solid was suspended in water and then filtered giving **12** as a yellow solid (710 mg, 89%). ^{1}H NMR (300 MHz, CD_3OD): δ 7.71 (s, 1H), 7.32 (s, 1H), 2.92 (s, 3H). ^{13}C NMR (125 MHz, CD_3OD): δ 159.61, 147.60, 146.20, 143.63, 121.12, 112.41, 14.32. ESI-HRMS calculated for $C_7H_7N_2OS$ $[M+H]^+$ 167.0274, found 167.0275.

Methyl 2-methyl-4-ureidothiophene-3-carboxylate (13)

Solid **4b** (1.0 g, 4.8 mmol) and potassium cyanate (670 mg, 8.2 mmol) were dissolved in a 50:50 mixture of water (8.2 mL) and acetic acid (8.2 mL). The resulting solution was stirred at room temperature overnight. The next day a brownish pink precipitate had formed and was filtered. The solid was rinsed with water. The solid was collected to yield **13** (0.97 g, 94%) as a brownish pink powder. ^{1}H NMR (300 MHz, $CDCl_3$): δ 9.44 (br s, 1H), 7.47 (s, 1H), 4.58 (br s, 2H), 3.92 (s, 3H), 2.67 (s, 3H). ^{13}C NMR (125 MHz, CD_3OD): δ 165.02, 157.54, 148.04, 137.54, 117.81, 102.74, 50.67, 15.81. ESI-HRMS calculated for $C_8H_{11}N_2O_3S$ $[M+H]^+$ 215.0485, found 215.0483.

5-methylthieno[3,4-*d*]pyrimidine-2,4(1*H*,3*H*)-dione (14)

Solid **13** (970 mg, 4.5 mmol) under argon was dissolved in 0.5 M sodium methoxide in methanol (20 mL, 10 mmol). The resulting solution was stirred at room temperature overnight. The next day a precipitate had formed and was filtered. The solid was collected to yield **14** (750 mg, 91%) as an off-white powder. ^{1}H NMR (300 MHz, DMSO-d_6): δ 10.66 (br s, 2H), 6.44 (s, 1H), 2.73 (s, 3H). ^{13}C NMR (125 MHz, DMSO-d_6): δ 160.52, 151.79, 146.98, 139.17, 117.73, 97.60, 15.25. ESI-HRMS calculated for $C_7H_5N_2O_2S$ $[M-H]^-$ 181.0077, found 181.0078.

(2*R*,5*R*)-2-((benzoyloxy)methyl)-5-(5-methyl-2,4-dioxo-3,4-dihydrothieno[3,4-*d*]pyrimidin-1(2*H*)-yl)tetrahydrofuran-3,4-diyl dibenzoate (15)

Solid **14** (710 g, 3.9 mmol) dried under high vacuum next to P_2O_5 overnight, under argon was dissolved in I (20 mL) that was dried on molecular sieves. *N,O*-bis(trimethylsilyl)acetamide (2380 g, 11.7 mmol) was added and the solution stirred for 2 hours at room temperature. B-D-ribofuranose 1-acetate 2,4,5-tribenzoate (2.16 g, 4.29 mmol), dried under high vacuum next to P_2O_5 overnight, and TMS triflate (1.1 mL, 6.2 mmol) were added and the resulting brown solution stirred at room temperature for 2 hours. The solution was brought to 70ºC and stirred for 1.5 hours. The solution was brought to room temperature and evaporated to a yellow foam. The foam was purified with column chromatography with a gradient of 0 to 40% EtOAc in

Hexanes. The desired fractions were evaporated to yield **15** (2.1 g, 85%) as a pale yellow solid. ^{1}H NMR (300 MHz, DMSO-d_6): δ 11.38 (s, 1H), 8.01-7.98 (m, 2H), 7.90-7.84 (m, 4H), 7.68-7.60 (m, 3H), 7.52-7.48 (m, 2H), 7.45-7.40 (m, 4H), 7.17 (s, 1H), 6.38 (d, *J* = 3.4 Hz, 1H), 6.12 (dd, *J* = 6.9, 3.5 Hz, 1H), 6.03 (t, *J* = 7.1 Hz, 1H), 4.77-4.67 (m, 2H), 4.61 (dd, *J* = 13.0, 6.0 Hz, 1H), 2.75 (s, 3H). ^{13}C NMR (125 MHz, DMSO-d_6): δ 165.91, 165.18, 165.14, 159.12, 150.40, 148.71, 137.37, 134.32, 134.28, 134.02, 129.79, 129.76, 129.63, 129.26, 129.14, 129.06, 128.99, 118.06, 100.54, 89.52, 78.41, 72.51, 70.38, 63.85, 15.47. ESI-HRMS calculated for $C_{33}H_{27}N_2O_9S$ $[M+H]^+$ 627.1432, found 627.1426.

(2*R*,5*R*)-2-(4-amino-5-methyl-2-oxothieno[3,4-*d*]pyrimidin-1(2*H*)-yl)-5-((benzoyloxy)methyl)tetrahydrofuran-3,4-diyl dibenzoate (16)

To pyridine (24 mL), dried overnight on molecular sieves, was added 1,2,4-triazole (1.92 g, 27.7 mmol) while stirring. The solution was placed in an ice bath and $POCl_3$ (0.85 mL, 9.1 mmol) was added slowly. After stirring on ice for 40 minutes, the solution was filtered and the yellow filtrate added to solid **15** (285 g, 0.46 mmol), dried under high vacuum next to P_2O_5 overnight, under argon while stirring at room temperature. After stirring for 1 hour, the solution was placed in an ice bath and concentrated ammonium hydroxide (5 mL) was added slowly. After 15 minutes, the solution was brought to room temperature and stirred for 1 hour. The solution was then co-evaporated with methanol (3x 20 mL) and DCM (3x 20 mL). The resulting solid was suspended in DCM (50 mL), filtered, and the filtrate extracted with water (3x 50 mL). The organic layers were combined, dried with sodium sulfate, evaporated to a residue. The residue was purified with column chromatography with a gradient of 0 to 100% EtOAc in Hexanes. The desired fractions were combined and evaporated to yield **16** (106 mg, 37%) as a yellow film. ^{1}H NMR (300 MHz, $CDCl_3$): δ 8.20 (s, 2H), 8.11-8.05 (m, 2H), 7.96-7.89 (m, 4H), 7.59-7.29 (m, 9H), 6.62 (s, 1H), 6.55 (d, *J* = 4.6 Hz, 1H), 6.25 (dd, *J* = 6.7, 4.9 Hz, 1H), 6.13 (t, *J* = 6.7 Hz, 1H), 4.86 (dd, *J* = 12.1, 3.0 Hz, 1H), 4.73 (dd, *J* = 12.1, 4.3 Hz, 1H), 4.69-4.63(m, 1H), 2.78 (s, 3H). ^{13}C NMR (125 MHz, $CDCl_3$): δ 166.19, 165.44, 165.33, 159.90, 155.96, 140.93,

139.59, 133.48, 133.45, 133.32, 129.86, 129.78, 129.57, 128.85, 128.57, 128.38, 114.77, 97.86, 88.79, 79.52, 71.49, 70.64, 64.00, 16.23. ESI-HRMS calculated for $C_{33}H_{28}N_3O_8S$ $[M+H]^+$ 626.1592, found 626.1587.

1-((2*R*,5*R*)-3,4-dihydroxy-5-(hydroxymethyl)tetrahydrofuran-2-yl)-5-methylthieno[3,4-*d*]pyrimidine-2,4(1*H*,3*H*)-dione (^{mth}U)

A solution of **15** (500 mg, 0.80 mmol) in methanolic ammonia (12 mL) was refluxed at 65ºC overnight. The next day the solution was allowed to cool to room temperature and evaporated to a residue. The residue was purified with column chromatography with a gradient of 0 to 100% EtOAc in Hexanes. The desired fractions were combined and evaporated to afford ^{mth}U (210 mg, 85%) as an off-white powder. ^{1}H NMR (300 MHz, CD_3OD): δ 7.16 (s, 1H), 6.09 (d, *J* = 6.1 Hz, 1H), 4.72 (t, *J* = 6.3 Hz, 1H), 4.30 (dd, *J* = 6.4, 4.7 Hz, 1H), 3.98-3.95 (m, 1H), 3.86, 3.78 (dABq, *J* = 6.0, 2.6 Hz, 2H), 2.82 (s, 3H). ^{13}C NMR (125 MHz, CD_3OD): δ 159.16, 151.01, 147.34, 135.87, 118.59, 102.03, 88.82, 85.31, 69.53, 68.42, 61.57, 15.41. ESI-HRMS calculated for $C_{12}H_{15}N_2O_6S$ $[M+H]^+$ 315.0645, found 315.0646.

4-amino-1-((2*R*,5*R*)-3,4-dihydroxy-5-(hydroxymethyl)tetrahydrofuran-2-yl)-5-methylthieno[3,4-*d*]pyrimidin-2(1*H*)-one (^{mth}C)

A solution of **16** (106 mg, 0.17 mmol) in methanolic ammonia (8 mL) was refluxed at 65ºC for 6 hours. The solution was allowed to cool to room temperature and evaporated to a residue. The residue was dissolved in water (40 mL) and extracted with DCM (3x 40 mL). The water phase was evaporated to a solid. The solid was loaded onto a reverse phase column and eluted with 2% I in water. The desired fractions were combined and evaporated to afford ^{mth}C (40 mg, 75%) as a white powder. ^{1}H NMR (300 MHz, CD_3OD): δ 7.06 (s, 1H), 6.09 (d, *J* = 5.5 Hz, 1H), 4.76 (t, *J* = 5.8 Hz, 1H), 4.31 (t, *J* = 4.6 Hz, 1H), 3.97 (s, 1H), 3.85, 3.77 (Abq, *J* = 7.5 Hz, 2H), 2.83 (s, 3H). ^{13}C NMR (125 MHz, CD_3OD): δ 159.51, 156.35, 140.93, 139.30, 115.19, 99.08, 89.63, 84.91, 69.68, 68.66, 61.71, 16.26. ESI-HRMS calculated for $C_{12}H_{16}N_3O_5S$ $[M+H]^+$ 314.0805, found 314.0800.

((2*R*,5*R*)-5-(2-amino-5-methyl-4-oxo-3,4-dihydrothieno[3,4-*d*]pyrimidin-7-yl)-3,4-dihydroxytetrahydrofuran-2-yl)methyl tetrahydrogen triphosphate (^{mth}GTP)

^{mth}G (23.8 mg, 0.076 mmol) was placed in a 10 mL round bottom flask and dried under vacuum next to P_2O_5 overnight. The next day dry trimethyl phosphate (0.71 mL) was added to the flask and the solution heated lightly until the solid dissolved. The solution was then placed in an ice bath while stirring. $POCl_3$ (0.035 mL, 0.38 mmol) was added dropwise and the solution stirred for 2 hours. In a separate flame dried flask, tributylammonium pyrophosphate (350 mg, 0.39 mmol) was dissolved in dry DMF (0.71 mL) and placed in an ice bath until equilibrated. The solution was then transferred to the reaction flask and then tributylamine (0.09 mL, 0.39 mmol) was added. Stirring continued for 1 hour in the ice bath. The reaction was quenched with cold (4ºC) 1 M TEAB (3 mL) and stirred for 5 minutes in the ice bath. The solution was then washed three times with ethyl acetate. The aqueous phase was evaporated to a residue. The residue was then subjected to ion exchange chromatography on a Sephadex DEAE A25 anion-exchange column, eluting with a gradient of 0.01 M to 1 M TEAB buffer at 4ºC. The desired fractions were collected, evaporated, and lyophilized. The resulting solid was dissolved in minimal water and subjected to reverse-phase HPLC. The gradient the compound was subjected to was 0.5% to 15% I in TEAA buffer (pH 6.7) over 20 minutes followed by a flush, 95% I for 5 minutes followed by re-equilibration for 5 minutes. The desired fractions were combined, evaporated, and lyophilized to afford the triethylammonium salt of ^{mth}GTP (4 mg, 5%) as an off-white powder. ^{1}H NMR (300 MHz, D_2O): δ 10.34 (d, *J* = 6.4 Hz, 1H), 6.03 (s, 2H), 5.11 (d, *J* = 6.6 Hz, 1H), 5.07 (d, *J* = 5.4 Hz, 1H), 4.85 (t, *J* = 5.6 Hz, 1H), 4.82 (d, *J* = 4.4 Hz, 1H), 3.93-3.86 (m, 2H), 3.71 (q, *J* = 2.7 Hz, 1H), 3.49-3.39 (m, 2H), 2.73 (s, 3H). ^{31}P NMR (202 MHz, D_2O): δ 160.06, 150.77, 147.61, 143.02, 120.88, 119.55, 85.11, 77.11, 76.68, 72.16, 62.80, 15.64. ESI-HRMS calculated for $C_{12}H_{15}N_3O_8PS^-$ 392.03, found 392.03. ESI-HRMS calculated for $C_{12}H_{16}N_3O_{11}P_2S^-$ 472.00, found 472.00.

2.9.2 X-ray Crystallography Experimental Summaries and Tables

For the ^{mth}U crystal structure, the single crystal X-ray diffraction studies were carried out on a Bruker Microstar APEX II CCD diffractometer equipped with Cu K_α radiation (λ =1.54178 Å).

Crystals of the subject compound were used as received (grown from MeOH). A 0.1 x 0.06 x 0.04 mm piece of a colorless crystal was mounted on a Cryoloop with Paratone oil. Data were collected in a nitrogen gas stream at 100(2) K using φ and ϖ scans. Crystal-to-detector distance was 45 mm and exposure time was 4, 6, 8, 10, or 20 seconds depending on the 2θ range per frame using a scan width of 1.25°. Data collection was 99.9 % complete to 67.679° in θ. A total of 9403 reflections were collected covering the indices, -19<=h<=18, -33<=k<=33, -8<=l<=8. 5820 reflections were found to be symmetry independent, with a R_{int} of 0.0235. Indexing and unit cell refinement indicated a **P**rimitive, **Monoclinic** lattice. The space group was found to be ***P*2$_1$**. The data were integrated using the Bruker SAINT Software program and scaled using the SADABS software program. Solution by direct methods (SHELXT) produced a complete phasing model consistent with the proposed structure.

All nonhydrogen atoms were refined anisotropically by full-matrix least-squares (SHELXL-2014). All carbon bonded hydrogen atoms were placed using a riding model. Their positions were constrained relative to their parent atom using the appropriate HFIX command in SHELXL-2014. Crystallographic data are summarized in Table 2.6.

Table 2.6 Crystal data and structure refinement for tor146 (^{mth}U)

Report date	2019-08-30	
Identification code	tor146_0m_a	
Empirical formula	C12 H16 N2 O7 S	
Molecular formula	C12 H14 N2 O6 S, H2 O1	
Formula weight	332.33	
Temperature	100.0 K	
Wavelength	1.54178 Å	
Crystal system	Monoclinic	
Space group	P 1 21 1	
Unit cell dimensions	a = 10.5481(3) Å	α= 90°.
	B = 5.25470(10) Å	β= 108.9760(10)°.
	C = 13.7012(3) Å	γ = 90°.
Volume	718.15(3) Å^3	
Z	2	
Density (calculated)	1.537 Mg/m^3	
Absorption coefficient	2.376 mm^{-1}	
F(000)	348	
Crystal size	0.1 x 0.06 x 0.04 mm^3	
Crystal color, habit	colourless block	
Theta range for data collection	3.411 to 68.224°.	
Index ranges	-12<=h<=12, -6<=k<=6, -16<=l<=15	
Reflections collected	9403	
Independent reflections	2645 [R(int) = 0.0235]	
Completeness to theta = 67.679°	99.9 %	
Absorption correction	Semi-empirical from equivalents	
Max. and min. transmission	0.5210 and 0.4164	
Refinement method	Full-matrix least-squares on F^2	
Data / restraints / parameters	2645 / 13 / 213	
Goodness-of-fit on F^2	1.040	
Final R indices [I>2sigma(I)]	R1 = 0.0259, wR2 = 0.0683	
R indices (all data)	R1 = 0.0263, wR2 = 0.0686	
Absolute structure parameter	-0.001(8)	
Extinction coefficient	n/a	
Largest diff. peak and hole	0.230 and -0.176 e.Å^{-3}	

For the **^{mth}I** crystal structure, the single crystal X-ray diffraction studies were carried out on a Bruker Microstar X8 CCD diffractometer equipped with Cu K_α radiation (= 1.54178). A 0.150 x 0.120 x 0.030 mm colorless crystal was mounted on a Cryoloop with Paratone oil.

Data were collected in a nitrogen gas stream at 100(2) K using φ and ϖ scans. Crystal-to-detector distance was 40 mm using exposure time 2, 4 and 8s s with a scan width of 1.25°. Data collection was 99.8% complete to 67.500° in *θ*.

A total of 5343 reflections were collected covering the indices, -6<=h<=5, -13<=k<13, -25<=l<=21. 2213 reflections were found to be symmetry independent, with a R_{int} of 0.0214. Indexing and unit cell refinement indicated a **P**rimitive, **Orthorhombic** lattice. The space group was found to be ***$P2_12_12_1$***. The data were integrated using the Bruker SAINT software program and scaled using the SADABS software program. Solution by direct methods (SHELXT) produced a complete phasing model consistent with the proposed structure.

All nonhydrogen atoms were refined anisotropically by full-matrix least-squares (SHELXL-2014). All carbon bonded hydrogen atoms were placed using a riding model. Their positions were constrained relative to their parent atom using the appropriate HFIX command in SHELXL-2014. All other hydrogen atoms (H-bonding) were located in the difference map (N-H, O-H). There positions were refined using “riding” model. Crystallographic data are summarized in Table 2.7.

Table 2.7 Crystal data and structure refinement for Tor_PL_mthI (^{mth}I)

Report date	2019-02-27	
Identification code	Tor_PL_mthI	
Empirical formula	C12 H14 N2 O5 S	
Molecular formula	C12 H14 N2 O5 S	
Formula weight	298.31	
Temperature	100.0 K	
Wavelength	1.54178 Å	
Crystal system	Orthorhombic	
Space group	$P2_12_12_1$	
Unit cell dimensions	a = 5.1329(3) Å	α= 90°.
	B = 11.1174(4) Å	β= 90°.
	c = 21.1792(10) Å	γ = 90°.
Volume	1208.58(10) $Å^3$	
Z	4	
Density (calculated)	1.639 Mg/m^3	
Absorption coefficient	2.623 mm^{-1}	
F(000)	624	
Crystal size	0.15 x 0.12 x 0.03 mm^3	
Crystal color, habit	colorless plate	
Theta range for data collection	4.175 to 68.821°.	
Index ranges	-6<=h<=5, -13<=k<=13, -25<=l<=21	
Reflections collected	5343	
Independent reflections	2213 [R(int) = 0.0214]	
Completeness to theta = 67.500°	99.8 %	
Absorption correction	Semi-empirical from equivalents	
Max. and min. transmission	0.5213 and 0.4324	
Refinement method	Full-matrix least-squares on F^2	
Data / restraints / parameters	2213 / 0 / 188	
Goodness-of-fit on F^2	1.029	
Final R indices [I>2sigma(I)]	R1 = 0.0253, wR2 = 0.0627	
R indices (all data)	R1 = 0.0266, wR2 = 0.0633	
Absolute structure parameter	0.010(7)	
Largest diff. peak and hole	0.260 and -0.192 e.$Å^{-3}$	

For the crystal structure of 15, the single crystal X-ray diffraction studies were carried out on a Bruker Pt 135 CCD diffractometer equipped with Cu $K_{\square}$ radiation ($\square$ = 1.54178).

A 0.220 x 0.080 x 0.060 mm colorless crystal was mounted on a Cryoloop with Paratone oil. Data were collected in a nitrogen gas stream at 100(2) K using $\square$ and $\square$ scans. Crystal-to-detector distance was 45 mm using exposure time 5, 20 and 30s s with a scan width of 1.50°. Data collection was 98.3% complete to 67.500° in $\square$.

A total of 23073 reflections were collected covering the indices, -6<=h<=6, -16<=k<16, -25<=l<=23. 10240 reflections were found to be symmetry independent, with a R_{int} of 0.0329. Indexing and unit cell refinement indicated a **P**rimitive, **Triclinic** lattice. The space group was found to be ***P*1**. The data were integrated using the Bruker SAINT software program and scaled using the SADABS software program. Solution by direct methods (SHELXT) produced a complete phasing model consistent with the proposed structure.

All nonhydrogen atoms were refined anisotropically by full-matrix least-squares (SHELXL-2014). All carbon bonded hydrogen atoms were placed using a riding model. Their positions were constrained relative to their parent atom using the appropriate HFIX command in SHELXL-2014. All other hydrogen atoms (H-bonding) were located in the difference map (N-H, O-H) . There positions were refined using “riding” model. Crystallographic data are summarized in Table 2.8. Notes: Excellent data and refinement, absolute stereochemistry conclusive, two molecules in asymmetric unit.

Table 2.8 Crystal data and structure refinement for Tor_MTHU3 (**15**)

Report date	2019-04-30	
Identification code	tor_mthu3	
Empirical formula	C33 H26 N2 O9 S	
Molecular formula	C33 H26 N2 O9 S	
Formula weight	626.62	
Temperature	100.15 K	
Wavelength	1.54178 Å	
Crystal system	Triclinic	
Space group	P1	
Unit cell dimensions	a = 5.40480(10) Å	α= 71.1950(10)°.
	b = 13.6367(4) Å	β= 85.3720(10)°.
	c = 20.6903(6) Å	γ = 85.7510(10)°.
Volume	1436.97(7) $Å^3$	
Z	2	
Density (calculated)	1.448 Mg/m^3	
Absorption coefficient	1.536 mm^{-1}	
F(000)	652	
Crystal size	0.22 x 0.08 x 0.06 mm^3	
Crystal color, habit	colorless block	
Theta range for data collection	2.260 to 72.648°.	
Index ranges	-6<=h<=6, -16<=k<=16, -25<=l<=23	
Reflections collected	23073	
Independent reflections	10240 [R(int) = 0.0329]	
Completeness to theta = 67.500°	98.3 %	
Absorption correction	Semi-empirical from equivalents	
Max. and min. transmission	0.7536 and 0.6731	
Refinement method	Full-matrix least-squares on F^2	
Data / restraints / parameters	10240 / 3 / 813	
Goodness-of-fit on F^2	1.027	
Final R indices [I>2sigma(I)]	R1 = 0.0273, wR2 = 0.0695	
R indices (all data)	R1 = 0.0285, wR2 = 0.0701	
Absolute structure parameter	0.024(5)	
Largest diff. peak and hole	0.207 and -0.197 e.$Å^{-3}$	

For the crystal structure of ^{mth}A in the alpha configuration, the single crystal X-ray diffraction studies were carried out on a Bruker SMART APEX II CCD diffractometer equipped with Cu K$_{\square}$ radiation ($\square$ = 1.54178). Crystals of the subject compound were used as received (grown by diffusion of MeOH into $CHCl_3$). A 0.210 x 0.030 x 0.010 mm translucent, colorless prism crystal was mounted on a Cryoloop with Paratone-N oil.

Data were collected in a nitrogen gas stream at 100(2) K using $\square\square$and$\square\square$ scans. Crystal-to-detector distance was 40 mm using exposure times of 5, 6, 11, 15, 22 and 60 seconds (depending on the 2$\square$ position) with a scan width of 1.40°. Data collection was 99.7 % complete to 67.500° in $\square$. A total of 16585 reflections were collected. 4632 reflections were found to be symmetry independent, with an R_{int} of 0.0350. Indexing and unit cell refinement indicated a **Primitive Monoclinic** lattice. The space group was found to be ***P2$_1$*****.** The data were integrated using the Bruker SAINT Software program and scaled using the SADABS software program. Solution by direct methods (SHELXT) produced a complete phasing model consistent with the proposed structure.

All non-hydrogen atoms were refined anisotropically by full-matrix least-squares (SHELXL-2014). All carbon bonded hydrogen atoms were placed using a riding model. Their positions were constrained relative to their parent atom using the appropriate HFIX command in SHELXL-2014. Crystallographic data are summarized in Table 2.9. Notes: Excellent data and refinement. Absolute stereochemistry established (Flack parameter, -0.007(13)).

Table 2.9 Crystal data and structure refinement for Tor152a (^{mth}A (alpha))

Report date	2019-11-19	
Identification code	Tor152a	
Empirical formula	C12 H15 N3 O4 S	
Formula weight	297.33	
Temperature	100.0 K	
Wavelength	1.54178 Å	
Crystal system	Monoclinic	
Space group	P 1 21 1	
Unit cell dimensions	a = 7.2609(2) Å	α= 90°.
	b = 15.7798(4) Å	β= 91.0260(10)°.
	c = 10.8048(3) Å	γ = 90°.
Volume	1237.77(6) Å^3	
Z	4	
Density (calculated)	1.596 Mg/m^3	
Absorption coefficient	2.519 mm^{-1}	
F(000)	624	
Crystal size	0.21 x 0.03 x 0.01 mm^3	
Theta range for data collection	4.092 to 71.479°.	
Index ranges	-8<=h<=8, -18<=k<=17, -13<=l<=11	
Reflections collected	16585	
Independent reflections	4632 [R(int) = 0.0350]	
Completeness to theta = 67.500°	99.7 %	
Absorption correction	Semi-empirical from equivalents	
Max. and min. transmission	0.7535 and 0.6553	
Refinement method	Full-matrix least-squares on F^2	
Data / restraints / parameters	4632 / 1 / 370	
Goodness-of-fit on F^2	1.067	
Final R indices [I>2sigma(I)]	R1 = 0.0330, wR2 = 0.0835	
R indices (all data)	R1 = 0.0344, wR2 = 0.0842	
Absolute structure parameter	-0.007(13)	
Extinction coefficient	n/a	
Largest diff. peak and hole	0.347 and -0.207 e.Å^{-3}	

2.9.3 General Spectroscopic Procedures

Spectroscopic grade DMSO and dioxane were obtained from Sigma Aldrich and aqueous solutions were prepared with de-ionized water. All the measurements were carried out in a 3 mL 1 cm four-sided quartz cuvette or 125 µL 1 cm four-sided quartz cuvette from Helma.

Absorption spectra were measured on a Shimadzu UV-2450 spectrophotometer setting the slit at 1 nm and using a resolution of 0.5 nm. All the spectra were corrected for the blank. Steady state emission spectra were measured on a Horiba Fluoromax-4 equipped with a cuvette holder with a stirring system setting the excitation slit at 2 nm and the emission slit at 3 nm, the resolution at 1 nm, and the integration time to 0.1 s. The steady state fluorescence spectra were performed upon excitation at the maximum wavelength of absorption.

All the spectra were corrected for the blank. Both instruments were equipped with a thermostat-controlled ethylene glycol-water bath fitted to specially designed cuvette holder and the temperature was kept at 25.0 ± 0.1 ºC.

Nucleosides were dissolved in DMSO to prepare highly concentrated stock solutions: ^{mth}**A** (8.74 mM), ^{mth}**C** (9.53 mM), ^{mth}**G** (4.95 mM), ^{mth}**U** (11.9 mM), ^{mth}**I** (8.88 mM).

2.9.4 Fluorescence Quantum Yield Evaluation

The samples concentrations were adjusted to have an optical density lower than 0.1 at the excitation wavelength (λ_{ex}). The fluorescence quantum yields (φ) were evaluated based on an external standard, quinine (for ^{mth}**A**, 0.55 in 2M sulfuric acid) or 2-aminopurine (for all others, 0.68 in water) by using the relative quantum yield equation (Eq. 2.1).

2.9.5 Sensitivity to Polarity

Experiments evaluating the effect of polarity were performed in water, dioxane and their mixtures (20, 40, 60, and 80 v/v % water in dioxane). The sample $E_T(30)$ values were determined by dissolving a small amount of Reichardt's dye in the mixture of the same solvent

used to dilute the nucleoside's DMSO sample.[22] The observed long wavelength absorption maximum (λ_{abs}^{max}) was converted to the $E_T(30)$ values with the $E_T(30)$ equation (Eq. 2.2).

2.9.6 General Enzyme Reaction Procedures

Bovine Spleen ADA was obtained from Sigma Aldrich (EC Number 232-817-5). The commercial solution (1150 U/mL in 3.2 M $(NH_4)_2SO_4$, 0.01 M potassium phosphate, pH 6.0) was diluted to 115 (^{mth}A reactions), 11.5 (thA reactions), or 1.15 (^{tz}A and adenosine reactions) U/mL by dissolving an aliquot (1 µL) in the appropriate amount of phosphate buffer (50 mM, pH 7.4). The enzyme solution was freshly prepared and kept on ice prior to use.

Human GDA expression was performed by Dr. Yao Li and Marcela Bucardo. Wild-type human GDA gene, cloned into pET-28B vector (Genescript, Piscataway Township, NJ), was expressed with an N-terminal hexahistidine tag. The construct was sequence-verified (GENEWIZ, South Plainfield, NJ). The plasmid (4 µg) was dissolved in water to a concentration of 28.8 ng/µL. *E. coli* BL21 (DE3) cells were transformed with the GDA containing plasmid. Overnight starter cultures were grown in Lubria Broth (LB) medium at 37ºC with 50 µg/mL of kanamycin. The overnight culture was used to inoculate 1 L of LB medium with 50 µg/mL kanamycin. Cells were grown while shaking at 37ºC until OD_{600} of 0.6 was reached and the culture was down tempered to 18ºC over a period of 1 hour. To induce target protein production, 0.5 mM IPTG was added, and the medium was left to stir at 18ºC overnight. Cells were harvested after overnight growth by centrifugation at 3500 rpm for 35 minutes at 4ºC.

Cells were resuspended in lysis buffer [20 mM HEPES, 500 mM NaCl, 10% glycerol, 0.5 mM TCEP (pH 7.5), supplemented with one tablet of Complete EDTA-free protease inhibitor (Roche Applied Science)] and lysed by sonication. Cell lysate was cleared by centrifugation at 10,000 rpm for 1 hour at 4ºC. The supernatant was decanted and filtered through a 0.45 µm syringe filter. GDA was purified by immobilized metal affinity chromatography. IMAC Ni-charged column [2 mL HisPur Ni-NTA Resin (Thermo Scientific)] was equilibrated with lysis buffer to

which the lysate was then added. The column was washed with 50 mL of wash buffer supplemented with 20 mM imidazole. The bound protein was eluted from the column with elution buffer (wash buffer supplemented with 200 mM imidazole). Fractions were analyzed by SDS-PAGE and those containing the target protein were pooled, subsequently concentrated and buffer exchanged into storage buffer [20 mM Tris-HCl buffer (pH 8.0), 10% glycerol, 1 mM DTT] using a centrifugal filter device with a 10,000 molecular weight cut off. After protein expression and purification, the final protein concentration was 5.3 mg/mL (0.1 mM) in a total volume of 1.7 mL. Protein aliquots were snap-frozen and stored at –80ºC until further use. Before use in enzymatic reactions the GDA protein stock was diluted 1:100 in phosphate buffer.

Concentrated stock solutions of ^{mth}A (8.74 mM), $^{mth}G_n$ (29.8 mM), ^{th}A (4.44 mM), $^{th}G_n$ (7.78 mM), ^{tz}A (8.69 mM), $^{tz}G_n$ (12.0 mM), and adenosine (3.51 mM) in DMSO were diluted in water to yield working stock solutions (1 mM). Guanine (10.6 mM) was separately prepared in water adjusted to pH 12.0 by 1M sodium hydroxide and diluted in water to yield a working stock solution (1 mM). The samples were prepared in a 125 µL 1 cm four-sided quartz cuvette from Helma and maintained at 25.0 ± 0.1 ºC during the course of the reaction. Reaction concentrations for adenosine and its analogues were 10 µM and reaction concentrations for guanine and its analogues were 3 µM.

2.9.7 Absorption and Emission Monitored Kinetic Assays

The ADA-mediated enzymatic conversion of adenosine (and its analogues) to inosine (and its analogues) was followed by absorbance and emission (for the emissive analogues) spectroscopy by monitoring the intensity variation at a fixed wavelength as a function of time. The real-time conversion of adenosine (and its analogues) to inosine (and its analogues) was performed on a Shimadzu UV-2450 spectrophotometer setting the slit at 1 nm and taking a point every 20 seconds for 600 seconds (1200 seconds for ^{mth}A) upon addition of ADA. The

enzymatic conversion was followed at 260 nm for adenosine to inosine, 340 nm for ^{tz}A to ^{tz}I and thA to thI, and 353 nm for ^{mth}A to ^{mth}I.

The enzymatic conversion was also followed by emission at 410 nm upon excitation at 322 nm for ^{tz}A to ^{tz}I, 391 nm upon excitation at 318 nm for thA to thI, and 415 nm upon excitation at 331 nm for ^{mth}A to ^{mth}I. The excitation wavelengths were all the respective isosbestic points. Excitation at the isosbestic point gives emission spectra that are unaffected by changes in optical density. The real-time conversion was measured on a Horiba Fluoromax-4 equipped with a cuvette holder with a built-in stirring system, setting the excitation and the emission slits at 2 and 3 nm respectively and taking a point every two seconds for 600 seconds upon addition of ADA.

Absorbance and emission signal were normalized and converted to concentration by multiplying the normalized data by the initial concentration. The apparent rate constant (k_{app}) and the reaction half-time ($t_{1/2}$) were determined by fitting a pseudo-first order curve to the data. The equations used were:

$$[A] = [A]_0 e^{-k_{app}t}$$

Equation 2.3 First Order Substrate Curve

$$[A] = [A]_0 (1 - e^{-k_{app}t})$$

Equation 2.4 First Order Product Curve

$$t_{1/2} = \frac{\ln (2)}{k_{app}}$$

Equation 2.5 First Order Half-Life Relation

where [A] is the concentration of adenosine or its analogue at a given time, $[A]_0$ is the initial concentration of adenosine or its analogue, k_{app} is the reaction rate, and t is time. If the signal was decreasing the first equation was used to determine k_{app}. If the signal was increasing the second equation was used to determine k_{app}. The reported values are the average of three independent sets of measurements.

The GDA-mediated enzymatic conversion of guanine (and its analogues) to xanthine (and its analogues) was followed by absorbance and emission on the same instruments as for ADA-mediated reactions. Slit widths were the same as for ADA-mediated reactions on both instruments and measurements were taken every 10 seconds for 600 seconds. The enzymatic conversion was followed by absorption at 270 nm for guanine to xanthine and at 355 nm for each analogue pair. The enzymatic conversion was followed by emission at 450 nm upon excitation at 328 nm for $^{tz}G_n$ to $^{tz}X_n$, 450 nm upon excitation at 360 nm for $^{th}G_n$ to $^{th}X_n$, and 450 nm upon excitation at 360 nm for $^{mth}G_n$ to $^{mth}X_n$. No signal change was observed in the reaction of $^{th}G_n$ and $^{mth}G_n$ over 600 seconds. A pseudo-first curve was fit to the resulting data to obtain k_{app} and $t_{1/2}$ values as described above.

2.9.8 T7 RNA Polymerase Reactions

The transcript was transcribed using T7 RNA polymerase (Fig. 2.). The single strand DNA template was annealed to a consensus 18-mer T7 RNA polymerase promoter in TE buffer (10 mM Tris-HCl, 1 mM EDTA, 100 mM NaCl, pH 7.8) by heating a 1:1 mixture (10 μM) at 90ºC for 3 minutes and cooling the solution slowly down to room temperature. Large scale transcription reactions were performed in buffer (40 mM Tris-HCl, pH 7.9) containing annealed templates (500 nM), dithiothreitol (10 mM), NaCl (10 mM), spermidine (2 mM), $MgCl_2$ (20 mM), RNase inhibitor (Ribolock, 1 U/μL), and T7 RNA polymerase (0.1 μg/μL) in a total volume of 200 μL. For the native transcript ATP (2 mM), GTP (2 mM), CTP (2 mM), and UTP (2 mM) were used. For lanes 1–4 on Figure 2.13, GTP was substituted for the corresponding GTP analogue (2 mM) listed. For lanes 5–8 in Figure 2.13, guanosine (10 mM), ^{tz}G, ^{th}G, or ^{mth}G were added to the reaction in large excess.

2.10 Acknowledgements

Chapter 2 is adapted from work currently being drafted for submission: Ludford III, P. T.; Yang, S.; Tor, Y. “The Next Generation of Emissive RNA Alphabets” *in preparation*. Permission to use materials from the manuscript was also obtained from co-authors Shenghua Yang and Yitzhak Tor. The dissertation author will be the first author.

2.11 References

1. Sinkeldam, R. W.; Greco, N. J.; Tor, Y. *Chem. Rev.* **2010**, *110*, 2579–2619.

2. Wilhelmsson, M. *Q. Rev. Biophys.* **2010**, *43*, 159–182.

3. Hawkins, M. E. *Cell Biochem. Biophys.* **2001**, *34*, 257–281.

4. Wilson, J. N.; Kool, E. T. *Org. Biomol. Chem.* **2006**, *4*, 4265–4274.

5. Okamoto, A.; Saito, Y.; Saito, I. *J. Photochem. Photobiol., C* **2005**, *6*, 108–122.

6. Dodd, D. W.; Hudson, R. H. E. *Mini-Rev. Org. Chem.* **2009**, *6*, 378–391.

7. Kimoto, M.; Cox, R. S., III; Hirao, I. *Expert Rev. Mol. Diagn.* **2011**, *11*, 321–331.

8. Rist, M. J.; Marino, J. P. *Curr. Org. Chem.* **2002**, *6*, 775–793.

9. Wierzchowski, J.; Antosiewicz, J. M.; Shugar, D. *Mol. BioSyst.* **2014**, *10*, 2756–2774.

10. Bood, M.; Sarangamath, S.; Wranne, M. S.; Grotli, M.; Wilhelmsson, L. M. *Beilstein J. Org. Chem.* **2018**, *14*, 114–129.

11. Gaied, N. B.; Glasser, N.; Ramalanjaona, N.; Beltz, H.; Wolff, P.; Marquet, R.; Burger, A.; Mely, Y. *Nucleic Acids Res.* **2005**, *33*, 1031–1039.

12. Nadler, A.; Strohmeier, J.; Diederichsen, U. *Angew. Chem., Int. Ed.* **2011**, *50*, 5392–5396.

13. Dumat, B.; Bood, M.; Wranne, M. S.; Lawson, C. P.; Foller Larsen, A.; Preus, S.; Streling, J.; Graden, H.; Wellner, E.; Grotli, M.; Wilhelmsson, L. M. *Chem. - Eur. J.* **2015**, *21*, 4039–4048.

14. Hopkins, P. A.; Sinkeldam, R. W.; Tor, Y. *Org. Lett.* **2014**, *6*, 25–64.

15. Shin, D.; Sinkeldam, R. W.; Tor, Y. *J. Am. Chem. Soc.* **2011**, *133*, 14912–14915.

16. Rovira, A. R.; Fin, A.; Tor, Y. *J. Am. Chem. Soc.* **2015**, *137*, 14602–14605.

17. Sinkeldam, R. W.; McCoy, L. S.; Shin, D.; Tor, Y. *Angew. Chem. Int. Ed.* **2013**, *52*, 14026–14030.

18. Ludford III, P. T.; Rovira, A. R.; Fin, A.; Tor, Y. *ChemBioChem* **2019**, *20*, 718–726.

19. Li, Y.; Ludford III, P. T.; Fin, A.; Rovira, A. R.; Tor, Y. *Chem. - Eur. J.* **2020**, *26*, 6076–6084.

20. Grimmet, M. R. *Science of Synthesis*, **2002**, *12*, 325–528.

21. Wang, S.; Fang, K.; Dong, G.; Chen, S.; Liu, N.; Miao, Z.; Yao, J.; Li, J.; Zhang, W.; Sheng, C. *J. Med. Chem.* **2015**, *58*, 6678–6696.

22. Reichardt, C. Chem. Rev. 1994, 94 (8), 2319–2358.

23. Bucardo, M.; Wu, Y.; Ludford III, P. T.; Fin, A.; Tor, Y. “Real-time Monitoring of Human Guanine Deaminase Activity by an Emissive Guanine Analog” *ACS Chem. Bio.*, **2021**, *in press*.

24. Ludford III, P. T.; Li, Y.; Yang, S.; Tor, Y. *Org. Biomol. Chem.*, **2021**, DOI: https://doi.org/10.1039/D1OB00705J.

25. McCoy, L. S.; Shin, D.; Tor, Y. Isomorphic Emissive GTP Surrogate Facilitates Initiation and Elongation of in Vitro Transcription Reactions. *J. Am. Chem. Soc.* **2014,** *136* (43), 15176–15184.

Chapter 3

Development of a High Throughput Screening Assay of Adenosine Deaminase

3.1 Brief Introduction to Adenosine Deaminase and Reported Inhibitors

Adenosine Deaminase (ADA) is a critically important enzyme involved in purine metabolism. ADA deaminates adenosine and 2'-deoxyadenosine to inosine and 2'-deoxyinosine, respectively.[1,2] It is a metalloenzyme containing a zinc metal ion.[3] The reaction mechanism begins by nucleophilic attack at the C6 position by a zinc activated hydroxide. The intermediate then rehybridizes (Fig. 3.1). This results in the release of ammonia, which can be used to monitor the reaction.[4,5]

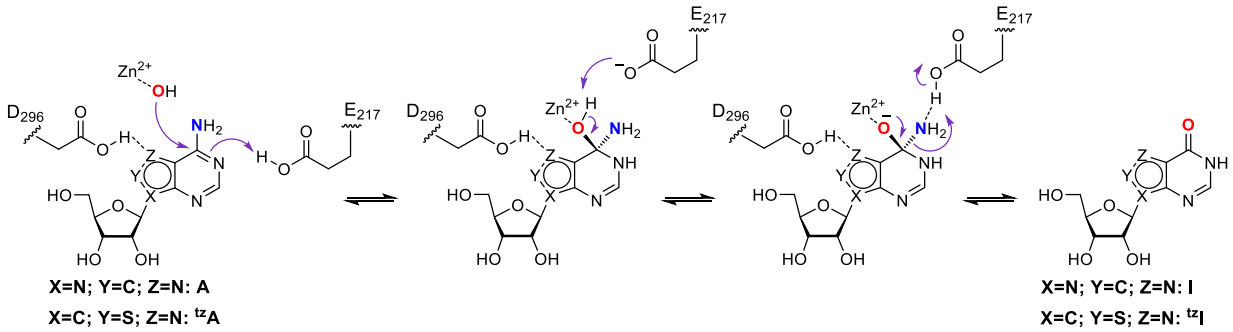

Figure 3.1 Mechanism of Deamination by Adenosine Deaminase

ADA has been implicated in certain types of cancer, notably leukemia and lymphoma, and is necessary for a properly functioning immune system.[6,7] This has made it attractive as a drug target. Inhibitors of ADA have thus been sought after as potential chemotherapeutic agents.[8–13] Two potent inhibitors, Pentostatin and Cladribine, have been FDA approved and have been used to treat hairy cell leukemia (Fig. 3.2).[1,14,15] EHNA, another inhibitor of ADA, is quite potent as well, but failed to make it into the clinic.[15–17] Thus the discovery of new ADA inhibitors is still a very real challenge.[18–21]

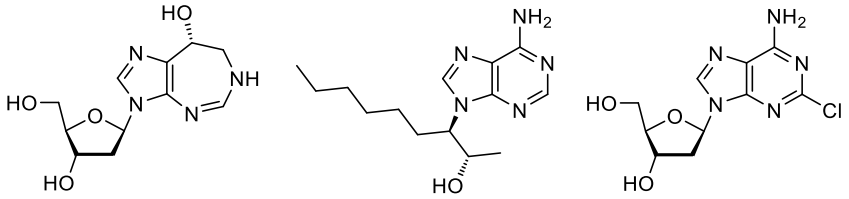

Figure 3.2 Potent Inhibitors of Adenosine Deaminase

Historically, methods of monitoring ADA activity included chromatographic separation,[20] a time-consuming task that does not yield results in real time, and absorption spectroscopy, which suffers from optical interference due to the low wavelength absorption bands of adenosine and inosine.[14,18,19,21] This left a vacancy for new methods of detecting ADA activity to be introduced. Other new methods of monitoring ADA activity and thereby screening inhibitors have been realized in recent years,[22–27] but herein we describe a method of screening potential inhibitors based on fluorescent adenosine and inosine surrogates, ^{tz}A and ^{tz}I respectively, in a high-throughput format.[28]

3.2 Synthesis of ^{tz}A and ^{tz}I

The synthetic route to ^{tz}A and ^{tz}I has been previously reported.[28] An ingenious nontraditional approach by Dr. Rovira was used to construct the nucleobase from the sugar. The underlying method used to construct the isothiazole ring structure is a Thorpe-Ziegler

cyclization. The route starts with construction of the sugar. Ribose with a methoxy moiety at the 1 position is protected with benzyl protecting groups via benzyl bromide, sodium hydride, and catalytic tetrabutylammonium iodide. The methoxy is removed by treatment with acid to yield **3**. The deprotected sugar then undergoes a Swern oxidation to give a benzyl protected lactone, **4**. The lactone is then attacked by methane diiodide using lithium halogen exchange giving **5**. The iodide is then displaced by thioacetate yielding **6**. Finally, compound **6** is reduced to a thiol (Scheme 3.1).

With the thiol sugar, **7**, synthesized, the nucleobase is ready to be constructed. Compound **7** is treated with **13** in a Thorpe-Ziegler reaction to give **8**. The hydroxyl moiety on **8** is then removed by treating with triethylsilane and $BF_3 \cdot OEt_2$ yielding **9**. The six-member pyrimidine ring is then cyclized by reacting **9** with triethylorthoformate. The resulting 10 can be deprotected to yield ^{tz}I or pushed forward to ^{tz}A. If pushing to ^{tz}A, **10** is treated with P_2S_5 to give **11**. Compound **11** undergoes ammonolysis and is then deprotected with ethanedithiol and $BF_3 \cdot OEt_2$ yielding ^{tz}A in 11 steps (Scheme 3.1).

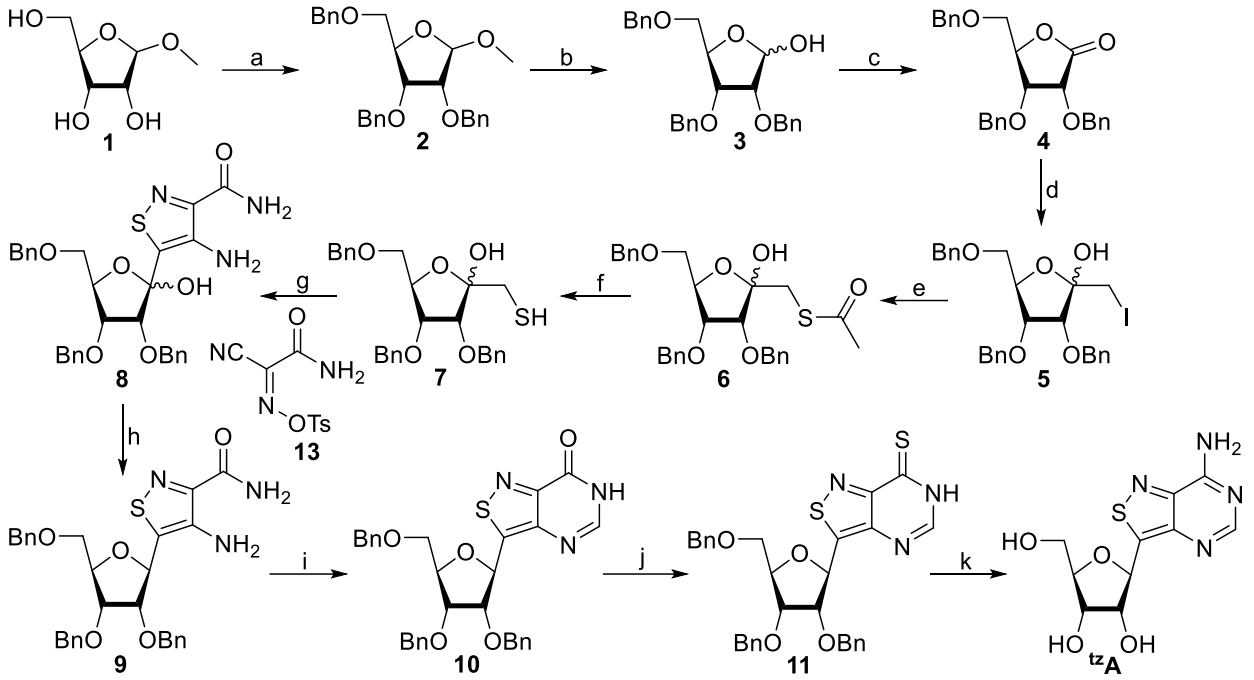

Scheme 3.1 ^{tz}A Synthetic Pathway. Reagents and Conditions: (a) Benzyl bromide, tetrabutylammonium iodide, sodium hydride (60% in mineral oil), DMF, 0ºC to RT, overnight, 82%. (b) Acetic acid (99%), water, RT, overnight, 84%. (c) Oxalyl chloride, DMSO, DCM, –78ºC, 1.5 h, 57%. (d) CH_2I_2, methyllithium, toluene, –78ºC, 1 h, 67%. (e) Potassium thioacetate, DMF, RT, 6 h, 74%. (f) OEt_2, $LiAlH_4$, 0ºC to RT, 1 h, >90%. (g) **13**, EtOH, morpholine, 5 h, 0ºC to RT, 79%. (h) Et_3SiH, $BF_3{\cdot}OEt_2$, DCM, –78ºC to RT, 4 h, 63%. (i) $CH(OEt)_3$, Ac_2O, 120ºC, 16 h, 69%. (j) P_2S_5, pyridine, 65ºC, 2 h. (k) i) NH_3, MeOH, 70ºC, 16 h; ii) Ethanedithiol, $BF_3{\cdot}OEt_2$, DCM, RT, 72 h, 32% over steps j and k.

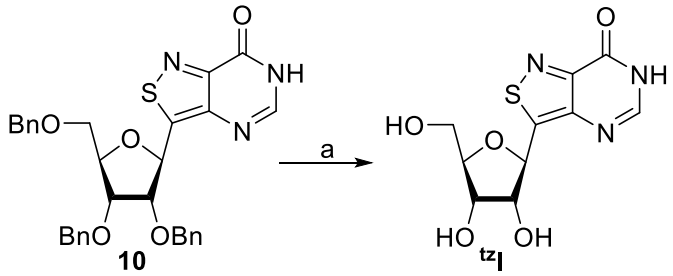

Scheme 3.2 Synthesis of ^{tz}I. Reagents and Conditions: a) Ethanedithiol, $BF_3{\cdot}OEt_2$, DCM, RT, 72 h, 30%.

3.3 Reported Kinetics of Adenosine Deaminase

The Michaelis-Menten kinetic parameters of ^{tz}A and ADA have been previously reported.[26] ^{tz}A as a substrate of ADA was found to have a K_M of 19 μM which was comparable to adenosine (28 μM) and its reaction $t_{1/2}$ (39 s) reported by Rovira et. al. was also comparable

to adenosine (57 s).[28] The method of detection used to monitor the reaction in all experiments was change in fluorescence. Due to the comparable binding and fast reaction times, ^{tz}A was the ideal candidate for monitoring ADA activity in a high throughput format.

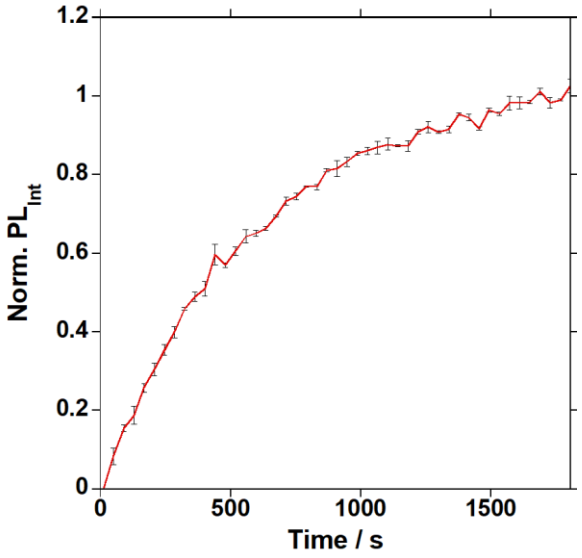

Figure 3.3 Example of a Typical Reaction of ^{tz}A with ADA on a Plate Reader

3.4 High Throughput Screen of the Cohen Lab Fragment Library

The Cohen Lab in recent years has assembled and screened a large metal binding pharmacophore (MBP) library against a number of metalloenzymes. These metalloenzymes have included glyoxalase-1, New Delhi metallo-β-lactamase-1, influenza PA_N endonuclease, proteasomal deubiquitinase Rpn11, MMP-12, and hCAII.[29–35] The MBPs are able to coordinate with the metal inside the binding pocket and thereby block it from catalysis. Due to the small size of these MBPs, they may be used as scaffolds with which to systematically build highly potent enzyme specific inhibitors. We sought to combine the real-time fluorescence-based assay using ^{tz}A with the MBP fragment library to hopefully identify a large number of new scaffolds for ADA inhibitors.

Once ^{tz}A had been obtained, we set out to screen ~350 MBPs from the Cohen Lab Fragment Library in collaboration with the Cohen Lab. The reaction of ^{tz}A with ADA in the presence of 200 μM of each inhibitor was monitored by emission at 410 nm upon excitation at 322 nm, the isosbestic point of ^{tz}A and ^{tz}I. The experiments were run in triplicate and a control with no enzyme was also run. The resulting reaction curves were converted to percent change relative to the initial time point and the value at 20 minutes compared to the same time point in a reaction without inhibitor. This yielded a wide range of percent inhibitions, from 87% to below 0% (Fig. 3.4). B26, at 89%, was found to have the highest percent inhibition from the initial library screen (Fig. 3.5).

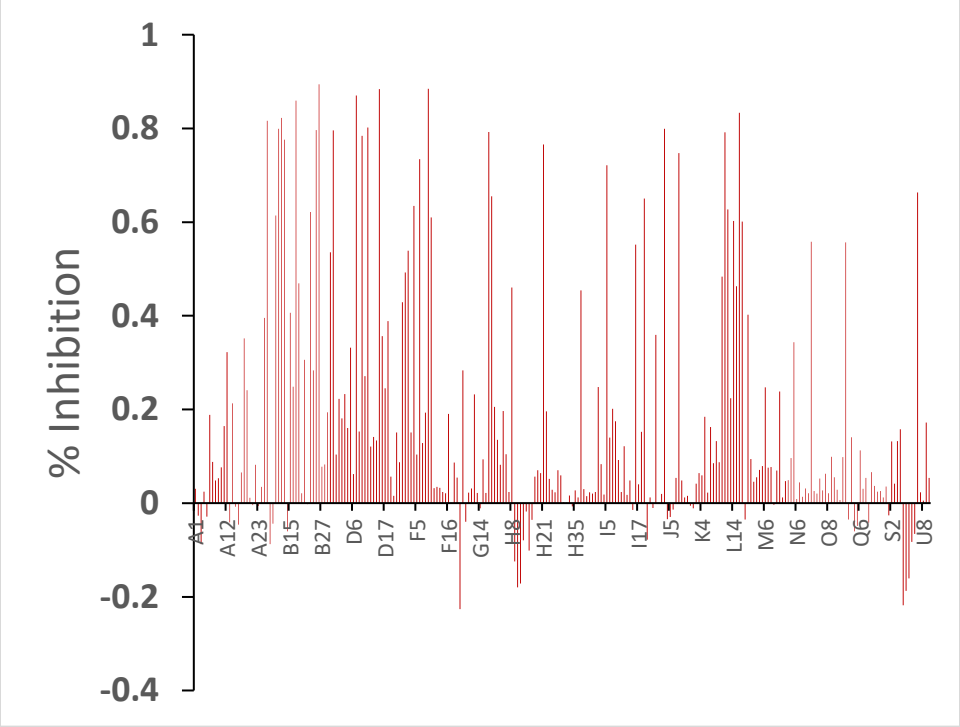

Figure 3.4 Results of a High Throughput Screen of the Cohen Lab Fragment Library. Results of the MBP library screen against ADA, represented as a bar graph of percent inhibition (relative to no inhibitor) of ADA in the presence of 200 μM MBP fragment.

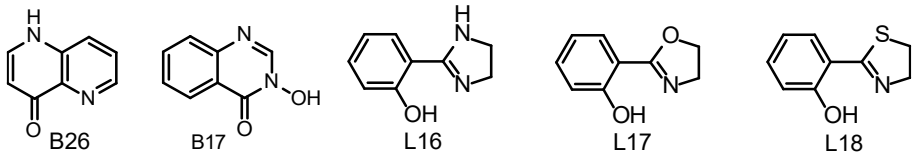

Figure 3.5 Notable Hits of the Initial Library Screen

We chose to run an IC_{50} experiment of two compounds in the high throughput format, B17 which had a percent inhibition of 86% and EHNA which was a known potent inhibitor and which would serve as a control (Fig. 3.5). The IC_{50} obtained for EHNA was 6 nM and the Cheng-Prusoff equation (Eq. 3.1) was used to calculate the K_I at 5 nM (Fig. 3.6, Table 3.1). This was in good agreement with previously reported K_I values of EHNA (Table 3.1). The IC_{50} of B17 was found to be 30 μM and the K_I was 25 μM (Figs. 3.7, 3.8). This was a promising start and so we decided to pick two hits from the initial screen, L16 and L17, with which to further investigate.

$$K_I = \frac{IC_{50}}{1 + \frac{[S]}{K_M}}$$

Equation 3.1 Cheng-Prusoff Equation

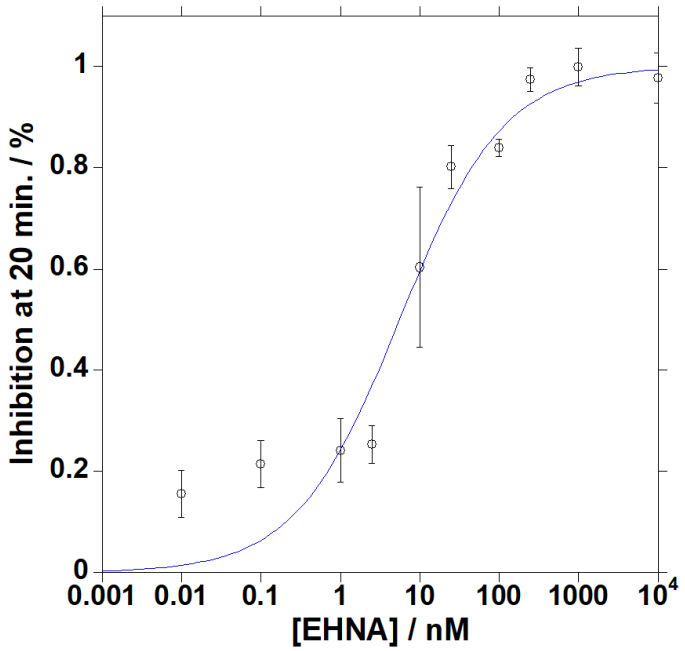

Figure 3.6 EHNA IC_{50} Analysis Using a Plate Reader. Semi-log plot of % inhibition in decimal form after 20 minutes versus [EHNA] fit to a sigmoidal Hill curve.

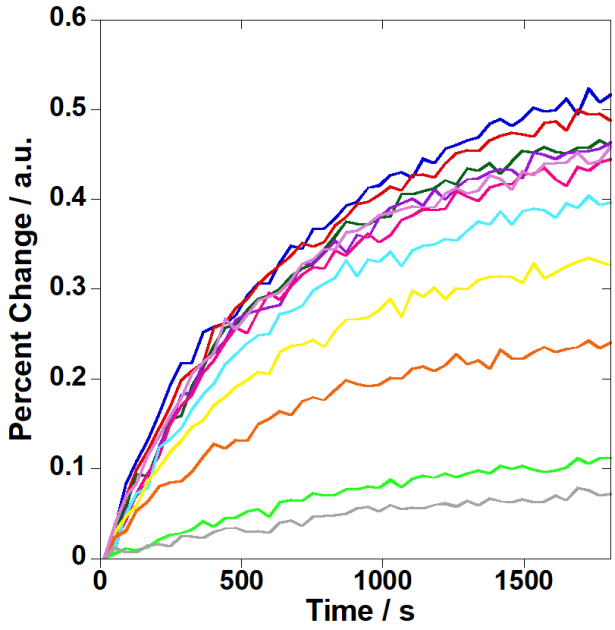

Figure 3.7 Conversion of ^{tz}A to ^{tz}I by ADA in the presence of various concentrations of B17 (0 μM (green), 0.001 μM (blue), 0.01 μM (red), 0.025 μM (purple), 0.1 μM (pink), 1 μM (dark pink), 2.5 μM (light blue), 10 μM (yellow), 25 μM (orange), 100 μM (light green), 250 μM (grey)).

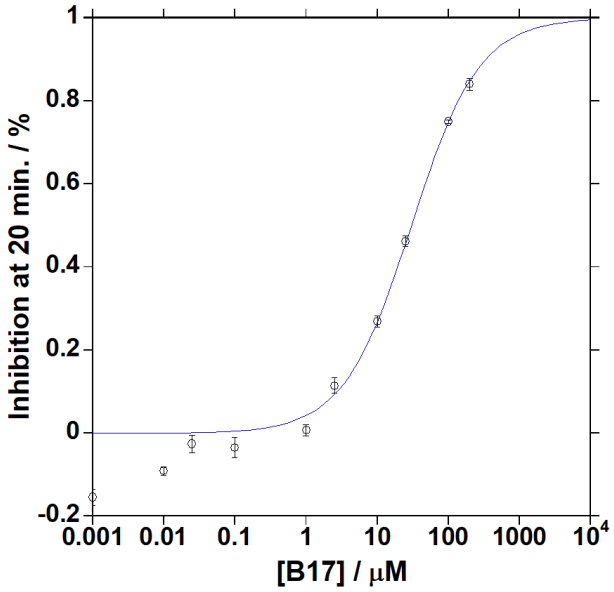

Figure 3.8 B17 IC_{50} Analysis Using a Plate Reader. Semi-log plot of % inhibition in decimal form after 20 minutes versus [B17] fit to a sigmoidal Hill curve.

3.5 Structure Activity Relationship Analysis of Derivatives of Selected Library Molecules

A member of the Cohen Lab, Dr. Rebecca Adamek, synthesized 12 derivatives of L17 (Fig. 3.9). The changes made were a methyl moiety was placed at each carbon position the was not sterically hindered, the benzene ring system was expanded to a naptholene, and the oxazoline ring was expanded (Fig. 3.9). An IC_{50} analysis was performed on L16, L17, and each of the 12 compounds using the ^{tz}A reaction with ADA to monitor the change in activity after 10 minutes. The goal was to determine a structure activity relationship (SAR) for the L17 derivatives.

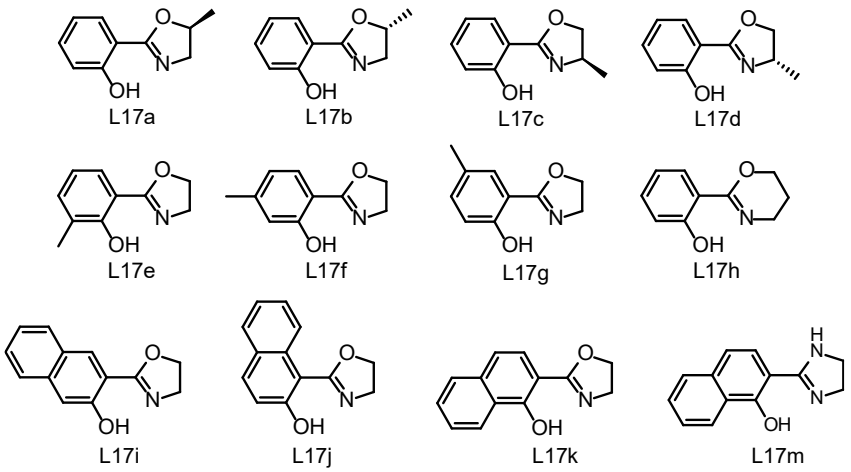

Figure 3.9 Structures of L16 and L17 Derivatives

IC_{50} values obtained for compounds L16, L17, and L17a–L17k ranged from 93 μM to above 700 μM. Based on the IC_{50} values, the methyl moiety lowered potency of all compounds except L17a and L17b. The expanded oxazoline ring also resulted in a severe loss of potency. The expansion of the aromatic ring system in compound L17i lowered its solubility in water to a degree that the IC_{50} could not be accurately determined. Compound L17j seemed to have a slightly negative or no effect on potency and compound L17k improved potency by over two-fold. These findings offered a few directions for designing an improved inhibitor.

Table 3.1 Experimentally Determined IC_{50} and K_I Values of Prepared L17 Derivatives

Compound	IC_{50} (μM)	K_I (μM)
EHNA	0.006 ± 0.002[a] 0.023 ± 0.004[b]	0.005 ± 0.002[a] 0.019 ± 0.004[b] ~0.005[c]
Pentostatin	0.0014 ± 0.0001[b]	0.0012 ± 0.0002[b] ~0.0000025[c]
L16	93 ± 17	77 ± 14
L17	260 ± 14	215 ± 12
L17a	194 ± 4	161 ± 3
L17b	188 ± 10	156 ± 8
L17c	455 ± 8	377 ± 7
L17d	> 700	n.d.
L17e	> 700	n.d.
L17f	618 ± 9	512 ± 7
L17g	372 ± 24	308 ± 20
L17h	> 700	n.d.
L17i	Insoluble	Insoluble
L17j	273 ± 19	226 ± 15
L17k	102 ± 17	85 ± 14
L17m	31 ± 1	26 ± 1

[a] Values were determined using a HTS assay format
[b] Values determined using a non-HTS assay format[26]
[c] Value reported in Cristalli et al.[1]

We decided to combine some of the structural features of L16 and L17k. Based on our SAR, we hypothesized that L17m might be a more potent inhibitor than any of the L17 derivatives tested so far. The synthesis of L17m had been previously reported and so we followed accordingly.[36] Methyl 1-hydroxy-2-naphthoate was refluxed in ethanediamine for 3 hours gave L17m (Scheme 3.3). Once obtained, an IC_{50} analysis was performed on L17m in the same manner as for the previous L17 derivatives. In accordance with our hypothesis and the SAR, L17m was the most potent derivative with an IC_{50} of 31 μM and a K_I of 26 μM.

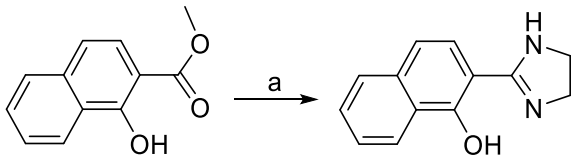

L17m

Scheme 3.3 Synthesis of L17m. Reagents and Conditions: (a) Methyl 1-hydroxy-2-naphthoate, ethylenediamine, reflux, 3 h, 47%.

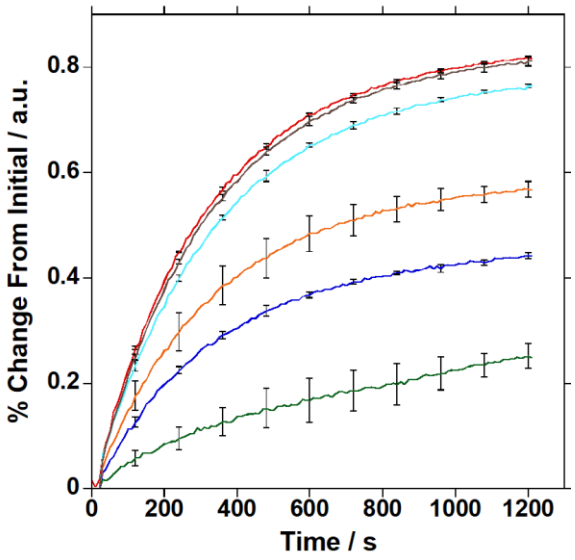

Figure 3.10 Conversion of ^{tz}A to ^{tz}I by ADA in the presence of various concentrations of L17m (0 μM (red), 0.1 μM (grey), 1 μM (light blue), 10 μM (orange), 25 μM (blue), 100 μM (green)).

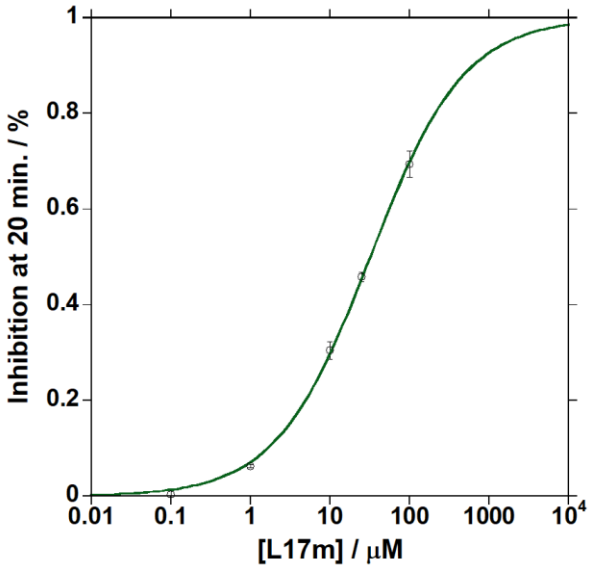

Figure 3.11 L17m IC_{50} Analysis. Semi-log plot of % inhibition in decimal form after 20 minutes versus [L17m] fit to a sigmoidal Hill curve.

3.6 Experimental Procedures

3.6.1 General Synthetic Procedures

^{tz}A was synthesized based on previously published procedures.[28] All of the compounds tested in the initial high throughput screen were provided by the Cohen Lab at UC San Diego.

The compounds L17a–k were synthesized and provided by Dr. Rebecca Adamek. Compound L17m was synthesized according to previously published procedures.[36]

3.6.2 General Methods for the High Throughput Screen

For all assay screening reactions, bovine spleen ADA was used. Bovine ADA has a 91% sequence similarity overall with human ADA1, and is highly conserved at the active site.[18] The values obtained using bovine spleen ADA should therefore be comparable to those that might be obtained using human ADA1. Concentrated stock solutions were prepared for ^{tz}A (8.4 mM) and potential inhibitors (50 mM) in DMSO. Bovine spleen ADA was obtained from Sigma Aldrich (EC Number 232-817-5). The commercial suspension (1150 U mL^{-1} in 3.2 M $(NH_4)_2SO_4$, 0.01 M potassium phosphate, pH 6.0) was diluted to 1.15 U mL^{-1} by dissolving an aliquot (1 µL) in freshly prepared phosphate buffer (999 µL, 50 mM, pH 7.4).

A freshly prepared enzyme stock solution was kept on ice prior to use for all reactions. Fresh dilutions of ^{tz}A (7.8 µM) and ADA (13.8 mU mL^{-1}) in freshly prepared phosphate buffer were made just before the reaction and kept at room temperature. All of the high throughput assays were run on a BioTek Synergy H4 microplate reader in Costar black 96-well plates that were filled and then inserted into the plate reader. The temperature was maintained at 37.0 ± 0.1 ºC. The reagents and enzymes were added in the following order: 20 µL of enzyme first, 30 µL of inhibitor second, and 50 µL of ^{tz}A last. Each well was excited at 322 nm and the emission intensity monitored at 410 nm. The intensity of emission was recorded every 37 seconds for just over 30 minutes.

3.6.3 High Throughput Screen of EHNA

Dilutions of EHNA (0.05, 0.5, 5, 12.5, 50, 125, 500, 1250, 5000, 50000 nM) were freshly prepared in phosphate buffer. ADA (20 µL of 13.8 mU mL^{-1} solution) and a respective EHNA (30 µL) dilution were added to successive wells in a row and thoroughly mixed. Phosphate

buffer was used in place of EHNA as a negative control. Two more rows were prepared in the same manner and a fourth row was prepared with phosphate buffer in place of ADA. After two minutes of incubation, ^{tz}A (50 µL, 7.8 µM) was added and thoroughly mixed. Wells were then excited at 322 nm and the emission intensity monitored at 410 nm. The intensity of emission was recorded every 37 seconds for just over 30 minutes.

3.6.4 High Throughput Screen of MBP Library

A fresh dilution of each inhibitor (1 mM) was made in phosphate buffer. 20 µL of 13.8 mU mL^{-1} ADA and 30 µL of each inhibitor were added to successive wells in a row and thoroughly mixed. As a negative and positive control, in the final two wells of the row, phosphate buffer and EHNA were added, respectively, in place of inhibitor. Two more rows were prepared in the same way as the first row and a fourth row was prepared with phosphate buffer substituted for ADA. After two minutes of incubation, ^{tz}A (50 µL of 7.8 µM) was added and thoroughly mixed. Each well was then excited sequentially at 322 nm and emission monitored at 410 nm. The intensity of emission was recorded every 37 seconds for just over 30 minutes.

3.6.5 IC_{50} Analysis of B26

Fresh dilutions of B26 at various concentrations (0.005, 0.05, 0.125, 0.5, 5, 12.5, 50, 125, 500, 1000 µM) in phosphate buffer were prepared. 20 µL of 13.8 mU mL^{-1} ADA and 30 µL of corresponding B26 solution were added to successive wells in a row and thoroughly mixed. As a negative and positive control, in the final two wells of the row, phosphate buffer and EHNA were added, respectively, in place of B26. Two more rows were prepared in the same manner and a fourth row was prepared with phosphate buffer substituted for ADA. After two minutes of incubation, ^{tz}A (50 µL of 7.8 µM) was added and thoroughly mixed. Each well was then excited

sequentially at 322 nm and emission monitored at 410 nm. The intensity of emission was recorded every 37 seconds for just over 30 minutes.

3.6.6 IC_{50} Analysis of L17 and L17 Derivatives

Concentrated stock solutions in DMSO of ^{tz}A (1 mM) and potential inhibitors (100 mM) were prepared. Bovine spleen ADA was purchased from Sigma Aldrich (EC Number 232-817-5). The commercial solution was diluted to 1.15 U mL^{-1} by dissolving an aliquot (1 µL) in freshly prepared phosphate buffer (999 µL, 50 mM, pH 7.4) to give a working stock solution. The working enzyme stock solution was freshly prepared and kept on ice prior to use for each set of experiments. Fresh dilutions of each compound tested in DMSO were prepared (1, 10 mM) from the 100 mM stock solution previously made. For L17m, one additional solution (0.1 mM) in DMSO was made. The change in emission intensity was monitored on a Horiba Fluoromax-4 equipped with a cuvette holder with a stirring system setting both the excitation and the emission slits at 3 nm, the resolution at 1 nm, and the integration time to 0.1 s. The Horiba Fluoromax-4 was equipped with a thermostat-controlled ethylene glycol-water bath fitted to a specially designed cuvette holder and the temperature was kept at 25.0 ± 0.1 ºC for all experiments. Reactions were stirred while monitoring in a 3 mL quartz cuvette. 1.7 mL of phosphate buffer was added to the cuvette. A volume equal to the sum of the ^{tz}A, ADA, and compound volumes was removed from the cuvette. If the final concentration of inhibitor was 10, 100, or 1000 µM, 17 µL of 1, 10, or 100 mM inhibitor solution was added, respectively. If the final concentration of inhibitor was 1 µM, 17 µL of 1 mM L17 derivative solution was added. If the final concentration of inhibitor was 25 or 250 µM, 4.25 µL of 10 or 100 mM L17 derivative solution was added, respectively. For a final concentration of 0.1 µM L17m, 1.7 µL of 0.1 mM solution was added. 6.6 µL of ^{tz}A was added to the cuvette and the solution was stirred for 1 minute. Initial emission at 410 nm upon excitation at 322 nm was measured. ADA was then added and measurements continued every 10 seconds for 20 minutes.

Note: For fragments L17i, L17j, and L17k at concentrations of 25 and 250 μM, 42.5 μL of 1 and 10 mM were added, respectively.

3.6.7 Data Analysis Methods

The emission intensity at each time point of the reaction of ^{tz}A with ADA was converted to a percent change relative to the initial intensity. The corresponding percent change values of the reaction without ADA were then subtracted from the reactions with ADA. The final value of each resulting curve was then divided by the final value of the run without inhibitor present to yield the percent activity for that inhibitor concentration. The percent activity of each inhibitor concentration was then subtracted from one to yield the percent inhibition. To obtain the IC_{50} value, the percent inhibition values were plotted against the respective inhibitor concentration on a logarithmic x-axis scale. The resulting plot was fit with a Hill curve and the IC_{50} value calculated from the two constants. K_I values were calculated from IC_{50} values using the Cheng-Prusoff equation.

3.7 Acknowledgements

Chapter 3 is adapted from the work: Adamek, R. N.* and Ludford III, P. T.*; Duggan, S. M.; Tor, Y.; Cohen, S. M. “Identification of Adenosine Deaminase Inhibitors by Metal-binding Pharmacophore Screening” *ChemMedChem*, *22*, 2151-2156. (*Shared first co-authorship). Permission to use materials from the manuscript was also obtained from co-authors Rebecca Adamek, Stephanie Duggan, Seth Cohen, and Yitzhak Tor. The dissertation author is the first co-author.

3.8 References

1. Cristalli, G.; Costanzi, S.; Lambertucci, C.; Lupidi, G.; Vittori, S.; Volpini, R.; Camaioni, E. *Med. Res. Rev.* **2001**, *21*, 105–128.

2. Tardif, V.; Muir, R.; Cubas, R.; Chakhtoura, M.; Wilkinson, P.; Metcalf, T.; Herro, R.; Haddad, E. K. *Nat. Commun.* **2019**, *10*, 823.

3. Chen, A. Y.; Adamek, R. N.; Dick, B. L.; Credille, C. V.; Morrison, C. N.; Cohen, S. M. *Chem. Rev.* **2019**, *119*, 1323–1455.

4. Wilson, D. K.; Quiocho, F. A. *Biochemistry* **1993**, *32*, 1689–1694.

5. Wilson, D. K.; Rudolph, F. B.; Quiocho, F. A. *Science* **1991**, *252*, 1278–1284.

6. Nakajima, Y.; Kanno, T.; Nagaya, T.; Kuribayashi, K.; Nakano, T.; Gotoh, A.; Nishizaki, T. *Cell. Physiol. Biochem.* **2015**, *35*, 51–60.

7. Kutryb-Zajac, B.; Koszalka, P.; Mierzejewska, P.; Bulinska, A.; Zabielska, M. A.; Brodzik, K.; Skrzypkowska, A.; Zelazek, L.; Pelikant-Malecka, I.; Slominska, E. M.; Smolenski, R. T. *J. Cell. Mol. Med.* **2018**, *22*, 5939–5954.

8. Sauer, A. V.; Brigida, I.; Carriglio, N.; Aiuti, A. *Front. Immunol.* **2012**, *3*, 265.

9. Mediero, A.; Cronstein, B. N. *Trends Endocrinol. Metab.* **2013**, *24*, 290–300.

10. B. Kutryb-Zajac, L. Mateuszuk, P. Zukowska, A. Jasztal, M. A. Zabielska, M. Toczek, P. Jablonska, A. Zakrzewska, B. Sitek, J. Rogowski, R. Lango, E. M. Slominska, S. Chlopicki, R. T. Smolenski, *Cardiovasc. Res.* **2016**, *112*, 590–605.

11. Cortes, A.; Gracia, E.; Moreno, E.; Mallol, J.; Lluis, C.; Canela, E. I.; Casado, V. *Med. Res. Rev.* **2015**, *35*, 85–125.

12. Antonioli, L.; Csoka, B.; Fornai, M.; Colucci, R.; Kokai, E.; Blandizzi, C.; Hasko, G. *Drug Discovery Today* **2014**, *19*, 1051–1068.

13. Antonioli, L.; Colucci, R.; La Motta, C.; Tuccori, M.; Awwad, O.; Da Settimo, F.; Blandizzi, C.; Fornai, M. *Curr. Drug Targets* **2012**, *13*, 842–862.

14. Schaeffer, H. J.; Schwender, C. F. *J. Med. Chem.* **1974**, *17*, 6–8.

15. Gillerman, I.; Fischer, B. *J. Med. Chem.* **2011**, *54*, 107–121.

16. McConnell, W. R.; El Dareer, S. M.; Hill, D. L. *Drug Metab Dispos* **1980**, *8*, 5–7.

17. Lambe, C. U.; Nelson, D. J. *Biochem Pharmacol* **1982**, *31*, 535–539.

18. Zimmermann, S. C.; Sadler, J. M.; O'Daniel, P. I.; Kim, N. T.; Seley-Radtke, K. L. *Nucleosides, Nucleotides Nucleic Acids* **2013**, *32*, 137–154.

19. Tite, T.; Lougiakis, N.; Myrianthopoulos, V.; Marakos, P.; Mikros, E.; Pouli, N.; Tenta, R.; Fragopoulou, E.; Nomikos, T. *Tetrahedron* **2010**, *66*, 9620–9628.

20. Li, G.; Nakagome, I.; Hirono, S.; Itoh, T.; Fujiwara, R. *Pharmacol. Res. Perspect.* **2015**, *3*, e00121

21. Da Settimo, F.; Primofiore, G.; La Motta, C.; Taliani, S.; Simorini, F.; Marini, A. M.; Mugnaini, L.; Lavecchia, A.; Novellino, E.; Tuscano, D.; Martini, C. *J. Med. Chem.* **2005**, *48*, 5162–5174.

22. Zhang, L.; Zhao, J.; Jiang, J.; Yu, R. *Chem. Commun. (Cambridge, U. K.)* **2012**, *48*, 10996–10998.

23. Xu, Y.; Venton, B. J. *Phys. Chem. Chem. Phys.* **2010**, *12*, 10027–10032.

24. Xing, X. J.; Liu, X. G.; Yue, H.; Luo, Q. Y.; Tang, H. W.; Pang, D. W. *Biosens. Bioelectron.* **2012**, *37*, 61–67.

25. Sinkeldam, R. W.; McCoy, L. S.; Shin, D.; Tor, Y. *Angew. Chem. Int. Ed. Engl.* **2013**, *52*, 14026–14030.

26. Ludford, III, P. T.; Rovira, A. R.; Fin, A.; Tor, Y. *ChemBioChem* **2019**, *20*, 718–726.

27. Hu, K.; Huang, Y.; Wang, S.; Zhao, S. *J. Pharm. Biomed. Anal.* **2014**, *95*, 164–168.

28. Rovira, A. R.; Fin, A.; Tor, Y. *J. Am. Chem. Soc.* **2015**, *137*, 14602–14605.

29. Yang, Y.; Hu, X. Q.; Li, Q. S.; Zhang, X. X.; Ruan, B. F.; Xu, J.; Liao, C. *Curr Top Med Chem* **2016**, *16*, 384–396.

30. Perez, C.; Barkley-Levenson, A. M.; Dick, B. L.; Glatt, P. F.; Martinez, Y.; Siegel, D.; Momper, J. D.; Palmer, A. A.; Cohen, S. M. *J. Med. Chem.* **2019**, *62*, 1609–1625.

31. Li, J.; Zhang, Y.; Da Silva Sil Dos Santos, B.; Wang, F.; Ma, Y.; Perez, C.; Yang, Y.; Peng, J.; Cohen, S. M.; Chou, T. F.; Hilton, S. T.; Deshaies, R. J. *Cell. Chem. Biol.* **2018**, *25*, 1350–1358 e1359.

32. Credille, C. V.; Dick, B. L.; Morrison, C. N.; Stokes, R. W.; Adamek, R. N.; Wu, N. C.; Wilson, I. A.; Cohen, S. M. *J. Med. Chem.* **2018**, *61*, 10206–10217.

33. Chen, A. Y.; Thomas, P. W.; Stewart, A. C.; Bergstrom, A.; Cheng, Z.; Miller, C.; Bethel, C. R.; Marshall, S. H.; Credille, C. V.; Riley, C. L.; Page, R. C.; Bonomo, R. A.; Crowder, M. W.; Tierney, D. L.; Fast, W.; Cohen, S. M. *J. Med. Chem.* **2017**, *60*, 7267–7283.

34. Chen, A. Y.; Thomas, P. W.; Cheng, Z.; Xu, N. Y.; Tierney, D. L.; Crowder, M. W.; Fast, W.; Cohen, S. M. *ChemMedChem* **2019**, *14*, 1271–1282.

35. Adamek, R. N.; Credille, C. V.; Dick, B. L.; Cohen, S. M. *J. Biol. Inorg. Chem.* **2018**, *23*, 1129–1138.

36. Sapegin, A.; Osipyan, A.; Krasavin, M. *Org. Biomol. Chem.* **2017**, *15*, 2906–2909.

Chapter 4

Investigation of Cytidine Deaminase with Three Fluorescent C Analogues

4.1 Introduction to CDA

Cytidine Deaminase (CDA) is an enzyme that converts cytidine and 2'-deoxycytidine to uridine and 2'-deoxyuridine (Fig. 4.1).[1] It is a key enzyme in the pyrimidine salvage pathway. The mechanism involves nucleophilic attack by a zinc activated hydroxide forming and intermediate which then rehybridizes by expulsion of an ammonia molecule (Fig. 4.1).[2–4] One of the key points of interest in this enzyme is that it has been shown to deaminate known chemotherapeutic agents cytarabine, gemcitabine, and 5-aza-2'-deoxycytidine thereby diminishing their potency.[5–8]

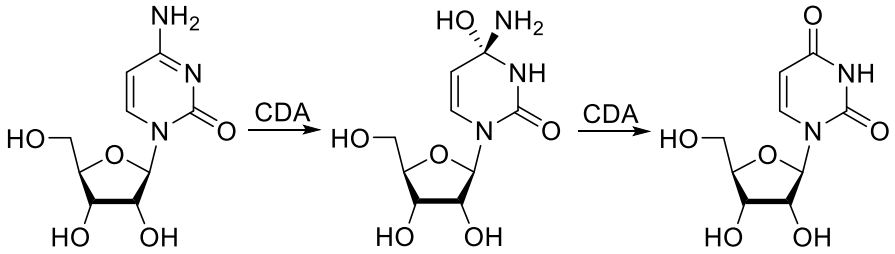

Figure 4.1 Reaction Pathway of Cytidine to Uridine Inside the CDA Binding Pocket

A variety of different inhibitors have been described over the years. One approach has been to mimic the intermediate state.[4,9–14] Molecules that resemble the intermediate state include tetrahydrouridine (THU), phosphapyrimidine riboside, and diazepinone riboside (Fig. 4.2).[13,15–17] Another potent inhibitor reported is zebularine (Fig. 4.2).[16,17] The only one of those

listed that has been co-administered with the previously mentioned chemotherapeutics is THU.[5–8]

As CDA has been found to interfere with chemotherapeutic agents, inhibitors are thus sought after for co-administration. Multiple methods of monitoring CDA activity have been reported. One such method is to monitor changes in absorption spectra.[1,18,19] Another is to monitor cytidine and uridine concentrations via high performance liquid chromatography.[20,21] Yet another is a colorimetric assay that monitors ammonia production.[22] The latter two suffer from lengthy time windows and the former can suffer from spectral overlap of the inhibitors. This leaves an opportunity for more sensitive real-time assays fit for high throughput operations to be developed.

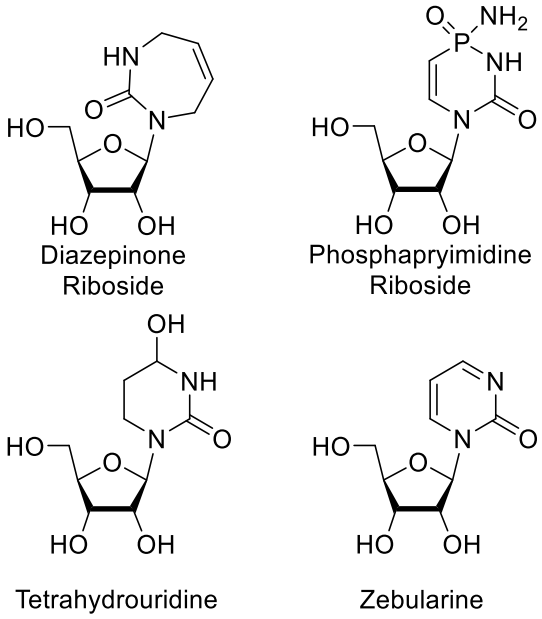

Figure 4.2 Inhibitors of CDA

4.2 Reactions of C Analogues with CDA

As we had recently synthesized a new cytidine analogue, ^{mth}C, and also had in hand two previously reported cytidine analogues, ^{tz}C and thC, we sought to test whether CDA would tolerate them as substrates.[23–25] Unlike in the adenosine and guanosine analogues where the

structural perturbations are mainly internal, the C and U analogues all contain an expanded ring system that is not present in the native cytidine and uridine. We were unsure whether this expanded ring would be too perturbing for CDA. However, the fact that diazepinone riboside, which also has an expanded ring, is a tight binding inhibitor suggested the C analogues may in fact be tolerated.[4,17]

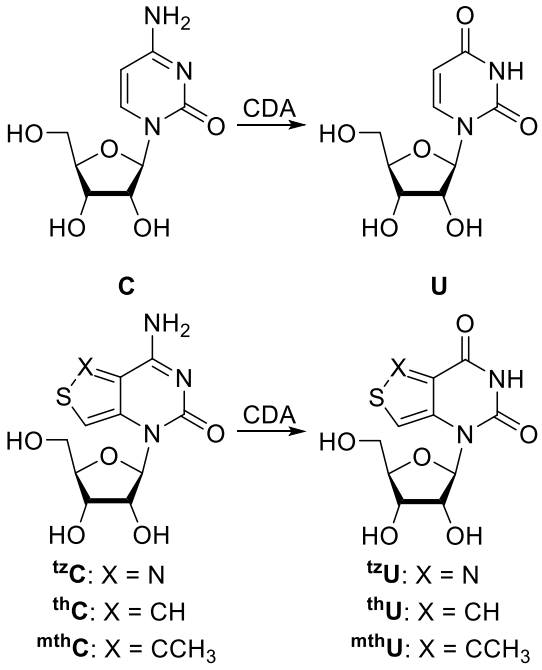

Figure 4.3 CDA Mediated Deamination of C and C Analogues to U and U Analogues

Cytidine, ^{tz}C, thC, and ^{mth}C were placed in the presence of CDA. The steady state absorption spectra were taken at multiple time windows and overlaid to observe the spectral changes (Figs. 4.4–4.7). The isosbestic points of ^{tz}C and ^{tz}U, thC and thU, and ^{mth}C and ^{mth}U were found to be 293 nm, 292 nm, and 305 nm respectively. Next, the steady state emission spectra were taken, exciting at the isosbestic point, at the same time windows and overlaid to observe the spectral changes (Figs. 4.8–4.10). All of these overlays revealed spectral changes that reflected a shift from the corresponding C analogue to the corresponding U analogue. To further corroborate these findings, reactions of each C analogue and CDA were incubated for 1 hour and subjected to analysis by HPLC. Compared with standards of the corresponding C and

U analogues, each reaction was found to only contain the corresponding U analogue (Figs. 4.11–4.14).

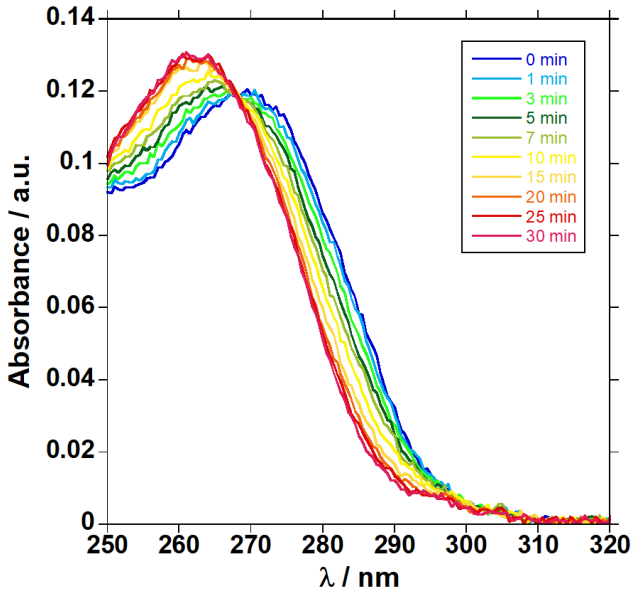

Figure 4.4 Steady state absorption traces of enzymatic conversion of cytidine to uridine by CDA over 30 minutes.

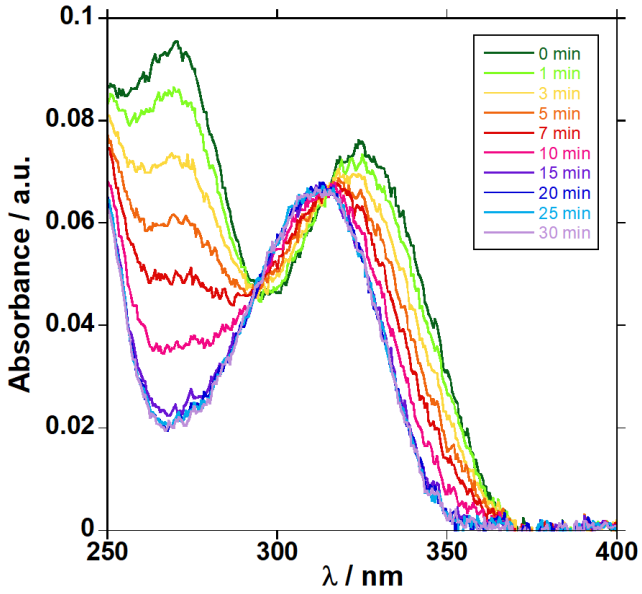

Figure 4.5 Steady state absorption traces of enzymatic conversion of ^{tz}C to ^{tz}U by CDA over 30 minutes

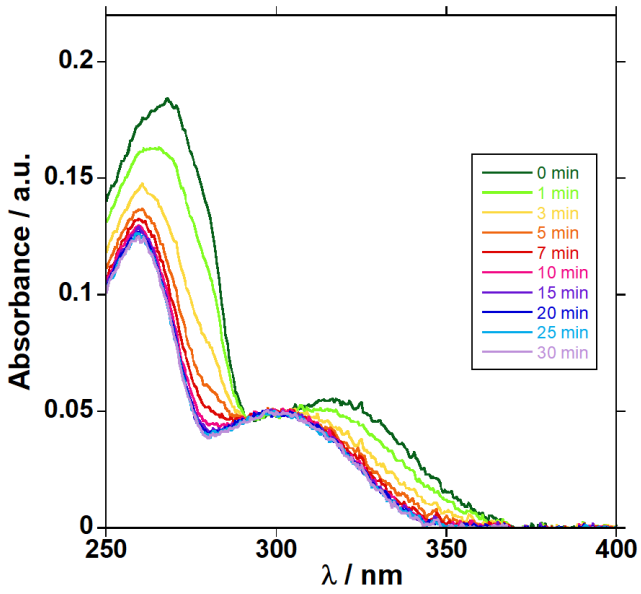

Figure 4.6 Steady state absorption traces of enzymatic conversion of thC to thU by CDA over 30 minutes

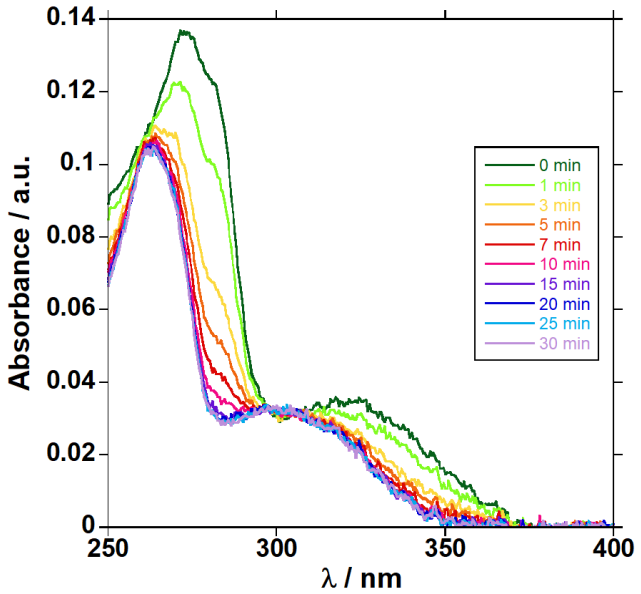

Figure 4.7 Steady state absorption traces of enzymatic conversion of ^{mth}C to ^{mth}U by CDA over 30 minutes

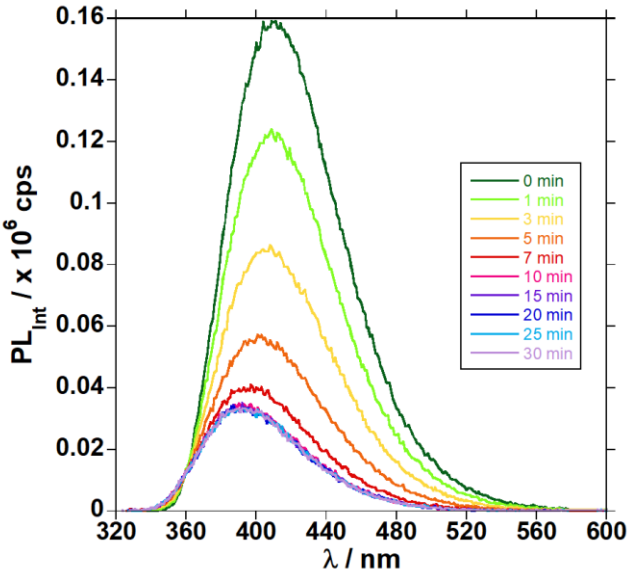

Figure 4.8 Steady state emission traces of enzymatic conversion of ^{tz}C to ^{tz}U by CDA over 30 minutes

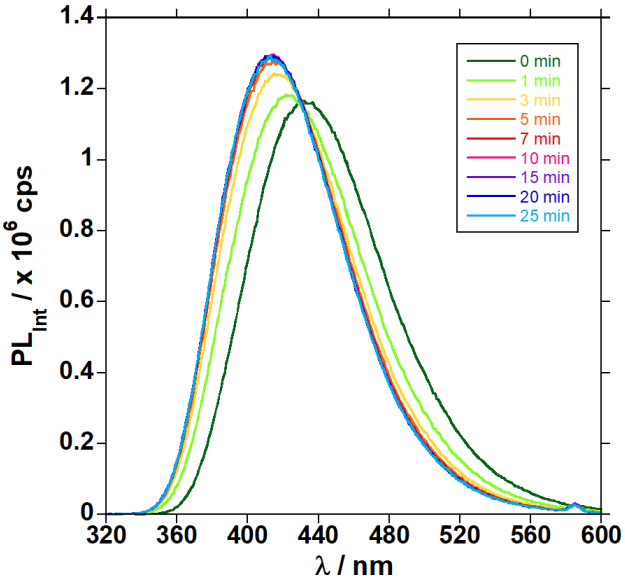

Figure 4.9 Steady state emission traces of enzymatic conversion of thC to thU by CDA over 30 minutes

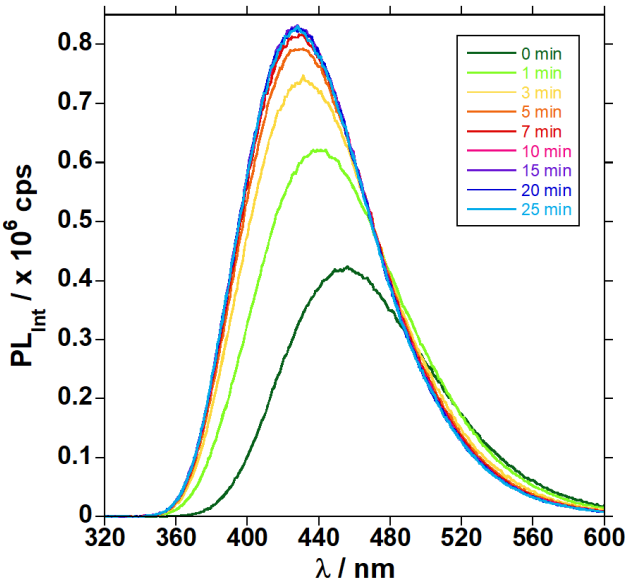

Figure 4.10 Steady state emission traces of enzymatic conversion of ^{mth}C to ^{mth}U by CDA over 30 minutes

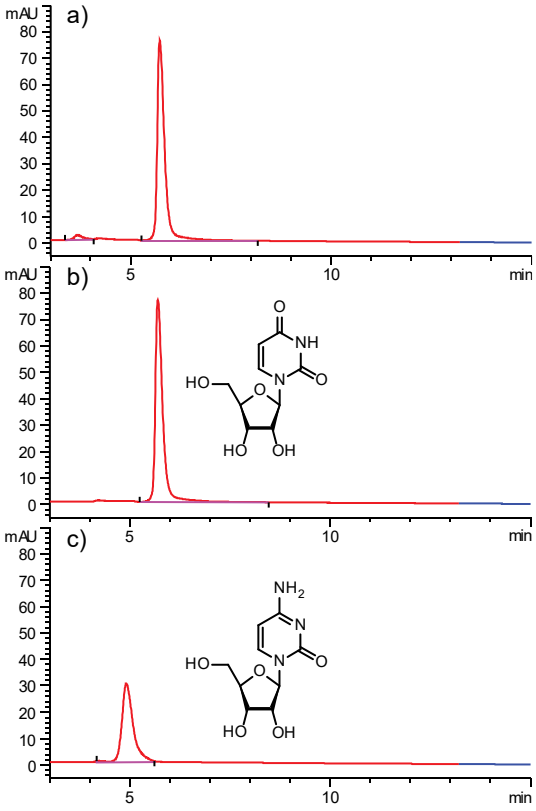

Figure 4.11 HPLC traces of the reaction of CDA with cytidine after 60 minutes (a), uridine (b), and cytidine (c) monitored by absorption at 260 nm. Inset: structures of uridine (b) and cytidine (c).

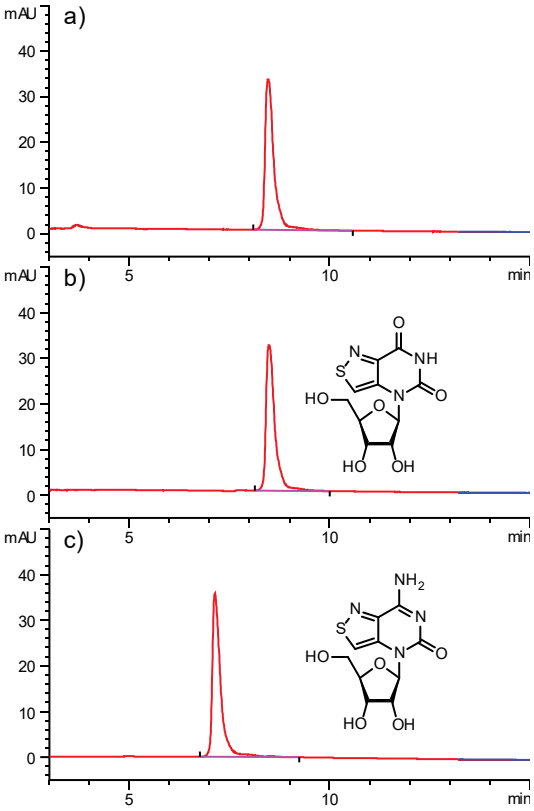

Figure 4.12 HPLC traces of the reaction of CDA with ^{tz}C after 60 minutes (a), ^{tz}U (b), and ^{tz}C (c) monitored by absorption at 320 nm. Inset: structures of ^{tz}U (b) and ^{tz}C (c).

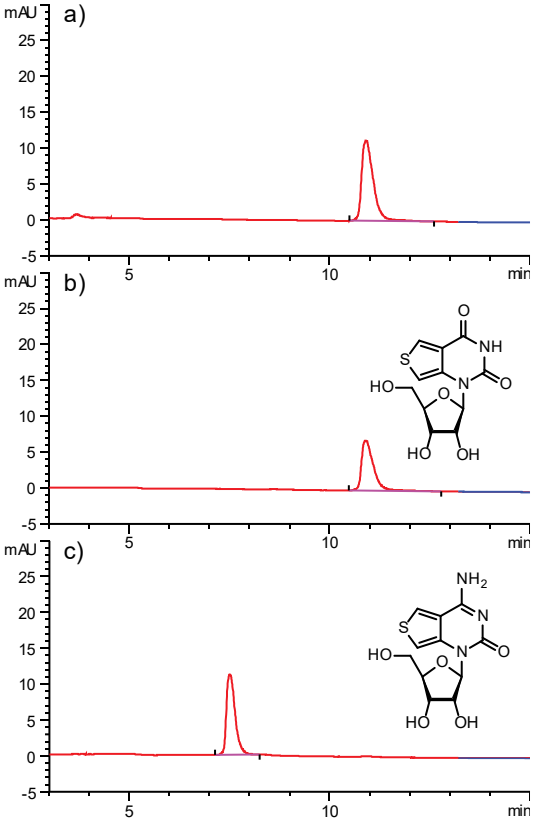

Figure 4.13 HPLC traces of the reaction of CDA with thC after 60 minutes (a), thU (b), and thC (c) monitored by absorption at 320 nm. Inset: structures of thU (b) and thC (c).

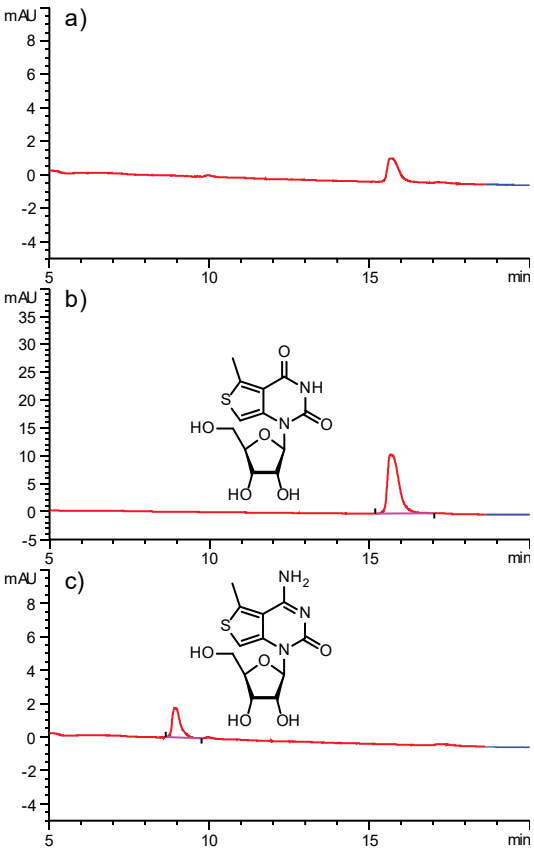

Figure 4.14 HPLC traces of the reaction of CDA with ^{mth}C after 60 minutes (a), ^{mth}U (b), and ^{mth}C (c) monitored by absorption at 320 nm. Inset: structures of ^{mth}U (b) and ^{mth}C (c).

4.3 Modeling and Analysis of CDA Kinetics

Upon confirming that a reaction took place when each C analogue was placed in the presence of CDA, we sought to characterize the reactions and compare substrates. To monitor the reactions of cytidine, ^{tz}C, thC, and ^{mth}C with CDA, we monitored the change in absorbance over 25 minutes at 260 nm, 340 nm, 330 nm, and 330 nm, respectively (Fig. 4.11). A pseudo-first order curve was fit to the data giving k_{app} values which were then converted to $t_{1/2}$ values (Table 4.1). We next monitored the reactions of ^{tz}C, thC, and ^{mth}C with CDA by emission at 408 nm, 400 nm, and 427 nm, respectively, upon excitation at the corresponding isosbestic point (Fig. 4.12). The same method of fitting the data and obtaining k_{app} and $t_{1/2}$ values was used yielding comparable results to those obtained from monitoring absorption.

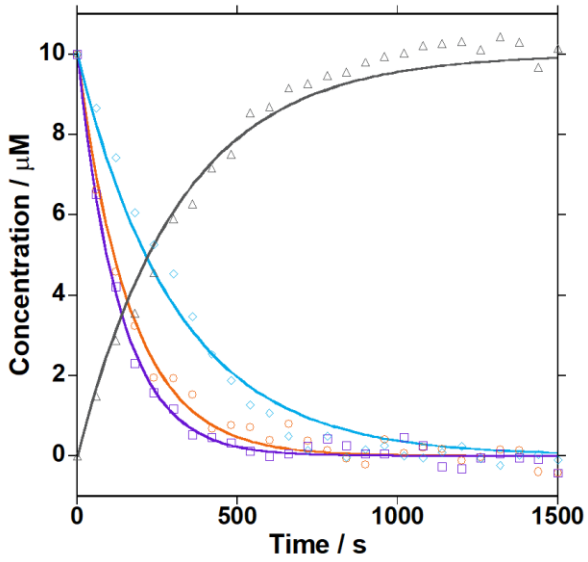

Figure 4.15 Enzymatic conversion of cytidine (grey), ^{tz}C (light blue), thC (purple), and ^{mth}C (orange) to uridine, ^{tz}U, thU, and ^{mth}U by CDA. Reactions were monitored by absorbance, normalized, converted to concentration, and fit with a pseudo-first order curve fit

Table 4.1 Pseudo-First Order Kinetic Parameters of CDA Reactions

		k_{app} (x 10^{-3}) s^{-1}	$t_{1/2}$ (s)	R^2
Abs	**C**	3.1 ± 0.1	220 ± 10	0.981
	^{tz}C	3.3 ± 0.1	210 ± 20	0.979
	thC	7.2 ± 0.2	92 ± 5	0.992
	^{mth}C	6.1 ± 0.2	110 ± 10	0.987
Em	**^{tz}C**	4.1 ± 0.1	170 ± 10	0.988
	thC	7.4 ± 0.1	94 ± 2	0.999
	^{mth}C	5.7 ± 0.1	120 ± 10	0.999

*Data are presented as mean ± SD.

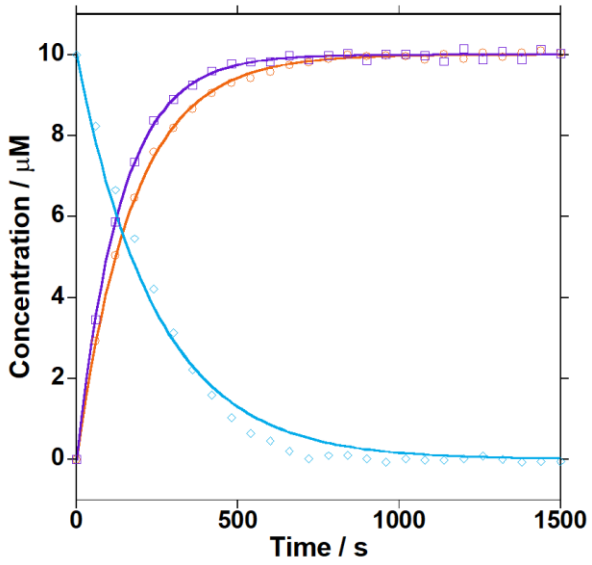

Figure 4.16 Enzymatic conversion of ^{tz}C (light blue), thC (purple), and ^{mth}C (orange) to ^{tz}U, thU, and ^{mth}U by CDA. Reactions were monitored by fluorescence, normalized, converted to concentration, and fit with a pseudo-first order curve fit

Interestingly, thC had the shortest $t_{1/2}$ value followed closely by ^{mth}C. ^{tz}C had a $t_{1/2}$ value that was slightly shorter than cytidine but much approximately double that of thC and ^{mth}C. Overall, all three analogues had shorter reaction $t_{1/2}$ values than cytidine suggesting the structural perturbation was actually a boon. The thiophene ring expansion at the 5/6 positions of the pyrimidine core appeared to be the most favored by CDA as both thC and ^{mth}C reacted much quicker than cytidine. Further, the methyl moiety projecting off the side of the thiophene in ^{mth}C seemed to also be tolerated although it slightly impacted acceptance by CDA as compared to thC. The isothiazole ring expansion at the 5/6 positions of the pyrimidine core also appeared to be favored by CDA, but not as much as the thiophene.

While the reaction data provided insight into the tolerance of the structural perturbations of the C analogues by CDA, they did not explain whether the shorter reaction $t_{1/2}$ values were due to binding or deamination rates. We thus used another model to fit the absorbance and emission data. A set of Michaelis-Menten equations (Eqs. 4.1–4.4) was solved using the Runge-Kutta method with a variable time step in MatLab (function ode45), setting the initial conditions to 10 µM for the C analogue, 8.7 nM for CDA, and 0 µM for the enzyme substrate

complex and product, the same as in each reaction.[26–28] An initial value was chosen for k_1 and k_2, and k_{-1} was set to 10% of k_1. The R^2 of the resulting fit to the data was calculated and the k_1 and k_2 values adjusted to improve R^2. This process was done iteratively until an optimized R^2 was obtained (Figs. 4.13, 4.14). The resulting kinetic parameters are listed in Table 4.2.

$$\frac{d[S]}{dt} = -k_1[E][S] + k_{-1}[ES]$$

Equation 4.1 Substrate Concentration Rate of Change Derived from Michaelis-Menten Kinetics

$$\frac{d[E]}{dt} = -k_1[E][S] + k_{-1}[ES] + k_2[ES]$$

Equation 4.2 Enzyme Concentration Rate of Change Derived from Michaelis-Menten Kinetics

$$\frac{d[ES]}{dt} = k_1[E][S] - k_{-1}[ES] - k_2[ES]$$

Equation 4.3 Enzyme-Substrate Complex Concentration Rate of Change Derived from Michaelis-Menten Kinetics

$$\frac{d[P]}{dt} = k_2[ES]$$

Equation 4.4 Product Concentration Rate of Change Derived from Michaelis-Menten Kinetics

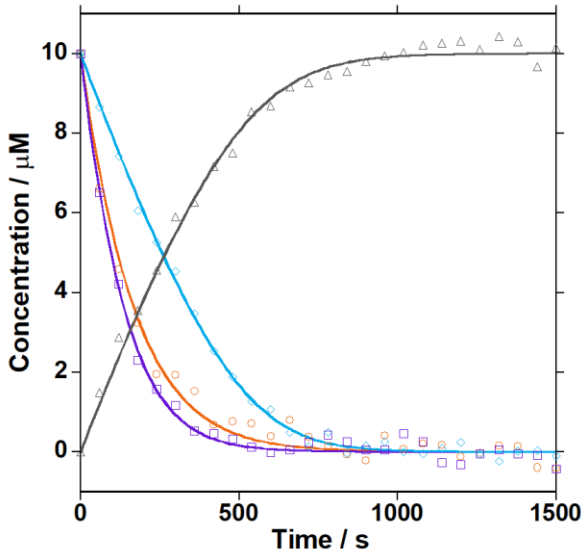

Figure 4.17 Enzymatic conversion of cytidine (grey), ^{tz}C (light blue), thC (purple), and ^{mth}C (orange) to uridine, ^{tz}U, thU, and ^{mth}U by CDA. Reactions were monitored by absorbance, normalized, converted to concentration, and fit with the integrated solution of a set of differential equations corresponding to the Michaelis-Menten kinetics

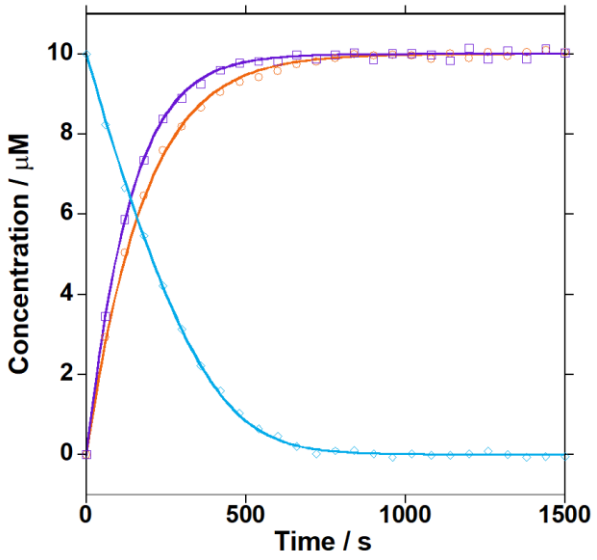

Figure 4.18 Enzymatic conversion of ^{tz}C (light blue), thC (purple), and ^{mth}C (orange) to ^{tz}U, thU, and ^{mth}U by CDA. Reactions were monitored by fluorescence, normalized, converted to concentration, and fit with the integrated solution of a set of differential equations corresponding to the Michaelis-Menten kinetics

Table 4.2 Michaelis-Menten Kinetic Parameters of CDA Reactions

		k_1 (μM^{-1} s^{-1})	k_{-1}[a] (s^{-1})	k_2 (s^{-1})	K_M (μM)[b]
Abs	**C**	0.91 ± 0.42	0.091	3.2 ± 2.1	3.6
	^{tz}C	1.04 ± 0.01	0.104	3.2 ± 0.3	3.1
	thC	1.01 ± 0.47	0.101	34 ± 7.2	34
	^{mth}C	0.75 ± 0.16	0.075	56 ± 5.9	75
Em	**^{tz}C**	1.06 ± 0.32	0.106	4.6 ± 1.3	4.4
	thC	0.95 ± 0.14	0.095	46 ± 5.3	49
	^{mth}C	0.71 ± 0.18	0.071	45 ± 2.3	63

*Data are presented as mean ± SD. [a] Values were assumed to be ≤10% of k_1. [b] Values calculated from k_1, k_{-1}, and k_2.

The results of the Michaelis-Menten model revealed that the isothiazole expanded ring system was actually tighter binding than the thiophene expanded ring system. Further, the methyl appendage off of the thiophene ring appeared to diminish binding slightly. The findings were surprising as they painted a different picture than that from the pseudo-first order model. However, the deamination rate explained the seeming discrepancy. The deamination rate was found to be fastest for ^{mth}C followed by thC. ^{tz}C had a much slower deamination rate that was closer to cytidine. This suggested the faster k_{app} observed for thC and ^{mth}C was driven by the

deamination rate, k_2. Further, the tighter binding constant of thC resulted in a faster reaction than that of ^{mth}C.

Overall, the findings indicated the CDA binding pocket was more tolerant of the isothiazole and thiophene expanded pyrimidine ring system than that of the native. The addition of a methyl moiety, however, diminished binding. We hope these findings may provide a possible route for future inhibitor design.

4.4 Development of Screening Assays for CDA

After analyzing the kinetic data and learning all we could, we sought to screen two inhibitors using the newly established substrates. The inhibitors we chose were THU and zebularine, well established potent inhibitors of CDA. We ran the same reactions we had previously, monitoring by emission in the same manner, but in the presence of increasing amounts of inhibitor. The runs with inhibitor presence were compared against runs without inhibitor yielding the percent inhibition of CDA. The percent inhibition was plotted against inhibitor concentration and a Hill curve fit to the data (Figs. 4.15, 4.16). The Hill curve parameters were then used to calculate the IC_{50} of the inhibitor (Table 4.3). The IC_{50} value was then converted to a K_I value using the Cheng-Prusoff equation and the K_M of the corresponding C analogue (Table 4.3).

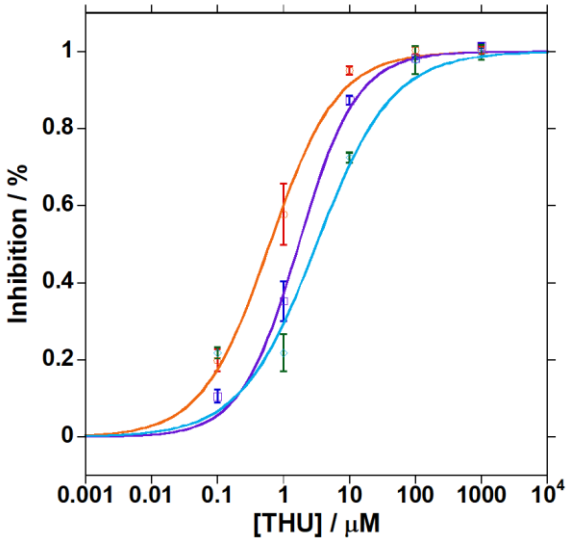

Figure 4.19 THU IC_{50} Analysis. Semi-log plot of % inhibition in decimal form after 20 minutes versus [THU] fit to a sigmoidal Hill curve

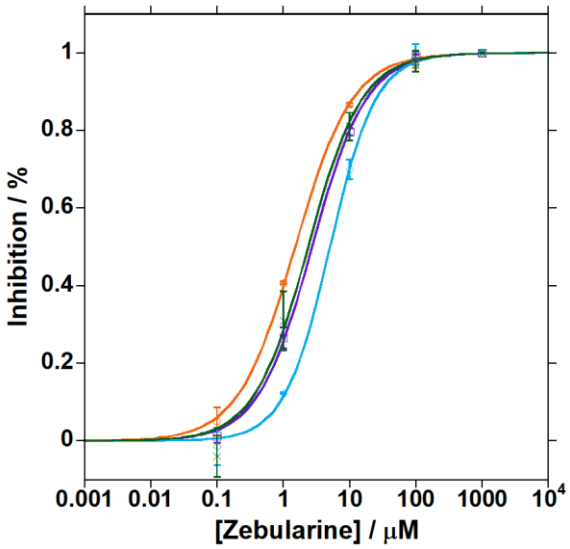

Figure 4.20 Zebularine IC_{50} Analysis. Semi-log plot of % inhibition in decimal form after 20 minutes versus [Zebularine] fit to a sigmoidal Hill curve.

Table 4.3 Experimentally Determined IC_{50} and K_I Values of Zebularine and THU

	Inh.	IC_{50} (μM)	K_I (μM)	R^2
^{tz}**C**	Zeb	5.0 ± 0.4	1.5 ± 0.1	0.999
th**C**	Zeb	2.7 ± 0.2	2.2 ± 0.1	0.999
^{mth}**C**	Zeb	1.5 ± 0.1	1.3 ± 0.1	0.999
^{mth}**C**[a]	Zeb	2.3 ± 0.6	2.0 ± 0.5	0.993
^{tz}**C**	THU	3.1 ± 0.5	0.95 ± 0.16	0.948
th**C**	THU	1.7 ± 0.3	1.4 ± 0.2	0.995
^{mth}**C**	THU	0.61 ± 0.11	0.53 ± 0.10	0.995

*Data are presented as mean ± SD. [a]Determined in the presence of 100 μM adenosine.

The K_I values were comparable to the K_I values previously reported for zebularine and THU. A similar experiment was run for zebularine in the presence of 100 μM adenosine to show the absorbance of the compound did not interfere with the assay (Fig. 4.16). The KI obtained from this experiment was within the range of those K_I values originally obtained using the C analogues. There was a slight variance (~0.9 μM) in K_I values determined by each C analogue for both zebularine and THU possibly indicating the inherent error with this method of measurement.

4.5 Experimental Procedures

4.5.1 General Spectroscopic Procedures

Spectroscopic grade DMSO and dioxane were obtained from Sigma Aldrich and aqueous solutions were prepared with MilliQ water. All measurements were carried out in a 3 mL, 1 cm four-sided quartz cuvette (extinction coefficient measurements) or a 125 μL, 1 cm four-sided quartz cuvette (quantum yield measurements) from Helma.

Absorption spectra were taken on a Shimadzu UV-2450 spectrophotometer setting the slit width to 1 nm and resolution to 0.5 nm. All spectra were corrected for the blank. Steady state emission spectra were taken on a Horiba Fluoromax-4 equipped with a cuvette holder with a stirring system setting the excitation slit width to 2 nm and the emission slit width to 3 nm, the

resolution to 1 nm, and the integration time to 0.1 s. Steady state fluorescence spectra used for quantum yield determinations were taken upon excitation at the corresponding molecules maximum wavelength of absorption. All spectra were corrected for the blank and instrument response.

Both instruments were equipped with a thermostat-controlled ethylene glycol-water bath fitted to specially designed cuvette holder and the temperature was kept at 25.0 ± 0.1 ºC.

Nucleosides were dissolved in DMSO to prepare highly concentrated stock solutions: ^{mth}**C** (9.53 mM), ^{mth}**U** (11.9 mM).

4.5.2 Fluorescence Quantum Yield Determination

The samples concentrations were adjusted to have an optical density lower than 0.07 at the excitation wavelength (λ_{ex}). The fluorescence quantum yields (φ) were evaluated based on an external standard, 2-aminopurine (0.68 in water), by using the relative quantum yield equation (Eq. 2.1).

4.5.3 General Methods for CDA Reactions

Recombinant human CDA variant Q27/A70 was obtained from BioVision (EC Number 7363-100) and stored in at –80ºC. The commercial solution [0.5 mg mL^{-1} in 20 mM Tris-HCl buffer (pH 8.0), 100 mM NaCl, 1 mM DTT, 2 mM EDTA, 40% glycerol] was diluted to 0.01 mg mL^{-1} by dissolving an aliquot (1 µL) in the same storage buffer (49 µL). The enzyme stock solution was freshly prepared, stored at –20ºC, and used for at most 2 hours of experimentation.

Concentrated stock solutions in DMSO were prepared for cytidine (4.47 mM), ^{tz}C (3.46 mM), thC (3.21 mM), and ^{mth}C (4.66 mM). A working solution (1 mM) was made the day of experimentation by dissolving an appropriate aliquot in MilliQ water for a total volume of (50 µL).

The CDA-mediated enzymatic conversion of cytidine (and its analogues) was followed by absorbance and emission (for the emissive analogues ^{tz}C, thC, and ^{mth}C) spectroscopy by

monitoring the intensity variation as a function of time. The real-time conversion of cytidine (and its analogues) to uridine (and the corresponding analogues) was performed on a Shimadzu UV-2450 spectrophotometer (slit width: 1nm, resolution 0.5 nm) and Horiba Fluoromax-4 (slit widths: 3 nm, resolution: 1 nm). Each instrument was equipped with a thermostat-controlled ethylene glycol/water bath fitted to a specially designed cuvette holder and the temperature was kept at 25.0 ± 0.1 ºC.

All measurements were carried out in a 125 µL, 1 cm four-sided quartz cuvette from Helma. Tris-HCl buffer (100 mM, pH 7.5) was freshly prepared. Buffer, cytidine or cytidine analogue, and CDA were diluted in water to final concentrations of 50 mM Tris-HCl, pH 7.5, 10 µM, and 0.16 µg mL^{-1} respectively.

4.5.4 Monitoring of Enzymatic Conversion of C and C Analogues to Corresponding U and U Analogues by Absorption Spectroscopy

The absorbance of cytidine, ^{tz}C, ^{th}C, and ^{mth}C was monitored at 260, 340, 330, and 330 nm respectively. MilliQ water, buffer, and cytidine analogue were added to the cuvette, thoroughly mixed, and an initial measurement at the respective wavelength was taken. An aliquot of enzyme stock solution was taken straight from the –20ºC freezer and added to the reaction cuvette. The reaction solution was mixed with a pipette several times and measurements were continued every 60 seconds. Cytidine was monitored for 3600 seconds. Cytidine analogues were monitored for 1560 seconds. All experiments were run in triplicate.

All absorption data were plotted against time. A pseudo-first order curve (Eqs. 1–2) was fit to each resulting time plot yielding k_{app} values and $t_{1/2}$ values. Averages and standard deviations of the k_{app} and $t_{1/2}$ values were calculated from cytidine and each cytidine analogues set of time plots. In addition, a set of ordinary differential equations (ODEs) (Eqs. 3–6) consistent with Michaelis-Menten kinetics was solved using the Runge-Kutta method with a variable time step in MatLab (function ode45). Initial concentrations used for each reaction

were given above. The resulting fitted curves for each species were optimized by iteratively testing k values (Table 1) that maximized R^2.

4.5.5 Monitoring of Enzymatic Conversion of C and C Analogues to Corresponding U and U Analogues by Fluorescence Spectroscopy

The emission intensity of ^{tz}C, thC, and ^{mth}C was monitored at 408, 400, and 427 nm upon excitation at 293, 292, and 305 nm, respectively. MilliQ water, buffer, and cytidine analogue were added to the cuvette, thoroughly mixed, and an initial measurement at the respective wavelength was taken. An aliquot of enzyme stock solution (kept at –20ºC) was added to the reaction cuvette. The reaction solution was mixed with a pipette several times and measurements were continued every 60 seconds for 1560 seconds. All experiments were run in triplicate.

All emission data were plotted against time. A pseudo-first order curve (Eqs. 1–2) was fit to each resulting time plot yielding k_{app} values and $t_{1/2}$ values. Averages and standard deviations of the k_{app} and $t_{1/2}$ values were calculated from each cytidine analogues set of time plots. In addition, a set of ordinary differential equations (ODEs) (Eqs. 3–6) consistent with Michaelis-Menten kinetics was solved using the Runge-Kutta method with a variable time step in MatLab (function ode45). Initial concentrations used for each reaction were given above. The resulting fitted curves for each species were optimized by iteratively testing k values (Table 1) that maximized R^2.

4.5.6 Analysis of CDA Inhibitors via Fluorescence Spectroscopy

The same procedure as described in section 4.3 was used for all measurements except for the addition of inhibition. Reactions were also only monitored for 600 seconds. Concentrated stock solutions of each inhibitor were prepared in MilliQ water (10 mM). An aliquot of the desired inhibitor was added to the reaction solution after the cytidine analogue and

before mixing. Inhibitors were tested at concentrations of 0, 0.1, 1, 10, 100, and 1000 µM. All experiments were run in triplicate.

All emission data for a give experiment were converted to a percent change relative to the initial time point. For a given cytidine analogue, percent change signal at one time point was divided by the percent change signal of the reaction without inhibitor present at the same time point to yield the percent activity. Percent activity was subtracted from 1 to yield percent inhibition. Percent inhibition was plotted against the corresponding inhibitor concentration. A Hill curve was fit to the resulting plot and the IC_{50} value was calculated from the obtained constants. The K_I was then calculated from the IC_{50} and K_M of the cytidine analogue used to monitor enzyme activity (Eq. 7).

4.5.7 HPLC End Point Analysis of CDA Activity On C, ^{tz}C, thC, and ^{mth}C

All HPLC experiments were performed by Dr. Yao Li. To corroborate the experiments above, CDA-mediated deamination of cytidine, ^{tz}C, thC, and ^{mth}C was monitored by chromatography. HPLC analysis was carried out with an Agilent 1200 series system with a Sepak Bio C18 analytical column (250 x 4.6 mm, 5 µm particle size). 0.1% formic acid stock solutions were prepared by dissolving 1 mL of formic acid (Acros, 99%) in 999 mL MilliQ water or HPLC grade acetonitrile (Sigma) and filtered using Millipore type GNWP 0.2 µM filters before use. Each injection (10 µL) was subjected to a gradient (20 minutes, from 0.5 to 20% acetonitrile 0.1% formic acid in water 0.1% formic acid) followed by a flush (10 minutes). A flow rate of 1 mL min^{-1} was used and the run was carried out at 25.0 ± 0.1 ºC. Each run was monitored at 260 nm and 320 nm with calibrated references at 650 nm and slit set at 4 nm.

4.6 Acknowledgements

Chapter 4 is adapted from the work: Ludford III, P. T.; Li, Y.; Yang, S.; Tor, Y. “Cytidine Deaminase Can Deaminate Fused Pyrimidine Ribonucleosides” *Org. Biomol. Chem.*, *in press*. Permission to use materials from the manuscript was also obtained from co-authors Yao Li, Shenghua Yang, and Yitzhak Tor. The dissertation author is the first author.

4.7 References

1. Micozzi, D.; Carpi, F. M.; Pucciarelli, S.; Polzonetti, V.; Polidori, P.; Vilar, S.; Williams, B.; Costanzi, S.; Vincenzetti, S. *Int. J. Biol. Macromol.*, **2014**, *63*, 64–74.

2. Cambi, A.; Vincenzetti, S.; Neuhard, J.; Costanzi, S.; Natalini, P.; Vita, A. *Protein Eng.*, **1998**, *11* (1), 59–63.

3. Teh, A. H.; Kimura, M.; Yamamoto, M.; Tanaka, N.; Yamaguchi, I.; Kumasaka, T. *Biochemistry*, **2006**, *45* (25), 7825–7833.

4. Chung, S. J.; Fromme, J. C.; Verdine, G. L. *J. Med. Chem.*, **2005**, *48* (3), 658–660.

5. Voorde, J. V.; Vervaeke, P.; Liekens, S.; Balzarini, J. *FEBS Open Bio* **2015**, *5*, 634–639.

6. Bjånes, T. K.; Jordheim, L. P.; Schjøtt, J.; Kamceva, T.; Cros-Perrial, E.; Langer, A.; de Garibay, G. R.; Kotopoulis, S.; McCormack, E.; Riedel, B. *Drug Metab. Dispos.* **2020**, *48* (3), 153–158.

7. Bowen, C.; Wang, S.; Licea-Perez, H. *J. Chromatogr. B Anal. Technol. Biomed. Life Sci.*, **2009**, *877* (22), 2123–2129.

8. Lavelle, D.; Vaitkus, K.; Ling, Y.; Ruiz, M. A.; Mahfouz, R.; Ng, K. P.; Negrotto, S.; Smith, N.; Terse, P.; Engelke, K. J.; Covey, J.; Chan, K. K.; DeSimone, J.; Saunthararajah, Y. *Blood*, **2012**, *119* (5), 1240–1247.

9. Liu, P. S.; Marquez, V. E.; Kelley, J. A.; Driscoll, J. S. *J. Org. Chem.*, **1980**, *45* (25), 5225–5227.

10. Marquez, V. E.; Liu, P. S.; Kelley, J. A.; Driscoll, J. S.; McCormack, J. J. *J. Med. Chem.*, **1980**, *23* (7), 713–715.

11. Kim, C. H.; Marquez, V. E.; Mao, D. T.; Haines, D. R.; McCormack, J. J. *J. Med. Chem.*, **1986**, *29* (8), 1374–1380.

12. McCormack, J. J.; Marquez, V. E.; Liu, P. S.; Vistica, D. T.; Driscoll, J. S. *Biochem. Pharmacol.*, **1980**, *29* (5), 830–832.

13. Ashley, G. W.; Bartlett, P. A. *J. of Biological Chemistry*, **1984**, *259* (21), 13621–13627.

14. Frick, L.; Yang, C.; Marquez, V. E.; Wolfenden, R. *Biochemistry*, **1989**, *28* (24), 9423–9430.

15. Funamizu, N.; Lacy, C. R.; Fujita, K.; Furukawa, K.; Misawa, T.; Yanaga, K.; Manome, Y. *PLoS One*, **2012**, *7* (5), e37424.

16. Marquez, V. E.; Barchi, J. J.; Kelley, J. A.; Rao, K. V. R.; Agbaria, R.; Ben-Kasus, T.; Cheng, J. C.; Yoo, C. B.; Jones, P. A. *Nucleosides, Nucleotides and Nucleic Acids*, **2005**, *24* (5–7), 305–318.

17. Laliberte, J.; Marquez, V. E.; Momparler, R. L. *Cancer Chemotherapy and Pharmacology*, **1992**, *30*, 7–11.

18. Wentworth, D. F.; Wolfenden, R. Biochemistry, **1975**, *14* (23), 5099–5105.

19. Frances, A.; Cordelier, P. *Mol. Therapy*, **2020**, *28* (2), 357–366.

20. Sherwood, R. A. *Biomed. Chromatogr.*, **1991**, *5* (6), 235–239.

21. Dutta, P. K.; Shanley, M. S.; O'Donovan, G. A. *J. Chromatogr. A*, **1990**, *512* (C), 395–401.

22. Okamura, T.; Kigasawa, K. *Prenat. Diagn.*, **1994**, *14* (3), 213–218.

23. Shin, D.; Sinkeldam, R. W.; Tor, Y. *J. Am. Chem. Soc.*, **2011**, *133* (38), 14912–14915.

24. Rovira, A. R.; Fin, A.; Tor, Y. *J. Am. Chem. Soc.*, **2015**, *137* (46), 14602–14605.

25. Rovira, A. R.; Fin, A.; Tor, Y. *Chem. Sci.*, **2017**, *8*, 2983–2993.

26. Ashyraliyev, M.; Fomekong-Nanfack, Y.; Kaandorp, J. A.; Blom, J. G. *FEBS Journal*, **2009**, *276*, 886–902.

27. Kutalik, Z.; Cho, K.-H.; Wolkenhauer, O. *BioSystems*, **2004**, *75*, 43–55.

28. Hoops, S.; Hontecillas, R.; Abedi, V.; Leber, A.; Philipson, C.; Carbo, A.; Bassaganya-Riera, J. in *Computational Immunology: Models and Tools*, ed. J. Bassaganya-Riera, Academic Press, **2016**, ch. 5, 63–78.

Chapter 5

Development of a Method to Deconvolute the Activities of Human Adenosine Deaminase 1 and 2

5.1 Introduction to Adenosine Deaminase 1 and 2

Human Adenosine Deaminase 1 (ADA1) and 2 (ADA2) are two enzymes that deaminate adenosine and 2'-deoxyadenosine converting them to inosine and 2'-deoxyinosine, respectively.[1] Despite having the same catalytic behavior, these enzymes are found in different regions of the body and are associated with separate diseases and disorders. ADA1 is primarily located in the cytoplasm and ADA2 is located in the extracellular membrane.[2–4] ADA1 has been shown to be associated with severe combined immunodeficiency disease and excess levels of adenosine can favor tumor progression by inhibiting the function of immune response cells.[5–8] Deficiency of adenosine deaminase 2 (DADA2) results in autoinflammatory disorder and may also cause susceptibility to Epstein Barr Virus (EBV)-induced disease.[9–14] ADA2 activity has also been used as a biomarker for HIV.[15] Some of these may in part be relate to the fact that cells become immunosuppressed when exposed to high concentrations of adenosine for extended periods.[5]

Historically, inhibitors of ADA activity in general have been sought after for chemotherapeutic potential.[18–23] ADA activity has been implicated in certain types of cancer,

notably leukemia and lymphoma.[24,25] Two potent inhibitors, Pentostatin and Cladribine, have both made it into the clinic to treat hairy cell leukemia (Fig. 5.1).[26,27] More inhibitors have been reported that are not FDA approved including EHNA, a potent inhibitor shown to be selective for ADA1 (Fig. 5.1).[17,28,29]

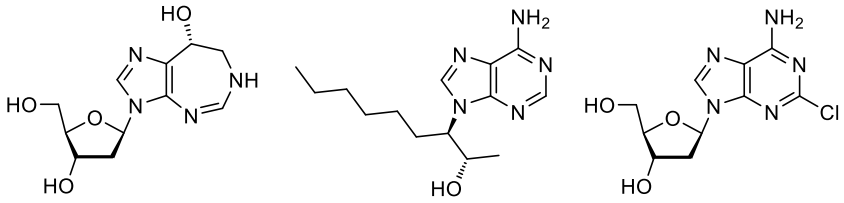

Figure 5.1 Structures of Cladribine, EHNA, and Pentostatin

The fact that these two enzymes are implicated in different diseases and disorders suggests the need to isolate the activity of each when both are present, such as in cell lysate. ADA activity has been monitored by chromatographic separation, ammonia production, and absorption spectroscopy.[26,30–32] These methods suffer from a lack of real time monitoring, time consuming tasks, and optical interference. With a new fluorescent adenosine analogue, ^{mth}A, on hand and two previously reported analogues, thA and ^{tz}A, we set out to establish a new assay for monitoring ADA1 and ADA2 activity.[33,34] The goal of the assay was to separate the activities of each enzyme when both are present by turning off one or the other with selective inhibitors.

5.2 Identifying Suitable Inhibitors for Selective Inhibition of ADA1 or ADA2

In the past, adenosine deaminase activity has been measured in blood plasma as a marker for disease.[3] These assays, however, do not distinguish between ADA1 or ADA2 activity. To the best of our knowledge, no assay has been reported that allows the user to choose which ADA to screen. We thus sought to develop such an assay.

We began by identifying selective inhibitors for ADA1 and ADA2. EHNA is a known potent inhibitor of ADA1 that does not inhibit ADA2 (Fig. 5.1).[17,28,29] We could therefore expect to turn off ADA1 selectively when both enzymes were present. However, no potent inhibitors of ADA2 have been reported that do not inhibit ADA1. The most potent inhibitors that have been reported for ADA2 but not reported for or not tested on ADA1 have K_I values in the hundreds of micromolar.[16] We therefore wanted to pick one that we thought would be the least likely to inhibit ADA1 or disrupt the assay.

Adenosine analogues such as Formycin A have in the past been reported to inhibit ADA1 and so we sought to avoid these types of structures. Nucleobases and structural analogues of them have not been shown to inhibit ADA1. We thus searched through the reported nucleobase analogue inhibitors of ADA2. A nucleobase analogue such as 4-fluoro-7-nitrobenzofurazan with a reported K_I of 167 μM might at first glance appear like a good choice.[16] However, some benzofurazans have been reported as excellent fluorophores and so we thought the molecule might drown out substrate signal.[35] Some purines such as adenine and guanine fluoresce so poorly that they are effectively dark.[36] With this in mind, we instead chose 2,6-dichloropurine, which happened to be the most potent nucleobase analogue inhibitor reported, to use as the “off-switch” for ADA2 in our assay (Fig. 5.2).

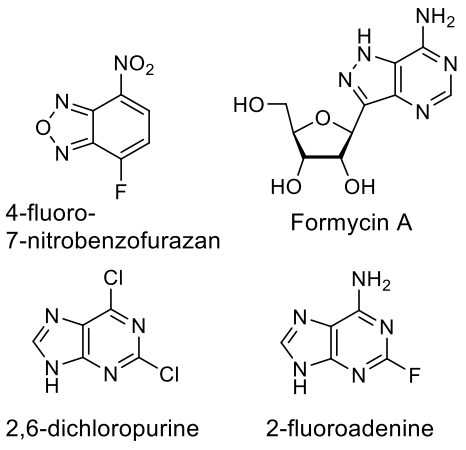

Figure 5.2 Structures of Various ADA2 Inhibitors

5.3 Reaction Kinetics of ADA1 and ADA2 with Three Adenosine Analogues

As 2,6-dichloropurine was reported to have a K_I of 110 uM, we needed a large excess to ensure ADA2 would not partially react with the substrate, in this case 10 mM.[16] 2,6-dichloropurine absorbs at all of the wavelengths that adenosine and inosine do. This meant the change in absorbance that is usually monitored during the reaction of adenosine with ADA could not be. We therefore needed new substrates that ideally absorbed above the range of 2,6-dichloropurine, and ideally fluoresced providing even further red-shifted signal. We chose the two previously reported fluorescent adenosine analogues, ^{tz}A and thA, and the newly synthesized ^{mth}A as potential substrates for ADA1 and ADA2. As all three had been shown to react with bovine ADA we suspected they would react with ADA1 and ADA2 as well.

Different reaction buffers are reported for ADA1 (Hepes buffer, pH 7.5) and ADA2 (1 M NaCl, 25 mM phosphate, pH 6.0). We chose to use the ADA2 reaction buffer to observe mixtures of each A and I analogue pair and to compare reactions of ADA1 and ADA2 due to the sensitivity to pH reported for ADA2. The absorption spectra of mixtures of ^{tz}A and ^{tz}I, thA and thI, and ^{mth}A and ^{mth}I were taken in reaction buffer (1 M NaCl, 25 mM phosphate, pH 6.0) to provide insight into how the reactions would look if they proceeded (Fig. 5.3–5.9). The isosbestic points of ^{tz}A and ^{tz}I, thA and thI, and ^{mth}A and ^{mth}I were found to be 324 nm, 317 nm, and 332 nm (Table 5.1). Next, the emission spectra of mixtures of ^{tz}A and ^{tz}I, thA and thI, and ^{mth}A and ^{mth}I upon excitation at the respective isosbestic points were taken in reaction buffer (1 M NaCl, 25 mM phosphate, pH 6.0) (Figs. 5.3–5.8). The isoemissive points of ^{tz}A and ^{tz}I, thA and thI, and ^{mth}A and ^{mth}I were found to be 369 nm, 438 nm, and 502 nm (Table 5.1).

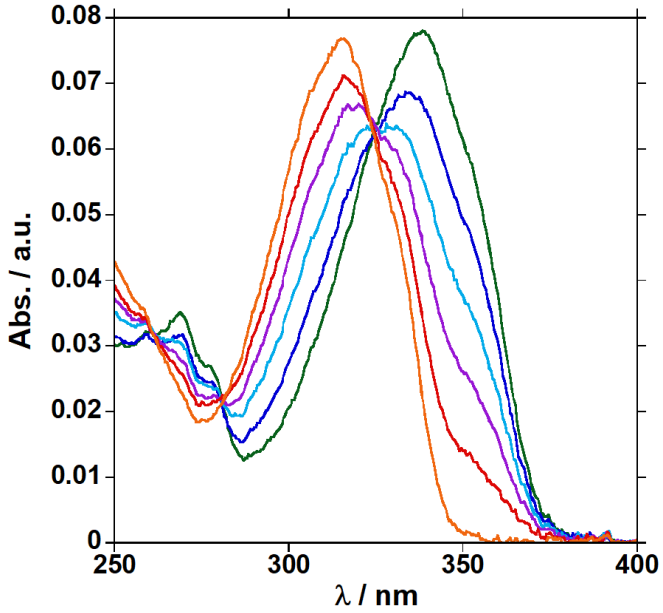

Figure 5.3 Absorption Spectra of ^{tz}A and ^{tz}I Mixtures in Buffer. Steady state absorption traces of isomolar (10 μM total analog) 0:1 (green), 1:4 (blue), 2:3 (light blue), 3:2 (purple), 4:1 (red), and 1:0 (orange) ^{tz}I:^{tz}A mixtures in 1 M NaCl, 25 mM phosphate, pH 6.0

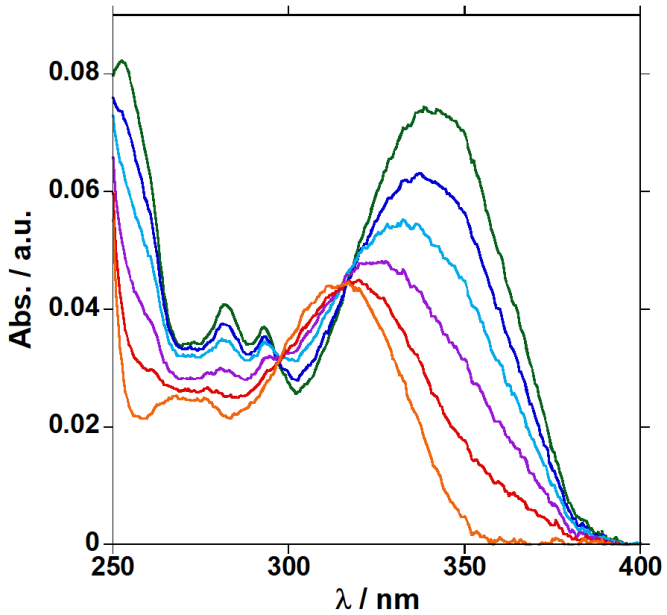

Figure 5.4 Absorption Spectra of thA and thI Mixtures in Buffer. Steady state absorption traces of isomolar (10 μM total analog) 0:1 (green), 1:4 (blue), 2:3 (light blue), 3:2 (purple), 4:1 (red), and 1:0 (orange) thI:thA mixtures in 1 M NaCl, 25 mM phosphate, pH 6.0

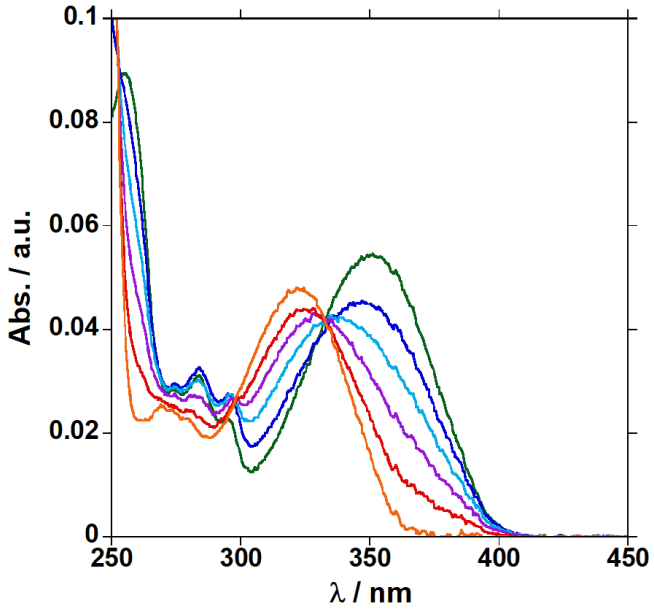

Figure 5.5 Absorption Spectra of ^{mth}A and ^{mth}I Mixtures in Buffer. Steady state absorption traces of isomolar (10 μM total analog) 0:1 (green), 1:4 (blue), 2:3 (light blue), 3:2 (purple), 4:1 (red), and 1:0 (orange) ^{mth}I:^{mth}A mixtures in 1 M NaCl, 25 mM phosphate, pH 6.0

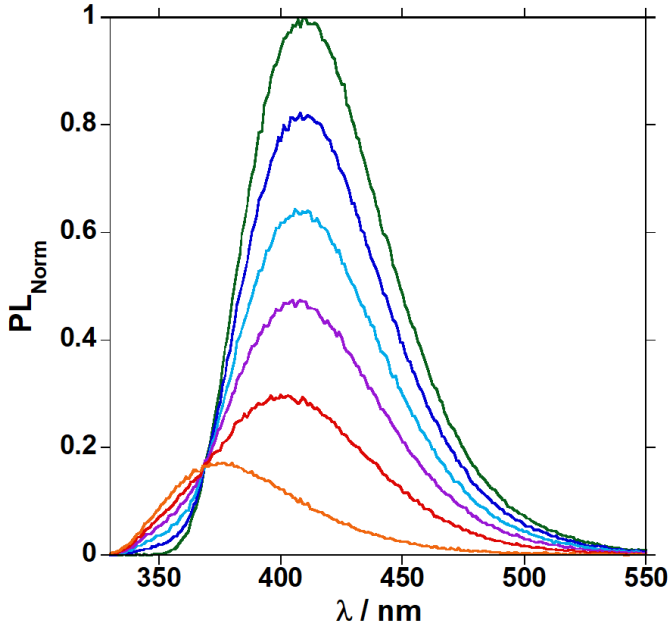

Figure 5.6 Emission Spectra of ^{tz}A and ^{tz}I Mixtures in Buffer. Steady state emission traces of isomolar (10 μM total analog) 0:1 (green), 1:4 (blue), 2:3 (light blue), 3:2 (purple), 4:1 (red), and 1:0 (orange) ^{tz}I:^{tz}A mixtures in 1 M NaCl, 25 mM phosphate, pH 6.0

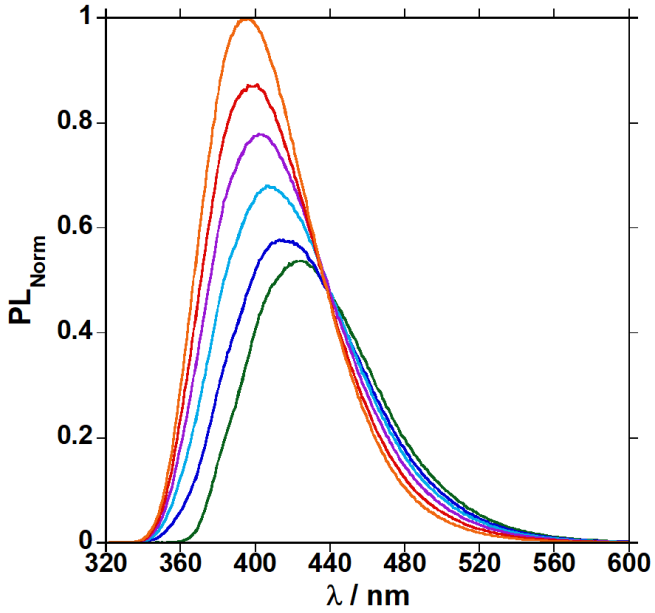

Figure 5.7 Emission Spectra of thA and thI Mixtures in Buffer. Steady state emission traces of isomolar (10 μM total analog) 0:1 (green), 1:4 (blue), 2:3 (light blue), 3:2 (purple), 4:1 (red), and 1:0 (orange) thI:thA mixtures in 1 M NaCl, 25 mM phosphate, pH 6.0

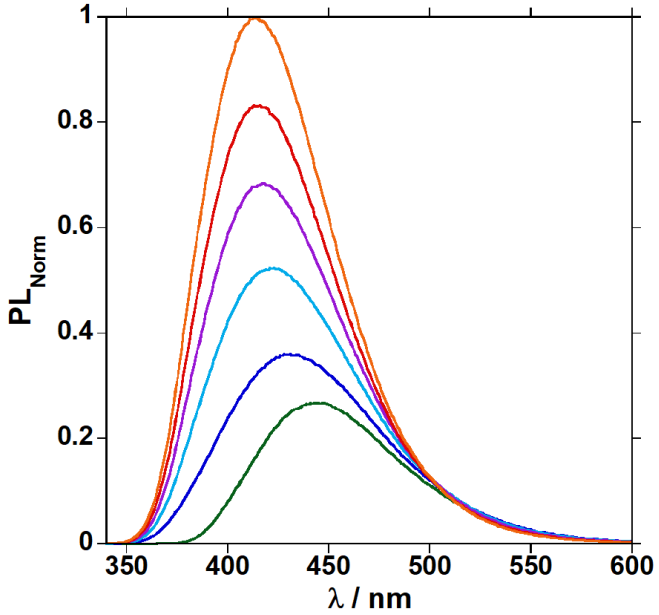

Figure 5.8 Emission Spectra of ^{mth}A and ^{mth}I Mixtures in Buffer. Steady state emission traces of isomolar (10 μM total analog) 0:1 (green), 1:4 (blue), 2:3 (light blue), 3:2 (purple), 4:1 (red), and 1:0 (orange) ^{mth}I:^{mth}A mixtures in 1 M NaCl, 25 mM phosphate, pH 6.0

Table 5.1 Isosbestic and Isoemissive Points

Compounds	Isosbestic Point	Isoemissive Point
^{tz}A and ^{tz}I	324 nm	369 nm
thA and thI	317 nm	438 nm
^{mth}A and ^{mth}I	332 nm	502 nm

Adenosine, ^{tz}A, thA, and ^{mth}A, all at 10 μM concentrations, were each placed in the presence of ADA1 or ADA2 in their reported reaction buffers. The change in absorption or emission was measured and plotted against time (Fig. 5.9, 5.10). The K_M of adenosine and ADA1 is reported as 100 μM, and the K_M of A and ADA2 is reported as 1.48 mM.[37] We hypothesized 10 μM of each A analogue would be sufficient to generate pseudo-first order conditions and thus fit a first order curve to each set of data. This yielded k_{app} values which could be converted to $t_{1/2}$ values or catalytic efficiency (k_{cat}/K_M) values listed in Tables 5.2 and 5.3. We also ran similar experiments for ADA1, but this time in the ADA2 reaction buffer and monitored the reactions by emission. This yielded k_{app}, $t_{1/2}$, and k_{cat}/K_M values listed in Table 5.4.

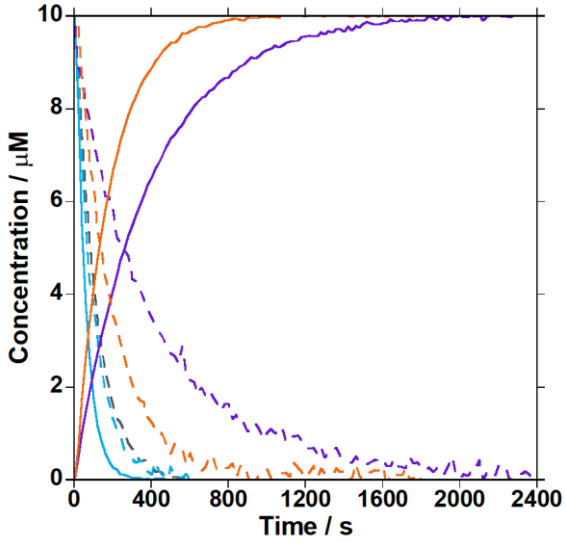

Figure 5.9 Reactions of adenosine (grey), ^{tz}A (light blue), thA (purple), and ^{mth}A (orange) with ADA1 in 1 M NaCl and 25 mM phosphate buffer, pH 6.0 monitored by absorption (dashed) or emission (solid)

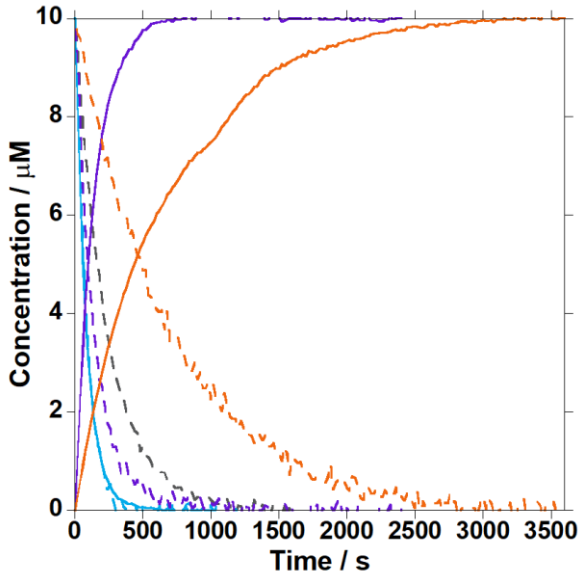

Figure 5.10 Reactions of adenosine (grey), ^{tz}A (light blue), thA (purple), and ^{mth}A (orange) with ADA2 in 1 M NaCl and 25 mM phosphate buffer, pH 6.0 monitored by absorption (dashed) or emission (solid)

Table 5.2 Pseudo-First Order Kinetic Parameters of ADA1 Reactions

		ADA1 (nM)	k_{app}	$t_{1/2}$	k_{cat}/K_M
Abs	**A**	2.4	8.7 ± 0.6	80 ± 5	3.6
	^{tz}A	2.4	10 ± 1	70 ± 4	4.2
	^{tz}A Adj.*	2.4	10 ± 1	70 ± 4	4.2
	thA	24	2.5 ± 0.2	280 ± 10	0.10
	thA Adj.*	2.4	0.25 ± 0.02	2800 ± 100	0.10
	^{mth}A	240	5.0 ± 0.1	140 ± 10	0.021
	^{mth}A Adj.*	2.4	0.050 ± 0.001	14000 ± 1000	0.021
Em	**^{tz}A**	2.4	16 ± 1	43 ± 6	6.7
	^{tz}A Adj.*	2.4	16 ± 1	43 ± 6	6.7
	thA	24	2.6 ± 0.3	270 ± 30	0.11
	thA Adj.*	2.4	0.26 ± 0.03	2700 ± 300	0.11
	^{mth}A	240	5.5 ± 0.1	130 ± 10	0.023
	^{mth}A Adj.*	2.4	0.055 ± 0.001	13000 ± 1000	0.023

[a] k_{app}, $t_{1/2}$, and k_{cat}/K_M values are in units of x 10^{-3} s^{-1}, s, and x 10^{6} M^{-1} s^{-1}, respectively. *values were adjusted to reflect an ADA1 concentration of 2.4 nM.

Table 5.3 Pseudo-First Order Kinetic Parameters of ADA2 Reactions

		ADA2 (nM)	k_{app}	$t_{1/2}$	k_{cat}/K_M
Abs	**A**	88	4.2 ± 0.1	170 ± 10	0.048
	^{tz}A	88	11 ± 1	62 ± 3	0.13
	thA	88	7.0 ± 1.0	100 ± 15	0.080
	^{mth}A	88	1.4 ± 0.1	490 ± 10	0.016
Em	**^{tz}A**	88	12 ± 1	60. ± 5	0.14
	thA	88	6.3 ± 0.6	110 ± 10	0.072
	^{mth}A	88	1.5 ± 0.1	460 ± 10	0.017

[a] k_{app}, $t_{1/2}$, and k_{cat}/K_M values are in units of x 10^{-3} s^{-1}, s, and x 10^{6} M^{-1} s^{-1}, respectively.

Table 5.4 Pseudo-First Order Kinetic Parameters of ADA1 Reactions in ADA2 Reaction Buffer

	ADA1 (nM)	k_{app}	$t_{1/2}$	k_{cat}/K_M
^{tz}A	2.4	14 ± 2	52 ± 8	5.8
^{tz}A Adj.*	2.4	14	52	5.8
thA	24	8.6 ± 0.2	80. ± 2	0.36
thA Adj.*	2.4	0.86	800	0.36
^{mth}A	240	9.7 ± 0.1	71 ± 1	0.040
^{mth}A Adj.*	2.4	0.097	7100	0.040

[a] k_{app}, $t_{1/2}$, and k_{cat}/K_M values are in units of x 10^{-3} s^{-1}, s, and x 10^{6} M^{-1} s^{-1}, respectively. *values were adjusted to reflect an ADA1 concentration of 2.4 nM.

In the case of ADA1, ^{tz}A displayed a $t_{1/2}$ comparable to adenosine. thA and ^{mth}A had a little over one order and two orders of magnitude larger $t_{1/2}$ values, respectively. This suggests the loss of the "N7" moiety in thA and introduction of a greasy moiety at that same position in ^{mth}A severely hindered the recognition of those compounds by ADA1. When the reactions with ADA1 were run in ADA2 reaction buffer, the $t_{1/2}$ value obtained for ^{tz}A remained roughly the same. However, the $t_{1/2}$ values for thA and ^{mth}A decreased by a factor of 1/3 and 1/2, respectively. It was not immediately clear why the change in reaction times was different across substrates. However, the pH was the main parameter changed suggesting it may have influenced the substrates differently from one another.

In the case of ADA2, ^{tz}A displayed the smallest $t_{1/2}$ value followed by thA and then followed by adenosine. ^{mth}A had the largest $t_{1/2}$ value, but only by a factor of three relative to adenosine. This suggests that ADA2 may not depend as heavily on the "N7" moiety for

substrate binding as ADA1 does. This insight may prove useful for future substrate or inhibitor design.

5.4 Selective Monitoring of ADA1 or ADA2 Reactions

With each A analogue confirmed as a substrate of ADA1 and ADA2, we next aimed to observe and isolate the activity of either enzyme when the other was also present. We started with isolating and monitoring ADA2 activity by introducing a selective inhibitor of ADA1, EHNA. We mixed ADA1, ADA2, EHNA, and an A analogue and observed the reaction by emission. The resulting signal data was plotted against time and a first order curve was fit to it (Fig 5.11). The $t_{1/2}$ values obtained for ^{tz}A, thA, and ^{mth}A were 59, 92, and 520 s, respectively, in good agreement with those obtained in reactions with just ADA2 (Table 5.3, 5.5). This indicated that all three analogues could be used to monitor the ADA2 reaction in the presence of ADA1 and EHNA.

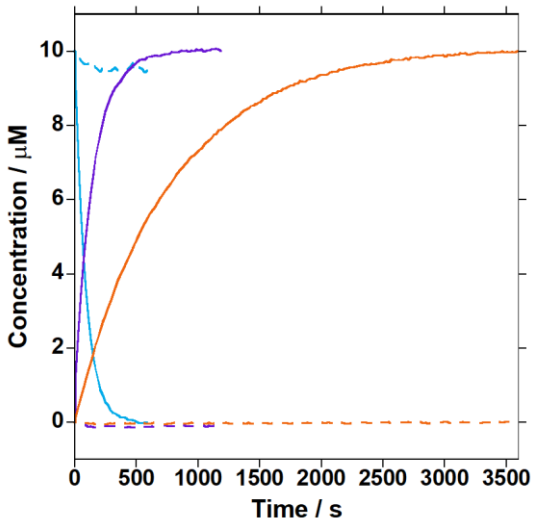

Figure 5.11 Reactions of adenosine (grey), ^{tz}A (light blue), thA (purple), and ^{mth}A (orange) with (solid) or without (dashed) ADA2 in 10 μM EHNA, 2.4 nM ADA1, 1 M NaCl, and 25 mM phosphate buffer, pH 6.0 monitored by emission

Table 5.5 Pseudo-First Order Kinetic Parameters of ADA1 + ADA2 Reactions in the Presence of 10 μM EHNA

	ADA1 (nM)	ADA2 (nM)	k_{app}	$t_{1/2}$	k_{cat}/K_M
^{tz}**A**	2.4	88	12 ± 1	59 ± 2	0.14
th**A**	2.4	88	7.6 ± 0.2	92 ± 2	0.086
^{mth}**A**	2.4	88	1.3 ± 0.1	520 ± 20	0.015

[a] k_{app}, $t_{1/2}$, and k_{cat}/K_M values are in units of x 10^{-3} s^{-1}, s, and x 10^6 M^{-1} s^{-1}, respectively.

We then sought to isolate and monitor ADA1 activity. We mixed ADA1, ADA2, 2,6-dichloropurine, and an A analogue and observed the reaction by emission in the same manner as before. The $t_{1/2}$ values obtained for ^{tz}A, thA, and ^{mth}A were 330, 6500, and 88000 s, respectively, when adjusted to reflect an ADA1 concentration of 2.4 nM. The reactions were slower than without ADA2 and 2,6-dichloropurine present, but we were still able to monitor activity. The catalytic efficiencies of the reactions with 2,6-dichloropurine and ADA2 present were found to be 16%, 12%, and 8% of the reactions without for ^{tz}A, thA, and ^{mth}A, respectively.

In each of the measurements of activity, we allowed the reaction to proceed to completion and then normalized the data and multiplied by the initial concentration. This allowed us to plot concentration versus time. In reactions of A analogue with ADA2 when ADA1 and EHNA were present the k_{app}, $t_{1/2}$, and catalytic efficiency values could be considered representative of ADA2 activity. In reactions of A analogue with ADA1 when ADA2 and 2,6-dichloropurine are present the k_{app}, $t_{1/2}$, and catalytic efficiency values need to be adjusted before being considered representative of the true ADA1 activity. This can be done simply by dividing the k_{app} value by the appropriate percentage listed above and then calculating the $t_{1/2}$ and catalytic efficiency from the adjusted k_{app} value.

The approaches listed above detailed information about the reaction, but in some cases it may be superfluous. One can also monitor a given reaction up to a given time point and then compare signal to another reaction signal at the same time point. In this case it may be advantageous to convert the signal to percent change relative to the initial before comparing different reactions. This should remove interference from the flux in absolute values.

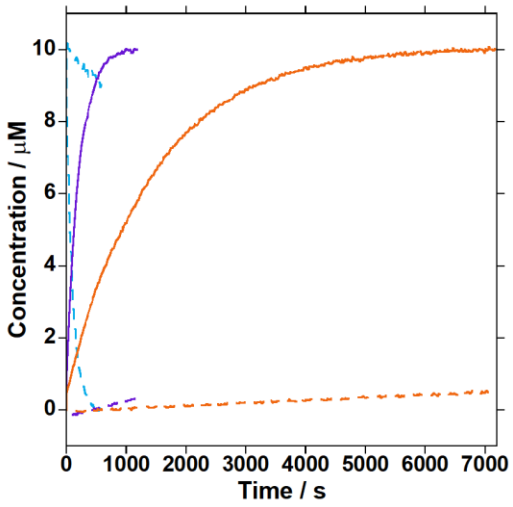

Figure 5.12 Reactions of adenosine (grey), ^{tz}A (light blue), thA (purple), and ^{mth}A (orange) with (solid) or without (dashed) ADA1 in 10 mM 2,6-dichloropurine, 88 nM ADA2, 1 M NaCl, and 25 mM phosphate buffer, pH 6.0 monitored by emission

Table 5.6 Pseudo-First Order Kinetic Parameters of ADA1 + ADA2 Reactions in the Presence of 10 mM 2,6-dichloropurine

	ADA1 (nM)	ADA2 (nM)	k_{app}	$t_{1/2}$	k_{cat}/K_M
^{tz}A	12	88	11 ± 1	66 ± 9	0.92
^{tz}A Adj.*	2.4	88	2.2	330	0.92
thA	120	88	5.3 ± 0.2	130 ± 10	0.044
thA Adj.*	2.4	88	0.106	6500	0.044
^{mth}A	240	88	0.77 ± 0.04	880 ± 50	0.0032
^{mth}A Adj.*	2.4	88	0.0077	88000	0.0032

[a] k_{app}, $t_{1/2}$, and k_{cat}/K_M values are in units of x 10^{-3} s^{-1}, s, and x 10^{6} M^{-1} s^{-1}, respectively. *values were adjusted to reflect an ADA1 concentration of 2.4 nM.

5.5 Experimental Procedures

5.5.1 General Procedure for Spectroscopic Measurements

Spectroscopic grade DMSO was obtained from Sigma Aldrich and aqueous solutions were prepared with MilliQ water. All measurements were carried out in a 3 mL, 1 cm four-sided quartz cuvette (absorption measurements) or a 125 μL, 1 cm four-sided quartz cuvette (emission measurements) from Helma.

Absorption spectra were taken on a Shimadzu UV-2450 spectrophotometer setting the slit width to 1 nm and resolution to 0.5 nm. All spectra were corrected for the blank. Steady

state emission spectra were taken on a Horiba Fluoromax-4 equipped with a cuvette holder with a stirring system setting the excitation slit width to 2 nm and the emission slit width to 3 nm, the resolution to 1 nm, and the integration time to 0.1 s. Steady state fluorescence spectra were taken upon excitation at the corresponding A and I analogues isosbestic point. All spectra were corrected for the blank and instrument response.

Both instruments were equipped with a thermostat-controlled ethylene glycol-water bath fitted to specially designed cuvette holder and the temperature was kept at 25.0 ± 0.1 ºC.

Concentrated stock solutions in DMSO were prepared for adenosine (4.23 mM), ^{tz}A (3.52 mM), thA (4.44 mM), and ^{mth}A (8.74 mM). A working solution (1 mM) was made the day of experimentation by dissolving an appropriate aliquot in autoclaved MilliQ water for a total volume of (50 µL). 2 M sodium chloride, 50 mM sodium phosphate buffer (pH 6.0) was freshly prepared. The buffer was diluted by half in all final solutions. Sample solutions of 10 µM A analog, 8 µM A analog and 2 µM I analog, 6 µM A analog and 4 µM I analog, 4 µM A analog and 6 µM I analog, 2 µM A analog and 8 µM I analog, and 10 µM I analog were prepared by diluting the appropriate workings solutions in MilliQ water and buffer for a total volume of 3 mL. 125 µL of sample solution was taken for measurements of emission. Absorption and emission spectra of samples of corresponding A and I analogs were normalized and overlaid to determine the isosbestic and isoemissive points.

5.5.2 General Procedures in Preparation for Enzymatic Reactions

Recombinant human adenosine deaminase (ADA1) was obtained from Novus Biologicals (Catalog Number 7048-AD-010) and stored in the freezer at –20ºC. The commercial solution [440 µg mL^{-1} in 20 mM Tris-HCl buffer (pH 7.5), 120 mM NaCl, 20% glycerol] was diluted to 10 µg mL^{-1} for assays involving ^{tz}A and 100 µg mL^{-1} for assays involving thA by dissolving an aliquot (1 µL for ^{tz}A, 10 µL for thA) in autoclaved MilliQ water (44 µL). The commercial solution was used as is for assays involving ^{mth}A. The enzyme stock solutions were

freshly prepared and stored on ice for each day of experiments. Final concentrations of ADA1 in reactions were 0.1 μg mL^{-1} (A and ^{tz}A), 1 μg mL^{-1} (thA), or 10 μg mL^{-1} (^{mth}A).

Expression of ADA2 was conducted by Dr. Phillip Bartels. Coding DNA for the ADA2 gene (Sino Biologicals) was cloned into pcDNA3.1/Myc-His (+) C (Invitrogen) using the HiFi DNA Assembly kit (New England Biolabs). The complete construct included a 5' GTC Kozak consensus sequence, the native ADA2 cleavable signal sequence and a C-terminal linker/hexahistidine tag.

Recombinant protein was expressed with the ExpiCHO overexpression system (ThermoFisher) for mammalian proteins using the MaxTiter protocol. Briefly, a 25 mL culture was expanded to a density of ~10 million cells/mL, then split to 6 million cells/mL in a final volume of 25 mL for transfection. 20 μg plasmid DNA was mixed with Expifectamine reagent in cold OptiPro medium and added to the cells with gentle swirling. The transfected cells were incubated at 37 ℃ and 8% CO_2 on a shaker (110 rpm) for ~20 hours, then 150 μL ExpiCHO enhancer and 4 mL ExpiCHO feed were added and the culture was transferred to a 32 ℃ incubator at 5% CO_2 with shaking (110 rpm) for 12 days. 5 days post-transfection, an additional 4 mL ExpiCHO feed was added. In a preliminary prep, Western blotting with THE™ 6x-His primary antibody (Genscript) revealed protein secretion from at least day 9 post-transfection with maximum yields obtained between days 12-14. For subsequent preps, cells were harvested on day 12.

ADA2 in the medium was isolated by centrifugation at 4500 x g for 30 minutes and 4 ℃ after which the supernatant was collected and filtered on a 0.22 μm PES membrane (Corning). Clarified medium was then loaded onto two 1 mL His HiTrap Ni columns (Cytiva) connected in series at a flow rate of 1 mL/minute on a peristaltic pump. The column was washed with 10 mL NiA buffer (25 mM HEPES, pH 7.5, 500 mM NaCl, 30 mM imidazole) followed by 10 mL NiB buffer (25 mM HEPES, pH 7.5, 500 mM NaCl, 300 mM imidazole). A substantial amount of protein from the initial prep was still present in the flow as determined by SDS-PAGE, so the

entire process (loading, NiA elution and NiB wash/elution) was repeated twice to maximize yield. SDS-PAGE showed that ADA2 eluted primarily in NiA, but some was still present in the high-imidazole NiB fraction. NiA and NiB fractions were combined and concentrated to ~1 mL using 20 mL 30 kDa MWCO Vivaspin PES columns (GE Healthcare) centrifuged at 3200 x g. Concentrated protein was then exchanged into size exclusion buffer (25 mM HEPES, pH 7.2, 300 mM NaCl, 5% glycerol) using a 2 mL 40 kDa MWCO Zeba desalting column (Thermo) prior to loading onto a pre-equilibrated Superdex 16/600 prep-grade column (GE Healthcare). ADA2 eluted as a single broad peak. 2 mL FPLC fractions were combined and concentrated a final time on a 20 mL Vivaspin PES column. Concentration was estimated by UV-vis using an extinction coefficient of 68,000 $M^{-1}cm^{-1}$ at 280 nm. Fully purified protein ran just below70 kDa by SDS-PAGE, dropping to the expected MW of 57 kDa following treatment with PNGase F (NEB) to remove N-linked glycans. The overall yield of purified protein was ~10 mg protein from a 25 mL cell culture (400 mg protein per liter of cell culture).

The resulting stock solution of ADA2 (6.26 μM) was used as a working solution for all reactions involving adenosine and its analogs. The final concentration of ADA2 in all reactions was 88 nM.

Concentrated stock solutions in DMSO were prepared for adenosine (4.23 mM), ^{tz}A (3.52 mM), thA (4.44 mM), and ^{mth}A (8.74 mM). A working solution (1 mM) was made the day of experimentation by dissolving an appropriate aliquot in autoclaved MilliQ water for a total volume of (50 μL).

The ADA1- and ADA2-mediated enzymatic conversion of adenosine (and its analogues) was followed by absorbance and emission (for the emissive analogues ^{tz}A, thA, and ^{mth}A) spectroscopy by monitoring the intensity variation as a function of time. The real-time conversion of adenosine (and its analogues) to inosine (and the corresponding analogues) was performed on a Shimadzu UV-2450 spectrophotometer (slit width: 1nm, resolution 0.5 nm) and Horiba Fluoromax-4 (ex. slit width: 2 nm, em. slit width: 3 nm, resolution: 1 nm). Each

instrument was equipped with a thermostat-controlled ethylene glycol/water bath fitted to a specially designed cuvette holder and the temperature was kept at 25.0 ± 0.1 ºC. All measurements were carried out in a 125 µL, 1 cm four-sided quartz cuvette from Helma. 100 mM Hepes buffer (pH 7.5) or 2 M sodium chloride, 50 mM sodium phosphate buffer (pH 6.0) were freshly prepared. Buffers were diluted by half for final reaction solutions.

5.5.3 Monitoring of ADA1 and ADA2 Conversion of A and A Analogs to Corresponding I and I Analogs by Absorption Spectroscopy

The absorbance of adenosine, ^{tz}A, thA, and ^{mth}A was monitored at 260, 340, 340, and 353 nm respectively. MilliQ water, buffer, and adenosine or adenosine analog were added to the cuvette, thoroughly mixed, and an initial measurement at the respective wavelength taken. An aliquot of enzyme working solution was added to the reaction cuvette. The reaction solution was mixed with a pipette several times and measurements were continued every 20 seconds. For reactions with ADA1, adenosine and ^{tz}A were monitored for 600 seconds, thA was monitored for 2400 seconds, and ^{mth}A was monitored for 1800 seconds. For reactions with ADA2, adenosine was monitored for 1800 seconds, ^{tz}A was monitored for 1200 seconds, thA for 2400 seconds, and ^{mth}A for 3600 seconds. All experiments were run in triplicate.

All absorption data were normalized, multiplied by the initial concentration of A analogue, and plotted against time. A pseudo-first order curve was fit to each resulting time plot yielding k_{app} values and $t_{1/2}$ values. Averages and standard deviations of the k_{app} and $t_{1/2}$ values were calculated from the set of time plots from adenosine and each adenosine analogs reactions.

5.5.4 Monitoring of ADA1 and ADA2 Conversion of A and A Analogs to Corresponding I and I Analogs by Fluorescence Spectroscopy

The emission intensity of ^{tz}A, thA, and ^{mth}A was monitored at 410, 391, and 415 nm upon excitation at 324, 323, and 332 nm, respectively. MilliQ water, buffer, and adenosine analog

were added to the cuvette, thoroughly mixed, and an initial measurement at the respective wavelength taken. An aliquot of enzyme working solution was added to the reaction cuvette. The reaction solution was mixed with a pipette several times and measurements were continued every 20 seconds. For reactions with ADA1, ^{tz}A were monitored for 600 seconds, thA was monitored for 2400 seconds, and ^{mth}A was monitored for 1800 seconds. For reactions with ADA2, ^{tz}A was monitored for 1200 seconds, thA for 2400 seconds, and ^{mth}A for 3600 seconds. All experiments were run in triplicate.

All emission data were normalized, multiplied by the initial concentration of A analogue, and plotted against time. A pseudo-first order curve was fit to each resulting time plot yielding k_{app} values and $t_{1/2}$ values. Averages and standard deviations of the k_{app} and $t_{1/2}$ values were calculated from each adenosine analogs set of time plots.

5.5.5 Monitoring of ADA2 Conversion of ^{tz}A to ^{tz}I, thA to thI, and ^{mth}A to ^{mth}I in the Presence of ADA1 and EHNA via Emission

The same procedure as described in section 5.5.4 was used except for the addition of ADA1 and EHNA. ADA1 and EHNA were added and thoroughly mixed before A analog.

The emission intensity data was normalized and multiplied by the initial concentration of A analogue. The resulting data was plotted against time. A pseudo-first order curve was fit to each resulting time plot yielding k_{app} values and $t_{1/2}$ values. Averages and standard deviations of the k_{app} and $t_{1/2}$ values were calculated from each adenosine analogs set of time plots. The k_{app} value was divided by the enzyme concentration to give the catalytic efficiency (k_{cat}/K_M) but the k_{app} value could also be divided by the catalytic efficiency to give the enzyme concentration in principle.

5.5.6 Monitoring of ADA1 Conversion of ^{tz}A to ^{tz}I, thA to thI, and ^{mth}A to ^{mth}I in the Presence of ADA2 and 2,6-dichloropurine via Emission

The same procedure as described in section 5.5.4 was used except for the addition of ADA2 and 2,6-dichloropurine. ADA2 and 2,6-dichloropurine were added and thoroughly mixed before A analog.

The emission intensity data was normalized and multiplied by the initial concentration of A analogue. The resulting data was plotted against time. A pseudo-first order curve was fit to each resulting time plot yielding k_{app} values and $t_{1/2}$ values. Averages and standard deviations of the k_{app} and $t_{1/2}$ values were calculated from each adenosine analogs set of time plots. The k_{app} value was divided by the enzyme concentration to give the catalytic efficiency (k_{cat}/K_M) but the k_{app} value could also be divided by the catalytic efficiency to give the enzyme concentration in principle.

5.6 Acknowledgements

Chapter 5 is adapted from work currently being drafted for submission: Ludford III, P. T.; Bartels, P. L.; Tor, Y. “Deconvoluting the Activity of Human Adenosine Deaminase 1 and 2” *in preparation*. Permission to use materials from the manuscript was also obtained from co-authors Phillip Bartels and Yitzhak Tor. The dissertation author will be the first author.

5.7 References

1. Cristalli, G.; Costanzi, S.; Lambertucci, C.; Lupidi, G.; Vittori, S.; Volpini, R.; Camaioni, E. *Med. Res. Rev.*, **2001**, *21*, 105–128.

2. Cortes, A.; Gracia, E.; Moreno, E.; Mallol, J.; Lluis, C.; Canela, E. I.; Casado, V. *Med. Res. Rev.*, **2015**, *35*, 85–125.

3. Khodadadi, I.; Abdi, M.; Ahmadi, A.; Wahedi, M. S.; Menbari, S.; Lahoorpour, F.; Rahbari, R. *Clinical Biochemistry*, **2011**, *44*, 980–983.

4. Conlon, B. A.; Law, W. R. *Clin. Exp. Immunol.*, **2004**, *138*, 14–20.

5. Gourdin, N.; Bossennec, M.; Rodriguez, C.; Vigano, S.; Machon, C.; Jandus, C.; Bauche, D.; Faget, J.; Durand, I.; Chopin, N.; Tredan, O.; Marie, J. C.; Dubois, B.; Guitton, J.; Romero, P.; Caux, C.; Menetrier-Caux, C. *Cancer Res.*, **2018**, *78*, 3604–3618.

6. Parish, S. T.; Kim, S.; Sekhon, R. K.; Wu, J. E.; Kawakatsu, Y.; Effros, R. B. *J. Immun.*, **2010**, *184*, 2847–2854.

7. Cortes, A.; Gracia, E.; Moreno, E.; Mallol, J.; Lluis, C.; Canela, E. I.; Casado, V. *Med. Res. Rev.*, **2015**, *35*, 85–125.

8. Yegutkin, G. G. *Biochimica et Biophysica Acta*, **2008**, *1783*, 673–694.

9. Carmona-Rivera, C.; Khaznadar, S. S.; Shwin, K. W.; Irizarry-Caro, J. A.; O'Neil, L. J.; Liu, Y.; Jacobson, K. A.; Ombrello, A. K.; Stone, D. L.; Tsai, W. L.; Kastner, D. L.; Aksentijevich, I.; Kaplan, M. J.; Grayson, P. C. *Blood*, **2019**, *134*, 395–406.

10. Kendall, J. L.; Springer, J. M. *Curr. Rheumatol. Rep.*, **2020**, *22*, 64.

11. Barzaghi, F.; Minniti, F.; Mauro, M.; De Bortoli, M.; Balter, R.; Bonetti, E.; Zaccaron, A.; Vitale, V.; Omrani, M.; Zoccolillo, M.; Brigida, I.; Cicalese, M. P.; Degano, M.; Hershfield, M. S.; Aiuti, A.; Bondarenko, A. V.; Chinello, M.; Cesaro, S. *Front. in Immun.*, **2019**, *9*, 2767.

12. Staples, E.; Simeoni, I.; Stephens, J. C.; Allen, H. L.; Wright, P.; Davies, E. G.; Javid, B.; Gkrania-Klotsas, E.; Gattens, M.; Firth, H.; Shamardina, O.; Deevi, S. V. V.; Prapa, M.; Uttenhal, B.; Kumararatne, D.; Thaventhiran, J. E. D. *Clinical Immunology*, **2020**, *215*, 108443.

13. Bowers, S. M.; Gibson, K. M.; Cabral, D. A.; Brown, K. L. *Pediatric Rheumatology*, **2020**, 18:54.

14. Samra, Y. A.; Saleh, H. M.; Hussein, K. A.; Elsherbiny, N. M.; Ibrahim, A. S.; Elmasry, K.; Fulzele, S.; El-Shishtawy, M. M.; Eissa, L. A.; El-Shabrawey, M.; Liou, G. I. *Invest. Ophthalmol. Vis. Sci.*, **2017**, *58*, 933–943.

15. Khodadadi, I.; Abdi, M.; Ahmadi, A.; Wahedi, M. S.; Menbari, S.; Lahoorpour, F.; Rahbari, R. *Clinical Biochemistry*, **2011**, *44*, 980–983.

16. Niedzwicki, J. G.; Abernethy, D. R. *Biochemical Pharmacology*, **1991**, *41*, 1615–1624.

17. Gillerman, J.; Fischer, B. *J. Med. Chem.*, **2011**, *54*, 107–121.

18. Sauer, A. V.; Brigida, I.; Carriglio, N.; Aiuti, A. *Front. Immunol.* **2012**, *3*, 265.

19. Mediero, A.; Cronstein, B. N. *Trends Endocrinol. Metab.* **2013**, *24*, 290–300.

20. Kutryb-Zajac, B.; Mateuszuk, L.; Zukowska, P.; Jasztal, A.; Zabielska, M. A.; Toczek, M.; Jablonska, P.; Zakrzewska, A.; Sitek, B.; Rogowski, J.; Lango, R.; Slominska, E. M.; Chlopicki, S.; Smolenski, R. T. *Cardiovasc. Res.* **2016**, *112*, 590–605.

21. Cortes, A.; Gracia, E.; Moreno, E.; Mallol, J.; Lluis, C.; Canela, E. I.; Casado, V. *Med. Res. Rev.* **2015**, *35*, 85–125.

22. Antonioli, L.; Csoka, B.; Fornai, M.; Colucci, R.; Kokai, E.; Blandizzi, C.; Hasko, G. *Drug Discovery Today* **2014**, *19*, 1051–1068.

23. Antonioli, L.; Colucci, R.; La Motta, C.; Tuccori, M.; Awwad, O.; Da Settimo, F.; Blandizzi, C.; Fornai, M. *Curr. Drug Targets* **2012**, *13*, 842–862.

24. Nakajima, Y.; Kanno, T.; Nagaya, T.; Kuribayashi, K.; Nakano, T.; Gotoh, A.; Nishizaki, T. *Cell. Physiol. Biochem.* **2015**, *35*, 51–60.

25. Kutryb-Zajac, B.; Koszalka, P.; Mierzejewska, P.; Bulinska, A.; Zabielska, M. A.; Brodzik, K.; Skrzypkowska, A.; Zelazek, L.; Pelikant-Malecka, I.; Slominska, E. M.; Smolenski, R. T. *J. Cell. Mol. Med.* **2018**, *22*, 5939–5954.

26. Schaeffer, H. J.; Schwender, C. F. *J. Med. Chem.* **1974**, *17*, 6–8.

27. McConnell, W. R.; El Dareer, S. M.; Hill, D. L. *Drug Metab Dispos* **1980**, *8*, 5–7.

28. Lambe, C. U.; Nelson, D. J. *Biochem Pharmacol* **1982**, *31*, 535-539.

29. Li, G.; Nakagome, I.; Hirono, S.; Itoh, T.; Fujiwara, R. *Pharma. Res. Per.*, **2015**, *3*, e00121.

30. Tite, T.; Lougiakis, N.; Myrianthopoulos, V.; Marakos, P.; Mikros, E.; Pouli, N.; Tenta, R.; Fragopoulou, E.; Nomikos, T. *Tetrahedron* **2010**, *66*, 9620–9628.

31. Da Settimo, F.; Primofiore, G.; La Motta, C.; Taliani, S.; Simorini, F.; Marini, A. M.; Mugnaini, L.; Lavecchia, A.; Novellino, E.; Tuscano, D.; Martini, C. *J. Med. Chem.* **2005**, *48*, 5162–5174.

32. Zimmermann, S. C.; Sadler, J. M.; O'Daniel, P. I.; Kim, N. T.; Seley-Radtke, K. L. *Nucleosides, Nucleotides Nucleic Acids* **2013**, *32*, 137–154.

33. Shin, D.; Sinkeldam, R. W.; Tor, Y. *J. Am. Chem. Soc.* **2011,** *133* (38), 14912–14915.

34. Rovira, A. R.; Fin, A.; Tor, Y. *J. Am. Chem. Soc.* **2015,** *137*, 14602–14605.

35. Imai, K.; Uzu, S.; Kanda, S. *Analytica Chimica Acta*, **1994**, *290*, 3-20.

36. Sinkeldam, R. W.; Greco, N. J.; Tor, Y. *Chem. Rev.* **2010,** *110* (5), 2579–2619.

37. Andreasyan, N. A.; Hairapetyan, H. L.; Sargisova, Y. G.; Mardanyan, S. S. *FEBS Letters*, **2005**, *579*, 643–647.

Chapter 6

Conclusions and Future Directions

6.1 Synopsis of Methylthieno[3,4-d]pyrimidine Based Ribonucleoside Alphabet

The synthesis of the methylthieno[3,4-d]pyrimidine based alphabet proved difficult but not insurmountable. The difficulties mainly resided with the ^{mth}A and ^{mth}C molecules because the initial attempts to activate the carbonyl moiety were unsuccessful. Two less common approaches to the activation of the carbonyl were taken. For ^{mth}A, the reagent BOP was used to activate the carbonyl in compound **10** which was then successfully displaced with an amine moiety by the introduction of excess ammonia gas. For ^{mth}C, the carbonyl in compound **15** was activated by treatment with an in situ generated tristriazole phosphoryl reagent. The resulting activated intermediate was not isolatable and had to be displayed using saturated ammonium hydroxide. The amount of time the intermediate was immersed in ammonium hydroxide had to be carefully balanced so that it underwent ammonolysis but also did not partially deprotect the sugar. Neither of the above described approaches was used in the activation of carbonyls in the isothiazolo[4,3-d]pyrimidine and thieno[3,4-d]pyrimidine based alphabets.

As was seen with the thieno[3,4-d]pyrimidine based alphabet, only the glycosylation step in the A analogue synthetic route produced two stereoisomers. Crystal structures and 2D NMR analysis revealed some interesting findings about how to identify which stereoisomer had been obtained. This culminated in the observation that the HH ^{3}J-coupling of the H1' on the ribose could indicate the stereochemistry, a very useful property that could almost certainly be exploited in future synthetic pursuits of ribonucleoside analogues.

The photophysical properties of the methylthieno[3,4-d]pyrimidine based alphabet were quite interesting. While the methyl moiety appeared to diminish the quantum yields relative to the thieno[3,4-d]pyrimidine based alphabet it also significantly red shifted the emission. ^{mth}A emission in particular was surprisingly red shifted relative to thA emission. Perhaps this observation might be exploitable in future fluorophore design. In addition, the ^{mth}A, ^{mth}C, and ^{mth}U all were most emissive in 60% dioxane in water. ^{mth}G emitted best in pure dioxane. This may suggest the analogues, except for ^{mth}G, prefer a mixed solvent environment.

6.2 Future Directions in Synthesis

The synthetic pathway developed for the methylthieno[3,4-d]pyrimidine based alphabet may be exploited to install other useful moieties at the “N7” position (purine numbering). One could imagine installing a bromobenzene using similar reactions that could then undergo palladium coupling to install any number of functional groups (Fig. 6.1). With a substitutable bromine, one could explore the effects of different moieties on the photophysical features of the base molecule. One could also imagine pursuing the same synthetic route but with a methyl moiety that has one or more fluorine atoms substituted for the hydrogen atoms (Fig. 6.2). The electron withdrawing nature of the fluorine atoms might affect the photophysical properties of the aromatic system in unexpected ways.

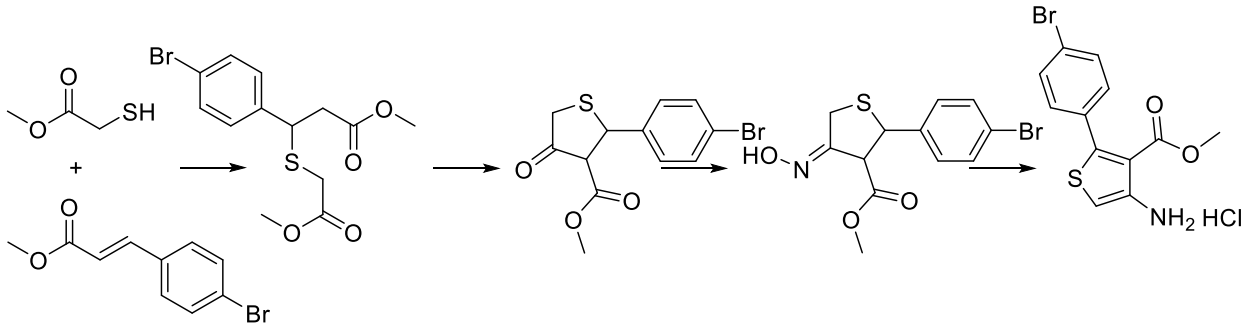

Figure 6.1 Proposed synthetic pathway to build a bromobenzenethiophene precursor

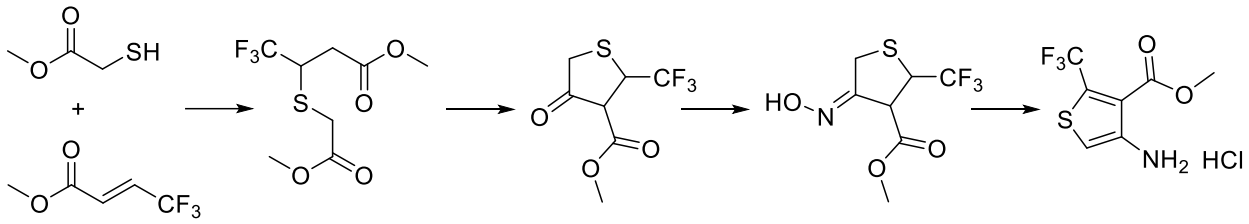

Figure 6.2 Proposed synthetic pathway to build a trifluoromethylthiophene precursor

In addition to potentially functionalizing the thieno[3,4-d]pyrimidine scaffold using the methylthieno[3,4-d]pyrimidine based alphabet as proof of concept, one could also build other interesting analogues. One that immediately comes to mind is an analogue of 2-aminopurine. If one were to successfully reduce the ester moiety in the methylthiophene precursor to an aldehyde, treatment of this intermediate with chloroformamidine might yield the ^{mth}2-AP nucleobase (Fig. 6.3). The photophysical properties of the ^{mth}2-AP nucleobase could then be analyzed to determine whether pursuing a full ribonucleoside would be worthwhile.

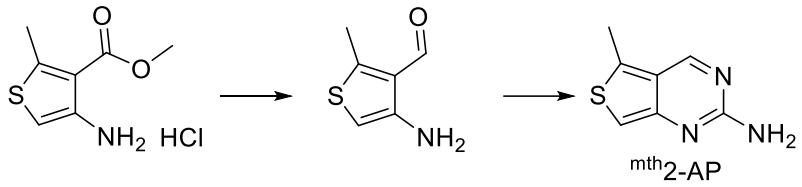

Figure 6.3 Proposed synthetic pathway to ^{mth}2-AP

Additionally, the ^{mth}A synthetic route could be exploited to synthesize some non-canonical ribonucleoside analogues. Those analogues are ^{mth}isoG, ^{mth}X, and ^{mth}2-AA. The synthesis of these molecules could be achieved from the ^{mth}A route because the methylthiophene precursor is glycosylated with a benzoate protected ribose, but still retains the ester and amine moieties necessary for pyrimidine ring formation. For the ^{mth}X, compound 9 could be deprotected and then treated with potassium cyanate to give a urea intermediate. The urea intermediate could then be cyclized by treatment with sodium methoxide (Fig. 6.4). For the ^{mth}isoG and ^{mth}2-AA, one could use the previously reported procedures for ^{tz}isoG and ^{tz}2-AA synthesis or attempt carbonyl activation using procedures described for the synthesis of ^{mth}A

and ^{mth}C (Fig. 6.4). These three molecules could be potentially useful from a photophysical perspective or a biological one.

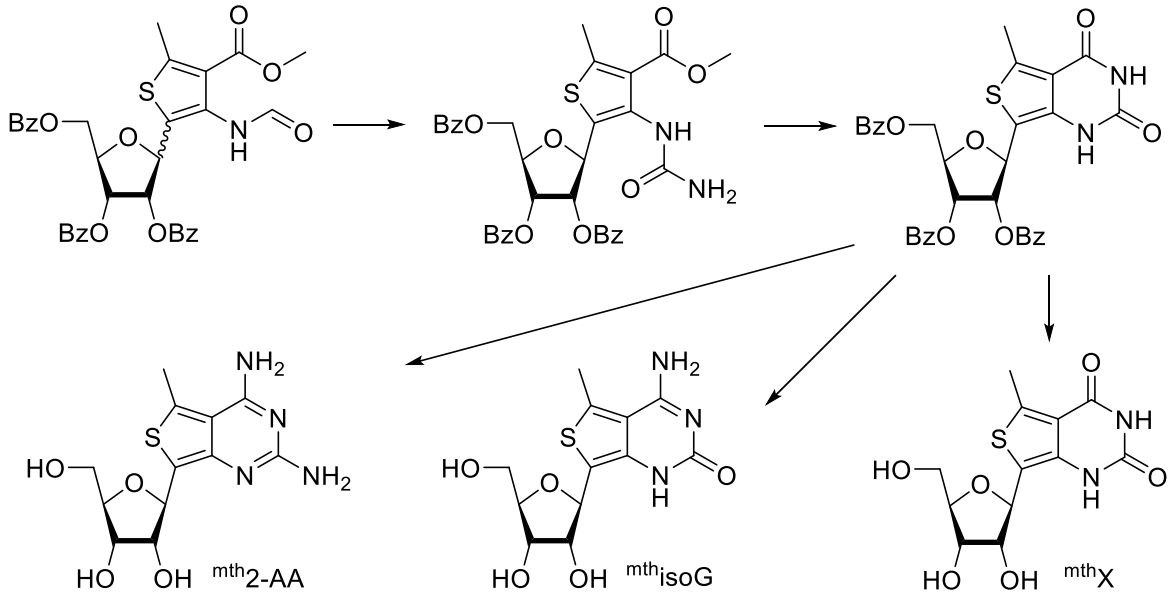

Figure 6.4 Proposed synthetic pathway to build ^{mth}X, ^{mth}isoG, and ^{mth}2-AA

Finally, no deoxyribonucleoside analogues based on the methylthieno[3,4-d]pyrimidine scaffold have been synthesized. One could potentially attempt the glycosylation step in each synthetic pathway with a deoxyribose instead of a ribose. However, this would likely require the separation of two stereoisomers at some point in the synthetic pathway.

6.3 What We Learned During Enzyme Studies

Studies of bovine ADA, CDA, GDA, ADA1, and ADA2 yielded results that indicate tolerance of the perturbing methyl moiety varies widely by enzyme. GDA did not recognize the corresponding ^{mth}G nucleobase as a substrate. Bovine ADA and ADA1 did recognize ^{mth}A as a substrate, but reacted much slower than with the native adenosine. CDA recognized ^{mth}C as a substrate and surprisingly reacted faster with ^{mth}C than cytidine the native substrate. ADA2 recognized ^{mth}A as a substrate and reacted with ^{mth}A roughly a third as fast as adenosine the

native substrate. This was in stark contrast with bovine ADA and ADA1, which both reacted with ^{mth}A at least a couple of orders of magnitude slower than the native substrate.

The findings for CDA were exciting because they indicated the enzyme binding pocket might be roomier than previously expected. Further, it was the only enzyme in which the methylthieno[3,4-d]pyrimidine based analogue reacted faster than the native substrate and the isothiazolo[4,3-d]pyrimidine based alphabet. This suggested that structural perturbations that might at first appear quite sterically bulky can still be quite useful for enzymatic studies. The thiophene and isothiazole ring expansions in thC and ^{tz}C, respectively, were found to be more tightly bound to the enzyme than cytidine. Those ring expansions or other five member rings might be worth adding to future inhibitor designs.

The inhibitors discovered for bovine ADA during the high throughput screening of the Cohen Library have so far only briefly been explored. There were so many hits that one could spend years optimizing each type of compound. The approach we took to build a structure activity relationship and then design a more potent inhibitor can be thought of as a proof of concept for any metal-binding pharmacophores one might want to test against bovine ADA.

We were also able to isolate and measure the activity of either ADA1 or ADA2 when the other was present by adding a selective inhibitor. The selective inhibitor for ADA1 was EHNA and the selective inhibitor for ADA2 was 2,6-dichloropurine. These methods to isolate activity were developed with the intent to be used for diagnostic tests of ADA activity in blood plasma or cell lysates someday. As many nucleobase inhibitors of ADA2 have been reported, it is feasible to think that the assay developed with 2,6-dichloropurine might be replicable with any of those other reported inhibitors for further optimization. As more inhibitors are inevitably developed for ADA2, they should be tested against ADA1 in tandem so as to determine whether they are selective.

On a slightly different note, T7 RNA polymerase was found to recognize ^{mth}GTP as a substrate and to incorporate it into RNA strands in the absence of GTP. The study of RNA is

extensive and ongoing with no end in sight so being able to incorporate the methylthieno[3,4-d]pyrimidine based analogues into RNA strands will make them all the more valuable.

6.4 Future Directions for Enzymatic Studies

That so many different enzymes were able to recognize molecules from the new ribonucleoside analogue alphabet as substrates is quite exciting. Some of the findings may provide new avenues for inhibitor design. That the CDA is able to bind thC and ^{tz}C tighter than cytidine may indicate that future inhibitors should incorporate an expanded ring system. In fact, one could imagine building a thieno[3,4-d]pyrimidine or isothiazolo[4,3-d]pyrimidine based zebularine analogue. This might be accomplished in a similar strategy as described above for the ^{mth}2-AP. One could perhaps reduce the ester moiety in the thiophene or isothiazole precursor to an aldehyde. The aldehyde intermediate could then be treated with potassium cyanate to give a urea which could then be treated with base to generate the pyrimidine ring with only one carbonyl similar to zebularine (Fig. 6.5). One could also imagine expanding the pyrimidine ring in cytidine with fused 6 member rings to generate new potential inhibitors or substrates of CDA. An example of ring systems that could be used as inspiration might be the quinazoline ring systems described by Dr. Yun Xie.[1–3]

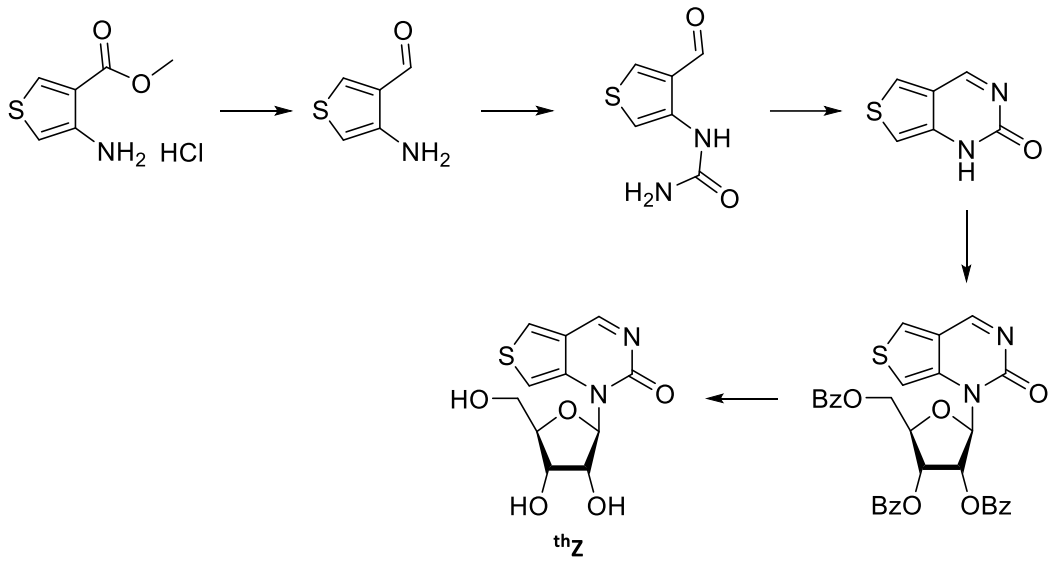

Figure 6.5 Proposed synthetic pathway to build thZ

The Cohen Lab library of MBPs could be screened against CDA, ADA1, ADA2, and GDA. GDA in particular may benefit from this approach because its native substrate is already so small. One could imagine small MBP fragments fitting quite well into the GDA binding pocket. Further, ADA2 which seems to be more susceptible to inhibition by nucleobase analogues may also be an excellent target for these MBPs. Any inhibitors discovered for ADA2 in this manner should also be tested against ADA1, as one may end up discovering a selective inhibitor for ADA2.

Finally, the derivatives of L16 and L17 could be further refined to give even more potent inhibitors. Different moieties such as cyano, nitro, benzene, and others could be substituted at different positions around the inhibitors to test for polar and nonpolar regions as well as empty pockets of space. It is imaginable that one could lower the K_I from low micromolar to low nanomolar with the right amount of persistent and systematic approaches.

6.5 A Relation Between K_I and Pseudo-first Order k_{app} Values

During the experiments monitoring ADA1 and ADA2 activity a potentially useful relation between the K_I of an inhibitor and the k_{app} value obtained from pseudo-first order conditions was discovered. In pseudo-first order conditions, substrate concentration is assumed to be significantly smaller than the K_M value. This transforms Equation 6.1 into Equation 6.2 and allows one to solve for Equation 6.3. A new apparent rate constant k_{app} appears which is described by Equation 6.4. If the initial enzyme concentration is known, k_{app}/K_M can be calculated.

$$-\frac{d[S]}{dt} = \frac{[E]_0 k_{cat}[S]}{K_M + [S]}$$

Equation 6.1 Michaelis-Menten Initial Rate Equation

$$-\frac{d[S]}{dt} = \frac{[E]_0 k_{cat}[S]}{K_M}$$

Equation 6.2 Pseudo-first Order Rate Equation

$$[S] = [S]_0 e^{-k_{app} t}$$

Equation 6.3 Pseudo-first Order Substrate Concentration Equation

$$k_{app} = \frac{[E]_0 k_{cat}}{K_M}$$

Equation 6.4 Pseudo-first Order k_{app} Equation

Next, if a competitive inhibitor is added to the reaction Equation 6.1 becomes Equation 6.5. If the reaction is in pseudo-first order conditions, Equation 6.5 transforms into Equation 6.6 and can then be solved to give Equation 6.7. This results in another apparent rate constant, denoted k'_{app} in Equation 6.7 and described by Equation 6.8. Equation 6.8 can be rearranged to give Equation 6.9 which shows that the K_I is only dependent on constants that can readily be obtained. The constant k'_{app} is obtained by fitting a first order curve to a reaction that is in pseudo-first order conditions and contains some amount of competitive inhibitor present. The constant k_{cat}/K_M is obtained by monitoring a reaction in pseudo-first order conditions without

inhibitor present and dividing the derived k_{app} value by initial enzyme concentration, $[E]_0$. The inhibitor concentration, [I], is known and finally the initial enzyme concentration is known. By applying all of these values to Equation 6.9, one can obtain a K_I value for the competitive inhibitor being tested.

$$-\frac{d[S]}{dt} = \frac{[E]_0 k_{cat}[S]}{K_M(1 + \frac{[I]}{K_I}) + [S]}$$

Equation 6.5 Competitive Inhibitor Michaelis-Menten Initial Rate Equation

$$-\frac{d[S]}{dt} = \frac{[E]_0 k_{cat}[S]}{K_M(1 + \frac{[I]}{K_I})}$$

Equation 6.6 Competitive Inhibitor Pseudo-first Order Rate Equation

$$[S] = [S]_0 e^{-k'_{app}t}$$

Equation 6.7 Competitive Inhibitor Pseudo-first Order Substrate Concentration Equation

$$k'_{app} = \frac{[E]_0 k_{cat}}{K_M(1 + \frac{[I]}{K_I})}$$

Equation 6.8 Competitive Inhibitor Pseudo-first Order k'_{app} Equation

$$K_I = \frac{[I]}{\frac{k_{cat}[E]_0}{K_M k'_{app}} - 1}$$

Equation 6.9 Competitive Inhibitor Pseudo-first Order K_I Equation

It is worth noting that this approach can be used for uncompetitive and noncompetitive inhibitors as well. However, in the case of noncompetitive inhibitors the exact same relation for K_I is obtained. This indicates that if using this method one cannot distinguish between competitive and noncompetitive inhibition. In the case of uncompetitive inhibitors, if pseudo-first order conditions are maintained between the reaction with inhibitor and the reaction without inhibitor, one will find there should be no change in the k_{app} values between the two reactions. This is because the substrate concentration term, which is being assumed to be effectively zero

in pseudo-first order conditions, is the term being adjusted by the inhibitor concentration. This then indicates that an uncompetitive inhibitor can be distinguished by this approach, but its K_I value cannot be obtained.

6.6 References

1. Xie, Y.; Maxson, T.; Tor, Y. *Org. Biomol. Chem.*, **2010**, *8*, 5053–5055.
2. Xie, Y.; Maxson, T.; Tor, Y. *J. Am. Chem. Soc.*, **2010**, *132* (34), 11896–11897.
3. Xie, Y.; Dix, A. V.; Tor, Y. *J. Am. Chem. Soc.*, **2009**, *131* (48), 17605–17614.